Re-entrant corner flows of Oldroyd-B fluids

O'Byrne, Aidan

Award date:
2010

Awarding institution:
University of Bath

Re-entrant corner flows of Oldroyd-B fluids

submitted by

Aidan T. O'Byrne

for the degree of Doctor of Philosophy

of the

University of Bath

Department of Mathematical Sciences

December 2010

Acknowledgements

I would like to especially thank my supervisor Dr Jonathan Evans for his patience, support and encouragement over the last four years and giving such an interesting topic to work on. Also the administration and postgraduate staff in the Mathematics department at Bath University for providing a supportive and stimulative environment in which to research.

A special thanks goes out to Dr David Sibley for his many insights and long discussions about the field of rheology during my time at Bath University and wish him the best of luck starting his post-doctoral career. Thanks go out to Dr Nick Gresham for being an excellent housemate with David and I over the last three years and Mr Sean Buckeridge for aid with deciphering Matlab.

I would also like to thank the Mathematics department at St. Andrews University during my undergraduate years for providing me with the motivation to study at postgraduate level. Finally to Michelle Hart for her support and encouragement. Without all of you this thesis would not have been possible.

Summary

We consider the planar flow of Oldroyd-B fluids around sharp corners. Two distinct cases arise for the corner geometry, where the corner angle is denoted by π/α. For $1/2 \leq \alpha < 1$ we have a re-entrant corner, whilst for $1 < \alpha < \infty$ a so called salient corner occurs. These two regimes have markedly different flow behaviour. The flow situation assumes complete flow around the corner with the absence of a lip vortex.

For the re-entrant corner problem a class of self-similar solutions has been identified with stress singularities of $O(r^{-2(1-\alpha)})$ and stream function behaviour $O(r^{(3-\alpha)\alpha})$ (r being the radial distance from the corner). These behaviours arise in a core flow region away from the walls and are shown to be solutions of the incompressible Euler equations. This region is reconciled with elastic boundary layers at the upstream and downstream walls using the method of matched asymptotic expansions. The analysis benefits from the representation of the stress in both Cartesian and natural stress formulations, and is performed when the Weissenberg number (the dimensionless relaxation time) is $O(1)$. These results hold for all values of the retardation parameter $\beta \in [0, 1)$, but breakdown in the Newtonian limit $\beta \to 1^-$. This latter singular limit is considered along with the other singular regimes of low and high Weissenberg number, in order to extend the parameter dependence of the solution.

For the salient corner case the mathematically simpler Newtonian balance for the flow and stress fields are shown to dominate away from the walls. This gives a stream function behaviour of $O(r^{1+\lambda_0})$ and stress behaviour $O(r^{\lambda_0 - 1})$, where λ_0 is the Newtonian problem eigenvalue. This behaviour is again reconciled with boundary layers at the walls which recover viscometric behaviour. These boundary layers are markedly different from those of the re-entrant corner case.

Contents

List of Figures

List of Tables

Chapter 1

Introduction

This thesis studies viscoelastic flows of Oldroyd-B type fluids in simple corner geometries. To introduce the subject, this chapter discusses the rheology behind viscometric materials, derivations of constitutive models leading up to Oldroyd-B type and a literature review of previous work undertaken in the field. To put this work into an industrial context, some relevant applications of Oldroyd-B type fluids are discussed. We begin with an introduction to basic rheological phenomena before going into detail on rheological concepts.

1.1 Introduction

Conservation laws for fluids state that particular measurable properties of an isolated physical system do not change as the system evolves. For example the Continuity Equation is a statement that mass is conserved within a system, whilst the Conservation of Linear and Angular Momentum states that the total linear and angular momentum respectively of a closed system of objects is constant. Similarly the Conservation of Energy states that the total amount of energy, again in a closed system, remains constant. However, there are generally more unknowns than equations requiring additional relations to be found in order to solve the systems. These additional relations are called *constitutive equations* and for fluids relate the motion of the fluid to the stresses present. An important class of fluid flow is Newtonian flow in which the extra stress tensor is proportional to the deformation tensor, with the proportionality being the viscosity of the fluid in question. Examples of materials which can be well described by Newtonian flow are water and air. Experimental data is well known to be modelled accurately by Newtonian flow theory for fluids which exhibit Newtonian flow characteristics.

However, many fluids show additional properties which are not modelled by Newto-

nian flow, for example paints can exhibit the shear-thinning effect, where the viscosity decreases with increasing shear rate. To explain this feature, imagine a polymer solution at rest with the molecules distributed at random. Any fluid trying to flow through this polymer will have to expend a lot of effort in order to make progress. In a simple shear flow, the molecules will align themselves with the fluid flow direction thus making it easier for the surrounding fluid molecules to flow past each other. This heuristic explanation of 'shear-thinning' explains why such fluids are very viscous at rest but flow easier when a stress is applied. Paint utilises this behaviour as one would like a less viscous substance while painting, but for it to be more viscous at rest to prevent dripping. A further example of non-Newtonian behaviour would be the presence of a yield stress. In this case, the stress upon a system has to pass a threshold before which the fluid does not flow. Particularly viscous materials such as toothpaste and ketchup are good examples where a yield-stress is present; fluids of this type are termed viscoplastic fluids. Fluids exhibiting this behaviour will not be discussed in this thesis but these examples serve to illustrate the many fluids which have a viscosity depending on shear rate. The need is clear for more complicated constitutive relations which can incorporate differing rheological qualia.

The development of constitutive equations and investigations into varying fluid behaviour is generally termed 'rheology'. For example, when modelling a polymer solution, a difference between Newtonian and non-Newtonian fluid mechanics is that the latter has to take into account the microstructure of the polymer in order to describe the observed effects. The varying size, shape and density of molecules that make up different polymer solutions can all give rise to differing rheological properties. Thus one can derive constitutive models by looking at the microstructure.

1.2 Viscoelasticity

Continuum mechanics provides the physical laws that materials obey and imparts requirements for the constitutive laws. There isn't a distinction in a continuum mechanical sense between solids and fluids though instinctively the difference is obvious: fluids 'flow' whereas solids do not. Alternatively, one can say that a solid is elastic, that is if a force is applied upon it the solid deforms, with the work stored as elastic energy. A fluid is viscous and transforms its work into heat. When the force is removed the solid returns to its original state (if it is a purely elastic material) but the fluid 'forgets' its original configuration. Viscoelastic materials lie somewhere in between the purely elastic and Newtonian flow characteristics. Some of the applied work done is stored as elastic energy with the rest transformed into heat. At a characteristic time λ say,

the material forgets its initial form after unloading some of its elastic energy into kinetic energy. For purely elastic materials $\lambda = \infty$, i.e. the material doesn't forget its original state and for purely viscous materials $\lambda = 0$. For materials which show both viscous and elastic properties, λ lies within these ranges and the material is termed a 'viscoelastic' material. It should be mentioned that there is the possibility of a range of different timescales within a single material: not every material has a unique characteristic time. For example, the characteristic relaxation time of isotactic polypropylene (iPP) increases with molecular weight.

It should be said that just knowing the characteristic time isn't generally that useful unless it is compared against the timescale of the flow (if the history of deformation is important). This introduces two dimensionless numbers in rheology, the Deborah number De and the Weissenberg number We. The Deborah number governs the degree to which elasticity shows itself in response to a deformation, it is the ratio of a characteristic time to the duration of the observation. Unless such a deformation is extremely slow or small, the behaiour of a viscoelastic fluid is nonlinear. The degree of nonlinearity is measured by the Weissenberg number: the product of a charteristic time of the fluid and the rate of deformation.

The key difference between these two measures is that We involves a characteristic rate of deformation and not the duration of observation (in this thesis the Weissenberg number is appropiately used due to the consideration of steady flow).

Since it is possible to characterise materials by the time it remembers its deformation history motivates calculating the total stress in a system over all past deformations, thus taking into account the memory of the fluid when calculating stress. We can formulate this by defining the total stress $\sigma(t)$ at a time t to be

$$\sigma(t) = -p\mathbf{I} + \mathbf{F}_{t'=-\infty}^{t'=\infty}\left(\mathbf{C}(t')\right), \tag{1.1}$$

where p is the pressure, $\sigma(t)$ is decomposed into an isotropic part and the extra-stress tensor with $\mathbf{C}$ a suitable strain tensor. The functional $\mathbf{F}$ weights the past deformations less than the most recent ones. Equation (1.1) in its general form can represent all possible viscoelastic models. Depending on the change of strain rate versus stress in a material the viscosity can be characterised as having a linear or non-linear response. In the former case this is termed a Newtonian fluid (i.e. the stress is directly proportional to the strain rate). When the response is non-linear it is said to be a non-Newtonian fluid.

It is possible to represent the functional $\mathbf{F}$ as an integral with a weighting function in it, the weighting function chosen to calibrate with real data (such as the measured

viscosity). This assumption on the functional gives rise to the linear viscoelastic model. However very few polymers can be said to be linearly viscoelastic and fails to model materials which change their properties under deformations. For example, variations of the Oldroyd-B model can be used to model the viscoelasticity of blood that characterize the shear thinning behaviour due to red blood cell aggregation and dispersion at low shear rate. The linear viscoelastic model cannot adequately describe such behaviour and is thus too limited for many non-Newtonian fluids.

As mentioned later in this introduction, the continuum approach to modelling viscoelastic fluids is limited and one is better served looking at the microstructure of fluids and building up constitutive models this way. The Oldroyd-B fluid is derived this way later from the properties of polymer molecules in such a fluid type.

1.3 Development of Viscoelastic Theory

The development and application of viscoelastic theory has arisen from the wide development of polymeric materials in industry. These materials display characteristics that cannot be adequately explained by the classical theories of elasticity or viscosity. Such studies lead to the need for a more general theory encompassing both fields. One way to characterise such materials, is to measure their response to a uniform stress. A standard elastic material when subject to such a stress, will respond instantaneously with a constant deformation. However, materials exist for which such a stress will induce an instant deformation that is not constant, i.e. some flow process will subsequently happen. This flow process may not be linear and may change with magnitude or form as time evolves. Materials which exhibit this are said to show creep characteristics. A Newtonian fluid shows creep characteristics which viscosity theory completely describes. More generally for non-Newtonian fluids neither theory on its own can fully describe it. For example the Oldroyd-B model includes both Newtonian and Maxwell models, allowing it to model, for example, the case where an elastic fluid obeying the Maxwell relation is mixed with a fluid governed by a Newtonian Law.

In addition, the application of a stress can produce an instantaneous deformation that in turn responds in a time-dependant manner to the stress first applied. A purely elastic material does not show this property: responses are governed at a particular time only by the total stress levels at that given moment. This property of 'memory' is of fundamental importance to viscoelastic fluids.

Viscoelastic fluids retain many of the properties associated with Newtonian Fluids; namely that stresses depends upon the current motion of the fluid, along with the property that stresses are dependent upon the history of its motion. Viscoelastic properties

are usually measured as responses to an instantaneously applied(removed) constant or dynamic stress or strain. The fluid can therefore be thought of as having both a viscous and an elastic element. Various fluid models exhibit viscoelastic behaviour and the reader is referred to [61] for examples of other constitutive models.

The flow of a fluid around a sharp re-entrant corner produces singularities in the stress field, causing significant numerical problems. The analysis here is confined to re-entrant corner flows between solid walls, with possible extensions to the analysis of different geometrical structures: wedge flows for example. In this paper, two formulations are considered: a Cartesian formulation and the natural stress basis, the latter chosen for simpler numerical implementation. It is assumed for simplicity that there is no re-circulation of flow at the upstream wall, i.e. lip vortices are not considered.

1.3.1 Balance Laws

Before deriving constitutive models, a more general discussion of the governing equations of many viscoelastic flows is useful. All fluid motion is governed by the balance laws of conservation of mass and of linear and angular momentum. If considering thermal effects, consideration of the energy balance is needed as well. For all models discussed here, thermal effects are not considered along with the added restriction that incompressible fluids are considered. These fluids are generally liquid at the temperatures used, hence this assumption has physical relevance. For incompressible fluids, the conservation of mass is

$$\nabla \cdot \mathbf{v} = 0, \tag{1.2}$$

where $\mathbf{v}$ is the velocity field of the fluid. Balance of linear momentum gives

$$\rho \left(\frac{\partial \mathbf{v}}{\partial t} + (\mathbf{v} \cdot \nabla)\mathbf{v} \right) = -\nabla p + \nabla \cdot \mathbf{T}, \tag{1.3}$$

where ρ is the density, $\mathbf{T}$ the extra stress tensor and p the pressure. The terms on the left are referred to as the inertial terms (representing the force of inertia) which in the majority of this thesis are found to be negligible. $\mathbf{T}$ represents the stress the fluid develops in response to the deformation. We define the total stress tensor σ to be

$$\sigma = -p\mathbf{I} + \mathbf{T}, \quad \text{with } \sigma = \sigma^T. \tag{1.4}$$

The symmetry of the stress tensor comes from the principle of conservation of angular momentum and balance of moment of momentum. Summming the moments around a point with the continuum assumed to be in equilibrium gives the stress tensor as

symmetric. In general this is not the case, for example if some force exists which is not proportional to the volume, and thus does not tend to zero in the limit as the volume goes to zero.

The conservation equations are not enough to determine the characteristics of the flow, motivating the need for constitutive equations relating the motion of the fluid to the stresses present.

1.3.2 Newtonian Fluids

An important class of fluid flow is Newtonian flow. This is a well known and widely discussed fluid flow type. For an incompressible Newtonian viscous fluid, the constitutive relation relating stresses to motion is known to be

$$\mathbf{T} = 2\eta\mathbf{D}, \tag{1.5}$$

where η is the viscocity and $\mathbf{D}$ the rate-of-strain (or deformation) tensor. The deformation tensor is related to the fluid motion, specifically it is the symmetric part of the velocity gradient tensor and written as

$$\mathbf{D} = \frac{1}{2}(\nabla\mathbf{v} + (\nabla\mathbf{v})^T). \tag{1.6}$$

For fluid flow behaviour where the stresses are dependant upon their history, or where solvent and polymer stresses are present a more complicated set of equations is needed to model this behaviour. Fluids which incorporate Maxwell effects as well as classical Newtonian qualities are ill-described by simple Newtonian flow.

1.3.3 Spring Dashpot derivation

There are several ways to derive models, one of which is to approach it via a mechanical analogy where springs and dashpots are considered in combination. Since viscoelastic fluids can consist of elastic and viscous elements, we can use the springs to represent elastic elements of the fluids and dashpots as viscous elements, see figure 1-1. We can derive Maxwell's one-dimensional linear model considering a spring and dashpot in series as in (A) of figure 1-1. Relating the elastic strain γ_e and elastic stress σ_e (the subscript e referencing the elastic element) via Hooke's Law

$$\sigma_e = k\gamma_e, \tag{1.7}$$

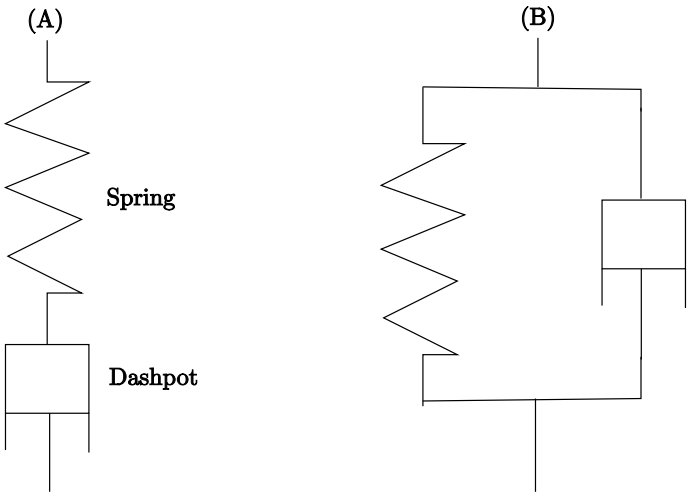

Figure 1-1: The spring and dashpot elements are shown in two possible configurations. (A) shows spring and dashpot elements arranged in a series to give a Maxwell element, and (B) in parallel to give a Kelvin-Voigt element.

with spring constant k. The dashpot as a viscous element with associated viscosity η, extends at a rate proportional to the force applied on it

$$\sigma_v = \eta \dot{\gamma}_v. \tag{1.8}$$

The total strain is the sum of the individual strains since the elements are in series, i.e.

$$\gamma = \gamma_e + \gamma_v. \tag{1.9}$$

Differentiating with respect to time the individual elements and noting that the stresses will be equal ($\sigma = \sigma_e = \sigma_v$) since the elements are connected in series, we obtain

$$\sigma + \frac{\eta}{k}\dot{\sigma} = \eta \dot{\gamma}, \tag{1.10}$$

where $\frac{\eta}{k}$ represents a relaxation time: a measure of the time for which the fluid remembers the flow history. Choosing to arrange the elements in parallel, see (B) of 1-1 gives the Kelvin-Voigt model. The derivation is similar to the one just performed, but since the elements are now connected in parallel, the total stress is the sum of individual stresses ($\sigma = \sigma_e + \sigma_v$) and the strains are equal ($\gamma = \gamma_e = \gamma_v$), giving

$$\sigma = k\gamma + \eta \dot{\gamma}. \tag{1.11}$$

We can note that (1.4) implies σ is a symmetric tensor field and that we can represent $\dot{\gamma}$ with the rate of deformation tensor $\mathbf{D}$. The one-dimensional Maxwell constitutive model can be generalised and written in tensor form as

$$\mathbf{T} + \frac{\eta}{k}\frac{\partial \mathbf{T}}{\partial t} = 2\eta \mathbf{D}. \tag{1.12}$$

1.4 Nonlinear Maxwell models

A natural extension to this is to consider nonlinear behaviour models for models to be applied to real fluids. In order to see why (1.12) is not sufficient to describe non-Newtonian fluids, we need to consider the work of Oldroyd in the 1950 paper [41], in which the principles that a constitutive equation must be based upon were laid out. A summary of Oldroyd's work is presented in [13].

Firstly, constitutive variables such as stress and strain, rates and gradients of these quantities are expressed in terms of their components in some coordinate system. To ensure that these variables are expressed in a form that does not limit them to a particular coordinate type, such as Cartesian, the variables are expressed as tensors. There are many ways of expressing tensors, what is important is that constitutive equations express the same relationship in all coordinate systems. This is what is termed the *Principle of coordinates invariance*.

Related to this principle is the *Principle of invariance*. Consider for example, the choice of a coordinate system in which some constitutive property of a fluid is to be measured. The principle of coordinate invariance means we need to formulate the constitutive equation so that we can express it in different co-ordinate systems. The natural question arises when a suitable system is chosen, how can we ensure that the constitutive equations are invariant to this choice? Important is the invariance of both the orientation of the co-ordinate system and its scale.

Therefore for constitutive equations to be invariant under a change of spatial frame, the so called *Principle of Objectivity* (a natural extension to the invariance property), wherein the deformation of a material is not affected by any rotation it may undergo. If the constitutive equation is satisfied for a motion, then the stresses within the fluid as a result are invariant spatially (i.e. they aren't influenced by the observer, only by the deformation itself). This principle is one that all linear constitutive models violate apart from Newtonian Flow, so a modification to the linear Maxwell model is needed. One way to approach this is to replace the time derivative with an invariant one: the

Gordon-Schowalter convected derivative

$$\frac{D\mathbf{T}}{Dt} = \frac{\partial \mathbf{T}}{\partial t} + \overset{\square}{\mathbf{T}}, \tag{1.13}$$

where

$$\overset{\square}{\mathbf{T}} = \mathbf{TW} - \mathbf{WT} - a\left(\mathbf{TD} + \mathbf{DT}\right), \quad \mathbf{W} = \frac{1}{2}\left(\nabla \mathbf{v} - (\nabla \mathbf{v})^T\right). \tag{1.14}$$

Here we have the parameter $a \in [-1, 1]$ and $\mathbf{W}$ is the vorticity tensor. This is the most general derivative used to describe viscometric behaviour. There are several Maxwell models which are specific cases of (1.13) (chosen to model specific viscometric behaviour). For $a = 1$, replacing the time derivative in (1.12) with the Gordon-Schowalter convected derivative we get the Upper Convected Maxwell (UCM) model

$$\mathbf{T} + \frac{\eta}{k}\left(\frac{\partial \mathbf{T}}{\partial t} + \overset{\triangledown}{\mathbf{T}}\right) = 2\eta \mathbf{D}, \tag{1.15}$$

and with $a = -1$, the Lower Convected Maxwell (LCM) model,

$$\mathbf{T} + \frac{\eta}{k}\left(\frac{\partial \mathbf{T}}{\partial t} + \overset{\triangle}{\mathbf{T}}\right) = 2\eta \mathbf{D}. \tag{1.16}$$

The symbols $\triangle$ and $\triangledown$ stand for the upper and lower convected derivatives respectively and are defined as

$$\overset{\triangledown}{\mathbf{T}} = (\mathbf{v} \cdot \nabla)\mathbf{T} - (\nabla \mathbf{v})\mathbf{T} - \mathbf{T}(\nabla \mathbf{v})^T, \quad \overset{\triangle}{\mathbf{T}} = (\mathbf{v} \cdot \nabla)\mathbf{T} + (\nabla \mathbf{v})^T\mathbf{T} + \mathbf{T}(\nabla \mathbf{v}). \tag{1.17}$$

1.4.1 Limitations of the Oldroyd-B model

Newtonian fluids are characterised by the assumption that the extra-stress tensor is a linear isotropic function of the velocity gradient. Such models cannot describe the shear thinning behaviour many polymer fluids exhibit. If the components of the extra stress tensor $\mathbf{T} = \sigma + p\mathbf{I}$ are assumed to depend only on the velocity, acceleration and higher order time derivatives, a set of constitutive models called the Order models can be developed. The Order models are also known as the slow flow expansion models - the asymptotic limit of all models in the limit of low Weissenberg numbers. This can be seen as a first attempt at modelling viscometric fluids and polymers. Given the initial assumptions on the extra stress tensor, a polynomial in $\mathbf{T}$ exists as well as the

Rivlin-Ericksen tensors $\{\mathbf{A}_k\}$ given by

$$\{\mathbf{A}_k\}(\mathbf{x},t) = \frac{\partial^k}{\partial t'^k}\mathbf{C}(\mathbf{x},t,t')_{t=t'}, \tag{1.18}$$

where the derivative follows the fluid particles and $\mathbf{C}(\mathbf{x},t,t')$ is the Cauchy-Green strain tensor. For $k=1$ (or defined as first order), we have

$$\{\mathbf{A}_1\}(\mathbf{x},t) = \nabla\mathbf{v} + (\nabla\mathbf{v})^T \tag{1.19}$$

Using identities in [43], pg.29 , we can deduce recurrance relations for arbitrary powers of k^{th} order

$$\{\mathbf{A}_{k+1}\}(\mathbf{x},t) = \frac{D\mathbf{A}_k}{Dt} + (\nabla\mathbf{v})\mathbf{A}_k + \mathbf{A}_k(\nabla\mathbf{v})^T, \qquad k = 1,2,3,\ldots. \tag{1.20}$$

For constitutive relations that are polynomial functions of the first N Rivlin-Ericksen tensors, $\mathbf{T} = f(\mathbf{A}_1,\mathbf{A}_2,\cdots,\mathbf{A}_N)$, the first three order fluids are given by

$$\begin{aligned}
\mathbf{T}_1 &= a_1\mathbf{A}_1\\
\mathbf{T}_2 &= a_1\mathbf{A}_1 + a_2\mathbf{A}_2 + a_{11}\mathbf{A}_1^2\\
\mathbf{T}_3 &= (a_1 + a_{1:11}tr(\mathbf{A}_1^2))\mathbf{A}_1 + a_2\mathbf{A}_2 + a_{11}\mathbf{A}_1^2 + a_3\mathbf{A}_3 + a_{12}(\mathbf{A}_1\mathbf{A}_2 + \mathbf{A}_2\mathbf{A}_1),
\end{aligned}$$

where the a_i's, a_{11}, a_{12}, $a_{1:11}$ are constant coefficients. The first order fluid is simply the Newtonian case, the second order fluid now has a normal stress difference through the existence of $\mathbf{A}_1$ and $\mathbf{A}_2$, and some viscoelastic properties (through $\mathbf{A}_2$). The third order fluid with suitable coefficients gives a viscosity decreasing with shear rate, though fails to allow for situations where strong shear rates are observed. Thus 'fast' flows or ones in which the tensors $\mathbf{A}_k$ vary rapidly, fail to be suitably modelled.

For simple steady shear flow, a constant viscosity is found which is suitable for many real world polymers flows subjected to shear, for example suitable for the class of Boger fluids. Further a quadratic first normal stress difference[1] and zero second normal stress difference are characteristics of Boger fluids (see, for example,[58] and [43]).

One limitation of the Oldroyd-B model is that fluids with varying viscosity are ill-suited to this model as well as problems that involve measuring extensional flow. As

[1]Normal stress is perpendicular to the plane of motion and are the diagonal components of the stress tensor. The deviatoric part of the stress tensor is important for deformation of fluids. If hydrostatic pressure is superimposed, it will change all normal components of the stress tensor but wouldn't influence flow. Therefore in order to characterize effects of normal stresses in shear flow it isn't the absolute value of the normal stress that is important but their differences.

an example, for the extensional flow

$$\mathbf{v} = \left(\dot{\epsilon} x, -\frac{\dot{\epsilon}}{2} y, -\frac{\dot{\epsilon}}{2} z \right), \tag{1.21}$$

with constant extensional rate $\dot{\epsilon}$, the Oldroyd-B model has an extensional viscosity η_e given by (see, e.g. [43])

$$\eta_\epsilon = \frac{3\eta(1 - \lambda_2\dot{\epsilon} - 2\lambda_1\lambda_2\dot{\epsilon}^2)}{(1 - 2\lambda_1\dot{\epsilon})(1 + \lambda_1\dot{\epsilon})}. \tag{1.22}$$

Here the constants λ_1 and λ_2 are characteristic relaxation and retardation times respectively (and defined below in section 1.4.2) and η is the total shear viscosity. Thus the extensional viscosity blows up at finite extensional rate $\dot{\epsilon} = \frac{1}{2\lambda_1}$. The elements in the dumbbell model used to derive the Oldroyd-B constitutive model are infinitely extensible and hence become infinitely extended in the flow at the critical value $\dot{\epsilon} = \frac{1}{2\lambda_1}$. In other words, the properties of constant viscosity and infinite extensibility of the Hookean connecting springs give extensional viscosity that blows up at finite extensional rates. When trying to model real world fluids subjected to extensional strain, this problem of non bounded extensional viscosity has lead to the development of models based upon finitely-extended dumbbells: the FENE models. This retains the constant shear viscosity of Boger fluids but with bounded extensional viscosities.

1.4.2 Derivation of the Oldroyd-B model

Classically, constitutive models were derived through continuum mechanics [40]. Recently, the basis of constitutive modelling has moved onto considering the microscopic properties of fluids, since, as said earlier the molecular composition has an important role to play in the macroscopic behaviour exhibited. This can be termed *kinetic theory* in which a mechanical model for the basic constituent of the molecules forming a non-Newtonian liquid is used. The main forces acting on these molecules are considered that define its motion, then these effects are averaged out over a large number of possible configurations that form the basic structure of the polymer. Thus this allows us to construct a model that has the relevant macroscopic properties from microscopic considerations.

For the Oldroyd-B model, kinetic theory can be used by consideration of a molecule being a pair of spheres connected by an Hookean spring; the dumbbell model. The following is a summary of one way in which this can be derived. The reader is referred to [42] and [43] for a more detailed treatment of this subject. The Navier Stokes equations are being used for the solvent in which the model bead-spring dumbbell is

immersed. The incompressible Navier Stokes equations are

$$\nabla \cdot \mathbf{v} = 0, \quad \rho \frac{D\mathbf{v}}{Dt} = \nabla \cdot \sigma, \tag{1.23}$$

with the associated constitutive equation

$$\sigma = -p\mathbf{I} + \mu(\nabla \mathbf{v} + (\nabla \mathbf{v})^T). \tag{1.24}$$

Here $\frac{D}{Dt}$ is the total time derivative, σ the stress tensor, ρ the density, μ the Newtonian viscosity and p pressure. At the microscopic level inertial forces are small compared to viscous forces, and thus the incompressible Navier Stokes equations simplify down to

$$\nabla \cdot \mathbf{v} = 0, \quad \mu \nabla^2 \mathbf{v} = \nabla p. \tag{1.25}$$

Consider now the flow of a small solid sphere in a Newtonian fluid. A sphere of radius a, moving with constant velocity $\mathbf{U}$ experiences a drag force $\mathbf{F} = -6\pi\mu a\mathbf{U}$. To model a polymer, a device is needed that remembers the flow history of an object. The simplest deformable object of this nature is to take two spherical beads and connect with a linear spring to form a dumbbell. There are three effects acting on each bead

- The spring force;
- The Stokes drag force from the solvent viscosity the dumbbell is suspended in, if moving relative to the fluid around it;
- Brownian motion at small enough scales.

Considering the spring force first, we have one bead of radius a at a position $\mathbf{x}$, with another bead at $\mathbf{x} + \mathbf{r}$ under the action of hydrodynamic and spring forces only, and neglecting brownian motion for the moment. The size of the beads are small, hence inertial forces are assumed zero and the total force on the bead is zero. We denote the spring force as $\lambda\mathbf{r}$ with λ the spring constant. The velocity $\mathbf{U}$ of a bead, in a fluid with velocity $\mathbf{v}(\mathbf{x})$ experiences a drag force of

$$6\pi\mu a(\mathbf{v}(\mathbf{x}) - \mathbf{U}). \tag{1.26}$$

The total force is therefore

$$\lambda\mathbf{r} + 6\pi\mu a(\mathbf{v}(\mathbf{x}) - \mathbf{U}) = 0. \tag{1.27}$$

Estimating the spring constant $\lambda = 3kT/a^2$ from thermal forces, the velocity of the

bead is

$$\mathbf{U} = \frac{kT}{2\pi\mu a^3}\mathbf{r} + \mathbf{v}(\mathbf{x}). \tag{1.28}$$

Calculating a similar velocity for the other bead at $\mathbf{x}+\mathbf{r}$, we can determine the evolution of $\mathbf{r}$ to be

$$\frac{d\mathbf{r}}{dt} = -\frac{kT}{\pi\mu a^3}\mathbf{r} + \mathbf{r}\cdot\nabla\mathbf{v}. \tag{1.29}$$

We denote $\frac{2kT}{\pi\mu a^3} = \frac{1}{\tau}$ as the relaxation time for the dumbbell following distortion caused by the flow. A suspension with a total m such small dumbbells will contribute extra stress. Furthermore, the fluid they are suspended in will contribute a Newtonian stress. In this case we are trying to find the polymer stress σ^p. We consider a small surface element area δS and a unit normal $\mathbf{n}$. The force associated with a dumbbell that crosses the surface is $\lambda\mathbf{r}$, dumbbells are more likely to cross the surface aligned with $\mathbf{n}$. Given m dumbbells per unit volume, we expect the number crossing the surface element to be $m\mathbf{r}\cdot\mathbf{n}\delta S$. From this, the extra stress exerted by the dumbbells is found as

$$\sigma^p = G\mathbf{r}\cdot\mathbf{r}, \quad G = \frac{3\pi\mu a m}{2\tau}. \tag{1.30}$$

Finally, Brownian motion needs to be considered to complete the model. Adding a standard three dimensional Brownian motion to the evolution of the vector $\mathbf{r}$:

$$d\mathbf{r} = (-\frac{1}{2\tau}\mathbf{r} + \mathbf{r}\cdot\nabla\mathbf{v})dt + \tau^{-1/2}d\mathbf{B}_t. \tag{1.31}$$

Introducing the conformation tensor $\mathbf{A}$, $\mathbf{A} =< \mathbf{r}, \mathbf{r} >$ used to describe the macroscopic polymer behaviour, consider the movement from position $\mathbf{x}$ of the dumbbell in a time dt, i.e. the movement is given by

$$\mathbf{x} + d\mathbf{x} = \mathbf{x} + \mathbf{v}(\mathbf{x})dt. \tag{1.32}$$

As we take a time step dt we get

$$\mathbf{A}(\mathbf{x} + \mathbf{v}dt, t + dt) =< (\mathbf{r} + d\mathbf{r}), (\mathbf{r} + d\mathbf{r}) > . \tag{1.33}$$

Evaluating these expressions, we obtain

$$\frac{\partial\mathbf{A}}{\partial t} + (\mathbf{v}\cdot\nabla)\mathbf{A} - \mathbf{A}\cdot\nabla\mathbf{v} - (\nabla\mathbf{v})^T\cdot\mathbf{A} = -\frac{1}{\tau}(\mathbf{A} - \mathbf{I}), \tag{1.34}$$

with polymer stress $\sigma^p = G\mathbf{A}$. The conformation tensor $\mathbf{A}$ is a positive definite, second order tensor that describes the microstructure of the polymer molecules at a continuum level. Putting these equations together gives

$$\nabla \cdot \mathbf{v} = 0, \quad \rho \frac{D\mathbf{v}}{Dt} = \nabla \cdot \sigma, \quad \sigma = -p\mathbf{I} + \mu(\nabla \mathbf{v} + (\nabla \mathbf{v})^T) + G\mathbf{A}, \tag{1.35}$$

$$\frac{\partial \mathbf{A}}{\partial t} + (\mathbf{v} \cdot \nabla)\mathbf{A} - \mathbf{A} \cdot \nabla \mathbf{v} - (\nabla \mathbf{v})^T \cdot \mathbf{A} = -\frac{1}{\tau}(\mathbf{A} - \mathbf{I}). \tag{1.36}$$

We may recast these equations using alternative notation. The total shear viscosity η of the suspension is comprised of Newtonian $\eta_s = \mu$ and polymer $\eta_p = G\tau$ components,

$$\eta = \mu + G\tau = \eta_s + \eta_p. \tag{1.37}$$

The relaxation time $\lambda_1 = \tau$ measures the transition from elastic to viscous behaviour. We introduce the retardation time λ_2 of the fluid, which characterises the response of a viscoelastic material to the instantaneous application of a constant stress. It is related to the relaxation time via

$$\lambda_2 = \frac{\tau \mu}{\mu + G\tau} = \frac{\eta_s}{\eta}\lambda_1. \tag{1.38}$$

Finally we introduce the polymer stress $\mathbf{T}^p$,

$$\mathbf{T}^p = G(\mathbf{A} - I) = \mathbf{T} - 2\eta_s \mathbf{D}, \tag{1.39}$$

with the deformation tensor defined in (1.6). Then the dimensional governing equations can alternatively be written as

$$\nabla \cdot \mathbf{v} = 0, \quad \rho\left(\frac{\partial \mathbf{v}}{\partial t} + (\mathbf{v} \cdot \nabla \mathbf{v})\right) = -\nabla p + \nabla \cdot \mathbf{T}^p + \eta_s \nabla^2 \mathbf{v},$$

$$\mathbf{T}^p + \lambda_1 \overset{\triangledown}{\mathbf{T}}{}^p = 2\eta_p \mathbf{D}, \tag{1.40}$$

with the upper convected derivative of the extra stress tensor as given in (1.17) and

$$\eta_p = \eta - \eta_s = \eta\left(1 - \frac{\lambda_2}{\lambda_1}\right).$$

Inertial terms will turn out to be negligible for flows considered in this thesis.

In [6], a 4-1 contraction flow was simulated for a viscoelastic polymer solution. Two Boger fluids PA100 and PA300 were examined: prepared by dissolving differing amounts of polyacrylamnide in a Newtonian solvent N91. Oldroyd-B type properties

Parameter values			
	$PA100$	$PA300$	PP
η	0.52	0.74	0.74
η_s	0.4	0.37	0.34
η_p	0.12	0.4	0.4
λ_1	1.947	1.942	1.947
λ_2	1.50	0.53	0.53

Table 1.1: Table showing parameter values for three Oldroyd-B type fluids. The viscosity η is split up into a solvent part η_s and a polymer part η_p. The third fluid type PP is a polyisobutylene-polybutene fluid. Viscosities are given in units $Pa.s$ and relaxation/retardation times in s. Reynolds numbers for all three fluids types were assumed small with Weissenberg numbers dependent upon the geometries used (not specifically given in the citations)

such as low shear thinning and very small second normal stress differences were retained. A three mode Oldroyd-B model[2] was fitted to experimental data. In [11], a polyisobutylene-polybutene solution is considered. Parameter values for these three polymer solutions (once changed to our notation) are given in table 1.1.

1.4.3 Nondimensionalisation

The Oldroyd-B model includes solvent stresses as well as polymeric stresses considered in the UCM model. It thus adds a Newtonian stress contribution to the UCM stresses. These two stresses can be written as $\mathbf{T}^p$ for the polymer stress and $\mathbf{T}^s$ for the solvent stress, with the total stress $\mathbf{T}$ being the sum of these individual stresses. This allows us to express the governing equations in two ways, one involving separate equations for the solvent and polymer stresses, and one involving the total stress only (eliminating explicit reference to the solvent and polymer stresses). The former statement is the one adopted in this thesis as in (1.40), which can be written as

$$\nabla \cdot \mathbf{v} = 0, \quad \rho\left(\frac{\partial \mathbf{v}}{\partial t} + (\mathbf{v} \cdot \nabla \mathbf{v})\right) = -\nabla p + \nabla \cdot \mathbf{T}, \tag{1.41}$$

$$\mathbf{T} = \mathbf{T}^p + \mathbf{T}^s, \quad \mathbf{T}^s = 2\eta_s \mathbf{D}, \quad \mathbf{T}^p + \lambda_1 \left(\frac{\partial \mathbf{T}^p}{\partial t} + \overset{\triangledown}{\mathbf{T}}^p\right) = 2\eta(1 - \frac{\lambda_2}{\lambda_1})\mathbf{D}. \tag{1.42}$$

We have defined λ_1 and λ_2 to be the characteristic relaxation and retardation times for the fluid, respectively. The relaxation time λ_1 measures the transition from elastic to viscous behaviour, whilst the retardation time λ_2 is a time characterising the response

[2]Multi-mode constitutive equations consider a spectrum of relaxation times with each mode i having a partial viscosity μ_i and relaxation time λ_i. Single mode verses multi mode modelling is considered for example in [38]

of a viscoelastic material to the instantaneous application of a constant stress. To nondimensionalise, we introduce a characteristic velocity scale U and length scale L. We then scale our variables as follows

$$\mathbf{x} = L\mathbf{x}^*, \quad t = \frac{L}{U}t^*, \quad \mathbf{v} = U\mathbf{v}^*, \quad p = \frac{U\eta}{L}p^*, \quad \mathbf{T}^p = \frac{U\eta}{L}\mathbf{T}^{p*}, \quad \mathbf{T}^s = \frac{U\eta}{L}\mathbf{T}^{s*}, \tag{1.43}$$

where * denotes the dimensionless variables. We introduce these into the dimensional equations (1.41)-(1.42) which, after dropping $*$'s, give the dimensionless governing equations as

$$\begin{aligned} \nabla \cdot \mathbf{v} = 0, \quad \mathrm{Re}\left(\frac{\partial \mathbf{v}}{\partial t} + (\mathbf{v}\cdot\nabla\mathbf{v})\right) &= -\nabla p + \nabla\cdot\mathbf{T}, \\ \mathbf{T} = \mathbf{T}^p + \mathbf{T}^s, \quad \mathbf{T}^s = 2\beta\mathbf{D}, \quad \mathbf{T}^p + \mathrm{We}\left(\frac{\partial \mathbf{T}^p}{\partial t} + \overset{\triangledown}{\mathbf{T}}^p\right) &= 2(1-\beta)\mathbf{D}, \end{aligned} \tag{1.44}$$

with dimensionless parameters

$$\mathrm{Re} = \frac{\rho U L}{\eta}, \quad \mathrm{We} = \frac{\lambda_1 U}{L}, \quad \beta = \frac{\lambda_2}{\lambda_1} = \frac{\eta_s}{\eta}. \tag{1.45}$$

These dimensionless parameters are the Reynolds number $\mathrm{Re} \geq 0$, the Weissenberg number $\mathrm{We} \geq 0$ (the dimensionless relaxation time) and the retardation parameter $\beta \in [0,1]$ (or dimensionless solvent viscosity).

We consider steady flow only for the problems addressed in this thesis, so that (1.44) reduce to

$$\begin{aligned} \nabla \cdot \mathbf{v} = 0, \quad \mathrm{Re}(\mathbf{v}\cdot\nabla\mathbf{v}) &= -\nabla p + \nabla\cdot\mathbf{T}, \\ \mathbf{T} = \mathbf{T}^p + \mathbf{T}^s, \quad \mathbf{T}^s = 2\beta\mathbf{D}, \quad \mathbf{T}^p + \mathrm{We}\,\overset{\triangledown}{\mathbf{T}}^p &= 2(1-\beta)\mathbf{D}, \end{aligned} \tag{1.46}$$

which will be the governing equations of interest. On occasion we will include the solvent stress explicitly in the momentum equation, so that the form

$$\begin{aligned} \nabla \cdot \mathbf{v} = 0, \quad \mathrm{Re}(\mathbf{v}\cdot\nabla\mathbf{v}) &= -\nabla p + \nabla\cdot\mathbf{T}^p + \beta\nabla^2\mathbf{v}, \\ \mathbf{T}^p + \mathrm{We}\,\overset{\triangledown}{\mathbf{T}}^p &= 2(1-\beta)\mathbf{D}, \end{aligned} \tag{1.47}$$

will be interchangeably used with (1.46).

1.5 Corner geometry

Figure 1-2 shows the re-entrant corner geometry. Using polar coordinates (r, θ) (centered on the corner itself), r is the distance away from the corner and θ the angle from the upstream wall. The domain is $0 < r < \infty$, $\theta \in [0, \pi/\alpha]$, where $\theta = 0$ is the upstream wall and $\theta = \pi/\alpha$ the downstream wall. The corner angle parameter satisfies $1/2 \leq \alpha < 1$ for re-entrant corners. The Cartesian axes (x, y) are aligned along the walls, with x aligned along the upstream wall and y at $\theta = \pi/2$. On both walls we prescribe no-slip and no normal velocity boundary conditions. As a note, in any subsequent derivation using the Cartesian form, only the alignment with the upstream wall is necessary, with the downstream formulation obtained through a suitable transformation which is described later.

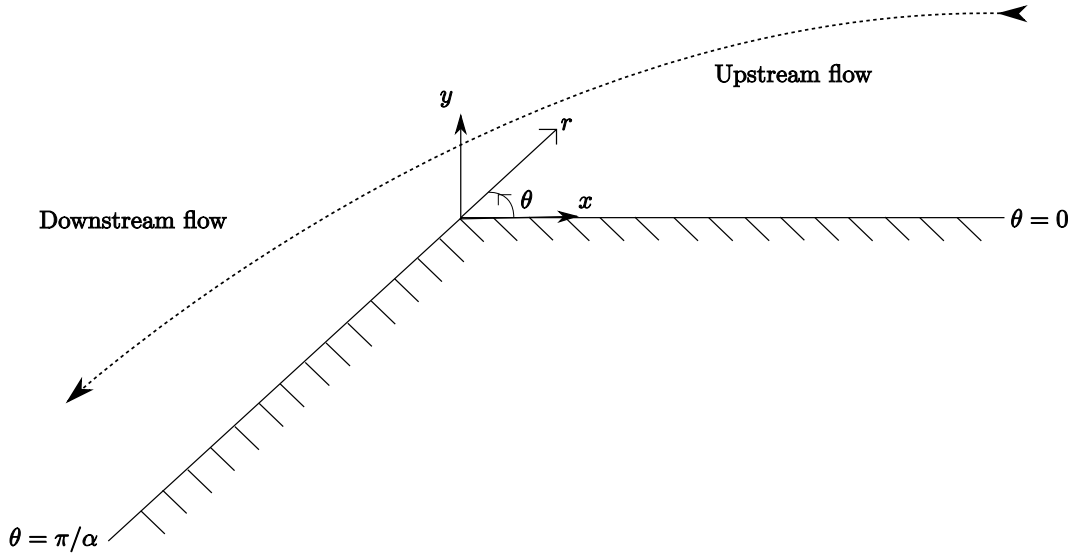

Figure 1-2: Diagram showing the local re-entrant corner geometry for Oldroyd-B fluids. Distances to and from the corner are assumed small. The Cartesian axes alignments are given and the direction of flow from upstream to downstream (from right to left) is indicated.

1.6 Literature Review

The main problem addressed in this thesis is flow at a re-entrant corner. These are corners whose angles are greater than 180^o and arise in many practical applications such as extrusion flows. It is a benchmark problem in the field of rheology and has received a lot attention due to the challenges and difficulties encountered when dealing with

flows involving high local stress concentrations[3] and thus in determining admissible asymptotic and numerical behaviours for certain viscoelastic differential constitutive models. In this respect, the Oldroyd-B (and Upper Convected Maxwell (UCM)) models have been particularly troublesome. The initial results of Hinch [30] for Oldroyd-B models generated a class of similarity solutions holding in a region local to the corner but away from the walls (a so called outer or core flow region). In this region, the upper convected stress derivative was assumed to dominate in the polymer constitutive equation and a stretching solution for the polymer stresses in the form

$$\mathbf{T}^p = \lambda(\psi)\mathbf{v}\mathbf{v}^T, \tag{1.48}$$

was identified. The similarity solutions predicted a stress singularity of $O(r^{-2(1-\alpha)})$ and stream function behaviour $O(r^{\alpha(3-\alpha)})$, where r is the radial distance to the corner and $\alpha \in [1/2, 1)$ the corner angle parameter (defined in chapter 3). This behaviour has subsequently been confirmed numerically for the benchmark corner angle of 270^o ($\alpha = 2/3$) by Singh and Leal [56], Baaijens [8], Xue et al. [60], Phillips and Williams [46], Alves et al. [4], Aboubacar and Webster [2], Aboubacar et al. [1] and Alves et al. [5] amongst others, despite initial setbacks (see, for example, Lipscomb et al. [36], Coates et al. [12]). The asymptotic solution has been completed with the determination of elastic wall boundary layers, the upstream case being first determined by Renardy [51], whilst the downstream case was considered by Rallison and Hinch [47] (see also Evans [17, 18]). These authors demonstrated matching between the respective boundary layers and Hinch's outer similarity solution, the analysis of [51] proceeding in a Cartesian formulation, whilst [47] used the natural stress formulation originally introduced in [49].

The essential features of the analysis in [47] was to demonstrate how the natural stress variables communicated the required information from the upstream boundary layer, through the outer region and into the downstream boundary layer. Further, it was identified that the downstream layer equations possessed an essential singularity (with one set of exponentially small terms explicitly identified, with the further two for Oldroyd-B given in Evans [18]). However, one noticeable failure of the analysis was the lack of convergence of a numerical solution to the downstream layer equations in the UCM case. The UCM case has subsequently been considered in [20] and [21], where the method of matched asymptotic expansions for the problem was set in a more systematic framework than that adopted in [47]. This setting afforded a consistent comparison between terms arising in the flow equations, so that they could be genuinely

[3]This is strongly related to the 'high Weissenberg number problem', see [59], [34] and [9],

compared. Detailed analysis of the boundary layer equations was also given, where the solution was shown to possess two sets of exponentially small terms at the downstream wall (these being associated with the essential singularity). Further it was shown how the complete local asymptotic solution could be expressed in terms of an upstream similarity parameter involving the upstream wall shear rate and pressure coefficients.

Our main intention in this thesis is to further the results of [47] for Oldroyd-B in the natural stress formulation. The approach adopted extends the matched asymptotic analysis framework used for the UCM case in [20] and [21].

Much of the early work on re-entrant corner flow started with investigation of UCM and Oldroyd-B type fluids, with results for the more complicated constitutive models such as PTT and Giesekus fluids following later. For a Newtonian fluid the stresses were known to grow very large as one approached a re-entrant corner and this was also expected for UCM type fluids. Preliminary investigations on the problem include Renardy [48], who considered the stresses in the UCM model for a 270^o corner when the velocity field is taken to be Newtonian. It was known that assuming a Newtonian velocity field was questionable but it allowed the main features of the flow to be considered. It was found that the convected derivative dominates at the corner away from the walls, with solution found to be proportional to $\mathbf{v}\mathbf{v}^T$ along streamlines and which was confirmed by numerical results. However, this core flow solution could not attain viscometric behaviour at the walls, thus determining the presence of boundary layers. The thickness of the boundary layers was found to be $\theta \sim r^{1-\lambda_0}$ (with r the radial distance away from the corner, θ the angle with the upstream wall and λ_0 a constant (the Newtonian flow eigenvalue), found to be $\lambda_0 \sim 0.54$ for a 270° corner angle). The Newtonian velocity field behaves as $\psi \sim r^{1+\lambda_0}$, the polymer stresses behave as $r^{-0.74}$ in the core and as $r^{-0.91}$ near the walls (the square of the velocity gradient).

The early work of both Hinch and Renardy was performed in the Cartesian stress basis. The discovery of Renardy that the stress close to the corner 'follows' the streamline coupled with the fact it becomes singular at the corner itself is the reason why numerical implementation is so difficult. Information from the stresses carry on downsteam past the corner; a Cartesian co-ordinate system has problems with the extreme accuracy required to calculate successful numerical results. Renardy in [49] builds upon the work in [48] which found that the upper convected derivative dominates in a core region, and is zero close to the corner. With the stresses of the form (1.48) it makes sense to introduce a 'natural stress' basis where $\mathbf{v}\mathbf{v}^T$ is one of the basis functions. In numerics, transforming tensor components to a basis aligned with streamlines was previously used in numerical work by Dupont et al. [16] and Keiller [33] but not in analysis pertaining to this problem. Davies and Devlin [14] approached the analysis of this prob-

lem in a different manner, looking at series expansions of the Oldroyd-B equations but formulated in terms of an Airy stress function and a stream function. They managed to find a set of eigenfunctions with associated eigenvalue problems, following the work of Dean and Montagon [15] where a similar method was applied to simple Newtonian flow. Their work is considered later in chapter 5, but in the context of Salient corner flow. Davis and Devlin showed that there existed two types of solutions, asymptotic Newtonian flow away from the walls and other UCM-like asymptotics. Though this approach is not employed in this thesis, the solutions found alternatively can be seen by balancing differing terms in the Oldroyd-B constitutive equations. A fuller discussion on the method used in [14] can be found in [18]. The contrasting approach by Hinch and Renardy of matched asymptotics is used instead here.

Additional work by Renardy in [52] and [50], examined the boundary layers present in high Weissenberg number flow. The context was general with no specific geometry selected other than being close to solid boundaries. However, the resulting equations are similar. In high Weissenberg flow, the upper convected derivatives in the constitutive equations dominate in regions away from solid boundaries. The equations governing UCM type flow can then be reduced to the compressible Euler equations; an important class of solutions to these being generated by potential flow. Near the walls, viscometric stress behaviour is recovered in elastic boundary layers. These high Weissenberg elastic boundary layer equations are the same as the wall boundary layer equations that occur near the re-entrant corner in Weissenberg order one flows. Thus the corner stress singularity seems to invoke the high Weissenberg behaviour even when Weissenberg is order one. The high Weissenberg analysis is thus relevant to corner flow, and aspects of it will be found in chapters 2 and 3. Since the elastic stress dominates the solvent stress (which is present in Oldroyd-B formulations), the results and analysis are very similar to those obtained with UCM flow. Renardy [51] showed that the boundary layer equations were little changed via the addition of a solvent stress.

Salient corners occur for angles less than 180^o and is another situation considered here. No analytical work has been done for flows at such corners for viscoelastic fluid models such as UCM and Oldroyd-B. There is a remark by Renardy [54] that the situation should be Newtonian dominated. Newtonian flows were considered first by Dean and Montagnon [15] and their analysis then extended by Moffatt [39], where a class of separable similarity solutions were discussed.

1.7 Structure of thesis

Chapter 1 has given an introduction to rheology and discussed the derivations of the Oldroyd-B fluid as well as a literature review. The non-dimensionalised equations for the Oldroyd-B have been stated, which are the equations that we wish to investigate for re-entrant and salient corner flow. Our study of these equations begins with a preliminary analysis in chapter 2, where we classify their type and give their 2-D component formulations in Cartesian and natural stress (see Renardy [49]) form. Extensive use of both of these formulations will be made in subsequent chapters, where steady planar flow only is considered. Also given are the solutions for steady simple shear and elongational flows, which are presented for reference. Finally in this chapter the Newtonian solution is given, used in the low Weissenberg limit in chapter 4 as well as the salient corner in chapter 5.

Chapter 3 considers the re-entrant corner problem for parameter values $\mathrm{We} = 1$ and $0 < \beta < 1$. The method of matched asymptotic expansions is used to identify a three region asymptotic structure local to the corner as well as to derive equations within them. The asymptotic regions comprise an outer (core flow) region away from the walls at which there are boundary layers. Self-similar solutions are identified and used to construct solutions. The upstream and downstream boundary layer equations are solved numerically. The derivation in this chapter using an artificial small parameter (introduced through a length scaling) for the asymptotic expansions, puts the work of Hinch [30], Renardy [51] and Rallison and Hinch [47] on a firmer footing.

Chapter 4 extends the solution of chapter 3 to other parameter regimes. Specifically (i) the low and high Weissenberg limits with $\beta \in (0, 1)$ kept fixed and (ii) the limits of β approaching 0 and 1 with now We held fixed and order one. The Weissenberg limits and the Newtonian limit of $\beta \to 1^-$ are singular and the goal is to identify their asymptotic structures.

In chapter 5, the salient corner is discussed. Crucially important to the understanding of which is Newtonian flow. The chapter follows the work of Dean and Montagnon [15] and Moffatt [39]. These solutions are then matched to wall boundary layers which recover viscometric behaviour for the Oldroyd-B fluid.

Finally in chapter 6, an overview of the results is presented, as well as possible extensions and open questions posed by this work.

Chapter 2

Preliminary analysis

This chapter introduces the main formulations and some preliminary results to be used later. We begin with analysis on the classification of the Oldroyd-B equations thus investigating questions of well-posedness and uniqueness. The Cartesian and natural stress formulations will be presented along with consideration of some simple flow types. The later can aid boundary layer considerations that we encounter in later chapters.

2.1 Classification of type

The dimensionless governing equations of the Oldroyd-B model for steady incompressible planar flow may be written as

$$\nabla.\mathbf{v} = 0, \quad \text{Re } (\mathbf{v}.\nabla)\mathbf{v} = -\nabla p + \nabla.\mathbf{T}^p + \beta\nabla^2\mathbf{v}, \tag{2.1}$$

$$\mathbf{T}^p + \text{We } \overset{\triangledown}{\mathbf{T}^p} = 2(1-\beta)\mathbf{D}. \tag{2.2}$$

Rewriting in Cartesian component form, with velocity field

$$\mathbf{v} = (u(x,y), v(x,y)), \tag{2.3}$$

the momentum and constitutive equations are given by

$$\text{Re } \mathbf{v}\cdot\nabla u = -\frac{\partial p}{\partial x} + \frac{\partial T^p_{11}}{\partial x} + \frac{\partial T^p_{12}}{\partial y} + \beta\left(\frac{\partial^2 u}{\partial x^2} + \frac{\partial^2 u}{\partial y^2}\right), \tag{2.4}$$

$$\text{Re } \mathbf{v}\cdot\nabla v = -\frac{\partial p}{\partial y} + \frac{\partial T^p_{12}}{\partial x} + \frac{\partial T^p_{22}}{\partial y} + \beta\left(\frac{\partial^2 v}{\partial x^2} + \frac{\partial^2 v}{\partial y^2}\right), \tag{2.5}$$

and

$$T_{11}^p + \mathrm{We}\left(u\frac{\partial T_{11}^p}{\partial x} + v\frac{\partial T_{11}^p}{\partial y} - 2\frac{\partial u}{\partial y}T_{12}^p - 2\frac{\partial u}{\partial x}T_{11}^p\right) = 2\left(1-\beta\right)\frac{\partial u}{\partial x}, \tag{2.6}$$

$$T_{12}^p + \mathrm{We}\left(u\frac{\partial T_{12}^p}{\partial x} + v\frac{\partial T_{12}^p}{\partial y} - \frac{\partial v}{\partial x}T_{11}^p - \frac{\partial u}{\partial y}T_{22}^p\right) = \left(1-\beta\right)\left(\frac{\partial u}{\partial y} + \frac{\partial v}{\partial x}\right), \tag{2.7}$$

$$T_{22}^p + \mathrm{We}\left(u\frac{\partial T_{22}^p}{\partial x} + v\frac{\partial T_{22}^p}{\partial y} - 2\frac{\partial v}{\partial x}T_{12}^p - 2\frac{\partial v}{\partial y}T_{22}^p\right) = 2\left(1-\beta\right)\frac{\partial v}{\partial y}. \tag{2.8}$$

Classification of the Oldroyd-B model is important to gain information about the existence of solutions and well-posedness of problems. Work in this chapter follows [28] and [29], which use the methods of discontinuous derivatives and stability of short waves. More general information on the classification of PDEs can be found in [31], [54] and the reader is referred to these texts for a detailed treatment. Analysis for the UCM model has been done in [28], [29] already; extending this to the Oldroyd-B model is possible since the presence of a Laplacian operator in the momentum equations (2.1) increases the order of the system, but does not significantly change the results already obtained. Following these two papers, the idea is to calculate the symbol of the differential operator for the model, then take the determinant and determine the principal part of the resulting polynomial. This is sufficient to classify the equations. A natural extension would be to determine the characteristic variables and compatibility equations but is not presented here.

As previously said, the Laplacian operator in the momentum equations requires the analysis in [28], [29] and [32] to be extended. The constitutive models considered, such as UCM and Johnson-Segalman, do not include a solvent viscosity and thus do not have any second derivatives of the velocity field. Initially (although the system is written as a first-order system later on in this section), we leave the system as second-order, writing the governing equations in the form

$$L\mathbf{q} = \mathbf{A}_1\frac{\partial \mathbf{q}}{\partial x} + \mathbf{A}_2\frac{\partial \mathbf{q}}{\partial y} + \mathbf{B}_1\frac{\partial^2 \mathbf{q}}{\partial x^2} + \mathbf{B}_2\frac{\partial^2 \mathbf{q}}{\partial y^2} + \mathbf{S}\mathbf{q} = \mathbf{0}, \tag{2.9}$$

where L is an operator acting on a vector $\mathbf{q} = (p, u, v, T_{11}^p, T_{12}^p, T_{22}^p)^T$. We define p, u, and v to be the pressure and velocity components in the x and y Cartesian directions respectively. The stress components T_{11}^p and T_{22}^p are the normal stresses in the x and

y directions respectively, and T^p_{12} is the shear stress. The matrices in (2.9) are

$$\mathbf{A}_1 = \begin{pmatrix} 0 & 1 & 0 & 0 & 0 & 0 \\ 1 & \text{Re } u & 0 & -1 & 0 & 0 \\ 0 & 0 & \text{Re } u & 0 & -1 & 0 \\ 0 & -2\text{We } T^p_{11} - 2(1-\beta) & 0 & \text{We } u & 0 & 0 \\ 0 & 0 & -2\text{We } T^p_{12} & 0 & 0 & \text{We } u \\ 0 & 0 & -\text{We } T^p_{11} - (1-\beta) & 0 & \text{We } u & 0 \end{pmatrix},$$

$$\mathbf{A}_2 = \begin{pmatrix} 0 & 0 & 1 & 0 & 0 & 0 \\ 0 & \text{Re } v & 0 & 0 & -1 & 0 \\ 1 & 0 & \text{Re } v & 0 & 0 & -1 \\ 0 & -2\text{We } T^p_{12} & 0 & \text{We } v & 0 & 0 \\ 0 & 0 & -2\text{We } T^p_{22} - 2(1-\beta) & 0 & 0 & \text{We } v \\ 0 & -\text{We } T^p_{22} - (1-\beta) & 0 & 0 & \text{We } v & 0 \end{pmatrix},$$

$$\mathbf{S} = \begin{pmatrix} 0 & 0 & 0 & 0 & 0 & 0 \\ 0 & 0 & 0 & 0 & 0 & 0 \\ 0 & 0 & 0 & 0 & 0 & 0 \\ 0 & 0 & 0 & 1 & 0 & 0 \\ 0 & 0 & 0 & 0 & 0 & 1 \\ 0 & 0 & 0 & 0 & 1 & 0 \end{pmatrix}, \quad \mathbf{B}_1 = \mathbf{B}_2 = \beta \begin{pmatrix} 0 & 0 & 0 & 0 & 0 & 0 \\ 0 & 1 & 0 & 0 & 0 & 0 \\ 0 & 0 & 1 & 0 & 0 & 0 \\ 0 & 0 & 0 & 0 & 0 & 0 \\ 0 & 0 & 0 & 0 & 0 & 0 \\ 0 & 0 & 0 & 0 & 0 & 0 \end{pmatrix}. \tag{2.10}$$

The matrices $\mathbf{B}_1$ and $\mathbf{B}_2$ are not present in [28], which arise from the extra momentum term. The UCM model in [28] considered unsteady planar flow, where the characteristic curves depended upon time. Our equations for Oldroyd-B are written in dimensionless form and consider steady flow only simplifying the analysis. Considering the stability of short waves solutions, we can consider plane wave solutions of (2.9) propagating in the $\boldsymbol{\xi}$-direction of the form

$$\mathbf{q}(\mathbf{x}) = \mathbf{q}_0 e^{i\boldsymbol{\xi}.\mathbf{x}}, \tag{2.11}$$

where $\boldsymbol{\xi} = \xi_1 \mathbf{e}_x + \xi_2 \mathbf{e}_y$ is a wave vector, $\mathbf{e}_x$, $\mathbf{e}_y$ are the unit vectors in the x and y directions respectively, with wave numbers ξ_1 and ξ_2 and the norm $|\boldsymbol{\xi}| = \sqrt{\xi_1^2 + \xi_2^2}$.

The linear operator we have chosen to look at contains the space co-ordinates $\mathbf{x} = (x, y)$ and partial derivatives. Decomposing solutions into a linear combination of the plane waves of (2.11), we take fourier transforms so that $\frac{\partial}{\partial x} = i\xi_1$ and $\frac{\partial}{\partial y} = i\xi_2$, the

higher order derivatives follow from this. The transformation of derivatives is therefore

$$\left(\mathbf{x}, \frac{\partial}{\partial x}, \frac{\partial^2}{\partial x^2}, \frac{\partial}{\partial y}, \frac{\partial^2}{\partial y^2}\right) \rightarrow \left(\mathbf{x}, i\xi_1, -\xi_1^2, i\xi_2, -\xi_2^2\right). \tag{2.12}$$

Substituting into our governing equations (2.9) yields

$$i(\xi_1\mathbf{A}_1 + \xi_2\mathbf{A}_2)\mathbf{q}_0 + (\mathbf{S} - \xi_1^2\mathbf{B}_1 - \xi_2^2\mathbf{B}_2)\mathbf{q}_0 = \mathbf{0}, \tag{2.13}$$

which will have a non-trivial solution for $\mathbf{q}_0$ if the determinant of (2.13) is zero,

$$\det\left(\xi_1\mathbf{A}_1 + \xi_2\mathbf{A}_2 - i(\mathbf{S} - \xi_1^2\mathbf{B}_1 - \xi_2^2\mathbf{B}_2)\right) = 0. \tag{2.14}$$

Following [28], the symbol of the differential operator defined by (2.9) is the response of the system to a solution of the form (2.11). Therefore the symbol, denoted $P(\mathbf{q}, i, \boldsymbol{\xi})$ for the Oldroyd-B model is

$$P(\mathbf{q}, i, \boldsymbol{\xi}) = i(\xi_1\mathbf{A}_1 + \xi_2\mathbf{A}_2 - i(\mathbf{S} - \xi_1^2\mathbf{B}_1 - \xi_2^2\mathbf{B}_2)). \tag{2.15}$$

The requirement that $\det P(\mathbf{q}, i, \boldsymbol{\xi}) = 0$, leads to the polynomial equation

$$(\xi_1^2 + \xi_2^2)\bar{W}^2\left(\boldsymbol{\xi}^T(\mathrm{We}\ \mathbf{T}^p + \mathbf{I})\boldsymbol{\xi} - i\beta\left(\xi_1^2 + \xi_2^2\right)\left(\bar{W} - i\right) - \mathrm{Re}\left(\mathbf{v}.\boldsymbol{\xi}\right)\bar{W}\right) = 0, \tag{2.16}$$

where $\bar{W} = (\mathrm{We}\left(\mathbf{v}.\boldsymbol{\xi}\right) - i)$ has been introduced for convenience. This polynomial equation in ξ_1 and ξ_2 is analogous to the result in [28] for the UCM model - setting $\beta = 0$ the two equations are the same (allowing for the difference in notation). The principal part of this polynomial are the terms of highest degree in ξ. The principal part of $\bar{W}$ is simply $\mathrm{We}\left(\mathbf{v}.\boldsymbol{\xi}\right)$ and thus the principal part of (2.16) after some simplification is

$$-i\beta\mathrm{We}^3(\xi_1^2 + \xi_2^2)^2\left(\mathbf{v}.\boldsymbol{\xi}\right)^3. \tag{2.17}$$

The real characteristics are associated with the real zeros of this expression, i.e.

$$\left(\mathbf{v}.\boldsymbol{\xi}\right)^3 = 0, \implies \left(\mathbf{v}.\boldsymbol{\xi}\right) = 0 \quad \text{(three times)}. \tag{2.18}$$

With reference to [28], [29] and [32] we can conclude for (2.17) for the Oldroyd-B symbol:

- The factor $(\xi_1^2 + \xi_2^2)$ corresponds to the symbol of the Laplace operator. This operator appears in the governing equations twice - once from the divergence of the velocity field and pressure gradient and secondly from the solvent viscosity.

This former part associated with the velocity field is always elliptic, irrespective of whether the flow is steady or unsteady. The factor associated with the solvent viscosity however can alternatively be associated with the principle part of the vorticity equation which is parabolic for time dependent flows, but elliptic for steady flows. For time dependent flow then, the Oldroyd-B model has both a elliptic and a parabolic part from this factor. For steady flow as considered here only the elliptic part is present.

- The other factor $(\mathbf{v}.\boldsymbol{\xi})^3$ demonstrates that there are three real characteristics $(\mathbf{v}.\boldsymbol{\xi}) = 0$. As such the system always has at least three linearly independent real eigenvectors associated with this factor. This gives the system a hyperbolic character. The Oldroyd-B model transfers an extra piece of information along the streamlines of the flow compared to UCM. It is noted in [43] that the contribution to the principal part of the symbol isn't strictly hyperbolic since the multiplicity is of order three, for practical purposes however the solutions behave as if they are hyperbolic.

- For comparison, we note that the UCM principal part of the symbol contained the factor

$$\boldsymbol{\xi}^T(\mathrm{We}\ \mathbf{T}^p + \mathbf{I})\boldsymbol{\xi} - \mathrm{Re}\ \ (\mathbf{v}.\boldsymbol{\xi})^2\,,$$

  which is associated with the vorticity equation. Looking at (2.16) we see that whilst this term is retained when $\beta = 0$, is it of a lower order in $\boldsymbol{\xi}$ than the terms multiplied by β.

From this we conclude that the system of partial differential equations for the steady Oldroyd-B model is of mixed elliptic-hyperbolic type, the elliptic nature coming from the presence of the Laplacian operator in the momentum equations and the hyperbolic nature coming from finding linearly independent real eigenvectors. A natural extension to this problem would be to determine the characteristic variables and the corresponding compatibility equations. Usually, finding the characteristic variables is of vital importance to prescribing the correct boundary conditions for numerical implementation as well as discretization, see [58]. The characteristic variables tell us the information that is being transmitted along streamlines. Finding the characteristics would be an interesting problem to persue to check that the boundary conditions prescribed by them are indeed the same as found later on in chapter 3 from the method of eigenmodes in the boundary layer analysis. The reader is referred to [29] for a detailed treatment of the UCM model, where similarities to the Oldroyd-B model are expected due to it being of a similar classification type.

In [28], it is noted that the system of equations can be written as first-order by introducing the gradients of the velocity components as new variables. This would be of use if one wanted to use the method of discontinuous derivatives in order to classify the system. In the two dimensional case these are surfaces $\phi(x, y) = 0$ across which the vector $\mathbf{q}$ is continuous with bounded jumps in the first derivative. For studying the stability of short wave solutions, writing the system as first-order does not change the result. For completeness we record this system firstly by defining

$$u_x = \frac{\partial u}{\partial x}, \quad u_y = \frac{\partial u}{\partial y}, \quad v_x = \frac{\partial v}{\partial x}, \quad v_y = \frac{\partial v}{\partial y}, \tag{2.19}$$

we don't need the matrices $\mathbf{B}_1$, $\mathbf{B}_2$ in (2.9) and instead have a ten-by-ten order system. Introducing a modified $\mathbf{q}$ vector as $\hat{\mathbf{q}} = (p, T^p_{11}, T^p_{12}, T^p_{22}, u_x, u_y, v_x, v_y, u, v)^T$, where p, u, and v are again the pressure and velocity components in the x and y Cartesian directions, T^p_{11} and T^p_{22} the normal stresses in the x and y directions respectively, and T^p_{12} is the shear stress. The four extra components come from writing the velocity gradients as first order variables as above. The new matrices resulting from

$$L\hat{\mathbf{q}} = \hat{\mathbf{A}}_1 \frac{\partial \hat{\mathbf{q}}}{\partial x} + \hat{\mathbf{A}}_2 \frac{\partial \hat{\mathbf{q}}}{\partial y} + \hat{\mathbf{S}}\hat{\mathbf{q}} = \mathbf{0} \tag{2.20}$$

in (2.20) are thus

$$\hat{\mathbf{A}}_1 = \begin{pmatrix} 0 & 1 & 0 & 0 & 0 & 0 & 0 & 0 & 0 & 0 \\ 1 & -1 & 0 & 0 & \beta & 0 & 0 & 0 & 0 & 0 \\ 0 & 0 & -1 & 0 & 0 & 0 & \beta & 0 & 0 & 0 \\ 0 & \mathrm{We}\, u & 0 & 0 & 0 & 0 & 0 & 0 & 0 & 0 \\ 0 & 0 & 0 & \mathrm{We}\, u & 0 & 0 & 0 & 0 & 0 & 0 \\ 0 & 0 & \mathrm{We}\, u & 0 & 0 & 0 & 0 & 0 & 0 & 0 \\ 0 & 0 & 0 & 0 & 0 & 0 & 0 & 0 & 1 & 0 \\ 0 & 0 & 0 & 0 & 0 & 0 & 0 & 0 & 0 & 0 \\ 0 & 0 & 0 & 0 & 0 & 0 & 0 & 0 & 0 & 1 \\ 0 & 1 & 0 & 0 & 0 & 0 & 0 & 0 & 0 & 0 \end{pmatrix},$$

$$\hat{\mathbf{A}}_2 = \begin{pmatrix} 0 & 0 & 0 & 0 & 0 & 0 & 0 & 0 & 0 & 0 \\ 0 & 0 & -1 & 0 & 0 & \beta & 0 & 0 & 0 & 0 \\ 1 & 0 & 0 & -1 & 0 & 0 & 0 & \beta & 0 & 0 \\ 0 & \mathrm{We}\ v & 0 & 0 & 0 & 0 & 0 & 0 & 0 & 0 \\ 0 & 0 & 0 & \mathrm{We}\ v & 0 & 0 & 0 & 0 & 0 & 0 \\ 0 & 0 & \mathrm{We}\ v & 0 & 0 & 0 & 0 & 0 & 0 & 0 \\ 0 & 0 & 0 & 0 & 0 & 0 & 0 & 0 & 0 & 0 \\ 0 & 0 & 0 & 0 & 0 & 0 & 0 & 0 & 1 & 0 \\ 0 & 0 & 0 & 0 & 0 & 0 & 0 & 0 & 0 & 0 \\ 0 & 1 & 0 & 0 & 0 & 0 & 0 & 0 & 0 & 1 \end{pmatrix},$$

$$\hat{\mathbf{S}} = \begin{pmatrix} 0 & 0 & 0 & 0 & 1 & 0 & 0 & 1 & 0 & 0 \\ 0 & 0 & 0 & 0 & \mathrm{Re}\ u & \mathrm{Re}\ v & 0 & 0 & 0 & 0 \\ 0 & 0 & 0 & 0 & 0 & 0 & \mathrm{Re}\ u & \mathrm{Re}\ v & 0 & 0 \\ 0 & 1 & 0 & 0 & \gamma_1 & -2\mathrm{We}\ T_{12}^p & 0 & 0 & 0 & 0 \\ 0 & 0 & 0 & 1 & 0 & 0 & -\mathrm{We}\ T_{12}^p & \gamma_2 & 0 & 0 \\ 0 & 0 & 1 & 0 & 0 & \gamma_3 & \gamma_4 & 0 & 0 & 0 \\ 0 & 0 & 0 & 0 & 1 & 0 & 0 & 0 & 0 & 0 \\ 0 & 0 & 0 & 0 & 0 & 1 & 0 & 0 & 0 & 0 \\ 0 & 0 & 0 & 0 & 0 & 0 & 1 & 0 & 0 & 0 \\ 0 & 0 & 0 & 0 & 0 & 0 & 0 & 1 & 0 & 0 \end{pmatrix},$$

where we introduce

$$\begin{aligned} &\gamma_1 = -2\mathrm{We}\ T_{11}^p - 2 + 2\beta, \quad \gamma_2 = -2\mathrm{We}\ T_{22}^p - 2 + 2\beta, \\ &\gamma_3 = -\mathrm{We}\ T_{22}^p - 1 + \beta, \quad \gamma_4 = -\mathrm{We}\ T_{11}^p - 1 + \beta. \end{aligned} \tag{2.21}$$

To show that this does not differ from the second-order system, here we are determining the stability of a short wave solution to (2.20) in the form

$$\hat{\mathbf{q}}(\mathbf{x}) = \hat{\mathbf{q}}_0 e^{i\boldsymbol{\xi}.\mathbf{x}}, \tag{2.22}$$

with a modified $\hat{\mathbf{q}}_0$. This has a non trivial solution for $\hat{\mathbf{q}}_0$ if

$$\det\left(\xi_1\hat{\mathbf{A}}_1 + \xi_2\hat{\mathbf{A}}_2 - i\hat{\mathbf{S}}\right) = 0. \tag{2.23}$$

Evaluating this gives the same polynomial equation as in (2.16).

2.2 Formulations of the governing equations

After the previous section which was concerned with classifying the Oldroyd-B model, we now state the problem in two different basis. One in the Cartesian basis and another using the natural stress basis where we express the stress tensor in a basis spanned by the velocity field and its orthogonal component. Noted also is a determinant relationship that links these two differing formulations.

2.2.1 Cartesian Formulation

The governing momentum and constitutive equations for Oldroyd-B type fluids are given in (2.4)-(2.8). Since flow is two-dimensional, the velocity field $\mathbf{v}$ is given by

$$\mathbf{v} = (u, v) = \left(\frac{\partial \psi}{\partial y}, -\frac{\partial \psi}{\partial x} \right),$$

with ψ the stream function for the flow. We can write the governing equations in terms of the stream function, which for reference are

$$\mathrm{Re}\ \left(\frac{\partial \psi}{\partial y}\frac{\partial^2 \psi}{\partial x \partial y} - \frac{\partial \psi}{\partial x}\frac{\partial^2 \psi}{\partial y^2} \right) = -\frac{\partial p}{\partial x} + \frac{\partial T^p_{11}}{\partial x} + \frac{\partial T^p_{12}}{\partial y} + \beta \left(\frac{\partial^3 \psi}{\partial x^2 \partial y} + \frac{\partial^3 \psi}{\partial y^3} \right), \tag{2.24}$$

$$\mathrm{Re}\ \left(-\frac{\partial \psi}{\partial y}\frac{\partial^2 \psi}{\partial x^2} + \frac{\partial \psi}{\partial x}\frac{\partial^2 \psi}{\partial x \partial y} \right) = -\frac{\partial p}{\partial y} + \frac{\partial T^p_{12}}{\partial x} + \frac{\partial T^p_{22}}{\partial y} + \beta \left(\frac{\partial^3 \psi}{\partial x^3} + \frac{\partial^3 \psi}{\partial x \partial y^2} \right), \tag{2.25}$$

and

$$T^p_{11} + \mathrm{We} \left(\frac{\partial \psi}{\partial y}\frac{\partial T^p_{11}}{\partial x} - \frac{\partial \psi}{\partial x}\frac{\partial T^p_{11}}{\partial y} - 2\frac{\partial^2 \psi}{\partial y^2} T^p_{12} - 2\frac{\partial^2 \psi}{\partial x \partial y} T^p_{11} \right) = 2\left(1-\beta\right)\frac{\partial^2 \psi}{\partial x \partial y}, \tag{2.26}$$

$$T^p_{12} + \mathrm{We} \left(\frac{\partial \psi}{\partial y}\frac{\partial T^p_{12}}{\partial x} - \frac{\partial \psi}{\partial x}\frac{\partial T^p_{12}}{\partial y} + \frac{\partial \psi}{\partial x^2} T^p_{11} - \frac{\partial^2 \psi}{\partial y^2} T^p_{22} \right) = (1-\beta)\left(\frac{\partial^2 \psi}{\partial y^2} - \frac{\partial^2 \psi}{\partial x^2} \right), \tag{2.27}$$

$$T^p_{22} + \mathrm{We} \left(\frac{\partial \psi}{\partial y}\frac{\partial T^p_{22}}{\partial x} - \frac{\partial \psi}{\partial x}\frac{\partial T^p_{22}}{\partial y} + 2\frac{\partial^2 \psi}{\partial x^2} T^p_{12} + 2\frac{\partial^2 \psi}{\partial x \partial y} T^p_{22} \right) = -2\left(1-\beta\right)\frac{\partial^2 \psi}{\partial x \partial y}. \tag{2.28}$$

This is a system of 5 coupled, non-linear, partial differential equations. The polymer stress tensor $\mathbf{T}^p$ satisfies the following relation found by Renardy in [50] for the UCM constitutive model

$$(\mathbf{v} \cdot \nabla)(\det(\mathrm{We}\mathbf{T}^p + \mathbf{I})) = -(\det(\mathrm{We}\mathbf{T}^p + \mathbf{I}))\mathrm{tr}\left((\mathrm{We}\mathbf{T}^p + \mathbf{I})^{-1}\mathbf{T}^p \right), \tag{2.29}$$

or alternatively

$$(\mathbf{v}\cdot\nabla)(\det(\mathrm{We}\mathbf{T}^p+\mathbf{I}))=-2(\det(\mathrm{We}\mathbf{T}^p+\mathbf{I}))+\mathrm{tr}(\mathrm{We}\mathbf{T}^p+\mathbf{I})). \tag{2.30}$$

For Oldroyd-B type fluids the analysis is similar, but here we relate the slightly modified determinant, $\det(\mathrm{We}\mathbf{T}^p+\mathbf{I}(1-\beta))$ with the stream function ψ. To this end, we can write the symmetric matrix $\mathrm{We}\mathbf{T}^p+\mathbf{I}(1-\beta))$ given by

$$\begin{pmatrix} \mathrm{We}T^p_{11}+(1-\beta) & \mathrm{We}T^p_{12} \\ \mathrm{We}T^p_{12} & \mathrm{We}T^p_{22}+(1-\beta) \end{pmatrix},$$

so the expressions $\det(\mathrm{We}\mathbf{T}^p+\mathbf{I}(1-\beta))$ and $\mathrm{tr}(\mathbf{T}^p+\mathbf{I}(1-\beta))$ are

$$\det(\mathrm{We}\mathbf{T}^p+\mathbf{I}(1-\beta))=(\mathrm{We}T^p_{11}+(1-\beta))(\mathrm{We}T^p_{22}+(1-\beta))-(\mathrm{We}T^p_{12})^2, \tag{2.31}$$

$$\mathrm{tr}(\mathrm{We}\mathbf{T}^p+\mathbf{I}(1-\beta))=\mathrm{We}T^p_{11}+\mathrm{We}T^p_{22}+2(1-\beta). \tag{2.32}$$

Rearranging the constitutive model (2.2), writing out the upper convected derivative and expressing $\mathbf{D}$ in terms of velocity components gives us

$$\mathrm{We}\,(\mathbf{v}\cdot\nabla)\,\mathbf{T}^p=(\nabla\mathbf{v})(\mathrm{We}\mathbf{T}^p+\mathbf{I}(1-\beta))+(\mathrm{We}\mathbf{T}^p+\mathbf{I}(1-\beta))(\nabla\mathbf{v})^T-\mathbf{T}^p. \tag{2.33}$$

In component form using the incompressibility condition $(u_x+v_y)=0$ (the subscripts x, y mean differentiation with respect to x and y as usual) where needed, (2.33) can be written as

$$\mathrm{We}(\mathbf{v}\cdot\nabla)T^p_{11}=2u_x\,(\mathrm{We}T^p_{11}+(1-\beta))+2\mathrm{We}u_yT^p_{12}-T^p_{11}, \tag{2.34}$$

$$\mathrm{We}(\mathbf{v}\cdot\nabla)T^p_{12}=v_x\,(\mathrm{We}T^p_{11}+(1-\beta))+u_y\,(\mathrm{We}T^p_{22}+(1-\beta))-T^p_{12}, \tag{2.35}$$

$$\mathrm{We}(\mathbf{v}\cdot\nabla)T^p_{22}=2v_y\,(\mathrm{We}T^p_{22}+(1-\beta))+2\mathrm{We}v_xT^p_{12}-T^p_{22}. \tag{2.36}$$

Using (2.34)-(2.36) along with the expressions for the determinant and the trace gives after rearranging

$$(\mathbf{v}\cdot\nabla)\det(\mathrm{We}\mathbf{T}^p+\mathbf{I}(1-\beta))=\mathbf{v}\cdot\nabla\left(\mathrm{We}(T^p_{11}+(1-\beta))(\mathrm{We}T^p_{22}+(1-\beta))-(\,\mathrm{We}T^p_{12}\,)^2\right) \tag{2.37}$$

$$=-2\det(\mathrm{We}\mathbf{T}^p+\mathbf{I}(1-\beta))+(1-\beta)\mathrm{tr}(\mathrm{We}\mathbf{T}^p+\mathbf{I}(1-\beta)), \tag{2.38}$$

which recovers (2.30) when $\beta=0$.

2.2.2 The natural stress basis formulation

For UCM and Oldroyd-B type fluids, it is well known that integrating the stresses close to a corner presents a serious numerical challenge. One of the first attempts to resolve this was by Dapont, Marchel and Crochet in [16] who used a curvilinear co-ordinate system to calculate stresses along streamlines by a finite-element method. This idea was extended by Keiller, [33] when investigating the efficacy of numerical techniques for flow around a corner. It was known at the time that simple explicit integration schemes produced poor stress approximations near curved boundaries - with this problem being particularly acute for Oldroyd-B fluids due to large normal stresses in shear flow. By aligning the polymer stress tensor $\mathbf{T}^p$ with the streamlines, the components of $\mathbf{T}^p$ and the velocity field are rotated and stretched with exactly the same deformations. This solved the previous problem of the rotational component of the velocity field being over-estimated for high Weissenberg flow.

Renardy in [49] used this information to motivate aligning the stress tensor along streamlines. Since the stresses act like $\mathbf{v}\mathbf{v}^T$, it is used as one of the basis functions in a natural stress formulation. The way to do this is to express the stress tensor with respect to a natural stress basis spanned by the velocity field and its orthogonal component. Specifically, by introducing the vector

$$\mathbf{w} = \left(-\frac{v}{u^2+v^2}, \frac{u}{u^2+v^2} \right), \tag{2.39}$$

orthogonal to $\mathbf{v} = (u, v)$ and satisfying $|\mathbf{v} \times \mathbf{w}| = 1$. Then $\mathbf{T}^p$ can be represented in a basis formed with the dyadic (or outer) products of $\mathbf{v}$ and $\mathbf{w}$ as

$$\mathbf{T}^p = \frac{-(1-\beta)}{\mathrm{We}}\mathbf{I} + \lambda\mathbf{v}\mathbf{v}^T + \mu(\mathbf{v}\mathbf{w}^T + \mathbf{w}\mathbf{v}^T) + \nu\mathbf{w}\mathbf{w}^T, \tag{2.40}$$

for variables λ, μ and ν. Written in component form, the Cartesian and natural stress basis are related through

$$T^p_{11} = \frac{-(1-\beta)}{\mathrm{We}} + \lambda u^2 - \frac{2\mu uv}{u^2+v^2} + \frac{\nu v^2}{(u^2+v^2)^2}, \tag{2.41}$$

$$T^p_{12} = \lambda uv + \frac{\mu(u^2-v^2)}{u^2+v^2} - \frac{\nu uv}{(u^2+v^2)^2}, \tag{2.42}$$

$$T^p_{22} = \frac{-(1-\beta)}{\mathrm{We}} + \lambda v^2 + \frac{2\mu uv}{u^2+v^2} + \frac{\nu u^2}{(u^2+v^2)^2}. \tag{2.43}$$

The variables $\lambda(x, y)$, $\mu(x, y)$ and $\nu(x, y)$ are aligned along streamlines and are termed the natural stress variables: λ the normal stress along a streamline, ν perpendicular

normal stress and μ represents a shear stress. The transformation from natural stress to Cartesian variables are recorded as well as

$$\lambda = (1-\beta)\frac{1}{\mathrm{We}\,(u^2+v^2)} + \frac{u^2}{(u^2+v^2)^2}T_{11}^p + \frac{2uv}{(u^2+v^2)^2}T_{12}^p + \frac{v^2}{(u^2+v^2)^2}T_{22}^p, \quad (2.44)$$

$$\mu = -\frac{uv}{(u^2+v^2)}T_{11}^p + \frac{uv}{(u^2+v^2)}T_{22}^p + \frac{(u^2-v^2)}{(u^2+v^2)}T_{12}^p, \quad (2.45)$$

$$\nu = \frac{(1-\beta)}{\mathrm{We}}(u^2+v^2) + u^2T_{22}^p + v^2T_{11}^p - 2uvT_{12}^p. \quad (2.46)$$

The vectors $\mathbf{v}$ and $\mathbf{w}$ are given in figure (2-1). We can now transform the momentum

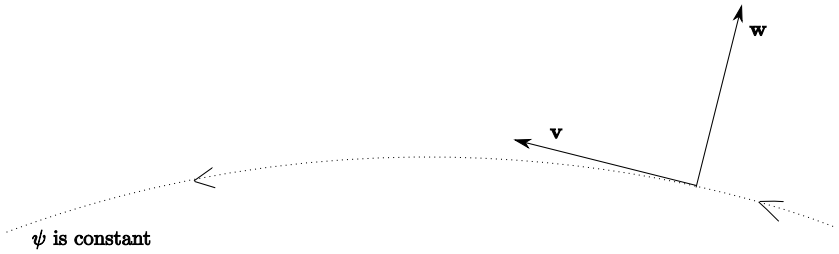

Figure 2-1: A representation of the velocity field $\mathbf{v}$ and vector $\mathbf{w}$ along a typical streamline, where $\mathbf{v} \perp \mathbf{w}$.

equations into the natural stress variables using the above relations (2.26)- (2.28),

$$\mathrm{Re}\ \ (\mathbf{v}\cdot\nabla u) = -\frac{\partial p}{\partial x} + \mathbf{v}\cdot\nabla(\lambda u) + \nabla\cdot\left(\mu u\mathbf{w} - (\mu\mathbf{v}+\nu\mathbf{w})\frac{v}{u^2+v^2}\right) + \beta\left(\frac{\partial^3\psi}{\partial x^2\partial y} + \frac{\partial^3\psi}{\partial y^3}\right), \quad (2.47)$$

$$\mathrm{Re}\ \ (\mathbf{v}\cdot\nabla v) = -\frac{\partial p}{\partial y} + \mathbf{v}\cdot\nabla(\lambda v) + \nabla\cdot\left(\mu u\mathbf{w} - (\mu\mathbf{v}+\nu\mathbf{w})\frac{u}{u^2+v^2}\right) + \beta\left(\frac{\partial^3\psi}{\partial x^3} + \frac{\partial^3\psi}{\partial x\partial y^2}\right) \quad (2.48)$$

and the constitutive equations from (2.26)- (2.28),

$$\lambda + \mathrm{We}\,(\mathbf{v}\cdot\nabla\lambda + 2\mu\nabla\cdot\mathbf{w}) = \frac{(1-\beta)}{\mathrm{We}\,(u^2+v^2)}, \quad (2.49)$$

$$\mu + \mathrm{We}\,(\mathbf{v}\cdot\nabla\mu + \nu\nabla\cdot\mathbf{w}) = 0, \quad (2.50)$$

$$\nu + \mathrm{We}\,(\mathbf{v}\cdot\nabla\nu) = \frac{(1-\beta)}{\mathrm{We}}(u^2+v^2). \quad (2.51)$$

The divergence of $\mathbf{w}$ here is

$$\nabla \cdot \mathbf{w} = \frac{1}{(u^2+v^2)^2}\left((v^2-u^2)\left(\frac{\partial v}{\partial x}+\frac{\partial u}{\partial y}\right)+4uv\frac{\partial u}{\partial x}\right).$$

It is noteworthy the significant decoupling that has taken place in the constitutive equations, although the momentum equations are now more complicated.

2.3 Simple flow types

Finally, this section investigates simple flow types - namely simple shear or viscometric flow and steady elongational flows. From these, we can deduce what terms are important as solid boundaries are approached. This gives us useful information on terms to be retained in the boundary layer equations. The second flow type discussed is steady elongational flows which highlights some limitations of the Oldroyd-B model.

2.3.1 Simple Shear Flow

There are several flows that can be considered for viscoelastic fluids that illustrate properties of the Oldroyd-B fluid as well as its limitations as a constitutive model. The first one is steady simple shear flow which introduces the rheological notion of viscosity. The viscosity can be defined as the ratio between the shear stress and shear rate in a simple shear flow. For a Newtonian flow this is constant - one of the defining features of this type of flow. For non-Newtonian flows, this ratio might vary with the shear rate, shear-thinning behaviour being one example of this phenomena. Indeed, for flows considered in this thesis, viscosity refers to shear-rate dependent viscosity. Renardy in [54] discusses steady simple shear flow for the UCM, PTT, Giesekus and Johnson-Segalman constitutive models. Results are given here for Oldroyd-B fluids and references given to the other non-Newtonian models where appropriate. For steady simple shear flow, the flow is two-dimensional with the velocity uni-directional along the x-axis only: $\mathbf{v} = (\dot{\gamma}y, 0, 0)$ where $\dot{\gamma}$ is a constant shear rate. The velocity gradient is the matrix

$$\begin{pmatrix} 0 & \dot{\gamma} & 0 \\ 0 & 0 & 0 \\ 0 & 0 & 0 \end{pmatrix} \tag{2.52}$$

and the stream function takes the form

$$\psi = \frac{1}{2}\dot{\gamma} y^2. \tag{2.53}$$

Moreover, the total extra stress tensor takes the form

$$\begin{pmatrix} T_{11} & T_{12} & 0 \\ T_{12} & T_{22} & 0 \\ 0 & 0 & T_{33} \end{pmatrix}, \tag{2.54}$$

where invariance under rotations fixes $T_{13} = T_{23} = 0$. Substituting the stream function form (2.53) into the constitutive equations (2.26)-(2.28) gives

$$\begin{aligned} &T^p_{11} + \mathrm{We}\left(-2\frac{\partial^2\Psi}{\partial y^2}T^p_{12}\right) = 0, \\ &T^p_{12} + \mathrm{We}\left(-\frac{\partial\Psi}{\partial y^2}T^p_{22}\right) = (1-\beta)\,\frac{\partial^2\Psi}{\partial y^2}, \\ &T^p_{22} = 0, \end{aligned} \tag{2.55}$$

which simplifies to

$$T^p_{11} = 2(1-\beta)\dot{\gamma}^2, \quad T^p_{12} = (1-\beta)\,\dot{\gamma}, \quad T^p_{22} = 0.$$

Further, we have that $T^p_{33} = 0$. Here we have found that there are contributions from the terms $\mathbf{T}^p$, $\overset{\triangledown}{\mathbf{T}}^p$ and $\mathbf{D}$. This indicates that these terms (or at least the corresponding components within them as shown in (2.55)) need to be retained in any boundary layer analysis. In other words, when considering viscometric behaviour at the wall as a boundary condition imposed on the system, the leading order behaviour described by the above equations will be required. Non-Newtonian flows with varying viscosities will have non-zero first and second normal stress differences, denoted N_1 and N_2 respectively

$$N_1 = T_{11} - T_{22}, \quad N_2 = T_{22} - T_{33}. \tag{2.56}$$

These, together with the viscosity function $\eta = T_{12}/\dot{\gamma}$ define three viscometric functions involving the total extra stress $\mathbf{T} = \mathbf{T}^p + \mathbf{T}^s$. For Oldroyd-B, we have

$$T_{11} = 2(1-\beta)\dot{\gamma}^2, \quad T_{22} = 0, \quad T_{33} = 0, \quad T_{12} = \dot{\gamma},$$

where $T_{12}^s = \beta\dot{\gamma}$ is the only non-zero component of the solvent extra stress. We can calculate the first and second normal stress differences from (2.56) to be

$$N_1 = 2\dot{\gamma}^2(1-\beta), \quad N_2 = 0, \tag{2.57}$$

whilst the viscosity function (dimensionless) here is a constant 1. The first normal stress difference tends to zero in the Newtonian limit $\beta \to 1$ as expected. Thus Oldroyd-B has a first normal stress difference that varies quadratically with the shear rate, whilst exhibiting a constant viscosity. As such it may be used to represent Boger fluids that exhibit this type of behaviour. However, in some fluids it is found as $\dot{\gamma}$ increases, η decreases which is so called 'shear thinning'. Also, N_1 may grow quadratically at low shear rates but then more slowly as $\dot{\gamma}$ increases further. This is not captured by Oldroyd-B and requires a more complicated non-Newtonian model such as PTT. Further, having a zero second normal stress difference isn't always found in some fluids which again can be picked up by the Johnson-Segalman model for example.

2.3.2 Steady Elongational Flows

Elongational flows are shear-free flows that have zero off diagonal components in the rate of strain and stress tensors. The diagonal components are called normal stresses since the component stresses act perpendicularly to a surface. The off diagonal components are called the 'shear components'. We can distinguish three types of elongational flows as follows

$$\text{Uniaxial elongational flow}\ , \quad \mathbf{v} = (\dot{\epsilon}x, -\dot{\epsilon}y/2, -\dot{\epsilon}z/2)\,, \tag{2.58}$$

$$\text{Planar elongational flow}\ , \quad \mathbf{v} = (\dot{\epsilon}x, -\dot{\epsilon}y, 0)\,, \tag{2.59}$$

$$\text{Biaxial stretching flow}\ , \quad \mathbf{v} = (-\dot{\epsilon}x, \dot{\epsilon}y/2, \dot{\epsilon}z/2)\,. \tag{2.60}$$

The function $\dot{\epsilon}$ is called the elongational rate, usually a function of time but for steady flow is a constant.

Planar flow has no stretching in the z direction (and we can think of it as stretching a rectangle out).

Bi-axial flow has the same velocity profile form as for uniaxial, but $\dot{\epsilon}$ has the opposite sign here. Examples of geometries that can produce bi-axial flow include film inflation and lubricated squeeze film where a lubricant is squeezed between two opposing plates.

For uniaxial flow $\dot{\epsilon}$ is positive and has strong stretching in the x direction with weaker contraction occuring in the y and z directions. This type of flow can be induced in filament stretching geometries found in ink printer rheology, or opposed-nozzle suc-

tion devices. uniaxial flow is more complicated than shear flow since the velocity components are non zero in all directions at points not on the co-ordinate axes. This contrasts with simple shear flow being uni-directional in the x direction only. All three velocity components are position dependent even for steady flows. The velocity gradient for this flow type is

$$\begin{pmatrix} \dot{\epsilon} & 0 & 0 \\ 0 & -\dot{\epsilon}/2 & 0 \\ 0 & 0 & -\dot{\epsilon}/2 \end{pmatrix}. \tag{2.61}$$

From the constitutive equations we can determine the polymer stress components to be

$$T^p_{11} = \frac{2(1-\beta)}{1-2\mathrm{We}\ \dot{\epsilon}}, \quad T^p_{12} = 0, \quad T^p_{22} = \frac{-(1-\beta)}{1+\mathrm{We}\ \dot{\epsilon}}. \tag{2.62}$$

The quantity $T^p_{11} - T^p_{22}$ is therefore

$$T^p_{11} - T^p_{22} = \frac{3(1-\beta)\dot{\epsilon}}{(1-2\mathrm{We}\ \dot{\epsilon})\,(1+\mathrm{We}\ \dot{\epsilon})}. \tag{2.63}$$

The extensional viscosity diverges at a strain rate of $\dot{\epsilon} = 1/(2\mathrm{We})$, and for strain rates slightly larger than this value, the viscosity value is negative. This consequence that we can have negative viscosities is unphysical. This is due to the fact that the Oldroyd-B model is derived from Hooke's Law springs which are infinitely extensible. Linear springs are fine for shear flows with moderate stretching. For strongly stretching flows however, a linear spring can stretch indefinitely hence giving infinite forces. This motivates the derivation of a model which has finitely extensible springs, termed the FENE model discussed in the introduction.

A further issue is that at specific elongation rates $\dot{\epsilon} = 1/(2\mathrm{We})$ the elongation viscosity is infinite. This is a well known problem with the Oldroyd-B model and thus is ill-suited to modelling fluids with steady elongational flows and large elongation rates. Polymeric fluids do show an increase in elongational viscosity with elongation rate, however the rate of increase can range from one order of magnitude to several. The prediction of a limiting elongational rate where the elongational viscosity becomes infinite can be reasonable for some fluids but not all. For reference, we determine the stresses and $T^p_{11} - T^p_{22}$ for the remaining two elongational flow types. For planar extension, we have

$$T^p_{11} = \frac{2(1-\beta)}{1-2\mathrm{We}\ \dot{\epsilon}}, \quad T^p_{12} = 0, \quad T^p_{22} = \frac{-2(1-\beta)}{1+2\mathrm{We}\ \dot{\epsilon}}, \tag{2.64}$$

with the quantity $T_{11}^p - T_{22}^p$

$$T_{11}^p - T_{22}^p = \frac{4(1-\beta)\dot{\epsilon}}{(1-2\text{We}\ \dot{\epsilon})\,(1+2\text{We}\ \dot{\epsilon})}. \tag{2.65}$$

Finally for biaxial extension,

$$T_{11}^p = \frac{-2(1-\beta)}{1+2\text{We}\ \dot{\epsilon}}, \quad T_{12}^p = 0, \quad T_{22}^p = \frac{(1-\beta)}{1-\text{We}\ \dot{\epsilon}}, \tag{2.66}$$

where

$$T_{11}^p - T_{22}^p = \frac{-3(1-\beta)\dot{\epsilon}}{(1+2\text{We}\ \dot{\epsilon})\,(1-\text{We}\ \dot{\epsilon})}. \tag{2.67}$$

Finding the elongational and shear viscosities are important in industry, especially chemical engineering, where a certain type of flow can be induced by a rheometer. The flows mentioned here are idealised flows so can only be approximated by certain geometries.

2.4 Newtonian corner flow

Early work was done by Dean and Montagnon [15] and extended by Moffat [39] to cover more situations, including flows in which eddies are present. The equations for Newtonian flow are

$$\nabla \cdot \mathbf{v} = 0, \quad \text{Re}\,(\mathbf{v} \cdot \nabla \mathbf{v}) = -\nabla p + \nabla \cdot \mathbf{T}, \quad \mathbf{T} = \mathbf{T}^s = 2\mathbf{D}, \tag{2.68}$$

where $\mathbf{T}$ is the total extra stress and $\mathbf{T}^s$ the solvent extra stress, these stresses being the same for Newtonian flow. Separable solutions for the stream function are known to exist in the form

$$\psi = c_0 r^{1+\lambda_0} f_0(\theta), \tag{2.69}$$

where c_0 is a constant, r the radius away from the corner $r \ll 1$ and λ_0 the eigenvalue which can be real or complex. The function f_0 is to be determined. Examining the relative sizes of the terms in the momentum and constitutive equations in terms of r from the stream function behaviour, we can deduce

$$\begin{aligned} &\psi = O(r^{1+\lambda_0}), \quad \mathbf{v} = O(r^{\lambda_0}), \quad (\mathbf{v} \cdot \nabla \mathbf{v}) = O(r^{2\lambda_0 - 1}), \quad \mathbf{D} = O(r^{\lambda_0 - 1}), \\ &\mathbf{T} = O(r^{\lambda_0 - 1}), \quad \nabla^2 \mathbf{v} = O(r^{\lambda_0 - 2}), \quad \nabla p = O(r^{\lambda_0 - 2}), \end{aligned}$$

where the scaling for p is chosen to retain it at leading order in the momentum equation. In the limit as $r \to 0$, the leading order momentum equation is

$$0 = -\nabla p + \nabla \cdot \mathbf{T}. \tag{2.70}$$

It is assumed that the stream function tends to zero as the corner is approached, hence $1 + \lambda_0 > 0$. The inertial terms in (2.70) are therefore subdominant. We can use the solution form for ψ from (2.69) here, the set of two simultaneous equations obtained reduce down, after eliminating p, to the bi-harmonic equation (the Laplacian is given in polar coordinates for reference)

$$\nabla^4 \psi = 0, \quad \nabla^2 = \frac{\partial^2}{\partial r^2} + \frac{1}{r}\frac{\partial}{\partial r} + \frac{1}{r^2}\frac{\partial^2}{\partial \theta^2}. \tag{2.71}$$

Substituting the stream function behaviour (2.69) into (2.71) gives a fourth-order linear differential equation for f_0 as

$$f_0'''' + 2(\lambda_0^2 + 1) f_0'' + (\lambda_0^2 - 1)^2 f_0 = 0, \tag{2.72}$$

where the $'$ denotes differentiation with respect to θ. We have no slip and no normal velocity boundary conditions at the wall

$$f_0(0) = f_0'(0) = f_0\left(\frac{\pi}{\alpha}\right) = f_0'\left(\frac{\pi}{\alpha}\right) = 0. \tag{2.73}$$

The general solution form for $f_0(\theta)$ is given in [15] as

$$f_0(\theta) = A\cos\left((\lambda_0 + 1)\,\theta\right) + B\sin\left((\lambda_0 + 1)\,\theta\right) + C\cos\left((\lambda_0 - 1)\,\theta\right) + D\sin\left((\lambda_0 - 1)\,\theta\right), \tag{2.74}$$

involving four arbitrary constants A, B, C, D. This formulation can be helpful when examining symmetric and anti-symmetric flow. Moffat gives the example of anti-symmetric flow between rigid boundaries (equivalent to the flow being considered here), where $f_0(\theta)$ is even about $\theta = \pi/2\alpha$. For flow between a rigid boundary and a free surface $f_0(\theta)$ is odd about $\theta = \pi/2\alpha$. For the former flow type then, using that the solution is required to be symmetric with respect to $\theta - \frac{\pi}{2\alpha}$, we have

$$f_0(\theta) = A\cos\left((\lambda_0 + 1)\left(\theta - \frac{\pi}{2\alpha}\right)\right) + C\cos\left((\lambda_0 - 1)\left(\theta - \frac{\pi}{2\alpha}\right)\right). \tag{2.75}$$

Applying the boundary conditions (2.73) to (2.75) gives two simultaneous equations to solve as

$$C\cos\left((\lambda_0-1)\frac{\pi}{2\alpha}\right)+A\cos\left((\lambda_0+1)\frac{\pi}{2\alpha}\right)=0, \tag{2.76}$$

$$C(\lambda_0-1)\sin\left((\lambda_0-1)\frac{\pi}{2\alpha}\right)+A(\lambda_0+1)\sin\left((\lambda_0+1)\frac{\pi}{2\alpha}\right)=0. \tag{2.77}$$

Combining these two equations gives a transcendental equation for λ_0 as

$$\sin\left(\frac{\lambda_0\pi}{\alpha}\right)=-\lambda_0\sin\left(\frac{\pi}{\alpha}\right). \tag{2.78}$$

We can determine A in terms of C from (2.76) thus eliminating one of the constants. The function $f_0(\theta)$ can then be written as

$$f_0(\theta)=C\cos\left((\lambda_0-1)\frac{\pi}{2\alpha}\right)\left[\frac{\cos\left((\lambda_0-1)\left(\theta-\frac{\pi}{2\alpha}\right)\right)}{\cos\left((\lambda_0-1)\frac{\pi}{2\alpha}\right)}-\frac{\cos\left((\lambda_0+1)\left(\theta-\frac{\pi}{2\alpha}\right)\right)}{\cos\left((\lambda_0+1)\frac{\pi}{2\alpha}\right)}\right]. \tag{2.79}$$

Taking the derivative of (2.79) twice with respect to θ evaluated at $\theta=0$ gives

$$f_0''(0)=4\lambda_0 C\cos\left((\lambda_0-1)\frac{\pi}{2\alpha}\right). \tag{2.80}$$

Solving for C, we can alternatively write (2.79) as

$$f_0(\theta)=\frac{f_0''(0)}{4\lambda_0}\left[\frac{\cos\left((\lambda_0-1)\left(\theta-\frac{\pi}{2\alpha}\right)\right)}{\cos\left((\lambda_0-1)\frac{\pi}{2\alpha}\right)}-\frac{\cos\left((\lambda_0+1)\left(\theta-\frac{\pi}{2\alpha}\right)\right)}{\cos\left((\lambda_0+1)\frac{\pi}{2\alpha}\right)}\right]. \tag{2.81}$$

Without loss of generality, we take $f_0''(0)=2$. For a given α, we can solve (2.78) numerically for λ_0. The pressure can then be determined from (2.70) given the stream function (using $v_r=\frac{1}{r}\psi_\theta$, $v_\theta=-\psi_r$ and the Laplacian in polar co-ordinates) in component form as

$$\frac{\partial p}{\partial r}=\frac{1}{r^2}\frac{\partial^2\psi}{\partial r\partial\theta}+\frac{1}{r}\frac{\partial^3\psi}{\partial r^2\partial\theta}+\frac{1}{r^3}\frac{\partial^3\psi}{\partial\theta^3}, \tag{2.82}$$

$$\frac{\partial p}{\partial\theta}=-r\frac{\partial^3\psi}{\partial r^3}-\frac{\partial^2\psi}{\partial r^2}-\frac{1}{r}\frac{\partial^3\psi}{\partial r\partial\theta^2}+\frac{1}{r}\frac{\partial\psi}{\partial r}+\frac{2}{r^2}\frac{\partial^2\psi}{\partial\theta^2}. \tag{2.83}$$

Substituting the behaviour for ψ from (2.69), we can write the pressure as

$$\frac{\partial p}{\partial r} = c_0 r^{\lambda_0 - 2}\big(f_0''' + (1+\lambda_0^2)^2 f_0'\big) \tag{2.84}$$

$$\frac{\partial p}{\partial \theta} = -c_0(\lambda_0 - 1) r^{\lambda_0 - 1}\big(f_0'' + (1+\lambda_0^2)^2 f_0\big). \tag{2.85}$$

Hence, p can be determined as

$$p = \frac{c_0}{(\lambda_0 - 1)} r^{\lambda_0 - 1}\left(f_0''' + (1+\lambda_0^2)^2 f_0'\right), \tag{2.86}$$

to within an arbitrary additive constant. The stress components in polar co-ordinates are

$$T_{rr} = \frac{\partial v_r}{\partial r} = 2c_0\lambda_0 r^{\lambda_0 - 1} f_0', \tag{2.87}$$

$$T_{r\theta} = \frac{\partial v_\theta}{\partial r} + \frac{1}{r}\frac{\partial v_r}{\partial \theta} - \frac{v_\theta}{r} = c_0 r^{\lambda_0 - 1}\big(f_0'' - (1-\lambda_0^2)^2 f_0\big), \tag{2.88}$$

$$T_{\theta\theta} = 2\frac{v_r}{r} + \frac{1}{r}\frac{\partial v_\theta}{\partial \theta} = -2c_0\lambda r^{\lambda_0 - 1} f_0'. \tag{2.89}$$

The equation (2.78) is transcendental and must be solved numerically. As noted in [15], for re-entrant corners and large enough salient corner angles (i.e. between 146.3° and 180°), the solution(s) to (2.78) are real and may be found by simply looking for the smallest positive root λ_0. For corner angles smaller than 146.3° the roots of (2.78) are complex and require further analysis. To start this we follow [39] in writing the root λ_0 as

$$\lambda_0 = x_0 + iy_0, \tag{2.90}$$

where x_0 is the real part and iy_0 the imaginary part. Substituting into (2.78) gives two equations (for the two unknowns x_0, y_0)

$$\sin\left(\frac{x_0\pi}{\alpha}\right)\cosh\left(\frac{y_0\pi}{\alpha}\right) = -x_0 \sin\left(\frac{\pi}{\alpha}\right) \tag{2.91}$$

$$\cos\left(\frac{x_0\pi}{\alpha}\right)\sinh\left(\frac{y_0\pi}{\alpha}\right) = -y_0 \sin\left(\frac{\pi}{\alpha}\right), \tag{2.92}$$

where the aim is to find (x_0, y_0). Since there are generally multiple solutions for this problem, the stream function can be expanded in a series

$$\psi = \sum_{n=0}^{\infty} c_n r^{1+\lambda_n} f_n(\theta), \tag{2.93}$$

where each $f_n(\theta)$ in (2.93) is dependant upon the value of λ_n. The roots are arranged by convention such that

$$0 < \mathrm{Re}(\lambda_0) < \mathrm{Re}(\lambda_1) < \cdots , \tag{2.94}$$

where the first inequality ensures that the velocity vanishes at the wall. Close to the corner where $r \to 0$, the first term in (2.93) dominates. For real eigenvalues, this is the natural way of picking the correct eigenvalue, for complex roots it is assumed by [15] that only the real part x_0 is relevant. The argument follows that the complex exponent in (2.90) corresponds to eddies found near the corner for sharp salient corner angles. This is found by using (2.69) with (2.75) and determining the transverse velocity component on $\theta = 0$. This component is found to change sign infinitely often as $r \to 0$ thus implying the existence of eddies in this limit. The geometry considered in the next section is only relevant then for real solutions to λ_0, i.e. for corner angles greater than 146.3° (for more acute corner angles λ_0 becomes complex). Figure 2-2 shows a sketch of the streamlines for where the corner angles $\theta < 146.3°$. In order to find (x_0, y_0) then, we can do this by trying to minimise the function

$$\left| \sin\left(\frac{x_0\pi}{\alpha}\right) \cosh\left(\frac{y_0\pi}{\alpha}\right) + x_0 \sin\left(\frac{\pi}{\alpha}\right) \right| + \left| \cos\left(\frac{x_0\pi}{\alpha}\right) \sinh\left(\frac{y_0\pi}{\alpha}\right) + y_0 \sin\left(\frac{\pi}{\alpha}\right) \right|. \tag{2.95}$$

For an initial guess, we can choose a large corner angle value of $\alpha = \frac{1}{2}$. Then in (2.78), we get $\sin(2\lambda_0\pi) = 0$, suggesting the smallest positive root is $\lambda_0 = 1/2$. Figure (2-3) shows the value of λ_0 for a range of α, where $1/2 \leq \lambda_0 < 1$ is taken for re-entrant corners and $\mathrm{Re}(\lambda_0) > 1$ for salient corners. We now record the limiting behaviour at the wall. No boundary layers are needed in the Newtonian case because all boundary conditions are satisfied. In the limit then as $\theta \to 0$ we determine f_0, f_0' and the pressure to be

$$f_0 \sim \theta^2, \quad f_0' \sim 2\theta \quad \text{and} \quad p \sim p_0 r^{\lambda_0 - 1} + 2c_0 r^{\lambda_0 - 1}(1 - \lambda_0)\theta. \tag{2.96}$$

The constant p_0 can be determined here by substituting the form of $f_0(\theta)$ from (2.81) into (2.86) and comparing with (2.96) to give

$$p_0 = 2c_0 \tan\left((\lambda_0 - 1)\,\frac{\pi}{2\alpha}\right). \tag{2.97}$$

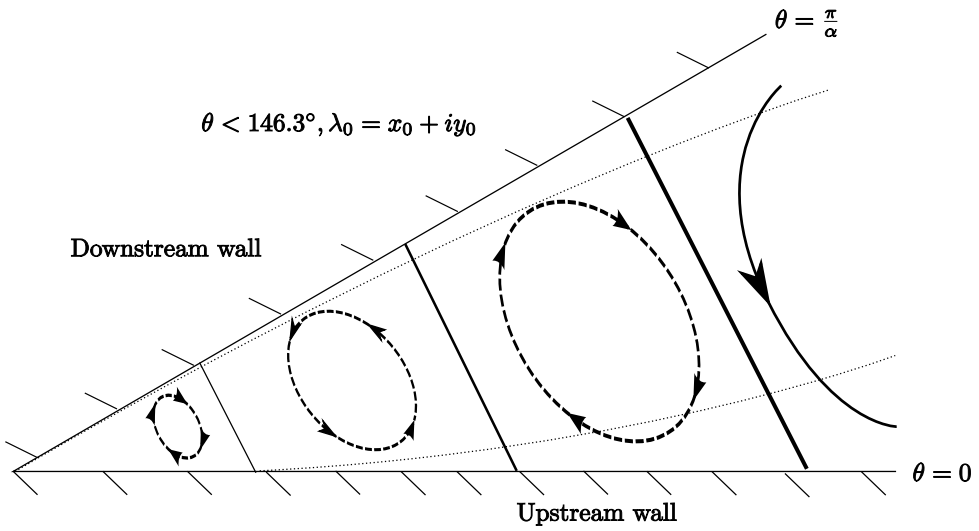

Figure 2-2: Sketch of the stream lines for corner angles $\theta < 146.3°$. In between the eddies are separating streamlines, the existence of eddies implied due to the transverse velocity component on the walls changing sign infinitely often as the corner is approached. The absolute size of the eddies are proportional to the length scale, determined by conditions far from the corner. The 'intensity' of successive eddies are found to depend upon the corner angle, with adjacent eddies up to a corner angle of 40° being of comparable size, for greater corner angles than this the relative size starts to drop off more and more quickly as the corner is approached. The reader is referred to [39] for more detail.

As a note we can transform between polar co-ordinates and Cartesian. This is recorded in [57] and is given in component form as

$$\begin{aligned} T_{11} &= \cos^2\theta T_{rr} - 2\sin\theta\cos\theta T_{r\theta} + \sin^2\theta T_{\theta\theta}, \\ T_{12} &= \sin\theta\cos\theta T_{rr} + (\cos^2\theta - \sin^2\theta) T_{r\theta} - \sin\theta\cos\theta T_{\theta\theta}, \\ T_{22} &= \sin^2\theta T_{rr} + 2\sin\theta\cos\theta T_{r\theta} + \cos^2\theta T_{\theta\theta}. \end{aligned} \tag{2.98}$$

In the limit then as $y \to 0$, the stream function and extra stress components behaviours are

$$\begin{aligned} &\psi \sim c_0 x^{\lambda_0 - 1} y^2, \quad p \sim p_0 x^{\lambda_0 - 1} + 2(1-\lambda_0) c_0 x^{\lambda_0 - 2} y, \\ &T_{11} \sim 4(\lambda_0 - 1) c_0 x^{\lambda_0 - 2} y, \quad T_{12} \sim 2 c_0 x^{\lambda_0 - 1}, \\ &T_{22} \sim -4(\lambda_0 - 1) c_0 x^{\lambda_0 - 2} y. \end{aligned} \tag{2.99}$$

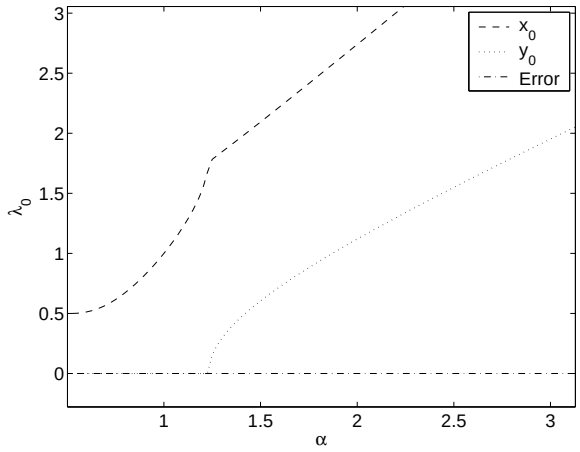

Figure 2-3: Plots of x_0 and y_0, the real and imaginary parts of λ_0 in (2.90). This figure shows the small α behaviour, with the corner angles shown from 360^o to 90^o. The 'Error' is the value of the minimised function in (2.95) and is a check that the calculations of (x_0, y_0) are correct. There is agreement with Table 1 of [39], for example at $\alpha = 2$ ($\theta = 90^o$), $\frac{\pi x_0}{\alpha} = 4.303$ and $\frac{\pi y_0}{\alpha} = 1.758$.

This completes the analysis for Newtonian corner flow and covers both the re-entrant and salient cases.

Chapter 3

Re-entrant Corner Flow
We $= O(1)$, $0 < \beta < 1$

3.1 Introduction

In this chapter we consider the asymptotics of fluid flow around a sharp corner (a corner angle greater than 180°) or so called re-entrant corner. This is contrasted with salient corner flow where the corner angle is less than 180°, this latter flow geometry is considered in chapter 5. Re-entrant corner flows appear naturally in contraction flows: where fluid flows between two joined pipes of differing diameters. It is well known that there are stress singularities at the corner making numerical simulation difficult, see [47], [7], [10]. An asymptotic approach is used to investigate two-dimensional planar flows, which have direct applications to contraction and extrusion flows that are benchmark problems for numerical schemes. This will allow us to investigate how the stresses behave close to the corner both in the upstream and the downstream flow regions.

Figure 1-2 in section 1.5 shows the re-entrant corner geometry. On both walls we prescribe no-slip and no normal velocity boundary conditions which in terms of the stream function are

$$\psi = \frac{\partial \psi}{\partial \theta} = 0, \quad \text{on } \theta = 0, \pi/\alpha. \tag{3.1}$$

Initially, we consider flow away from the walls in an outer (core) flow region and look to find a dominant balance in the constitutive equations (2.2). As a note, in any subsequent derivation using the Cartesian form, only the alignment with the upstream wall is necessary, with the downstream formulation obtained through a suitable transformation. For the downstream layer, Cartesian axes are taken with the x axis along the downstream wall $\theta = \pi/\alpha$ and y orthogonal to the wall along $\theta = \pi/\alpha + \pi/2$, preserving

the orientation relative to the upstream axes. In terms of polar co-ordinates we have $x = r\cos(\pi/\alpha - \theta)$, $y = -r\sin(\pi/\alpha - \theta)$. The domain is now

$$x \geq 0, \quad y \leq 0. \tag{3.2}$$

Figure 3-1 shows the downstream axes alignment.

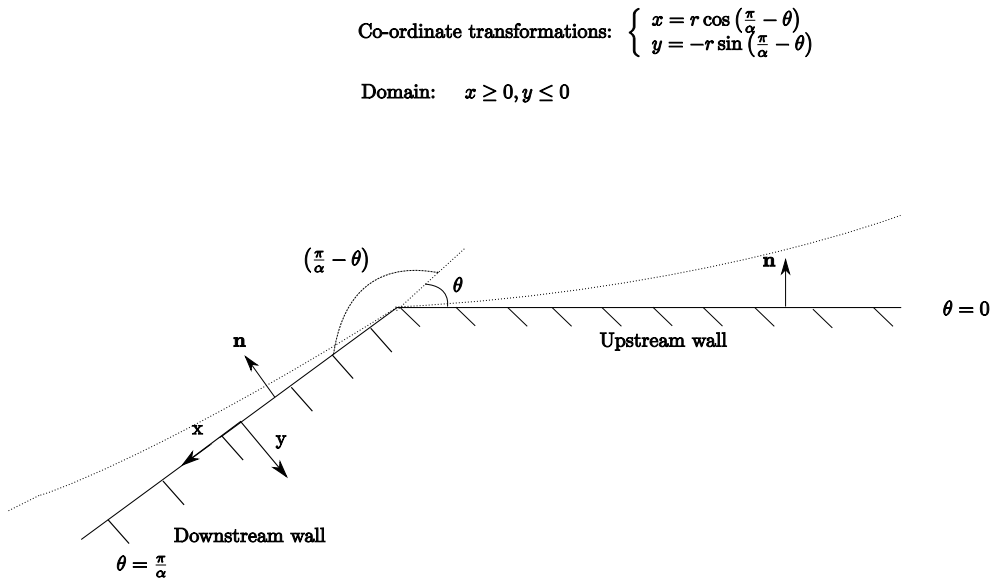

Figure 3-1: Re-entrant corner geometry, with the downstream axes alignment shown. The normals $\mathbf{n}$ are given on both upstream and downstream walls, along with the (x, y) alignment shown for the downstream wall. The domain (3.2) is given, where y is now aligned into the wall rather than out from it as in the upstream case. The co-ordinate transformations from Cartesian to polars are given, with the relevant angles indicated on the corner.

3.1.1 Weissenberg scalings

For this geometry there is no natural length scale and thus we may scale our variables as follows

$$r \mapsto \frac{r}{\mathrm{We}^{1/2}}, \quad v \mapsto \mathrm{We}^{1/2} v, \quad \mathbf{T}^p \mapsto \mathrm{We}\mathbf{T}^p, \quad p \mapsto \mathrm{We}\, p. \tag{3.3}$$

This has the effect of removing We from the equations (2.1)–(2.2). Thus in this chapter we set $\mathrm{We} = 1$ throughout.

3.1.2 Core Balance

Intuitively, considering solutions in an outer region, as $r \to 0$ for some k and m, we expect for the stream function ψ, and the extra polymer stress tensor $\mathbf{T}^p$ to behave like

$$\psi \sim O(r^k), \quad \mathbf{T}^p \sim O(r^{-m}). \tag{3.4}$$

Here we assume a stress singularity at the corner as $r \to 0$, anticipating m to be positive. These scalings allow us to consider the relative sizes of terms in (2.26)- (2.28) as

$$\mathbf{T}^p \sim O(r^{-m}), \quad \mathbf{D} \sim O(r^{k-2}), \quad \overset{\triangledown}{\mathbf{T}}{}^p \sim O(r^{k-2-m}). \tag{3.5}$$

The upper convected derivative will dominate the rate of strain terms $\mathbf{D}$ in the constitutive equations provided $m > 0$ (as already stated if a stress singularity is expected as $r \to 0$). As the re-entrant corner is approached, the stream function vanishes and is non-singular, thus $k > 0$. Further, it is expected the upper convected derivative will also dominate over the polymer stress terms $\mathbf{T}^p$. This assumption is based on expecting the fluid to accelerate around a reentrant corner, becoming infinite as $r \to 0$ (which is physically realistic) hence $k < 2$. With these assumptions in place, the dominant balance in the outer region is

$$\overset{\triangledown}{\mathbf{T}}{}^p + o(1) = 0, \quad r \to 0. \tag{3.6}$$

This analysis to follow is similar to that done by Renardy, [50] where the core balance considered above is the same as for the UCM model and the reader is referred to Renardy for a more detailed treatment if inertial effects or time dependent flows are considered. Other core balances can hold in differing geometries or constitutive models. For example in chapter 4, the $\beta \to 1$ limiting case has the upper convected derivative terms subdominant in a outer core region and is discussed later.

3.1.3 Core Solution

In the core region away from the boundaries, we expect the upper convected derivative to dominate as in (3.6), along with the momentum and constitutive equations. We will show together with (2.24), there exists a potential flow solution ψ, where ψ is a stream

function associated with the velocity field, and a solution for $\mathbf{T}^p$ given by

$$\psi = c_0 r^{\alpha n} \sin^n(\alpha\theta), \quad \mathbf{T}^p = \lambda(\psi)\mathbf{v}\mathbf{v}^T, \quad \text{as} \quad r \to 0, \tag{3.7}$$

for some function $\lambda = \lambda(\psi)$, constant c_0 and parameter n. Firstly, this solution form is physically relevant since we expect the fluid to advect and deform affinely (no polymer slip), hence stresses occur along streamlines. This balance is advantageous to use since from the natural stress formulation presented later we will show that the natural stress variables are constant along streamlines, as opposed to the Cartesian basis with arbitrarily chosen axes. To show that (3.7) is a solution, we write the momentum equations in component form as

$$\text{Re } v_k \frac{\partial}{\partial x_k} v_i = -\frac{\partial p}{\partial x_i} + \frac{\partial T_{ik}}{\partial x_k}. \tag{3.8}$$

Substituting in the solution form for $\mathbf{T}^p$ from (3.7) gives after differentiation

$$\text{Re } v_k \frac{\partial}{\partial x_k} v_i = -\frac{\partial p}{\partial x_i} + v_i v_k \frac{\partial \lambda(\psi)}{\partial x_k} + \lambda(\psi) v_k \frac{\partial v_i}{\partial x_k} + \lambda(\psi) \frac{\partial v_k}{\partial x_k}, \tag{3.9}$$

then collecting terms

$$(\text{Re} - \lambda(\psi))\, \mathbf{v} \cdot \nabla v_i = -\frac{\partial p}{\partial x_i}, \tag{3.10}$$

which is a particular form of the Euler equations. Assuming the inertial terms are subdominant to the pressure and velocity terms in the momentum equations in (2.1), $\lambda(\psi) \gg \text{Re}$, after dropping subscripts we have

$$-\mathbf{v} \cdot \nabla(\lambda \mathbf{v}) = -\nabla p. \tag{3.11}$$

Introducing the vector $\mathbf{u} = \lambda^{1/2}\mathbf{v}$, (3.11) becomes

$$\mathbf{u} \cdot \nabla \mathbf{u} = \nabla p. \tag{3.12}$$

This vector satisfies the continuity equation automatically

$$\nabla \cdot \mathbf{u} = \nabla \cdot \left(\lambda^{1/2}\mathbf{v}\right) = \mathbf{v} \cdot \nabla \left(\lambda^{1/2}\right) + \lambda^{1/2} \nabla \cdot \mathbf{v} = 0. \tag{3.13}$$

Also,

$$\nabla p = \mathbf{u} \cdot \nabla \mathbf{u} = (\nabla \times \mathbf{u}) \times \mathbf{u} + \nabla \left(\frac{1}{2} |\mathbf{u}|^2 \right), \tag{3.14}$$

where $\nabla \times \mathbf{u}$ is the associated vorticity Ω. Taking the curl of both sides of (3.14) then, we have

$$0 = \nabla \times (\Omega \times \mathbf{u}), \tag{3.15}$$

which after some simplification yields

$$\begin{aligned} 0 = \nabla \times (\Omega \times \mathbf{u}) &= (\mathbf{u} \cdot \nabla)\, \Omega + (\nabla \cdot \mathbf{u})\, \Omega - (\nabla \cdot \Omega)\, \mathbf{u} - (\Omega \cdot \nabla)\, \mathbf{u} \\ &= (\mathbf{u} \cdot \nabla)\, \Omega. \end{aligned} \tag{3.16}$$

The vorticity direction $\underline{k}$ is orthogonal to the plane of flow. In component form,

$$\Omega \underline{k} = \left(\frac{\partial \hat{v}}{\partial x} - \frac{\partial \hat{u}}{\partial y} \right) \underline{k} = -\nabla^2 \hat{\psi} \underline{k}, \tag{3.17}$$

where $\mathbf{u} = (\hat{u}, \hat{v})$ and $\hat{\psi}$ is the associated stream function. Solving (3.16) is then equivalent to solving the Poisson equation

$$\nabla^2 \hat{\psi} = f(\hat{\psi}), \tag{3.18}$$

where f is an arbitrary function of $\hat{\psi}$. In the literature, [30], [48], $f(\hat{\psi})$ has been taken to be zero giving Laplace's equation. To recap, our momentum equations can be written in the form (3.12) for a modified vector $\mathbf{u}$. This has a potential flow solution $\nabla^2 \hat{\psi} = 0$: Laplace's equation. This is related to the velocity field $\mathbf{v}$ through $\mathbf{u} = \lambda^{1/2} \mathbf{v}$, the fields being parallel and hence have the same streamlines. A particular solution form for $\hat{\psi}$ is

$$\hat{\psi} = \hat{c}_0 r^\alpha \sin(\alpha \theta), \quad \hat{\psi} = 0 \quad \text{on } \theta = 0, \pi/\alpha, \tag{3.19}$$

for some real constant $\hat{c}_0$. The stream function we are interested in, ψ, due to the above arguments, will be a function of $\hat{\psi}$ (sharing the same streamlines). Mathematically we can write this as, $\psi = h(\hat{\psi})$, for some unknown function h. Making the assumption that

$$\psi = h(\hat{\psi}) = \hat{c}_1 \hat{\psi}^n, \tag{3.20}$$

for some constant $\hat{c}_1$, ψ is of power law form. Differentiating with respect to y and using the chain rule, we can re-arrange for λ as

$$\lambda^{1/2} = (\hat{c}_1 n \hat{\psi}^{n-1})^{-1}. \tag{3.21}$$

Therefore we obtain

$$\lambda(\psi) = c_1 \left(\frac{\psi}{c_0 \alpha^n} \right)^{2/n-2}, \quad \psi = c_0 r^{\alpha n} \sin^n(\alpha\theta), \tag{3.22}$$

where c_0 and c_1 are constants (combinations of $\hat{c}_0$, $\hat{c}_1$ and n), n an unknown exponent to be found. For the first equation in (3.22), ψ has been divided through by $c_0\alpha^n$ for later convenience.

After having found a solution for ψ, it is instructive to go back to (3.11) and solve for the pressure gradient. Combining the gradients in (3.14) then taking the dot product with $\mathbf{u}$ on both sides gives

$$\mathbf{u} \cdot \nabla \left(\nabla p - \frac{1}{2}|\mathbf{u}|^2 \right) = 0, \implies p = P_0(\psi) + \frac{1}{2}\lambda |\mathbf{v}|^2, \tag{3.23}$$

where P_0 is an arbitrary function of ψ resulting from the integration. Writing $|\mathbf{v}|^2$ in polar co-ordinates, $|\mathbf{v}|^2 = \left(\frac{1}{r}\psi_\theta\right)^2 + (\psi_r)^2$ along with (3.22) means we can write the pressure in terms of r, this being after some simplification

$$p = P_0(\psi) + \frac{1}{2} p_0 r^{-2(1-\alpha)}, \tag{3.24}$$

where $p_0 = c_1 c_0^2 n^2 \alpha^{2n}$.

A possible core flow has thus been determined (with $f(\hat{\psi})$ taken arbitrarily to be zero in (3.18)) subject to the constants c_0, p_0 (c_1 is a combination of these two and is thus dependent) and the undetermined exponent n. This is unlikely to be the unique solution, if $f(\hat{\psi})$ is assumed to be non-zero then different core flow behaviour is assumed to hold. The exponent n will be determined by matching to the wall boundary layers. Using our assumed solution form for ψ and $\mathbf{T}^p$ in (3.22) along with our intuitive expectations of how these functions behave in the limit $r \to 0$, this class of self-similar solutions for the flow and stress fields gives

$$\psi = O(r^{n\alpha}), \quad \mathbf{T}^p = O(r^{-2(1-\alpha)}), \quad \mathbf{D} = O(r^{n\alpha-2}), \quad \overset{\triangledown}{\mathbf{T}}{}^p = O(r^{\alpha(2+n)-4}), \tag{3.25}$$

holding in the core outer region away from the walls. It is notable that the polymer extra stress behaviour is independent of n, unlike the stream function.

3.2 Asymptotic Analysis

The results in the previous section 3.1 allow us to approach the re-entrant corner problem, where we begin by determining the main asymptotic regions and corresponding solution structures in each of them. We have introduced the Cartesian and natural stress formulations in chapter 2, the results here are presented in both bases concurrently. Relevant highlights or differences between the two are commented on where appropriate.

The main asymptotic regions that need to be considered are more easily seen with the Cartesian formulation than natural stress. It is therefore ideal to consider Cartesian as an introductory basis used as a preliminary aid to investigate the results. However, the natural stress basis is required later on for the complete downstream solution when transitioning from the upstream to downstream boundary layers. The advantages of the natural stress basis are discussed later on in this thesis.

To make clear the size of the terms in the governing equations and to formulate a singular perturbation problem, a small parameter ϵ, $0 < \epsilon \ll 1$ is introduced for the length scales. The three main asymptotic regions local to the corner are presented in figure 3-2 comprising the outer (core) flow away from the boundaries and the boundary layers at the upstream and downstream walls. The analysis will proceed as follows. In section 3.2.1 the core balance assumed in (3.6) will be verified, motivating core scalings for the variables. In order to satisfy viscometric behaviour at the walls, the core solution is matched into boundary layers in 3.2.2. The boundary layer equations admit a similarity solution which is to be solved numerically. To do this, the wall behaviour of both formulations is examined in 3.2.4 and far-field behaviour in 3.2.5. This determines that the upstream system can be solved as an IVP shooting from the wall into the far-field using the upstream wall shear rate coefficient. The downstream system can then be solved as a boundary value problem giving the downstream wall rate.

3.2.1 The outer (core) region

The analysis of the re-entrant corner takes place in a region close to the corner. We scale distances with an artificially small parameter ϵ. With reference to the order magnitude assumptions in (3.25), suggested scalings for the stream function, velocity and stresses are

$$r = \epsilon R^*, \quad x = \epsilon X^*, \quad y = \epsilon Y^*, \quad \psi = \epsilon^{n\alpha}\Psi^*, \quad \mathbf{v} = \epsilon^{\alpha n-1}\mathbf{v}^*, \quad \mathbf{w} = \epsilon^{1-n\alpha}\mathbf{w}^*,$$
$$\mathbf{T}^p = \epsilon^{-2(1-\alpha)}\mathbf{T}^{p*}, \quad p = \epsilon^{-2(1-\alpha)}p^*, \quad \lambda = \epsilon^{-2\alpha(n-1)}\lambda^*, \quad \mu = \gamma_2\mu^*, \quad \nu = \gamma_3\nu^*.$$

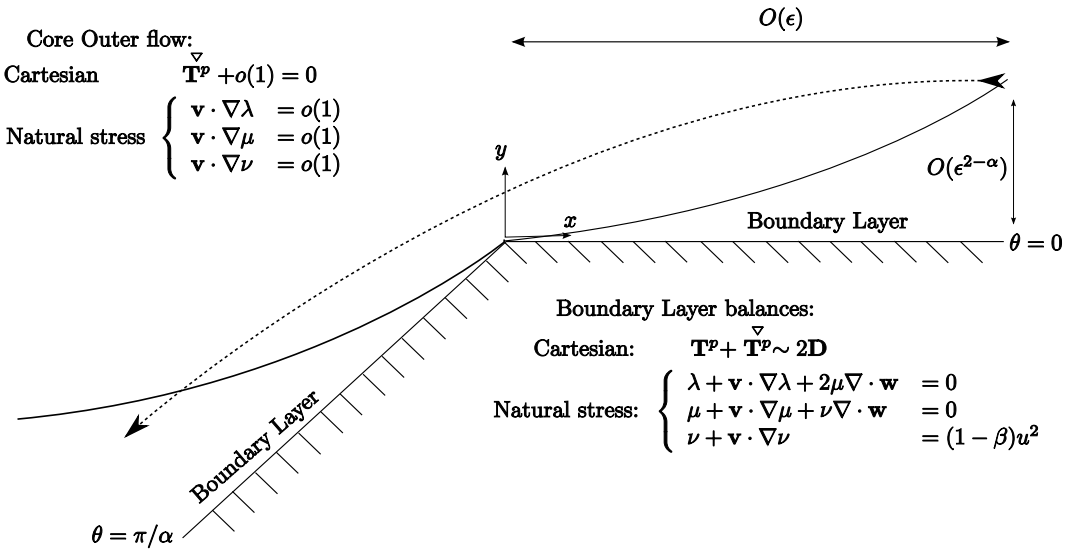

Figure 3-2: Illustration of the main asymptotic regions close to the corner for Oldroyd-B fluids with We $= O(1)$. Distances to the corner are assumed to be small of $O(\epsilon)$. In the core region the upper convected derivative dominates, self-similar solutions of the form (3.7) can be matched to upstream and downstream boundary layers at the walls. The fluid flows completely around the corner, so lip vortices are assumed not to be present. The leading order core and boundary layer equations are shown in the natural stress formulation. The boundary layer has a thickness of $O(\epsilon^{2-\alpha})$.

The scaling for the natural stress variable, λ, comes naturally from (3.22). For μ and ν the scalings are initially left unknown, determined by the small gauges $\gamma_2(\epsilon)$, $\gamma_3(\epsilon)$. These are found along with the exponent n when matching into the boundary layer later on. The scaling for the pressure gradient has been chosen so as to retain it at leading order within the momentum equation. Since we are away from the walls, the region considered is one for which $X^* = O(1)$, $Y^* = O(1)$.

The momentum equations in Cartesian become in component form,

$$\text{Re}\ \epsilon^{2\alpha(n-1)}\mathbf{v}^*\cdot\nabla^* u^* = -\frac{\partial p^*}{\partial X^*} + \frac{\partial T_{11}^{p*}}{\partial X^*} + \frac{\partial T_{12}^{p*}}{\partial Y^*} + \epsilon^{\alpha(n-2)}\beta\left(\frac{\partial^2 u^*}{\partial X^{*2}} + \frac{\partial^2 u^*}{\partial Y^{*2}}\right), \quad (3.26)$$

$$\text{Re}\ \epsilon^{2\alpha(n-1)}\mathbf{v}^*\cdot\nabla^* v^* = -\frac{\partial p^*}{\partial Y^*} + \frac{\partial T_{12}^{p*}}{\partial X^*} + \frac{\partial T_{22}^{p*}}{\partial Y^*} + \epsilon^{\alpha(n-2)}\beta\left(\frac{\partial^2 v^*}{\partial X^{*2}} + \frac{\partial^2 v^*}{\partial Y^{*2}}\right). \quad (3.27)$$

In the natural stress basis these are

$$\text{Re }\epsilon^{2\alpha(n-1)}\mathbf{v}^*\cdot\nabla^* u^* = -\frac{\partial p^*}{\partial X^*} + \mathbf{v}^*\cdot\nabla^*(\lambda^* u^*) + \delta_1\nabla^*\cdot\left(\mu^* u^*\mathbf{w}^* - \mu^*\mathbf{v}^*\frac{v^*}{u^{*2}+v^{*2}}\right)$$
$$- \delta_2\nabla^*\cdot\left(\nu^*\mathbf{w}^*\frac{v^*}{u^{*2}+v^{*2}}\right) + \beta\epsilon^{\alpha(n-2)}\left(2\frac{\partial^2 u^*}{\partial X^{*2}} + \frac{\partial^2 u^*}{\partial Y^{*2}} + \frac{\partial^2 v^*}{\partial X^*\partial Y^*}\right), \tag{3.28}$$

$$\text{Re }\epsilon^{2\alpha(n-1)}\mathbf{v}^*\cdot\nabla^* v^* = -\frac{\partial p^*}{\partial Y^*} + \mathbf{v}^*\cdot\nabla^*(\lambda^* v^*) + \delta_1\nabla^*\cdot\left(\mu^* v^*\mathbf{w}^* - \mu^*\mathbf{v}^*\frac{u^*}{u^{*2}+v^{*2}}\right)$$
$$+ \delta_2\nabla^*\cdot\left(\nu^*\mathbf{w}^*\frac{u^*}{u^{*2}+v^{*2}}\right) + \beta\epsilon^{\alpha(n-2)}\left(\frac{\partial^2 u^*}{\partial X^*\partial Y^*} + \frac{\partial^2 v^*}{\partial X^{*2}} + 2\frac{\partial^2 v^*}{\partial Y^{*2}}\right), \tag{3.29}$$

where we have set

$$\delta_1 = \gamma_2\epsilon^{2(1-\alpha)}, \quad \delta_2 = \gamma_3\epsilon^{4-2n\alpha-2\alpha}, \tag{3.30}$$

for convenience. For the inertial terms to be subdominant in either formulation, we require $n > 1$ to hold (since α is positive). The constitutive equations with these scalings in component form are

$$\epsilon^{2-n\alpha}T_{11}^{p*} + \left(u^*\frac{\partial T_{11}^{p*}}{\partial X^*} + v^*\frac{\partial T_{11}^{p*}}{\partial Y^*} - 2\frac{\partial u^*}{\partial Y^*}T_{12}^{p*} - 2\frac{\partial u^*}{\partial X^*}T_{11}^{p*}\right)$$
$$= 2\epsilon^{2(1-\alpha)}(1-\beta)\frac{\partial u^*}{\partial X^*}, \tag{3.31}$$

$$\epsilon^{2-n\alpha}T_{12}^{p*} + \left(u^*\frac{\partial T_{12}^{p*}}{\partial X^*} + v^*\frac{\partial T_{12}^{p*}}{\partial Y^*} - \frac{\partial v^*}{\partial X^*}T_{11}^{p*} - \frac{\partial u^*}{\partial Y^*}T_{22}^{p*}\right)$$
$$= \epsilon^{2(1-\alpha)}(1-\beta)\left(\frac{\partial u^*}{\partial Y^*} + \frac{\partial v^*}{\partial X^*}\right), \tag{3.32}$$

$$\epsilon^{2-n\alpha}T_{22}^{p*} + \left(u^*\frac{\partial T_{22}^{p*}}{\partial X^*} + v^*\frac{\partial T_{22}^{p*}}{\partial Y^*} - 2\frac{\partial v^*}{\partial X^*}T_{12}^{p*} - 2\frac{\partial v^*}{\partial Y^*}T_{22}^{p*}\right)$$
$$= 2\epsilon^{2(1-\alpha)}(1-\beta)\frac{\partial v^*}{\partial Y^*}. \tag{3.33}$$

For the upper convected derivative to dominate at leading order in the constitutive equations we require

$$\epsilon^{2-n\alpha} \ll 1, \quad \epsilon^{2(1-\alpha)} \ll 1. \tag{3.34}$$

The first of these in (3.34) implies $n < 2/\alpha$, the second $\alpha < 1$. For the inertial terms to be subdominant as already discussed, $n > 1$. The geometry of the re-entrant corner restricts the values of alpha to be $\alpha \in [1/2, 1)$, and we have a lower and upper bound

on the value of n

$$1 < n < 2/\alpha. \tag{3.35}$$

For reference, we can express these equations in full form in the Cartesian basis as

$$\text{Re } \epsilon^{2\alpha(n-1)\alpha}\mathbf{v}^* \cdot \nabla^*\mathbf{v}^* = -\nabla p^* + \nabla^* \cdot \mathbf{T}^{p*} + 2\epsilon^{\alpha(n-2)}\beta\nabla^* \cdot \mathbf{D}^*, \tag{3.36}$$

$$\epsilon^{2-n\alpha}\mathbf{T}^{p*} + \overset{\triangledown}{\mathbf{T}}^{p*} = 2(1-\beta)\epsilon^{2(1-\alpha)}\mathbf{D}^*. \tag{3.37}$$

In natural stress, the constitutive equations are

$$\epsilon^{2-\alpha n}\lambda^* + \mathbf{v}^* \cdot \nabla^*\lambda^* + 2\gamma_2\epsilon^{2-2\alpha}\mu^*\nabla^* \cdot \mathbf{w}^* = \epsilon^{4-2\alpha-n\alpha}(1-\beta)\frac{1}{(u^{*2}+v^{*2})}, \tag{3.38}$$

$$\epsilon^{2-\alpha n}\nu^* + \mathbf{v}^* \cdot \nabla^*\nu^* = \frac{1}{\gamma_3}\epsilon^{n\alpha}(1-\beta)(u^{*2}+v^{*2}), \tag{3.39}$$

$$\epsilon^{2-n\alpha}\mu^* + \mathbf{v}^* \cdot \nabla^*\mu^* + \frac{\gamma_3}{\gamma_2}\epsilon^{2-2n\alpha}\nu^*\nabla^* \cdot \mathbf{w}^* = 0. \tag{3.40}$$

The two formulations can be related, by writing (2.41)-(2.43) in outer variables

$$T_{11}^{p*} = -(1-\beta)\epsilon^{2(1-\alpha)} + \lambda^* u^{*2} - \gamma_2\epsilon^{2(1-\alpha)}\frac{2\mu^* u^* v^*}{(u^{*2}+v^{*2})} + \gamma_3\epsilon^{4-2n\alpha-\alpha}\frac{\nu^* v^{*2}}{(u^{*2}+v^{*2})^2}, \tag{3.41}$$

$$T_{12}^{p*} = \lambda^* u^* v^* + \gamma_2\epsilon^{2(1-\alpha)}\frac{\mu^*(u^{*2}-v^{*2})}{(u^{*2}+v^{*2})} - \gamma_3\epsilon^{4-2n\alpha-\alpha}\frac{\nu^* u^* v^*}{(u^{*2}+v^{*2})^2}, \tag{3.42}$$

$$T_{22}^{p*} = -(1-\beta)\epsilon^{2(1-\alpha)} + \lambda^* v^{*2} - \gamma_2\epsilon^{2(1-\alpha)}\frac{2\mu^* u^* v^*}{(u^{*2}+v^{*2})} + \gamma_3\epsilon^{4-2n\alpha-\alpha}\frac{\nu^* u^{*2}}{(u^{*2}+v^{*2})^2}. \tag{3.43}$$

Posing the expansions

$$\begin{gathered}\Psi^* = \Psi^{*(0)} + o(1), \quad \mathbf{T}^{p*} = \mathbf{T}^{p*(0)} + o(1), \quad p^* = p^{*(0)} + o(1), \\ \lambda^* = \lambda^{*(0)} + o(1), \quad \mu^* = \mu^{*(0)} + o(1), \quad \nu^* = \nu^{*(0)} + o(1), \quad \text{as } \epsilon \to 0,\end{gathered} \tag{3.44}$$

we look for the leading order behaviours as $\epsilon \to 0$. In order to progress, assumptions about the size of various terms for the natural stress formulation will have to be made along with (3.34). The validity of these will be verified retrospectively once the values of n, γ_2, γ_3 have been determined. So, assuming that

$$\gamma_2\epsilon^{2(1-\alpha)} \ll 1, \quad \frac{\gamma_3}{\gamma_2}\epsilon^{2(1-n\alpha)} \ll 1, \quad \frac{1}{\gamma_3}\epsilon^{n\alpha} \ll 1, \quad \gamma_3\epsilon^{4-2n\alpha-2\alpha} \ll 1, \tag{3.45}$$

the leading order momentum and constitutive equations in the core region are

$$0 = -\nabla^* p^{*(0)} + \nabla^* \cdot \mathbf{T}^{p*(0)}, \quad \overset{\triangledown}{\mathbf{T}}{}^{p*(0)} = 0, \tag{3.46}$$

$$\mathbf{v}^{*(0)} \cdot \nabla^* \lambda^{*(0)} = 0, \quad \mathbf{v}^{*(0)} \cdot \nabla^* \mu^{*(0)} = 0, \quad \mathbf{v}^{*(0)} \cdot \nabla^* \nu^{*(0)} = 0. \tag{3.47}$$

In starred outer variables, these equations have solutions

$$\Psi^{*(0)} = c_0 R^{*n\alpha} \sin^n(\alpha\theta), \quad \lambda^{*(0)} = c_1 \left(\frac{\Psi^{*(0)}}{c_0 \alpha^n} \right)^{2/n-2}, \quad p^{*(0)} = p_0 R^{*-2(1-\alpha)}, \tag{3.48}$$

which satisfy no normal velocity on the wall, $\Psi^{*(0)} = 0$ on $\theta = 0$ and $\theta = \pi/\alpha$. We have assumed the solution form for $\mathbf{T}^{*p(0)}$ from (3.7), so we can use the stream function form in (3.48) to express the core extra stress components in terms of this stream function as

$$T_{11}^{p*(0)} = c_1 \left(\frac{\Psi^{*(0)}}{c_0 \alpha^n} \right)^{\frac{2}{n}-2} \left(\frac{\partial \Psi^{*(0)}}{\partial Y^*} \right)^2, \tag{3.49}$$

$$T_{12}^{p*(0)} = -c_1 \left(\frac{\Psi^{*(0)}}{c_0 \alpha^n} \right)^{\frac{2}{n}-2} \left(\frac{\partial \Psi^{*(0)}}{\partial X^*} \frac{\partial \Psi^{*(0)}}{\partial Y^*} \right), \tag{3.50}$$

$$T_{22}^{p*(0)} = c_1 \left(\frac{\Psi^{*(0)}}{c_0 \alpha^n} \right)^{\frac{2}{n}-2} \left(\frac{\partial \Psi^{*(0)}}{\partial X^*} \right)^2. \tag{3.51}$$

Mathematically, (3.47) tells us that the leading order natural stress variables, $\lambda^{*(0)}$, $\mu^{*(0)}$ and $\nu^{*(0)}$ are constant along streamlines. Thus any information contained within them remains unchanged as the core outer region is traversed from upstream to downstream. Equivalently, we can say that $\lambda^{*(0)}$, $\mu^{*(0)}$ and $\nu^{*(0)}$ are functions of $\Psi^{*(0)}$ and are anticipated to be of a power law form as with the Cartesian formulation. We thus consider power-law form solutions

$$\lambda^{*(0)} = d_1 \left(\frac{\Psi^{*(0)}}{c_0 \alpha^n} \right)^{n_1}, \quad \mu^{*(0)} = d_2 \left(\frac{\Psi^{*(0)}}{c_0 \alpha^n} \right)^{n_2}, \quad \nu^{*(0)} = d_3 \left(\frac{\Psi^{*(0)}}{c_0 \alpha^n} \right)^{n_3}, \tag{3.52}$$

for undetermined constants d_1, d_2, d_3, c_0 and exponents n_1, n_2, n_3. To match with the upstream boundary layer we consider the behaviour as $Y^* \to 0$, which corresponds to $\theta \to 0$. Noting that for small θ, $R^* \sim X^*$, $\theta^* \sim Y^*/X^*$, our scalings for the stream

function and extra polymer stress components become

$$\Psi^{*(0)} \sim C_0 X^{*n(\alpha-1)} Y^{*n}, \quad T_{11}^{p*(0)} \sim C_1 X^{*(2\alpha-2)}, \tag{3.53}$$

$$T_{12}^{p*(0)} \sim C_1(1-\alpha) X^{(2\alpha-3)} Y^{*}, \quad T_{22}^{p*(0)} \sim C_1(1-\alpha)^2 X^{*(2\alpha-4)} Y^{*2}, \tag{3.54}$$

where $C_0 = c_0\alpha^n$. The pressure balance comes from the momentum equation, and is given by

$$p^{*(0)} \sim p_0 X^{*2\alpha-2}. \tag{3.55}$$

In natural stress the corresponding limiting behaviour is

$$\lambda^{*(0)} \sim d_1 X^{*2(n-1)(1-\alpha)} Y^{*2(1-n)}, \tag{3.56}$$

$$\mu^{*(0)} \sim d_2 X^{*n(\alpha-1)n_2} Y^{*nn_2}, \tag{3.57}$$

$$\nu^{*(0)} \sim d_3 X^{*n(\alpha-1)n_3} Y^{*nn_3}, \tag{3.58}$$

where the constants C_0, C_1, p_0 and hence d_1 (which is found by comparing with (3.48)) are given by

$$d_1 = c_1, \quad C_0 = c_0\alpha^n, \quad C_1 = c_1 n^2 C_0^2, \quad p_0 = \frac{1}{2}C_1, \tag{3.59}$$

The stream function in (3.48) and extra stresses (3.49)-(3.51) do not give viscometric flow behaviour near the walls found in 2.3.1. This motivates the consideration of boundary layers.

3.2.2 The upstream wall boundary layer analysis

To start the boundary layer analysis, we need to scale into the walls. Terming this the 'inner' solution, we define inner barred variables as

$$\begin{gathered} X^* = \bar{X}, \quad Y^* = \delta\bar{Y}, \quad \Psi^* = \delta^n\bar{\Psi}, \quad p^* = \bar{p}, \\ T_{11}^{p*} = \bar{T}_{11}^{p}, \quad T_{12}^{p*} = \delta\bar{T}_{12}^{p}, \quad T_{22}^{p*} = \delta^2\bar{T}_{22}^{p}, \quad u^* = \delta^{n-1}\bar{u}, \quad v^* = \delta^n\bar{v}, \\ \lambda^* = \delta^{2(1-n)}\bar{\lambda}, \quad \mu^* = \delta^{nn_2}\bar{\mu}, \quad \nu^* = \delta^{nn_3}\bar{\nu}. \end{gathered} \tag{3.60}$$

We scale with δ in the Y^* variable only, where necessarily, $\delta \ll 1$, with $\delta = \delta(\epsilon)$. The boundary layer region is thus $\bar{X} = O(1)$, $\bar{Y} = O(1)$. In the Cartesian stress basis the

constitutive equations are

$$\epsilon^{2-n\alpha}\delta^{1-n}\bar{T}^p_{11} + \left(\bar{u}\frac{\partial \bar{T}^p_{11}}{\partial \bar{X}} + \bar{v}\frac{\partial \bar{T}^p_{11}}{\partial \bar{Y}} - 2\frac{\partial \bar{u}}{\partial \bar{Y}}\bar{T}^p_{12} - 2\frac{\partial \bar{u}}{\partial \bar{X}}\bar{T}^p_{11}\right) = 2\epsilon^{2(1-\alpha)}\left(1-\beta\right)\frac{\partial \bar{u}}{\partial \bar{X}}, \tag{3.61}$$

$$\epsilon^{2-n\alpha}\delta^{1-n}\bar{T}^p_{12} + \left(\bar{u}\frac{\partial \bar{T}^p_{12}}{\partial \bar{X}} + \bar{v}\frac{\partial \bar{T}^p_{12}}{\partial \bar{Y}} - \frac{\partial \bar{v}}{\partial \bar{X}}\bar{T}^p_{11} - \frac{\partial \bar{u}}{\partial \bar{Y}}\bar{T}^p_{22}\right) = \frac{1}{\delta^2}\epsilon^{2(1-\alpha)}\left(1-\beta\right)\left(\frac{\partial \bar{u}}{\partial \bar{Y}} + \delta^2\frac{\partial \bar{v}}{\partial \bar{X}}\right), \tag{3.62}$$

$$\epsilon^{2-n\alpha}\delta^{1-n}\bar{T}^p_{22} + \left(\bar{u}\frac{\partial \bar{T}^p_{22}}{\partial \bar{X}} + \bar{v}\frac{\partial \bar{T}^p_{22}}{\partial \bar{Y}} - 2\frac{\partial \bar{v}}{\partial \bar{X}}\bar{T}^p_{12} - 2\frac{\partial \bar{v}}{\partial \bar{Y}}\bar{T}^p_{22}\right) = 2\frac{1}{\delta^2}\epsilon^{2(1-\alpha)}\left(1-\beta\right)\frac{\partial \bar{v}}{\partial \bar{Y}}, \tag{3.63}$$

and in the natural stress

$$\epsilon^{2-\alpha n}\delta^{1-n}\bar{\lambda} + \bar{\mathbf{v}}\cdot\bar{\nabla}\bar{\lambda} + 2\gamma_2\epsilon^{2-2\alpha}\delta^{nn_2-1}\bar{\mu}\bar{\nabla}\cdot\bar{\mathbf{w}} = \epsilon^{4-2\alpha-n\alpha}\delta^{1-n}(1-\beta)\frac{1}{\bar{u}^2+\delta^2\bar{v}^2}, \tag{3.64}$$

$$\epsilon^{2-\alpha n}\delta^{1-n}\bar{\nu} + \bar{\mathbf{v}}\cdot\bar{\nabla}\bar{\nu} = \frac{\epsilon^{n\alpha}\delta^{n-1-nn_3}}{\gamma_3}(1-\beta)(\bar{u}^2+\delta^2\bar{v}^2), \tag{3.65}$$

$$\epsilon^{2-n\alpha}\delta^{1-n}\bar{\mu} + \bar{\mathbf{v}}\cdot\bar{\nabla}\bar{\mu} + \frac{\gamma_3}{\gamma_2}\epsilon^{2-2n\alpha}\frac{\delta^{nn_3}}{\delta^{nn_2+2n-1}}\bar{\nu}\bar{\nabla}\cdot\bar{\mathbf{w}} = 0, \tag{3.66}$$

where

$$\bar{\nabla}\cdot\bar{\mathbf{w}} = \frac{\partial}{\partial \bar{Y}}\left(\frac{\bar{u}}{\bar{u}^2+\delta^2\bar{v}^2}\right) - \delta^2\frac{\partial}{\partial \bar{X}}\left(\frac{\bar{v}}{\bar{u}^2+\delta^2\bar{v}^2}\right) = \frac{\partial}{\partial \bar{Y}}\left(\frac{1}{\bar{u}}\right) + O(\delta^2). \tag{3.67}$$

The momentum equations in Cartesian form are

$$\text{Re }\epsilon^{2\alpha(n-1)}\delta^{2n-2}\bar{\mathbf{v}}\cdot\bar{\bar{\nabla}}\bar{u} = -\frac{\partial \bar{p}}{\partial \bar{X}} + \frac{\partial \bar{T}^p_{11}}{\partial \bar{X}} + \frac{\partial \bar{T}^p_{12}}{\partial \bar{Y}} + \epsilon^{\alpha(n-2)}\delta^{n-3}\beta\left(\delta^2\frac{\partial^2 \bar{u}}{\partial \bar{X}} + \frac{\partial^2 \bar{u}}{\partial \bar{Y}^2}\right), \tag{3.68}$$

$$\text{Re }\epsilon^{2\alpha(n-1)}\delta^{2n}\bar{\mathbf{v}}\cdot\bar{\bar{\nabla}}\bar{v} = -\frac{\partial \bar{p}}{\partial \bar{Y}} + \delta^2\left(\frac{\partial \bar{T}^p_{12}}{\partial \bar{X}} + \frac{\partial \bar{T}^p_{22}}{\partial \bar{Y}}\right) + \epsilon^{\alpha(n-2)}\delta^{n-1}\beta\left(\delta^2\frac{\partial^2 \bar{v}}{\partial \bar{X}} + \frac{\partial^2 \bar{v}}{\partial \bar{Y}^2}\right), \tag{3.69}$$

and in natural stress

$$\begin{aligned}\text{Re } \epsilon^{2(2-\alpha)}\bar{\mathbf{v}}\cdot\bar{\nabla}\bar{u} = &-\frac{\partial\bar{p}}{\partial\bar{X}} + \bar{\mathbf{v}}\cdot\bar{\nabla}(\bar{\lambda}\bar{u}) + \frac{\partial}{\partial\bar{Y}}\left(\bar{\mu}\frac{\bar{u}^2-\delta^2\bar{v}^2}{\bar{u}^2+\delta^2\bar{v}^2}\right) - \delta^2\frac{\partial}{\partial\bar{X}}\left(\frac{2\bar{\mu}\bar{u}\bar{v}}{\bar{u}^2+\delta^2\bar{v}^2}\right)\\ &- \delta^2\left(\frac{\partial}{\partial\bar{Y}}\left(\frac{\bar{\nu}\bar{u}\bar{v}}{(\bar{u}^2+\delta^2\bar{v}^2)^2}\right) - \delta^2\frac{\partial}{\partial\bar{X}}\left(\frac{\bar{\nu}\bar{v}^2}{(\bar{u}^2+\delta^2\bar{v}^2)^2}\right)\right)\\ &+ \beta\left(\delta^2 2\frac{\partial^2\bar{u}}{\partial\bar{X}^2} + \frac{\partial^2\bar{u}}{\partial\bar{Y}^2} + \delta^2\frac{\partial^2\bar{v}}{\partial\bar{X}\partial\bar{Y}}\right), \qquad (3.70)\end{aligned}$$

$$\begin{aligned}\text{Re } \epsilon^{2(2-\alpha)}\delta^2\bar{\mathbf{v}}\cdot\bar{\nabla}\bar{v} = &-\frac{\partial\bar{p}}{\partial\bar{Y}} + \delta^2\bar{\mathbf{v}}\cdot\bar{\nabla}(\bar{\lambda}\bar{v}) + \delta^2\frac{\partial}{\partial\bar{X}}\left(\bar{\mu}\frac{\bar{u}^2-\delta^2\bar{v}^2}{\bar{u}^2+\delta^2\bar{v}^2}\right) + \delta^2\frac{\partial}{\partial\bar{Y}}\left(\frac{2\bar{\mu}\bar{u}\bar{v}}{\bar{u}^2+\delta^2\bar{v}^2}\right)\\ &+ \delta^2\left(-\delta^2\frac{\partial}{\partial\bar{X}}\left(\frac{\bar{\nu}\bar{u}\bar{v}}{(\bar{u}^2+\delta^2\bar{v}^2)^2}\right) + \frac{\partial}{\partial\bar{Y}}\left(\frac{\bar{\nu}\bar{u}^2}{(\bar{u}^2+\delta^2\bar{v}^2)^2}\right)\right)\\ &+ \beta\delta^2\left(\delta^2\frac{\partial^2\bar{v}}{\partial\bar{X}^2} + 2\frac{\partial^2\bar{v}}{\partial\bar{Y}^2} + \frac{1}{\delta}\frac{\partial^2\bar{u}}{\partial\bar{X}\partial\bar{Y}}\right). \qquad (3.71)\end{aligned}$$

Next we seek expressions for the exponent n of the stream function and δ (which allows us to determine the boundary layer thickness). To this end we attempt to keep the maximum number of terms in (3.61)-(3.63) and (3.64)-(3.66) as possible. Fullest balance is obtained when

$$\begin{aligned}&\epsilon^{2-\alpha n}\delta^{1-n} = 1, \quad \gamma_2\epsilon^{2(1-\alpha)}\delta^{nn_2-1} = 1, \quad \frac{\gamma_3}{\gamma_2\delta^{nn_2}}\epsilon^{2(1-n\alpha)}\delta^{nn_3+1-2n} = 1,\\ &\frac{\epsilon^{n\alpha}\delta^{n-1}}{\gamma_3\delta^{nn_3}} = 1, \quad \frac{1}{\delta^2}\epsilon^{2(1-\alpha)} = 1, \qquad (3.72)\end{aligned}$$

where we retain the linear stress and rate of strain terms. This determines n and δ to be

$$\delta = \epsilon^{1-\alpha}, \quad n = 3-\alpha \qquad (3.73)$$

and also

$$\gamma_2\delta^{nn_2} = \epsilon^{\alpha-1}, \quad \gamma_3\delta^{nn_3} = \epsilon^2. \qquad (3.74)$$

The boundary layer thickness is thus $\epsilon^{2-\alpha}$. The leading order boundary layer momentum equations are

$$0 = -\frac{\partial\bar{p}}{\partial\bar{X}} + \frac{\partial\bar{T}^p_{11}}{\partial\bar{X}} + \frac{\partial\bar{T}^p_{12}}{\partial\bar{Y}} + \beta\frac{\partial^3\bar{\Psi}}{\partial\bar{Y}^3}, \qquad (3.75)$$

$$0 = -\frac{\partial\bar{p}}{\partial\bar{Y}}, \qquad (3.76)$$

from which it is clear the pressure is a function of $\bar{X}$ only. The leading order constitutive equations in the boundary layer are

$$\bar{T}^p_{11} + \left(\frac{\partial \bar{\Psi}}{\partial \bar{Y}} \frac{\partial \bar{T}^p_{11}}{\partial \bar{X}} - \frac{\partial \bar{\Psi}}{\partial \bar{X}} \frac{\partial \bar{T}^p_{11}}{\partial \bar{Y}} - 2 \frac{\partial^2 \bar{\Psi}}{\partial \bar{Y}^2} \bar{T}^p_{12} - 2 \frac{\partial^2 \bar{\Psi}}{\partial \bar{X} \partial \bar{Y}} \bar{T}^p_{11} \right) = 0, \tag{3.77}$$

$$\bar{T}^p_{12} + \left(\frac{\partial \bar{\Psi}}{\partial \bar{Y}} \frac{\partial \bar{T}^p_{12}}{\partial \bar{X}} - \frac{\partial \bar{\Psi}}{\partial \bar{X}} \frac{\partial \bar{T}^p_{12}}{\partial \bar{Y}} + \frac{\partial^2 \bar{\Psi}}{\partial \bar{X}^2} \bar{T}^p_{11} - \frac{\partial^2 \bar{\Psi}}{\partial \bar{Y}^2} \bar{T}^p_{22} \right) = (1-\beta) \frac{\partial^2 \bar{\Psi}}{\partial \bar{Y}^2}, \tag{3.78}$$

$$\bar{T}^p_{22} + \left(\frac{\partial \bar{\Psi}}{\partial \bar{Y}} \frac{\partial \bar{T}^p_{22}}{\partial \bar{X}} - \frac{\partial \bar{\Psi}}{\partial \bar{X}} \frac{\partial \bar{T}^p_{22}}{\partial \bar{Y}} + 2 \frac{\partial^2 \bar{\Psi}}{\partial \bar{X}^2} \bar{T}^p_{12} + 2 \frac{\partial^2 \bar{\Psi}}{\partial \bar{Y} \partial \bar{X}} \bar{T}^p_{22} \right) = -2(1-\beta) \frac{\partial^2 \bar{\Psi}}{\partial \bar{Y} \partial \bar{X}}. \tag{3.79}$$

In the natural stress basis, the leading order momentum equations are

$$0 = -\frac{\partial \bar{p}}{\partial \bar{X}} + \bar{\mathbf{v}} \cdot \bar{\nabla}(\lambda \bar{u}) + \frac{\partial \bar{\mu}}{\partial \bar{Y}} + \beta \frac{\partial^2 \bar{u}}{\partial \bar{Y}^2}, \tag{3.80}$$

$$0 = -\frac{\partial \bar{p}}{\partial \bar{Y}}, \tag{3.81}$$

agreeing with the Cartesian formulation that the pressure is a function of $\bar{X}$ only. The leading order constitutive equations are

$$\bar{\lambda} + \bar{\mathbf{v}} \cdot \bar{\nabla} \bar{\lambda} + 2\bar{\mu} \bar{\nabla} \cdot \bar{\mathbf{w}} = 0, \tag{3.82}$$

$$\bar{\mu} + \bar{\mathbf{v}} \cdot \bar{\nabla} \bar{\mu} + \bar{\nu} \bar{\nabla} \cdot \bar{\mathbf{w}} = 0, \tag{3.83}$$

$$\bar{\nu} + \bar{\mathbf{v}} \cdot \bar{\nabla} \bar{\nu} = (1-\beta) u^2. \tag{3.84}$$

The two formulations are linked (at leading order) in the boundary layer through the transformations

$$\bar{T}^p_{11} = \bar{\lambda} \bar{u}^2, \quad \bar{T}^p_{12} = \bar{\lambda} \bar{u} \bar{v} + \bar{\mu}, \quad \bar{T}^p_{22} = -(1-\beta) + \bar{\lambda} \bar{v}^2 + \left(\frac{2\bar{\mu}\bar{v}}{\bar{u}} \right) + \left(\frac{\bar{\nu}}{\bar{u}^2} \right), \tag{3.85}$$

or equivalently the inverse relationships

$$\bar{\lambda} = \frac{\bar{T}^p_{11}}{\bar{u}^2}, \quad \bar{\mu} = \bar{T}^p_{12} - \frac{\bar{T}^p_{11} \bar{v}}{\bar{u}}, \quad \bar{\nu} = \bar{\mu}^2 (1-\beta) + \bar{u}^2 \bar{T}^p_{22} + \bar{v}^2 \bar{T}^p_{11} - 2\bar{u}\bar{v}\bar{T}^p_{12}. \tag{3.86}$$

These relations are the same as derived by Renardy in [52] for the high Weissenberg UCM boundary layer fluid. Alternatively, the leading order boundary layer equations

(3.80)-(3.84) can be expressed in terms of the stream function as

$$0 = -\frac{d\bar{p}}{d\bar{X}} + \left(\frac{\partial\bar{\Psi}}{\partial\bar{Y}}\right)\frac{\partial}{\partial\bar{X}}\left(\bar{\lambda}\frac{\partial\bar{\Psi}}{\partial\bar{Y}}\right) - \left(\frac{\partial\bar{\Psi}}{\partial\bar{X}}\right)\frac{\partial}{\partial\bar{Y}}\left(\bar{\lambda}\frac{\partial\bar{\Psi}}{\partial\bar{Y}}\right) + \frac{\partial\bar{\mu}}{\partial\bar{Y}} + \beta\frac{\partial^2}{\partial\bar{Y}^2}\left(\frac{\partial\bar{\Psi}}{\partial\bar{Y}}\right), \tag{3.87}$$

$$0 = \left(\frac{\partial\bar{\Psi}}{\partial\bar{Y}}\right)^2\left(\frac{\partial\bar{\Psi}}{\partial\bar{Y}}\frac{\partial\bar{\lambda}}{\partial\bar{X}} - \frac{\partial\bar{\Psi}}{\partial\bar{X}}\frac{\partial\bar{\lambda}}{\partial\bar{Y}} + \bar{\lambda}\right) - 2\frac{\partial^2\bar{\Psi}}{\partial\bar{Y}^2}\bar{\mu}, \tag{3.88}$$

$$0 = \left(\frac{\partial\bar{\Psi}}{\partial\bar{Y}}\right)^2\left(\frac{\partial\bar{\Psi}}{\partial\bar{Y}}\frac{\partial\bar{\mu}}{\partial\bar{X}} - \frac{\partial\bar{\Psi}}{\partial\bar{X}}\frac{\partial\bar{\mu}}{\partial\bar{Y}} + \bar{\mu}\right) - \frac{\partial^2\bar{\Psi}}{\partial\bar{Y}^2}\bar{\nu} - \beta\left(\frac{\partial\bar{\Psi}}{\partial\bar{Y}}\right)^2\frac{\partial^2\bar{\Psi}}{\partial\bar{Y}^2}, \tag{3.89}$$

$$0 = \left(\frac{\partial\bar{\Psi}}{\partial\bar{Y}}\frac{\partial\bar{\nu}}{\partial\bar{X}} - \frac{\partial\bar{\Psi}}{\partial\bar{X}}\frac{\partial\bar{\nu}}{\partial\bar{Y}}\right) + \bar{\nu} - (1-\beta)\left(\frac{\partial\bar{\Psi}}{\partial\bar{Y}}\right)^2. \tag{3.90}$$

This system is completed with the solid boundary and no-slip condition at the wall

$$\text{on } \bar{Y} = 0, \quad \Psi = \frac{\partial\Psi}{\partial\bar{Y}} = 0, \tag{3.91}$$

along with the matching conditions as $\bar{Y} \to \infty$

$$\begin{aligned}
&\bar{\Psi} \sim C_0\bar{X}^{(\alpha-1)n}\bar{Y}^n, \quad \bar{T}^p_{11} \sim C_1\bar{X}^{2\alpha-2}, \quad \bar{T}^p_{12} \sim C_1(1-\alpha)\bar{X}^{2\alpha-3}\bar{Y}, \\
&\bar{T}^p_{22} \sim C_1(1-\alpha)^2\bar{X}^{2\alpha-4}\bar{Y}^2, \quad \bar{p} \sim p_0\bar{X}^{-2(1-\alpha)}, \\
&\bar{\lambda} \sim d_1\bar{X}^{2(n-1)(1-\alpha)}\bar{Y}^{2(1-n)}, \quad \bar{\mu} \sim d_2\bar{X}^{n(\alpha-1)n_2}\bar{Y}^{nn_2}, \quad \bar{\nu} \sim d_3\bar{X}^{nn_3(\alpha-1)}\bar{Y}^{nn_3},
\end{aligned} \tag{3.92}$$

with the exponents n_2, n_3 currently unknown. We next seek a self-similar solution to these equations. To this end, we look for invariance under a one parameter scaling group. Rescaling the barred (inner) variables gives a one parameter scaling group in γ say, as

$$\begin{aligned}
\bar{X} = \gamma\hat{X}, \quad \bar{Y} = \gamma^{2-\alpha}\hat{Y}, \quad \bar{\Psi} = \gamma^{3-\alpha}\hat{\Psi}, \quad \bar{p} = \gamma^{2(\alpha-1)}\hat{p}, \\
\bar{T}^p_{11} = \gamma^{2(\alpha-1)}\hat{T}^p_{11}, \quad \bar{T}^p_{12} = \gamma^{\alpha-1}\hat{T}^p_{12}, \quad \bar{T}^p_{22} = \hat{T}^p_{22}, \\
\bar{\lambda} = \gamma^{-2(2-\alpha)}\hat{\lambda}, \quad \bar{\mu} = \gamma^{\alpha-1}\hat{\mu}, \quad \bar{\nu} = \gamma^2\hat{\nu}.
\end{aligned} \tag{3.93}$$

This allows us to determine the exponents n_2 and n_3 to be

$$n_2 = -\frac{(1-\alpha)}{3-\alpha}, \quad n_3 = \frac{2}{n}, \tag{3.94}$$

which determines the remaining exponents in the leading order core behaviour. From this it is possible to determine the gauges γ_2 and γ_3 as

$$\gamma_2 = \epsilon^{-\alpha(1-\alpha)}, \quad \gamma_3 = \epsilon^{-2(\alpha^2-3\alpha+1)}, \tag{3.95}$$

This allows us to verify that the assumptions made in (3.45) were valid, namely

$$\begin{aligned} \gamma_2\epsilon^{2(1-\alpha)} = \epsilon^{(2-\alpha)(1-\alpha)} \ll 1, \quad \frac{\gamma_3}{\gamma_2}\epsilon^{2(1-n\alpha)} = \epsilon^{\alpha(1-\alpha)} \ll 1, \\ \frac{1}{\gamma_3}\epsilon^{n\alpha} = \epsilon^{(2-\alpha)(1-\alpha)} \ll 1, \quad \gamma_3\epsilon^{4-2n\alpha-2\alpha} = \epsilon^{2(1-\alpha)} \ll 1. \end{aligned} \tag{3.96}$$

The above scaling group suggests a similarity solution, which we can also use to to scale p_0 out of the governing equations. The similarity solution is

$$\begin{aligned} \xi = p_0^{\frac{1}{2}}\frac{\bar{Y}}{\bar{X}^{2-\alpha}}, \quad \bar{\Psi} = \bar{X}^{3-\alpha}p_0^{-\frac{1}{2}}f(\xi), \quad \bar{p} = p_0\bar{X}^{-2(1-\alpha)}, \\ \bar{T}_{11} = p_0\bar{X}^{2\alpha-2}t_{11}(\xi), \quad \bar{T}_{12} = p_0^{\frac{1}{2}}\bar{X}^{\alpha-1}t_{12}(\xi), \quad \bar{T}_{22} = t_{22}(\xi), \\ \bar{\lambda} = p_0\bar{X}^{-2(2-\alpha)}\tilde{\lambda}(\xi), \quad \bar{\mu} = p_0^{\frac{1}{2}}\bar{X}^{\alpha-1}\tilde{\mu}(\xi), \quad \bar{\nu} = \bar{X}^2\tilde{\nu}(\xi). \end{aligned} \tag{3.97}$$

The leading order Cartesian statement of the boundary layer equations are

$$2(\alpha-1)(t_{11}^p - 1) - (2-\alpha)\xi t_{11}^{p'} + t_{12}^{p'} + \beta f''' = 0, \tag{3.98}$$

$$t_{11}^p + \left(-(3-\alpha)ft_{11}^{p'} + 2(\alpha-2)t_{11}^p(f' - f''\xi) - 2f''t_{12}^p\right) = 0, \tag{3.99}$$

$$\begin{aligned} t_{22}^p + \Bigg(&- (3-\alpha)ft_{22}^{p'} + 2(2-\alpha)\left((3-\alpha)f - (3-\alpha)\xi f' + (2-\alpha)\xi^2 f''\right)t_{12}^p \\ &+ 2t_{22}^p\left(f' - (2-\alpha)\xi f''\right)\Bigg) = -2\left(1-\beta\right)\left(f' - (2-\alpha)\xi f''\right), \end{aligned} \tag{3.100}$$

$$\begin{aligned} t_{12}^p + \Bigg(&- (3-\alpha)ft_{12}^{p'} + (\alpha-1)f't_{12}^p + (2-\alpha)\left((3-\alpha)(f - \xi f') + (2-\alpha)\xi^2 f''\right)t_{11}^p \\ &- t_{22}^p f''\Bigg) = (1-\beta)\, f'', \end{aligned} \tag{3.101}$$

where the $'$ denotes differentiation with respect to ξ. In the natural stress formulation this becomes

$$\tilde{\mu}' + 2(1-\alpha) + \frac{2f''}{f'}\tilde{\mu} - (f'(1-f') + (3-\alpha)ff'')\tilde{\lambda} + \beta f''' = 0, \tag{3.102}$$

$$(3-\alpha)f\tilde{\lambda}' + (2(2-\alpha)f' - 1)\tilde{\lambda} + \frac{2f''}{(f')^2}\tilde{\mu} = 0, \tag{3.103}$$

$$(3-\alpha)f\tilde{\mu}' + \tilde{\mu}((1-\alpha)f' - 1) + \tilde{\nu}\frac{f''}{(f')^2} = 0, \tag{3.104}$$

$$(3-\alpha)f\tilde{\nu}' - (1+2f')\tilde{\nu} + (1-\beta)(f')^2 = 0. \tag{3.105}$$

The systems are completed with the wall and far-field behaviours

$$\text{at } \xi = 0, \quad f'' \sim \frac{a^{sp}}{2}\xi^2 \tag{3.106}$$

$$\text{as } \xi \to \infty, \quad f \sim C_0^{sp}\xi^{3-\alpha}, \quad t_{11}^p \sim C_1^{sp}, \quad t_{12}^p \sim C_1^{sp}(1-\alpha)\xi, \quad t_{22}^p \sim C_1^{sp}(1-\alpha)^2\xi^2 \tag{3.107}$$

$$\tilde{\lambda} \sim d_1^{sp}\xi^{-2(2-\alpha)}, \quad \tilde{\mu} \sim d_2^{sp}\xi^{-1+\alpha}, \quad \tilde{\nu} \sim d_3^{sp}\xi^2. \tag{3.108}$$

The similarity parameters a^{sp}, C_0^{sp}, C_1^{sp}, d_1^{sp}, d_2^{sp} and d_3^{sp} are defined by

$$a^{sp} = \frac{a}{p_0^{1/2}}, \quad C_0^{sp} = \frac{C_0}{p_0^{1-\frac{\alpha}{2}}}, \quad C_1^{sp} = \frac{C_1}{p_0} = 2, \quad d_1^{sp} = \frac{d_1}{p_0^{-1+\alpha}}, \quad d_2^{sp} = \frac{d_2}{p_0^{\alpha}} \quad d_3^{sp} = \frac{d_3}{p_0}, \tag{3.109}$$

where the parameter a arises in the wall behaviour

$$\text{as } \bar{Y} \to 0, \qquad \bar{\Psi} \sim \frac{1}{2}a\bar{X}^{\alpha-1}\bar{Y}^2, \tag{3.110}$$

corresponding to (3.106). As is seen, the extra stress equations in component form, now readily agree with the UCM model, while the momentum equation is changed with the presence of a higher order retardation term. The two points $\xi = 0$, $\xi = \infty$ are singular points for the system, so further analysis is required to investigate local behaviours.

3.2.3 The downstream wall boundary layer

The reader is referred to section 3.1 for the geometry involved for the downstream boundary layer in figure 3-1. In outer variables, $R^* \sim X^*$ as usual, but $(\pi/\alpha - \theta) \sim -Y^*/X^*$ as the downstream wall is approached. In the core region, the solution form

for $\Psi^{*(0)}$ in (3.48) as the downstream wall is approached behaves like

$$\Psi^{*(0)} = c_0 R^{*n\alpha} \sin^n(\alpha\theta) \sim C_0 R^{*n\alpha} \left(\frac{-Y^*}{X^*}\right)^n = C_0 X^{*n(\alpha-1)}(-Y^*)^n. \tag{3.111}$$

Similarly the limiting behaviours of the other variables are

$$\begin{aligned}
&\Psi^{*(0)} \sim C_0 X^{*n(\alpha-1)}(-Y^*)^n, \quad T_{11}^{p*(0)} \sim C_1 X^{*(2\alpha-2)}, \\
&T_{12}^{p*(0)} \sim C_1(1-\alpha) X^{(2\alpha-3)}(-Y^*), \quad T_{22}^{p*(0)} \sim C_1(1-\alpha)^2 X^{*(2\alpha-4)}(-Y^*)^2, \\
&\lambda^{*(0)} \sim d_1 X^{*2(n-1)(1-\alpha)}(-Y^*)^{2(\alpha-2)}, \quad \mu^{*(0)} \sim d_2 X^{*n(\alpha-1)n_2}(-Y^*)^{\alpha-1}, \\
&\nu^{*(0)} \sim d_3 X^{*n(\alpha-1)n_3}(-Y^*)^2.
\end{aligned} \tag{3.112}$$

For the boundary layer matching conditions, (3.92), the sign of d_2 will also change with the other polymer stress components and natural stress variables remaining unchanged. We note that changing the sign of the following variables leaves the governing equations unchanged and changes the sign of C_0 and d_2 only.

$$\bar{\Psi} \mapsto -\bar{\Psi}, \quad \bar{Y} \mapsto -\bar{Y}, \quad \bar{T}_{12}^p \mapsto -\bar{T}_{12}^p, \quad \bar{\mu} \mapsto -\bar{\mu}. \tag{3.113}$$

Consequently the matching conditions (3.92) remain the same with the signs of C_0, d_2 and a^{sp} reversed. The similarity solution and matching conditions found for the upstream region are therefore valid for the downstream region with the above transformations. Figure 3-1 shows the downstream axes alignment.

3.2.4 Behaviour at the wall and Eigenmode analysis

The system under consideration in both stress basis is a 6th order system: the dependent variables in the Cartesian statement are (f,f',f'',t_{11}^p,t_{12}^p,t_{22}^p) and in the natural stress statement (f,f',f'',λ,μ,ν). We are interested in viscometric behaviour at the walls. Performing a local analysis in Cartesian firstly for (3.98)-(3.101) at $\xi = 0$ and assuming a regular power series expansion for $f(\xi), t_{11}^p(\xi), t_{12}^p(\xi), t_{22}^p(\xi)$, i.e.

$$f(\xi) = \sum_{i=2}^{\infty} \frac{f_i \xi^i}{i!}, \quad t_{ij}^p = \sum_{k=0}^{\infty} a_{ijk} \xi^k, \tag{3.114}$$

we obtain the two-term solution as

$$f(\xi) = \frac{a^{sp}}{2}\xi^2 + \frac{b^{sp}}{6}\xi^3 + O(\xi^4), \tag{3.115}$$

$$t^p_{11}(\xi) = 2\left(a^{sp}\right)^2(1-\beta) - 6(1-\beta)a^{sp}\left(\left(a^{sp}\right)^2(\alpha-1) - \frac{2}{3}b^{sp}\right)\xi + O(\xi^2), \tag{3.116}$$

$$t^p_{12}(\xi) = (1-\beta)a^{sp} + (1-\beta)(3\left(a^{sp}\right)^2(1-\alpha) + b^{sp})\xi + O(\xi^2), \tag{3.117}$$

$$t^p_{22}(\xi) = -2(1-\beta)(1-\alpha)a^{sp}\xi + 4(1-\beta)\left(\left(a^{sp}\right)^2\left(\alpha - \frac{5}{4}\right)(\alpha-1) - \frac{1}{2}b^{sp}\alpha + \frac{3}{4}b^{sp}\right)\xi^2 + O(\xi^3). \tag{3.118}$$

In the natural stress basis this is

$$\tilde{\lambda}(\xi) = 2(1-\beta)\frac{1}{\xi^2} - \frac{2(1-\beta)(-3\left(a^{sp}\right)^2 - b^{sp} + 3\alpha\left(a^{sp}\right)^2)}{a^{sp}}\frac{1}{\xi} + O(1), \tag{3.119}$$

$$\tilde{\mu}(\xi) = (1-\beta)a^{sp} - (1-\beta)(-b^{sp} + 2\left(a^{sp}\right)^2 + 2\alpha\left(a^{sp}\right)^2)\xi + O(\xi^2), \tag{3.120}$$

$$\tilde{\nu}(\xi) = (1-\beta)\left(a^{sp}\right)^2\xi^2 - (1-\beta)\left((\alpha-1)\left(a^{sp}\right)^2 - b^{sp}\right)\xi^3 + O(\xi^4), \tag{3.121}$$

where $a^{sp} = f''(0)$ is free whilst $b^{sp} = f'''(0)$ satisfies

$$b^{sp} = (1-\alpha)\left((1-\beta)\left(a^{sp}\right)^2 - 2\right). \tag{3.122}$$

Setting $\beta = 0$ recovers the UCM solution in [20] as expected. To determine the number of degrees of freedom contained in this asymptotic behaviour at the wall, an eigenmode analysis is necessary. The analysis is presented separately for each stress basis.

Cartesian wall analysis

To do an eigenmode analysis, we consider the perturbation

$$f(\xi) \sim f^{(0)}(\xi) + \bar{\delta}\bar{f}(\xi), \qquad t^p_{ij}(\xi) \sim t^{p(0)}_{ij}(\xi) + \bar{\delta}\bar{t}^p_{ij}(\xi), \tag{3.123}$$

where $\bar{\delta} \ll 1$, and $f^{(0)}(\xi)$ and $t^{p(0)}_{ij}(\xi)$ represent the regular power series expansion. The perturbed terms are $\bar{f}(\xi)$ and $\bar{t}^p_{ij}$. Linearizing by keeping terms of $O(\bar{\delta})$ and neglecting the forcing terms gives a sixth-order homogeneous linear ode (obtained using Maple and not recorded for brevity) to determine the perturbed terms. The six linearly

independent solutions are the eigenmodes, which to leading order are

$$\left.\begin{aligned}&\bar{f}(\xi)\sim 1\\&\bar{t}^p_{11}\sim -2a^{sp}(3-\alpha)(4\alpha(a^{sp})^2-3b^{sp})(1-\beta)\\&\bar{t}^p_{12}\sim -(3-\alpha)((a^{sp})^2(\alpha+3)-b^{sp})(1-\beta)\\&\bar{t}^p_{22}\sim -2a^{sp}(3-\alpha)(1-\beta)\end{aligned}\right\},\quad \left.\begin{aligned}&\bar{f}(\xi)\sim \xi\\&\bar{t}^p_{11}\sim 6(a^{sp})^2(1-\beta)(1-\alpha)\\&\bar{t}^p_{12}\sim -a^{sp}(1-\beta)(1+\alpha)\\&\bar{t}^p_{22}\sim -2(1-\beta)\end{aligned}\right\}, \tag{3.124}$$

$$\left.\begin{aligned}&\bar{f}(\xi)\sim \xi^2\\&\bar{t}^p_{11}\sim 8a^{sp}(1-\beta)\\&\bar{t}^p_{12}\sim 2(1-\beta)\\&\bar{t}^p_{22}\sim 4(1-\beta)(1-\alpha)\xi\end{aligned}\right\},\quad \left.\begin{aligned}&\bar{f}(\xi)\sim \xi^{m_1}\exp\left(\frac{-2}{a^{sp}\beta(3-\alpha)\xi}\right)\\&\bar{t}^p_{11}\sim -\frac{8(1-2\beta)}{a^{sp}\beta(3-\alpha)^2(1-\beta)}\xi^{m_1-4}\exp\left(\frac{-2}{a^{sp}\beta(3-\alpha)\xi}\right)\\&\bar{t}^p_{12}\sim \frac{-4}{(a^{sp})^2\beta(3-\alpha)^2}\xi^{m_1-4}\exp\left(\frac{-2}{a^{sp}\beta(3-\alpha)\xi}\right)\\&\bar{t}^p_{22}\sim \frac{-8(2-\alpha)}{(a^{sp})^2\beta(3-\alpha)^2}\xi^{m_1-3}\exp\left(\frac{-2}{a^{sp}\beta(3-\alpha)\xi}\right)\end{aligned}\right\}, \tag{3.125}$$

$$\left.\begin{aligned}&\bar{f}(\xi)\sim \xi^{m_2}\exp\left(\frac{-2}{a^{sp}(3-\alpha)\xi}\pm\frac{4}{((3-\alpha)a^{sp}\xi)^{1/2}}\right)\\&\bar{t}^p_{11}\sim \mp\frac{8(1-2\beta)}{a(1-\beta)(3-\alpha)^2\beta}\xi^{m_2-4}\exp\left(\frac{-2}{a^{sp}(3-\alpha)\xi}\pm\frac{4}{((3-\alpha)a^{sp}\xi)^{1/2}}\right)\\&\bar{t}^p_{12}\sim -\frac{4}{(a^{sp})^2\beta(3-\alpha)^2}\xi^{m_2-4}\exp\left(\frac{-2}{a^{sp}(3-\alpha)\xi}\pm\frac{4}{((3-\alpha)a^{sp}\xi)^{1/2}}\right)\\&\bar{t}^p_{22}\sim \mp\frac{8(2-\alpha)}{(a^{sp})^2\beta(3-\alpha)^2}\xi^{m_2-3}\exp\left(\frac{-2}{a^{sp}(3-\alpha)\xi}\pm\frac{4}{((3-\alpha)a^{sp}\xi)^{1/2}}\right)\end{aligned}\right\}. \tag{3.126}$$

The constants m_1 and m_2 are defined as

$$m_1=\frac{-\beta(a^{sp})^2(3-\alpha)+\beta(11-5\alpha)+2(\alpha-2)}{\beta(1-\beta)(3-\alpha)},$$
$$m_2=\frac{\beta^3(3\alpha-9)+\beta(a^{sp})^2(12-4\alpha)+\beta(5\alpha-11)-(2\alpha-4)}{\beta(3-\alpha)(1-\beta)}.$$

Thus the sixth order homogeneous equation for the perturbed terms have six leading order asymptotic behaviours. We can deduce the following:

- In the case $a^{sp}<0$ relevant to the upstream boundary layer, only the third mode is consistent with the viscometric wall expansion. This implies that it has one degree of freedom associated with the free constant a^{sp}. As expected

the parameter b^{sp} is not free but determined through (3.122). The local wall expansion will be analytic in this case.

- For the downstream case, $a^{sp} > 0$, all of the exponential behaviours are consistent, along with the third mode, giving four degrees of freedom. The constant a^{sp} is associated with one degree of freedom, the remaining three associated with the exponential modes. Therefore, the wall expansion isn't analytic, with the exponential modes needing to be included in a full wall expansion. These occur as smaller terms in the expansion, their derivation being equivalent to a WKBJ-type expansion. Associating the constants K_1, K_2, K_3 with the three exponential

terms, the full wall expansion downstream takes the form

$$f(\xi) = \frac{a^{sp}}{2}\xi^2 + \frac{b^{sp}}{6}\xi^3 + O(\xi^4) + K_1\xi^m \exp\left(\frac{-2}{a^{sp}\beta(3-\alpha)\xi}\right)(1+O(\xi))$$
$$+ K_2\xi^{m_2} \exp\left(\frac{-2}{a^{sp}(3-\alpha)\xi} + \frac{4}{((3-\alpha)a^{sp}\xi)^{1/2}}\right)(1+O(\xi))$$
$$+ K_3\xi^{m_2} \exp\left(\frac{-2}{a^{sp}(3-\alpha)\xi} - \frac{4}{((3-\alpha)a^{sp}\xi)^{1/2}}\right)(1+O(\xi)), \tag{3.127}$$

$$t^p_{11}(\xi) = 2(a^{sp})^2(1-\beta) + O(\xi)$$
$$+ K_1\frac{-8(1-2\beta)}{a^{sp}(1-\beta)(3-\alpha)^2}\xi^{m_1-4} \exp\left(\frac{-2}{a^{sp}\beta(3-\alpha)\xi}\right)(1+O(\xi))$$
$$+ K_2\frac{-8(1-2\beta)}{a^{sp}(1-\beta)(3-\alpha)^2}\xi^{m_1-4} \exp\left(\frac{-2}{a^{sp}(3-\alpha)\xi} + \frac{4}{((3-\alpha)a^{sp}\xi)^{1/2}}\right)(1+O(\xi))$$
$$+ K_3\frac{-8(1-2\beta)}{a^{sp}(1-\beta)(3-\alpha)^2}\xi^{m_2-4} \exp\left(\frac{-2}{a^{sp}(3-\alpha)\xi} - \frac{4}{((3-\alpha)a^{sp}\xi)^{1/2}}\right)(1+O(\xi)), \tag{3.128}$$

$$t^p_{12}(\xi) = (1-\beta)a^{sp} + O(\xi)$$
$$+ K_1\frac{-4}{(a^{sp})^2\beta(3-\alpha)^2}\xi^{m_1-4} \exp\left(\frac{-2}{a^{sp}\beta(3-\alpha)\xi}\right)(1+O(\xi))$$
$$+ K_2\frac{-4}{(a^{sp})^2\beta(3-\alpha)^2}\xi^{m_1-4} \exp\left(\frac{-2}{a^{sp}(3-\alpha)\xi} + \frac{4}{((3-\alpha)a^{sp}\xi)^{1/2}}\right)(1+O(\xi))$$
$$+ K_3\frac{-4}{(a^{sp})^2\beta(3-\alpha)^2}\xi^{m_2-4} \exp\left(\frac{-2}{a^{sp}(3-\alpha)\xi} - \frac{4}{((3-\alpha)a^{sp}\xi)^{1/2}}\right)(1+O(\xi)), \tag{3.129}$$

$$t^p_{22}(\xi) = -2(1-\beta)(1-\alpha)a^{sp}\xi + O(\xi^2)$$
$$+ K_1\frac{-8(2-\alpha)}{(a^{sp})^2\beta(3-\alpha)^2}\xi^{m_1-3} \exp\left(\frac{-2}{a^{sp}\beta(3-\alpha)\xi}\right)(1+O(\xi))$$
$$+ K_2\frac{-8(2-\alpha)}{(a^{sp})^2\beta(3-\alpha)^2}\xi^{m_1-3} \exp\left(\frac{-2}{a^{sp}(3-\alpha)\xi} + \frac{4}{((3-\alpha)a^{sp}\xi)^{1/2}}\right)(1+O(\xi))$$
$$+ K_3\frac{8(2-\alpha)}{(a^{sp})^2\beta(3-\alpha)^2}\xi^{m_2-3} \exp\left(\frac{-2}{a^{sp}(3-\alpha)\xi} - \frac{4}{((3-\alpha)a^{sp}\xi)^{1/2}}\right)(1+O(\xi)). \tag{3.130}$$

These local wall expansions can be viewed as composed of an analytical part (the power series terms in regular powers of ξ) and a non-analytical part consisting of three exponentially small terms, for the case $a^{sp} > 0$.

Natural stress wall analysis

As for the Cartesian formulation, we aim to determine the degrees of freedom in the natural stress wall asymptotic behaviour. We consider a perturbation of the form, (as $\xi \to 0$)

$$\left(f(\xi), \tilde{\lambda}(\xi), \tilde{\mu}(\xi), \tilde{\nu}(\xi)\right) = \left(f_0(\xi), \tilde{\lambda}_0(\xi), \tilde{\mu}_0(\xi), \tilde{\nu}_0(\xi)\right) + \hat{\delta}\left(\hat{f}(\xi), \hat{\lambda}(\xi), \hat{\mu}(\xi), \hat{\nu}(\xi)\right). \tag{3.131}$$

We again linearise with the parameter $\hat{\delta}$ to obtain at $O(\hat{\delta})$ a homogeneous sixth order system of equations to determine the eigenmodes (obtained using Maple and not recorded for brevity). Three are algebraic and three exponential, namely

$$\left.\begin{aligned} f(\xi) &\sim 1 \\ \tilde{\lambda}(\xi) &\sim \frac{-2(-3+\alpha)(4\alpha(a^{sp})^2 - 3b^{sp})(-1+\beta)}{a^{sp}}\frac{1}{\xi^2} \\ \tilde{\mu}(\xi) &\sim 2a^{sp}(-1+\beta)(-3+\alpha)\frac{1}{\xi} \\ \tilde{\nu}(\xi) &\sim 2(a^{sp})^2(-1+\beta)(-3+\alpha)\xi \end{aligned}\right\}, \tag{3.132}$$

$$\left.\begin{aligned} f(\xi) &\sim \xi \\ \tilde{\lambda}(\xi) &\sim -\frac{4(1-\beta)}{a^{sp}}\frac{1}{\xi^3} \\ \tilde{\mu}(\xi) &\sim -(-3+\alpha)(7\alpha(a^{sp})^2 - 3a^{sp} - 4b^{sp})(-1+\beta) \\ \tilde{\nu}(\xi) &\sim 2a^{sp}(1-\beta)\xi \end{aligned}\right\}, \qquad \left.\begin{aligned} f(\xi) &\sim \xi^2 \\ \tilde{\lambda}(\xi) &\sim \frac{2(1-\beta)}{a^{sp}}\frac{1}{\xi^2} \\ \tilde{\mu}(\xi) &\sim 2(1-\beta) \\ \tilde{\nu}(\xi) &\sim 4a^{sp}(1-\beta)\xi^2 \end{aligned}\right\}, \tag{3.133}$$

$$\left.\begin{aligned} f(\xi) &\sim \xi^{q_1}\exp\left(\frac{-2}{a^{sp}\beta(3-\alpha)\xi}\right) \\ \tilde{\lambda}(\xi) &\sim -\frac{8(1-2\beta)}{\beta(a^{sp})^3(3-\alpha)^2(1-\beta)}\xi^{q_1-6}\exp\left(\frac{-2}{a^{sp}\beta(3-\alpha)\xi}\right) \\ \tilde{\mu}(\xi) &\sim \frac{-4}{(a^{sp})^2\beta(3-\alpha)^2}\xi^{q_1-4}\exp\left(\frac{-2}{a\beta(3-\alpha)\xi}\right) \\ \tilde{\nu}(\xi) &\sim \frac{-4}{(3-\alpha)}\xi^{q_1-1}\exp\left(\frac{-2}{a^{sp}\beta(3-\alpha)\xi}\right) \end{aligned}\right\}, \tag{3.134}$$

$$\left.\begin{aligned} f(\xi) &\sim \exp\left(\frac{-2}{a^{sp}(3-\alpha)\xi} \pm \frac{4}{((3-\alpha)a^{sp}\xi)^{\frac{1}{2}}}\right) \\ \tilde{\lambda}(\xi) &\sim -\frac{8(1-2\beta)}{\beta(a^{sp})^3(3-\alpha)^2(1-\beta)}\xi^{q_1-6}\exp\left(\frac{-2}{a^{sp}(3-\alpha)\xi} \pm \frac{4}{((3-\alpha)a^{sp}\xi)^{\frac{1}{2}}}\right) \\ \tilde{\mu}(\xi) &\sim \frac{-4}{(a^{sp})^2\beta(3-\alpha)^2}\xi^{q_1-4}\exp\left(\frac{-2}{a^{sp}(3-\alpha)\xi} \pm \frac{4}{((3-\alpha)a^{sp}\xi)^{\frac{1}{2}}}\right) \\ \tilde{\nu}(\xi) &\sim \frac{-4}{(3-\alpha)}\xi^{q_1-1}\left(\frac{-2}{a^{sp}(3-\alpha)\xi} \pm \frac{4}{((3-\alpha)a^{sp}\xi)^{\frac{1}{2}}}\right) \end{aligned}\right\}, \tag{3.135}$$

where

$$q_1 = \frac{3-\beta}{1-\beta} - \frac{1}{\beta(1-\beta)}. \tag{3.136}$$

The conclusions are similar to the Cartesian statement. The wall behaviour analysis has allowed us determine the conditions imposed upon the system by specifying the asymptotic behaviour (3.106) as $\xi \to 0$. A similar analysis is now done for the far-field behaviour.

3.2.5 Far-field behaviour

Cartesian analysis

Here we consider the degrees of freedom exhibited by the far-field behaviour. We pose

$$\begin{gathered} f \sim C_0^{sp}\xi^{3-\alpha}\big(1+\hat{\delta}\hat{f}(\xi)\big), \quad t_{11}^p \sim C_1^{sp}\big(1+\hat{\delta}\hat{t}_{11}^p(\xi)\big), \\ t_{12}^p \sim C_1^{sp}(1-\alpha)\xi\big(1+\hat{\delta}\hat{t}_{12}^p(\xi)\big), \quad t_{22}^p \sim C_1^{sp}(1-\alpha)^2\xi^2\big(1+\hat{\delta}\hat{t}_{22}^p(\xi)\big), \end{gathered} \tag{3.137}$$

then linearise using the parameter $\hat{\delta}$, where $\hat{\delta}$ is assumed small. We assume power law behaviours in the expansion for $\hat{f}$ and the perturbed extra polymer stresses as

$$\hat{f}(\xi) = \xi^m, \quad \hat{t}_{11}^p = A_{11}\xi^m, \quad \hat{t}_{12}^p = A_{12}\xi^m, \quad \hat{t}_{22}^p = A_{22}\xi^m, \tag{3.138}$$

aiming to find expressions for m and the A_{ij}. Substituting for these expressions, we obtain five algebraic asymptotic behaviours whilst the remaining one is exponential.

$$\left.\begin{array}{l}\hat{f}=1\\ \hat{t}^p_{11}=0\\ \hat{t}^p_{12}=0\\ \hat{t}^p_{22}=0\end{array}\right\},\qquad \left.\begin{array}{l}\hat{f}=\xi^{2(\alpha-2)}\\ \hat{t}^p_{11}=-\dfrac{2(2\alpha+1)}{\alpha}\\ \hat{t}^p_{12}=\dfrac{-4(\alpha^2-3\alpha-3)}{\alpha(\alpha-3)}\\ \hat{t}^p_{22}=\dfrac{-2(2\alpha^4-11\alpha^3+25\alpha^2-27\alpha+12)}{\alpha(\alpha-3)(\alpha-1)^2}\end{array}\right\},$$

$$\left.\begin{array}{l}\hat{f}=\xi^{-1}\\ \hat{t}^p_{11}=0\\ \hat{t}^p_{12}=-\dfrac{1}{(\alpha-1)(-3+\alpha)}\xi^{-1}\\ \hat{t}^p_{22}=-\dfrac{2}{3+\alpha^2-4\alpha}\xi^{-1}\end{array}\right\},\qquad \left.\begin{array}{l}\hat{f}=\xi^{\alpha-2}\\ \hat{t}^p_{11}=\dfrac{-2(\alpha-1)}{(\alpha+1)(\alpha-3)}\\ \hat{t}^p_{12}=\dfrac{-2(\alpha^2-2\alpha+2)}{(\alpha^2-1)(\alpha-3)}\\ \hat{t}^p_{22}=\dfrac{-2}{\alpha-1}\end{array}\right\},\tag{3.139}$$

$$\left.\begin{array}{l}\hat{f}=\xi^{2(\alpha-1)}\\ \hat{t}^p_{11}=-\dfrac{2(2\alpha-1)}{\alpha-3}\\ \hat{t}^p_{12}=-\dfrac{4(\alpha-1)}{\alpha-3}\\ \hat{t}^p_{22}=-\dfrac{2(2\alpha-3)}{\alpha-3}\end{array}\right\},\qquad \left.\begin{array}{l}\hat{f}=\xi^{1-\alpha}\exp\left(\dfrac{C_1^{sp}}{\beta C_0^{sp}(3-\alpha)\alpha}\xi^{\alpha}\right)\\ \hat{t}^p_{11}=\dfrac{2C_1^{sp}}{\beta C_0^{sp}(3-\alpha)^2}\exp\left(\dfrac{C_1^{sp}}{\beta C_0^{sp}(3-\alpha)\alpha}\xi^{\alpha}\right)\\ \hat{t}^p_{12}=\dfrac{((3-2\alpha))C_1^{sp}}{(1-\alpha)(3-\alpha)^2C_0^{sp}\beta}\exp\left(\dfrac{C_1^{sp}}{\beta C_0^{sp}(3-\alpha)\alpha}\xi^{\alpha}\right)\\ \hat{t}^p_{22}=\dfrac{2C_1^{sp}(2-\alpha)}{C_0^{sp}\beta(1-\alpha)(3-\alpha)^2}\exp\left(\dfrac{C_1^{sp}}{\beta C_0^{sp}(3-\alpha)\alpha}\xi^{\alpha}\right)\end{array}\right\}.\tag{3.140}$$

The above eigenmodes are all consistent with the far-field behaviour (3.107)-(3.108). As such they identify the homogeneous terms in the full far-field expansion, which is expected to contain the five free constants C_0^{sp}, C_2, C_3, C_4, C_5. These constants are associated with each of the above five modes. Inhomogeneous or forcing terms are also expected to be present in the full far-field expansion which are lost during the linearisation (and admission of the forcing terms). It is noted that there is no mode associated with the parameter C_1^{sp}. Proceeding systematically, we identify and

determine successive terms in the expansion as

$$f(\xi) \sim C_0^{sp}\xi^{3-\alpha}\Bigg(1 + F_1\xi^{-\alpha} + C_2\xi^{2\alpha-2} + F_2\xi^{-2\alpha} + C_3\xi^{-1} + \left(C_4 - \frac{1}{2C_0^{sp}(\alpha-2)}\right)\xi^{\alpha-2}$$
$$+ F_3\xi^{-2} + F_4\xi^{-3\alpha} + F_5\xi^{-4\alpha} + F_6\xi^{-2-\alpha} + C_5\xi^{-4+2\alpha}\Bigg), \tag{3.141}$$

$$t_{11}^p(\xi) \sim C_1^{sp}\Bigg(1 + A_1\xi^{-\alpha} - \frac{2C_2(2\alpha-1)}{\alpha-3}\xi^{2\alpha-2} + A_2\xi^{-2\alpha} - \frac{2(\alpha-1)C_4}{(\alpha+1)(\alpha-3)}\xi^{\alpha-2}$$
$$+ A_3\xi^{-2} + A_4\xi^{-3\alpha} + A_5\xi^{-4\alpha} + A_6\xi^{-2-\alpha} - A_7\xi^{-4+2\alpha}\Bigg), \tag{3.142}$$

$$t_{12}^p(\xi) \sim C_1^{sp}(1-\alpha)\xi\Bigg(1 + B_1\xi^{-\alpha} - \frac{4C_2(\alpha-1)}{\alpha-3}\xi^{2\alpha-2} + B_2\xi^{-2\alpha} - \frac{C_3}{(\alpha-1)(\alpha-3)}\xi^{-1}$$
$$- \frac{2C_4(\alpha^2-2\alpha+2)}{(\alpha+1)(\alpha-3)(\alpha-1)}\xi^{\alpha-2} - B_3\xi^{-2} + B_4\xi^{-3\alpha} + B_5\xi^{-4\alpha} + B_6\xi^{-2-\alpha} - B_7\xi^{-4+2\alpha}\Bigg), \tag{3.143}$$

$$t_{22}^p(\xi) \sim C_1^{sp}(1-\alpha)^2\xi^2\Bigg(1 + D_1\xi^{-\alpha} - \frac{2C_2(-3+2\alpha)}{\alpha-3}\xi^{2\alpha-2} + D_2\xi^{-2\alpha}$$
$$- \frac{2C_4(\alpha^2-2\alpha+3)}{(\alpha-1)(\alpha-3)(\alpha+1)}\xi^{\alpha-2} - D_3\xi^{-2} + D_4\xi^{-3\alpha} + D_5\xi^{-4\alpha} + D_6\xi^{-2-\alpha} - D_7\xi^{-4+2\alpha}\Bigg), \tag{3.144}$$

where the constants F_i, A_i, B_i, D_i, are given in Appendix A. Noteworthy are the following:

- The above expansions are found with C_2, C_3 set to zero. The terms in which they first arise have been included (modes two and three) but subsequent forcing terms including them have been omitted. This is done under the assumption that C_2, C_3 do not contribute towards determining parameters associated with the natural stress formulation, verified in the natural stress analysis performed in the next section.

- The expansions are not uniform in α. The terms associated with the eigenmodes keep their positioning in the expansion relative to each other. However, the forcing terms change their relative ordering. This is seen with the UCM model by Evans, [20], where with $C_2 \neq 0$, additional terms of order $O(\xi^{-4+4\alpha})$, $O(\xi^{-6+6\alpha})$ are included. As $\alpha \to 1^-$, an ever-increasing number of like terms will enter the expansion.

- The coefficients of the forcing terms in this expansion are singular at $\alpha = 2/3$. This suggests that the expansion needs to be modified to accommodate this. Following Sibley [57], we look for behaviour of the form $(\ln(\xi)\xi^{-\alpha})$ instead of $\xi^{-\alpha}$ for example. The expansion at the singular point $\alpha = 2/3$ is included in appendix B.

Natural stress analysis

Here, we consider the asymptotic far-field behaviourin the natural stress formulation. Linearising by using the small parameter $\hat{\delta}$ via

$$\tilde{f} \sim C_0^{sp}\xi^{3-\alpha}\left(1+\hat{\delta}\hat{f}(\xi)\right), \quad \tilde{\lambda} \sim d_1^{sp}\xi^{-4+2\alpha}\left(1+\hat{\delta}\hat{\lambda}(\xi)\right),$$
$$\tilde{\mu} \sim d_2^{sp}\xi^{-1+\alpha}\left(1+\hat{\delta}\hat{\mu}(\xi)\right), \quad \tilde{\nu} \sim d_3^{sp}\xi^{2}\left(1+\hat{\delta}\hat{\nu}(\xi)\right), \tag{3.145}$$

we keep terms of $O(\delta)$ and ignore the forcing terms. We thus again obtain a sixth order homogeneous linearised system to determine the eigenmodes. These are found (using Maple) to be:

$$\left.\begin{aligned}\hat{f} &= 1\\ \hat{\lambda} &= -2\\ \hat{\mu} &= 0\\ \hat{\nu} &= 0\end{aligned}\right\}, \quad \left.\begin{aligned}\hat{f} &= 0\\ \hat{\lambda} &= 0\\ \hat{\mu} &= 1\\ \hat{\nu} &= 0\end{aligned}\right\}, \quad \left.\begin{aligned}\hat{f} &= 0\\ \hat{\lambda} &= 0\\ \hat{\mu} &= 0\\ \hat{\nu} &= 1\end{aligned}\right\}, \quad \left.\begin{aligned}\hat{f} &= \xi^{-2+2\alpha}\\ \hat{\lambda} &= -2\frac{(2-\alpha)}{3-\alpha}\xi^{-2+2\alpha}\\ \hat{\mu} &= -\frac{(1-\alpha)}{3-\alpha}\xi^{-2+2\alpha}\\ \hat{\nu} &= \frac{2}{3-\alpha}\xi^{-2+2\alpha}\end{aligned}\right\}, \tag{3.146}$$

$$\left.\begin{aligned}\hat{f} &= \xi^{-1}\\ \hat{\lambda} &= -2\frac{(2-\alpha)}{3-\alpha}\xi^{-1}\\ \hat{\mu} &= -\frac{(1-\alpha)}{3-\alpha}\xi^{-1}\\ \hat{\nu} &= \frac{2}{3-\alpha}\xi^{-1}\end{aligned}\right\}, \quad \left.\begin{aligned}\hat{f} &= \xi^{-3-\alpha}\exp\left(\frac{2}{\beta\alpha(3-\alpha)C_0^{sp}}\xi^{\alpha}\right)\\ \hat{\lambda} &= -2\frac{(2-\alpha)}{3-\alpha}\exp\left(\frac{2}{\beta\alpha(3-\alpha)C_0^{sp}}\xi^{\alpha}\right)\\ \hat{\mu} &= -\frac{(1-\alpha)}{3-\alpha}\xi^{-3-\alpha}\exp\left(\frac{2}{\beta\alpha(3-\alpha)C_0^{sp}}\xi^{\alpha}\right)\\ \hat{\nu} &= \frac{2}{3-\alpha}\xi^{-3-\alpha}\exp\left(\frac{2}{\beta\alpha(3-\alpha)C_0^{sp}}\xi^{\alpha}\right)\end{aligned}\right\}, \tag{3.147}$$

that correspond to the linearly independent solutions. The first eigenmode emphasises that d_1^{sp} is related to C_0^{sp}, see (3.59) and is consistent with the far-field behaviour (3.108). Further the first mode corresponds to small changes in C_0^{sp}, similarly the second mode corresponds to changes in d_2^{sp} and the third mode with d_3^{sp}. The fourth and fifth modes are associated with two further free parameters in the system, which

were denoted C_2, C_3 in the Cartesian full far-field. Since the system is sixth-order we expect six eigenmodes. The final eigenmode is exponentially small when $C_0^{sp} < 0$ in the upstream case. An expansion of the type (3.145) will not be analytic due to the existence of this eigenmode. Further, we can now determine the constants d_1^{sp}, d_2^{sp}, d_3^{sp} in terms of the C_i's, $i = 1, .., 5$. Expressions for d_1^{sp}, d_2^{sp} and d_3^{sp} are found to be as follows

$$d_1^{sp} = \frac{C_1^{sp}}{(3-\alpha)^2(C_0^{sp})^2}, \quad d_2^{sp} = \frac{C_1^{sp}}{2(3-\alpha)C_0^{sp}}\Big(1 + \frac{2\alpha(1-\alpha)C_0^{sp}C_4}{(1+\alpha)}\Big), \tag{3.148}$$

$$d_3^{sp} = \frac{C_1^{sp}}{4} + \frac{2C_1^{sp}(C_0^{sp})^2C_5(3-\alpha)(3-2\alpha)}{\alpha} + \frac{(2\alpha^4 - 5\alpha^3 - \alpha^2 + 9\alpha - 9)C_1^{sp}C_0^{sp}C_4}{2\alpha(1+\alpha)(2-\alpha)} \tag{3.149}$$

$$+ \frac{(\alpha^3 - 3\alpha^2 + 4\alpha - 3)C_1^{sp}(C_0^{sp})^2C_4^2}{\alpha}. \tag{3.150}$$

In the particular case $C_4 = 0$, the expressions are

$$d_1^{sp} = \frac{C_1^{sp}}{(3-\alpha)^2(C_0^{sp})^2}, \quad d_2^{sp} = \frac{C_1^{sp}}{2(3-\alpha)C_0^{sp}}, \quad d_3^{sp} = \frac{C_1^{sp}}{4} + \frac{2C_1^{sp}(C_0^{sp})^2C_5(3-\alpha)(3-2\alpha)}{\alpha}, \tag{3.151}$$

which are the same expressions for UCM-type fluids given in [21].

3.2.6 Boundary Layer analysis summary

Summarising the results from the wall and far field analysis of sections 3.2.4 and 3.2.5:

- The upstream boundary layer is the case for which $a^{sp} < 0$. The Cartesian wall system (3.98)-(3.101) or natural stress wall system ((3.102))-(3.105) with the appropriate wall behaviours (3.115)-(3.118), (3.119)-(3.121) respectively can be used as a IVP in order to arrive at the far-field behaviours (3.107)-(3.108). The parameters a and p_0 are related through the similarity parameter a^{sp} in (3.106).

- The downstream case is a two point boundary value problem. Imposing the wall behaviour with a^{sp} unspecified gives two conditions only, with the remaining four from prescribing C_0^{sp}, d_2^{sp}, d_3^{sp} in the natural stress formulation, or C_0^{sp} with any two from (C_2,C_3,C_4,C_5) in the Cartesian basis. Consistency with the natural stress formulation suggests the choice of C_4, C_5. The wall shear rate coefficient $a^{sp} < 0$ is to be determined.

3.3 Numerical Analysis

For numerical implementation the system is re-arranged to form an explicit system with the highest derivative of f isolated. Here the Cartesian basis is examined first, with some numerical difficulties associated with it highlighted. The natural stress formulation is then used, since it is able to connect efficiently the information from the upstream and downstream boundary layers.

3.3.1 Cartesian upstream problem

Firstly we consider the upstream boundary layer case. We are interested in solving the sixth order system (3.98)-(3.101) subject to asymptotic behaviour both at the wall (3.115)-(3.118), and the far-field (3.107). Imposing the wall behaviour with a^{sp} specified gives 6 boundary conditions for the sixth order system. For a chosen α, the IVP has one free parameter, a^{sp}, with b^{sp} fixed through (3.122), giving us a one-dimensional parameter space to classify solutions. The far-field behaviour (3.141)-(3.144) involves the five free constants $(C_0^{sp}, C_2, C_3, C_4, C_5)$ which can be numerically determined, with the constant $C_1^{sp} = 2$. In order to distinguish between the upstream and downstream cases, we introduce the index u to the upstream constants. Introducing

$$(a^{sp}, b^{sp}, C_0^{sp}, C_2, C_3, C_4, C_5) = (a_u^{sp}, b_u^{sp}, C_{0u}^{sp}, C_{2u}, C_{3u}, C_{4u}, C_{5u}), \tag{3.152}$$

we can write an expression for b_u in terms of a_u^{sp} as

$$b_u^{sp} = 2(1-\alpha)(\frac{(1-\beta)(a_u^{sp})^2}{2} - 1). \tag{3.153}$$

The process for numerically solving these systems of equations starts by treating the upstream as an initial-value problem using MATLAB's stiff `ode15s` solver. To make the system explicit, we can re-arrange (3.98)-(3.101) for $f'''(\xi)$ as

$$\begin{aligned} f''' = \frac{-1}{f\beta(3-\alpha)}\Big(& f''\left(4\xi^2 t_{11}^p(\alpha(\alpha-1)+1) + t_{12}^p(2\xi(\alpha-2)+1) + (1-\beta)\right) \\ & + f'\left(-\xi t_{11}^p(2-\alpha)(1-\alpha) + t_{12}^p(1-\alpha)\right) \\ & + f\left(\alpha t_{11}^p(3-\alpha) - 2(3-\alpha)(1-\alpha)\right) + \xi t_{11}^p(2-\alpha) - t_{12}^p\Big), \end{aligned} \tag{3.154}$$

therefore allowing us to write the system as a set of first order equations involving $(f, f', f'', t_{11}^p, t_{12}^p, t_{22}^p)$. Tolerances $AbsTol = 10^{-13}$ and $RelTol = 10^{-13}$ were used on the domain $[\xi_0, \xi_\infty]$ where ξ_0 is taken suitably small and ξ_∞ large. The figures in 3-3 show the upstream solutions for a re-entrant corner with $\xi_0 = 10^{-6}$, $\xi_\infty = 10^{10}$,

$a_u^{sp} = -1,\ \alpha = 0.66$					
C_{0u}^{sp}					
ξ_0/ξ_∞	10^2	10^3	10^4	10^5	10^6
10^{-2}	-0.419335	-0.426934	-0.429564	-0.430536	-0.430803
10^{-3}	-0.419631	-0.426860	-0.430010	-0.430990	-0.431258
10^{-4}	-0.419660	-0.426891	0.430054	-0.431034	-0.431303
10^{-5}	-0.419663	-0.426895	-0.430059	-0.431039	-0.431308
10^{-6}	-0.419662	-0.426894	-0.430057	-0.431037	-0.431306

Table 3.1: Table showing convergence of C_{0u}^{sp} for decreasing ξ_0 and increasing ξ_∞

$a_u^{sp} = -1$, $\alpha = 0.66$, $\beta = 0.1$, as well as the stream function and stresses scaled with their far-field behaviours to show convergence. At $\xi_\infty = 10^{30}$, estimates for C_{0u}^{sp} and C_1^{sp} are

$$\frac{f}{\xi^{3-\alpha}} \approx C_{0u}^{sp} = -0.43318500489 \tag{3.155}$$

$$t_{11}^p \approx 1.999999999984978, \quad t_{11}^p = C_1^{sp} = 2, \tag{3.156}$$

$$\frac{t_{12}^p}{\xi_\infty} \approx 0.666666666656527, \quad \frac{t_{12}^p}{\xi_\infty} = C_1^{sp}(1-\alpha) = 0.\dot{6}, \tag{3.157}$$

$$\frac{t_{22}^p}{\xi_\infty^2} \approx 0.222222222217130, \quad \frac{t_{22}^p}{\xi_\infty} = C_1^{sp}(1-\alpha)^2 = 0.\dot{2}, \tag{3.158}$$

giving agreement to 10 decimal places. Convergence to this amount of significant figures requires very large ξ_∞ values for close approximation. To illustrate, table 3.1 shows convergence of C_{0u}^{sp} for varying domains $[\xi_0, \xi_\infty]$. To complete the solution, we need the value of at least three of $C_{0u}^{sp}, C_{2u}, C_{3u}, C_{4u}, C_{5u}$ so the downstream problem can be well posed. The value of C_{0u}^{sp} we have at leading order (calculating $f/\xi^{3-\alpha}$ at the far-field) but two more are needed. To illustrate the difficulties this can cause in the numerical stability of the solution we go back to the far-field analysis. We look at the first few terms in (3.141)-(3.144) in order to see how C_{2u} would be determined. Taking the first three terms in each of the far-field expansions, four possible approximations to C_{2u} (the superscripts relate to which of the far-field expansions the estimate for C_{2u}

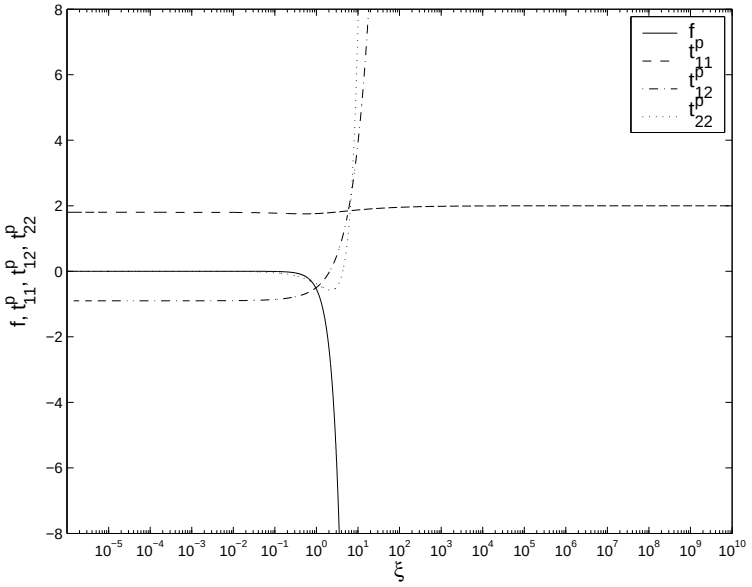

(a) Solution profiles for f, t^p_{11}, t^p_{12}, t^p_{22}

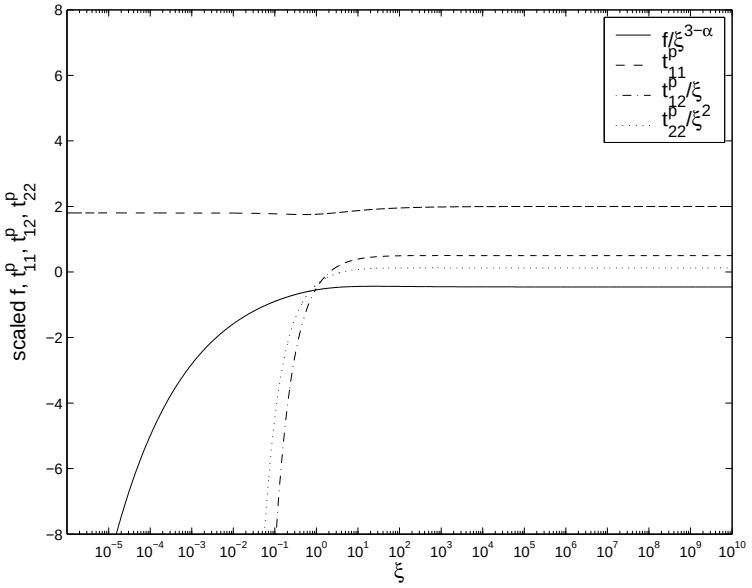

(b) Solution profiles for f, t^p_{11}, t^p_{12}, t^p_{22} scaled with ξ to show convergence to upstream far-field constants.

Figure 3-3: Solution profiles in the Cartesian formulation of the IVP for the upstream boundary layer. Scheme parameters used were $a_u^{sp} = -1$, $\alpha = 0.66$, $\beta = 0.1$, with $\xi_0 = 10^{-6}$, $\xi_\infty = 10^{10}$. The polymer stress components t^p_{11}, t^p_{12}, t^p_{22} and f are shown in (A) and scaled with their far-field behaviours in (B) where we expect convergence for large ξ.

comes from) would be,

$$C_{2u}^{f} = \left(\frac{f}{C_{0u}^{sp} \xi_\infty^{3-\alpha}} - 1 - \frac{\beta C_{0u}^{sp} (\alpha-2)(\alpha-3)^2}{C_{1u}^{sp}(3\alpha-2)} \xi_\infty^{-\alpha} \right) \xi_\infty^{2-2\alpha}, \tag{3.159}$$

$$C_{2u}^{t_{11}^p} = \frac{(\alpha-3)}{(2\alpha-1)} \left(-\frac{t_{11}^p}{C_{1u}^{sp}} + 1 - \frac{2\beta C_{0u}^{sp}(\alpha-1)(\alpha-2)(\alpha-3)}{C_{1u}^{sp}(3\alpha-2)} \xi_\infty^{-\alpha} \right) \xi_\infty^{2-2\alpha}, \tag{3.160}$$

$$C_{2u}^{t_{12}^p} = -\frac{(\alpha-3)}{4(\alpha-1)} \left(\frac{t_{12}^p}{C_{1u}^{sp}(1-\alpha)\xi_\infty} - 1 - \frac{\beta C_{0u}^{sp}(2\alpha-1)(\alpha-3)(\alpha-2)^2}{C_{1u}^{sp}(3\alpha-2)(\alpha-1)} \xi_\infty^{-\alpha} \right) \xi_\infty^{2-2\alpha}, \tag{3.161}$$

$$C_{2u}^{t_{22}^p} = -\frac{(\alpha-3)}{2(-3+2\alpha)} \left(\frac{t_{22}^p}{C_{1u}^{sp}(1-\alpha)^2\xi_\infty^2} - 1 - \frac{2\beta C_{0u}^{sp}(\alpha-2)(\alpha-3)(\alpha^2-3\alpha+1)}{C_{1u}^{sp}(3\alpha-2)(\alpha-1)} \xi_\infty^{-\alpha} \right) \xi_\infty^{2-2\alpha}. \tag{3.162}$$

To make this easier, we restrict the alpha range $\alpha > 2/3$ so that the first forcing terms are subdominant, the above expressions are

$$C_{2u}^{f} = \left(\frac{f}{C_{0u}^{sp} \xi_\infty^{3-\alpha}} - 1 \right) \xi_\infty^{2-2\alpha}, \tag{3.163}$$

$$C_{2u}^{t_{11}^p} = \frac{(\alpha-3)}{2(2\alpha-1)} \left(1 - \frac{t_{11}^p}{C_{1u}^{sp}} \right) \xi_\infty^{2-2\alpha}, \tag{3.164}$$

$$C_{2u}^{t_{12}^p} = -\frac{(\alpha-3)}{4(\alpha-1)} \left(\frac{t_{12}^p}{C_{1u}^{sp}(1-\alpha)\xi_\infty} - 1 \right) \xi_\infty^{2-2\alpha}, \tag{3.165}$$

$$C_{2u}^{t_{22}^p} = -\frac{(\alpha-3)}{2(-3+2\alpha)} \left(\frac{t_{22}^p}{C_{1u}^{sp}(1-\alpha)\xi_\infty^2} - 1 \right) \xi_\infty^{2-2\alpha}. \tag{3.166}$$

For large values of ξ_∞ there is a large amount of numerical instability in determining C_{2u}. This is probably due to the bracketed expressions in each approximation tending to 0 as ξ_∞ increases. Since these are multiplied by $\xi_\infty^{2-2\alpha}$ in each case, which grows extremely large, any small numerical errors in determining C_{0u}^{sp} or C_{1u}^{sp} are multiplied to the point where for sufficiently large ξ_∞ the numerical approximations break down. Figure 3-4 shows the numerical instability discussed, where all four approximations converge slowly for a moderately large ξ_∞, after which they break down. In order to determine other constants further down in the full far-field, these numerical instabilities will grow and make it extremely difficult to accurately determine any further constants. A downstream numerical scheme cannot therefore be accurately implemented for the Cartesian basis. The information required to transition to downstream in the natural stress basis is all contained at leading order in the upstream, eliminating the problem that the Cartesian basis has.

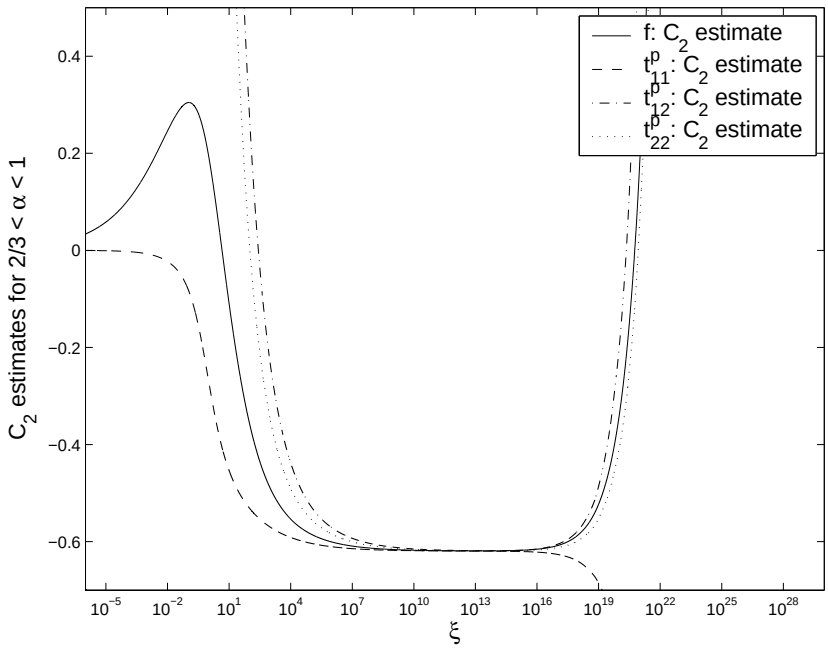

Figure 3-4: Diagram showing approximations for C_{2u} from (3.163)-(3.166), convergence is seen at around $\xi_\infty \sim 10^{15}$, after which divergence happens for increasing ξ_∞. Parameter values are $a_u^{sp} = -1$, $\alpha = 0.75$, $\beta = 0.1$, $\xi_0 = 10^{-6}$, $\xi_\infty = 10^{30}$

3.3.2 Natural stress upstream problem

Firstly we consider the upstream boundary layer case. We are interested in solving the system (3.102)-(3.105) subject to asymptotic behaviour both at the wall (3.119)-(3.121) and far-field (3.108). Imposing the wall behaviour with a^{sp} specified gives 6 boundary conditions for the sixth order system. For a chosen α, the IVP has one free parameter, a^{sp}, with b^{sp} fixed through (3.122), giving us a one-dimensional parameter space to classify solutions. The far field parameters are related to the Cartesian formulation through

$$d_{1u}^{sp} = \frac{C_{1u}^{sp}}{(3-\alpha)^2 (C_{0u}^{sp})^2}, \quad d_{2u}^{sp} = \frac{C_{1u}^{sp}}{2(3-\alpha) C_{0u}^{sp}} \Big(1 + \frac{2\alpha(1-\alpha) C_{0u}^{sp} C_{4u}}{(1+\alpha)} \Big), \tag{3.167}$$

$$d_{3u}^{sp} = \frac{C_{1u}^{sp}}{4} + \frac{2 C_{1u}^{sp} (C_{0u}^{sp})^2 C_{5u} (3-\alpha)(3-2\alpha)}{\alpha} + \frac{(2\alpha^4 - 5\alpha^3 - \alpha^2 + 9\alpha - 9) C_{1u}^{sp} C_{0u}^{sp} C_{4u}}{2\alpha(1+\alpha)(2-\alpha)}. \tag{3.168}$$

Since $\xi = 0$ is a singular point for the system, we use the wall asymptotic behaviour at the point $\xi = \xi_0 > 0$, where ξ_0 is necessarily very small. As for the Cartesian formulation, the system is solved on a finite domain $[\xi_0, \xi_\infty]$. Our initial conditions at

ξ_0 are the leading-order wall behaviours. The two-term wall behaviours for the natural stress formulation in terms of the similarity parameter a_u^{sp} are

$$f = \frac{1}{2}a_u^{sp}\xi_0^2 + \frac{1}{3!}b_u^{sp}\xi_0^3, \tag{3.169}$$

$$\tilde{\lambda} = 2(1-\beta)\frac{1}{\xi_0^2} - \frac{2(1-\beta)(-3(a_u^{sp})^2 - b_u^{sp} + 3\alpha(a_u^{sp})^2}{a_u^{sp}}\frac{1}{\xi_0}, \tag{3.170}$$

$$\tilde{\mu} = (1-\beta)a_u^{sp} - (1-\beta)(-b_u^{sp} + 2(a_u^{sp})^2 + 2\alpha(a_u^{sp})^2)\xi_0, \tag{3.171}$$

$$\tilde{\nu} = (1-\beta)(a_u^{sp})^2\xi_0^2 - (1-\beta)(-(a_u^{sp})^2 + \alpha(a_u^{sp})^2 - b_u^{sp})\xi_0^3. \tag{3.172}$$

For numerical implementation, the following rescaling is introduced

$$l(\xi) = f'(\xi)^2\tilde{\lambda}(\xi), \quad m(\xi) = \tilde{\mu}(\xi), \quad n(\xi) = f'(\xi)^{-2}\tilde{\nu}(\xi), \tag{3.173}$$

so that the wall behaviours are of $O(1)$. For implementation purposes, we use the leading order wall behaviour, in terms of our rescaled variables the initial conditions are

$$\text{at } \xi = \xi_0, \quad f = \frac{1}{2}a_u^{sp}\xi_0^2, \quad l = 2(1-\beta)(a_u^{sp})^2, \quad m = (1-\beta)a_u^{sp}, \quad n = (1-\beta). \tag{3.174}$$

For the far-field conditions, as $\xi \to \infty$, $f \sim C_{0u}^{sp}\xi^{3-\alpha}$. Substituting this into (3.108) with the scaled variables (3.173),

$$\text{at } \xi = \xi_\infty, \quad f = C_{0u}^{sp}\xi_\infty^{3-\alpha}, \quad l = 2, \quad m = d_{2u}^{sp}\xi^{\alpha-1}, \quad n = \frac{d_{3u}^{sp}}{(3-\alpha)^2(C_{0u}^{sp})^2}\xi^{2(\alpha-1)}, \tag{3.175}$$

where

$$d_{1u}^{sp} = \frac{2}{(3-\alpha)^2(C_{0u}^{sp})^2}. \tag{3.176}$$

The rescaled similarity solution is now

$$2(1-\alpha)f' + 2f''m + f'm' + \beta f'f''' - l\left(1 - f' + (3-\alpha)\frac{ff''}{f'}\right) = 0, \tag{3.177}$$

$$(3-\alpha)fl' - 2(3-\alpha)\frac{ff''}{f'}l' + (2(2-\alpha)f' - 1)l + 2f''m = 0, \tag{3.178}$$

$$(3-\alpha)fm' + m((1-\alpha)f' - 1) + nf'' = 0, \tag{3.179}$$

$$(3-\alpha)fn' - (1+2f')n + (1-\beta) + 2(3-\alpha)n\frac{ff''}{f'} = 0. \tag{3.180}$$

Rearranging to form an explicit system, we may obtain for f''' the expression

$$f''' = \frac{2(\alpha-1)}{\beta} + \frac{f''}{\beta}\left(\frac{n}{(3-\alpha)f} - \frac{2m}{f'} + \frac{(3-\alpha)fl}{(f')^2}\right) + \frac{l}{\beta}\left(\frac{1-f'}{f'}\right) + m((1-\alpha)f' - 1)\frac{1}{\beta(3-\alpha)f}. \tag{3.181}$$

As a result, (3.181) allows an explicit statement of the system involving f, f', f'', l, m, n.

The IVP is solved using MATLAB `ode15s`, the upstream numerical results are now presented. Solution profiles are given with $a_u^{sp} = -1$, $\alpha = 0.66$ with $\xi_0 = 10^{-6}$, $\xi_\infty = 10^8$. Estimates of the far-field constants $C_{0u}^{sp}, d_{1u}^{sp}, d_{2u}^{sp}, d_{3u}^{sp}$ for specified α, a_u^{sp} can be plotted and are given in 3-5. For large upstream wall shear coefficients, larger ξ_∞ values are needed for convergence. For the upstream case we can also vary β for fixed a_u^{sp}, starting to investigating the limits $\beta \to 0$ and $\beta \to 1$. This is plotted in 3-6 and 3-7 for varying a_u^{sp}. A surface plot of C_{0u}^{sp} for varying small $-a_u^{sp}$ and β for fixed α is given in 3-8. We can test convergence of d_i^{sp} and C_{0u}^{sp} for particular values of α and a_u^{sp}. The far-field behaviour is used to provide estimates for the constants C_{0u}^{sp}, d_{1u}^{sp}, d_{2u}^{sp}, d_{3u}^{sp} by evaluating the functions at selected ξ_∞ values. Table 3.2(a) shows convergence as ξ_∞ increases for these constants. Convergence as ξ_0 becomes increasingly small is shown in table 3.2(b) to show convergence in both limits. Also for the upstream wall, we can fix β and vary a_u^{sp} between small and large wall shear rates for selected corner angles α. Numerical instability is apparent for large wall shear rates as the corner angle tends to 180°. Solution profiles for $\beta = 0.1$, $\beta = 0.4$ and $\beta = 0.8$ are shown in figures 3-9, 3-10 and 3-11 respectively.

3.3.3 Natural stress downstream boundary layer

For the downstream problem, flow is away from the corner with $a_u^{sp} > 0$. We solve the re-scaled system (3.177)-(3.180) with the explicit f''' as in (3.181). The wall conditions (3.174) give us two conditions when a_u^{sp} is unspecified, with the far-field behaviour

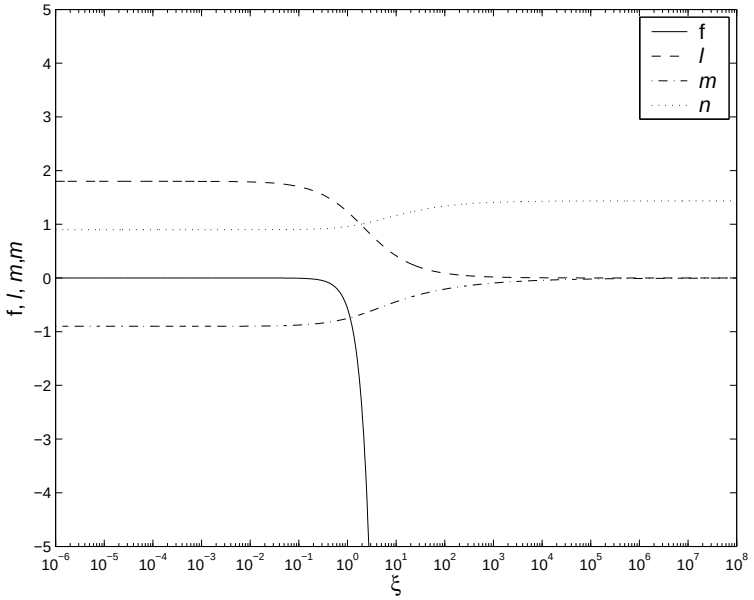

(a) Solution profiles for f, l, m, n

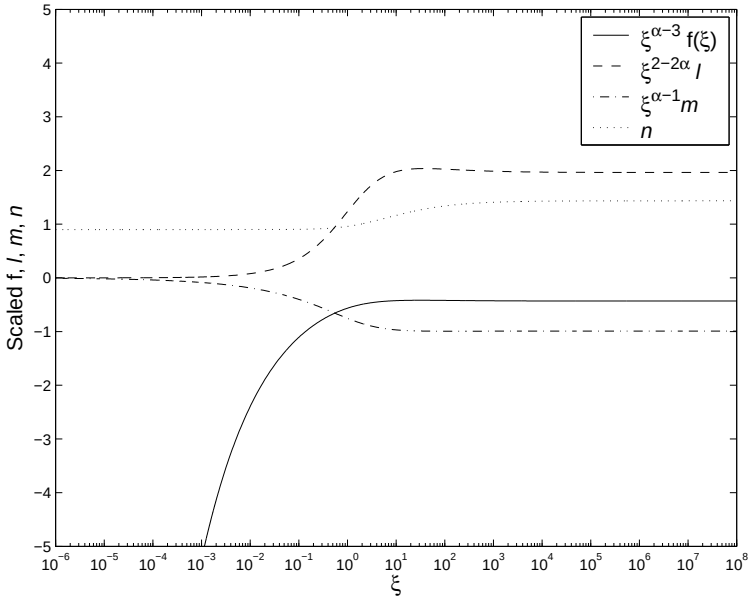

(b) Solution profiles for f, l, m, n scaled with ξ

Figure 3-5: Solution profiles in the natural stress formulation of the IVP for the upstream boundary layer. Scheme parameters used were $a_u^{sp} = -1$, $\alpha = 0.66$ with $\xi_0 = 10^{-6}$, $\xi_\infty = 10^8$. The related natural stress variables l, m, n defined in 3.173 are shown in (A) and scaled with their far-field behaviours in (B) where we expect convergence for large ξ.

(3.175) providing the remaining four. The system is solved on a restricted domain $[\xi_0, \xi_\infty]$ with (3.174) imposed at ξ_0 and (3.175) at ξ_∞ - the domain end points. Introducing the subscript d to refer to downstream parameters, the upstream and downstream constants are linked through the axis transformation (3.113), hence the required transformations needed are

$$C_{0d}^{sp} = -C_{0u}^{sp}, \quad d_{2d}^{sp} = -d_{2u}^{sp}, \quad d_{3d}^{sp} = d_{3u}^{sp}. \tag{3.182}$$

The upstream solutions gives us C_{0u}^{sp}, d_{2u}^{sp}, d_{3u}^{sp} which can used for the downstream problem via the above transformations. The downstream numerical solution is a significantly harder problem than the upstream, the steps taken to solve this are given below.

- The upstream problem is solved as an IVP on $[\xi_0 = 10^{-5}, \xi_\infty = 10^{10}]$ to obtain estimates for C_{0u}^{sp}, d_{2u}^{sp}, d_{3u}^{sp}. Using (3.182), the downstream version of these constants is obtained. The sign of the upstream f profile is changed, then put into (3.177)-(3.180). These constitutive equations are then rearranged for l, m and n and solved as an IVP from the far-field into the wall. This is done on a reduced domain $[\xi_\infty = 10^6, \xi_0 = 10^{-5}]$.

- The data points obtained from the above procedure are interpolated on $[\xi_0 = 10^{-5}, \xi_\infty = 10^6]$. A mesh is created on the restricted domain $[\xi_0 = 10^{-2.5}, \xi_\infty = 10^3]$ and the interpolated solution obtained is used as an initial guess for the Matlab boundary value problem solver `bvp4c` on loose tolerances $RelTol = 10^{-5}$, $AbsTol = 10^{-5}$.

- The domain is then extended towards the corner for as far as possible. The initial solution obtained from the previous step is used as a guess on a slightly extended domain. Using `bvp4c` with the above tolerances, the largest extended domain achieved was $[\xi_0 = 1.7 \times 10^{-4}, \xi_\infty = 10^3]$.

- When varying a_u^{sp}, the above steps are repeated for each a_u^{sp}. Taking small a_u^{sp} values first, a_u^{sp} is initially solved with $a_u^{sp} = -1$, then increased by 0.01 until $a_u^{sp} = -0.01$ is reached.

- Then increasing $-a_u^{sp}$ is examined. Care has to be taken since upstream convergence for far-field parameters is sensitive to the initial ξ_0 that the IVP shoots from. Therefore, for $-a_u^{sp} = O(10^2)$ the upstream ξ_0 should be taken smaller to around 10^{-7} to ensure convergence for C_{0u}^{sp}, d_{2u}^{sp} and d_{3u}^{sp}. This substantially increases computational time so is only used when $-a_u^{sp} > 10$.

- The data for small and large $-a_u^{sp}$ is combined for plotting 3-13.

3.3.4 Discussion

A class of self-similar solutions for the Oldroyd-B model at a re-entrant corner has been described that are associated with the upper convected stress derivative dominating in a core flow region near to the corner (but away from the walls). These give a polymer stress singularity of $O(r^{-2(1-\alpha)})$. The stream function behaves as $O(r^{n\alpha})$, with $n = 3 - \alpha$ determined by matching into wall boundary layers which are needed to recover viscometric behaviour at the wall. Consequently the solvent stresses are weaker and $O(r^{n\alpha-2})$. In summary we have

$$\mathbf{T}^p = O(r^{-2(1-\alpha)}), \quad \mathbf{T}^s = O(r^{-(2-\alpha)(1-\alpha)}), \quad \mathbf{v} = O(r^{(3-\alpha)\alpha-1}) \quad \text{as } r \to 0.$$

The solution structure has wall boundary layers in addition to the outer core region. The complete solution depends upon two parameters, the pressure coefficient p_0 and the wall shear rate coeficient a (or equivalently p_0 and the coefficient of the core stream function C_0). One of these parameters can however be scaled out in the similarity solution reducing the parameter space of solutions for classification by one, the choice here taken was to scale p_0 out. This is equivalent to introducing the similarity combination $a/p_0^{1/2}$, which can be used to determine the other parameters arising in the upstream far-field behaviour and downstream wall beahviour.

The stress singularity, stream function behaviour and boundary layer thickness are found to be the same as the UCM model. The difference with the Oldroyd-B model is the inclusion of the retardation parameter β. Setting $\beta = 0$ recovers the UCM results in the similarity solution. The similarity equations reduce now from an explicit sixth-order system to an implicit fifth-order system. We loose an exponential eigenmode in the wall and far-field asymptotic behaviours. Accordingly, the numerical scheme presented here needs modification to solve the UCM fifth-order system.

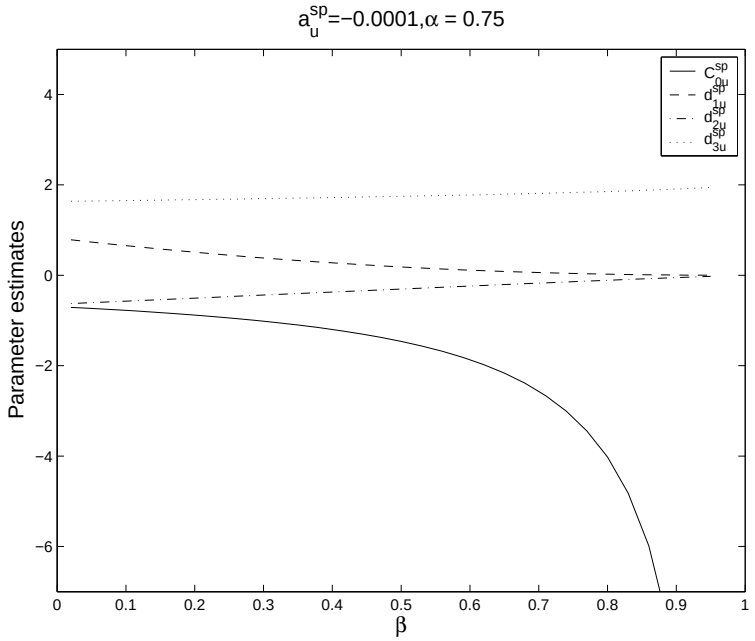

(a) Solution profiles for C_{0u}^{sp}, d_{1u}^{sp}, d_{2u}^{sp}, d_{3u}^{sp} for a fixed $a_u^{sp} = -0.00001$, $\alpha = 0.75$.

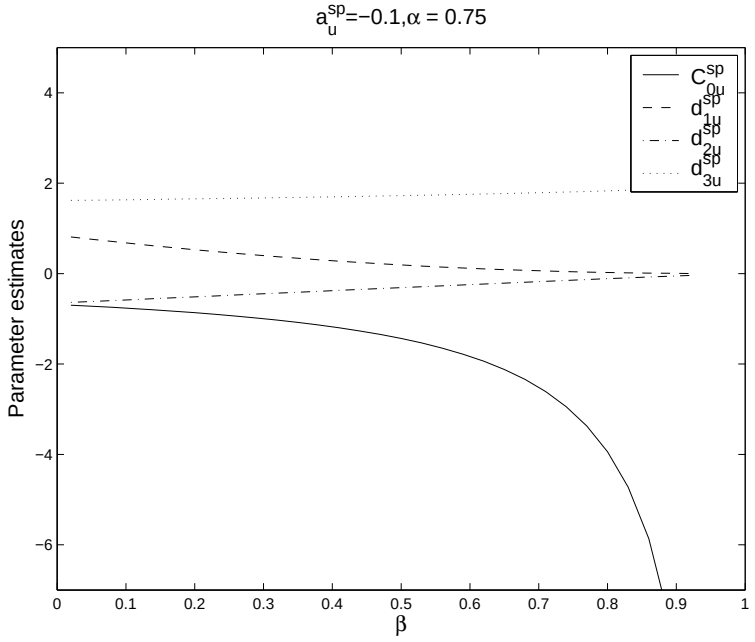

(b) Solution profiles for C_{0u}^{sp}, d_{1u}^{sp}, d_{2u}^{sp}, d_{3u}^{sp} for a fixed $a_u^{sp} = -0.1$, $\alpha = 0.75$.

Figure 3-6: Estimates of the far-field constants C_{0u}^{sp}, d_{1u}^{sp}, d_{2u}^{sp}, d_{3u}^{sp} for fixed a_u^{sp} and α. The IVP was solved with $\xi_0 = 10^{-10}$, $\xi_\infty = 10^{40}$, the large domain needed for parameter convergence as $\beta \to 1$. As $\beta \to 1$, C_{0u}^{sp} takes large negative values and Matlab exhibits numerical instabilties as this limit is approached.

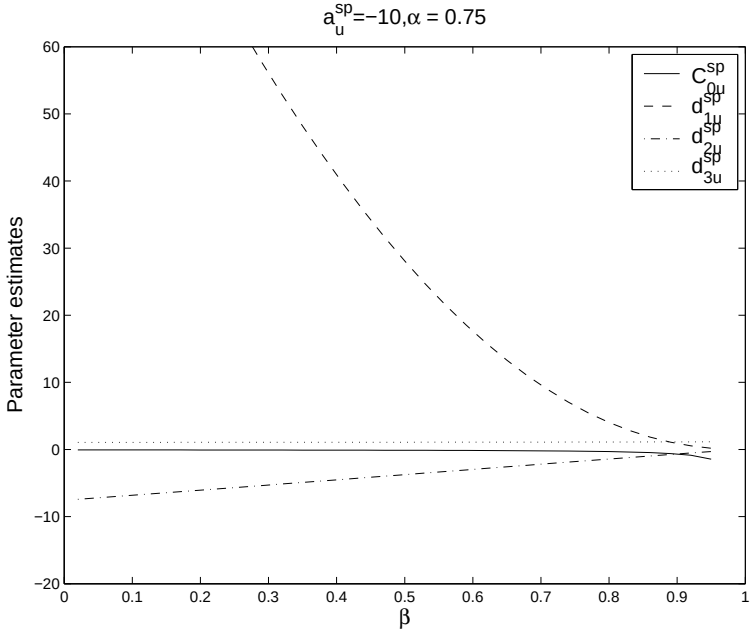

Figure 3-7: Estimates of the far-field constants C_{0u}^{sp}, d_{1u}^{sp}, d_{2u}^{sp}, d_{3u}^{sp} for a fixed large $a_u^{sp} = -10$ and $\alpha = 0.75$. The IVP was solved with $\xi_0 = 10^{-7}$, $\xi_\infty = 10^{35}$, the large values of ξ_∞ required as $\beta \to 1$. As $-a_u^{sp}$ increases in size past $O(10)$ the value of d_{1u}^{sp} increases in size as $\beta \to 0$. In the limit as $\beta \to 1$ numerical instability is more apparent than for smaller values of $-au^{sp}$.

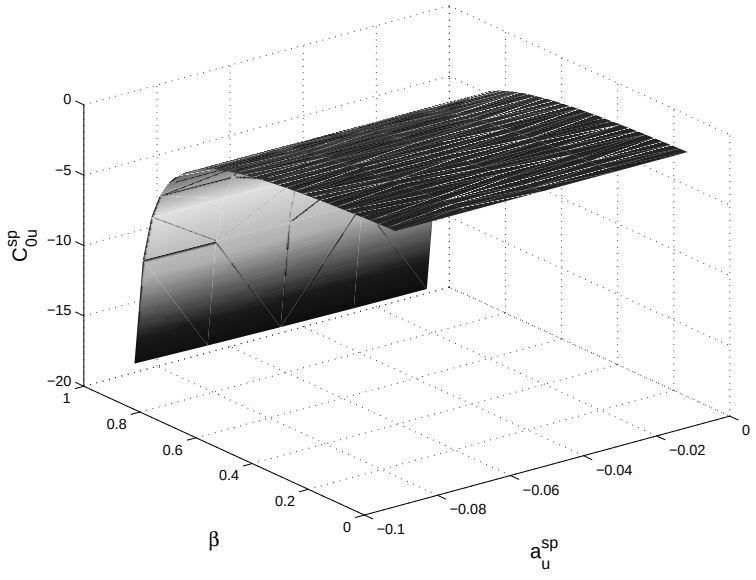

Figure 3-8: Estimate of the far-field constants C_{0u}^{sp} for varying a_u^{sp}, β and fixed $\alpha = 0.75$. The IVP was solved with $\xi_0 = 10^{-7}$, $\xi_\infty = 10^{35}$. A surface plot is given with $-a_u^{sp}$ varying between $[-0.01, -0.09]$ and β in $[0.02, 0.95]$.

(a) Convergence for fixed ξ_0 and increasing ξ_∞ for the natural stress upstream constants

$a_u^{sp} = -1$, $\alpha = 2/3$, $\beta = 1/9$ $\xi_0 = 10^{-7}$					
	C_{0u}^{sp} estimates	d_{1u}^{sp} estimates	d_{2u}^{sp} estimates		d_{3u}^{sp} estimates
ξ_∞	$f\xi^{\alpha-3}$	$\frac{2}{(3-\alpha)^2(C_{0u}^{sp})^2}$	$m\xi^{1-\alpha}$	$\frac{C_{1u}^{sp}}{2(3-\alpha)C_{0u}^{sp}}$	$(3-\alpha)^2(C_{0u}^{sp})^2 n\xi^{2-2\alpha}$
10^2	-0.425227	2.031588	-0.979751	-1.007866	1.314828
10^3	-0.433632	1.953588	-0.978294	-0.988329	1.389040
10^4	-0.437245	1.921437	-0.977196	-0.980163	1.414183
10^5	-0.438371	1.911579	-0.976840	-0.977645	1.421291
10^6	-0.438683	1.908859	-0.976741	-0.976950	1.423152
10^7	-0.438765	1.908148	-0.976715	-0.976767	1.423621

(b) Convergence for fixed ξ_∞ and decreasing ξ_∞ for the natural stress upstream constants

$a_u^{sp} = -1$, $\alpha = 2/3$, $\beta = 1/9$ $\xi_\infty = 10^7$					
	C_{0u}^{sp} estimates	d_{1u}^{sp} estimates	d_{2u}^{sp} estimates		d_{3u}^{sp} estimates
ξ_0	$f\xi^{\alpha-3}$	$\frac{2}{(3-\alpha)^2(C_{0u}^{sp})^2}$	$m\xi^{1-\alpha}$	$\frac{C_{1u}^{sp}}{2(3-\alpha)C_{0u}^{sp}}$	$(3-\alpha)^2(C_{0u}^{sp})^2 n\xi^{2-2\alpha}$
10^{-2}	-0.438279	1.912381	-0.977798	-0.977850	1.422963
10^{-3}	-0.438717	1.908564	-0.976821	-0.976874	1.423556
10^{-4}	-0.438760	1.908191	-0.976726	-0.976778	1.423615
10^{-5}	-0.438765	1.908153	-0.976716	-0.976769	1.423620
10^{-6}	-0.438765	1.908148	-0.976715	-0.976767	1.423621
10^{-7}	-0.438765	1.908148	-0.976715	-0.976767	1.423621

Table 3.2: Table showing convergence for Natural stress constants C_{0u}^{sp}, d_{1u}^{sp}, d_{2u}^{sp} and d_{3u}^{sp} to six decimal places. For (a), ξ_0 is fixed with varying ξ_∞. Estimates for d_{3u}^{sp} and d_{1u}^{sp} converge slower than C_{0u}^{sp} and d_{2u}^{sp} for smaller values of ξ_∞. The second table (b) fixes ξ_∞ for varying ξ_0. Convergence for all four constants is accurate to six decimal places when $\xi_0 = 10^{-6}$ with the value of ξ_∞ being more important. The estimates for d_{1u}^{sp} and d_{2u}^{sp} (with $C_{4u} = 0$) are found from (3.167), with an additional check on d_{2u}^{sp} from (3.175). Estimating d_{3u}^{sp} from (3.167) is complicated since determining C_{5u} from the Cartesian formulation is fraught with numerical difficulty as discussed earlier, the estimate for this constant again comes from rearranging the last expression in (3.175).

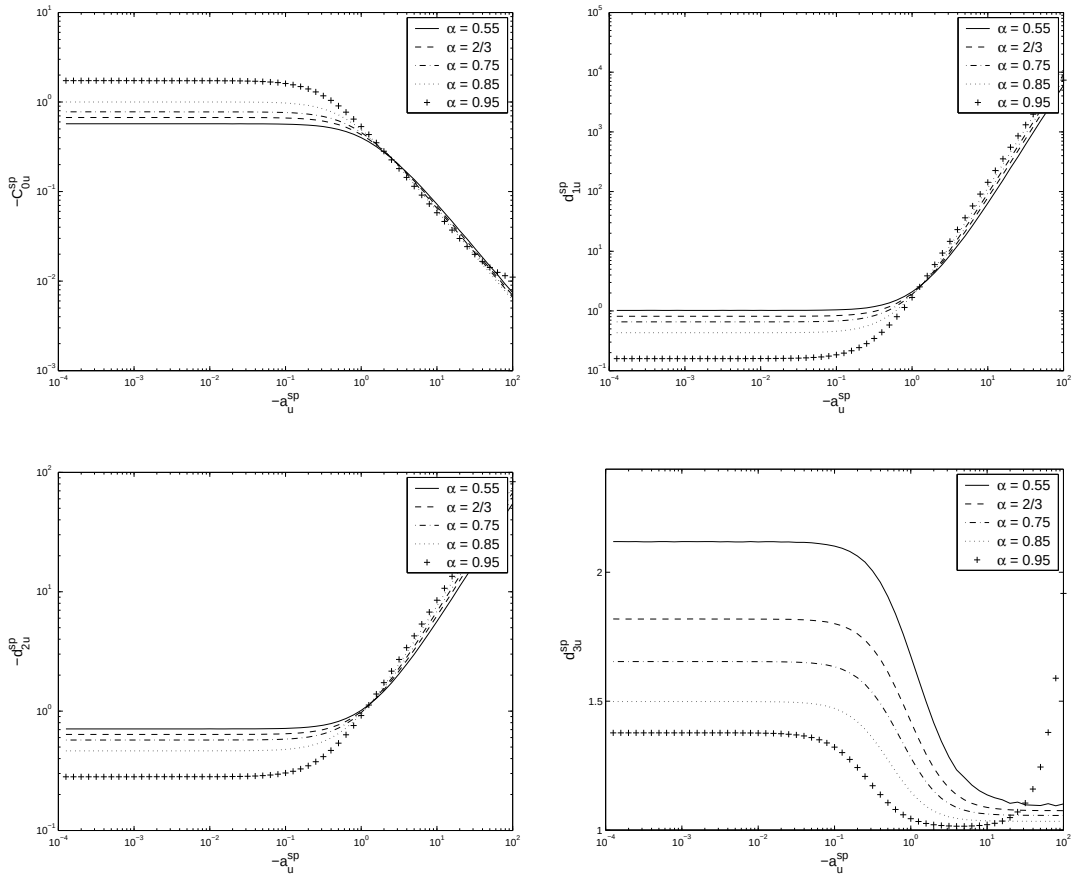

Figure 3-9: Solution profiles for $\beta = 0.1$. Estimates of the upstream far-field similarity parameters, varying the wall similarity parameter a_u^{sp} for selected corner angle values α. The IVP was solved with $\xi_0 = 10^{-6}$, $\xi_\infty = 10^{35}$. Numerical instability is seen for when $-a_u^{sp}$ is $O(10^2)$ for large values of α, especially for d_{3u}^{sp}.

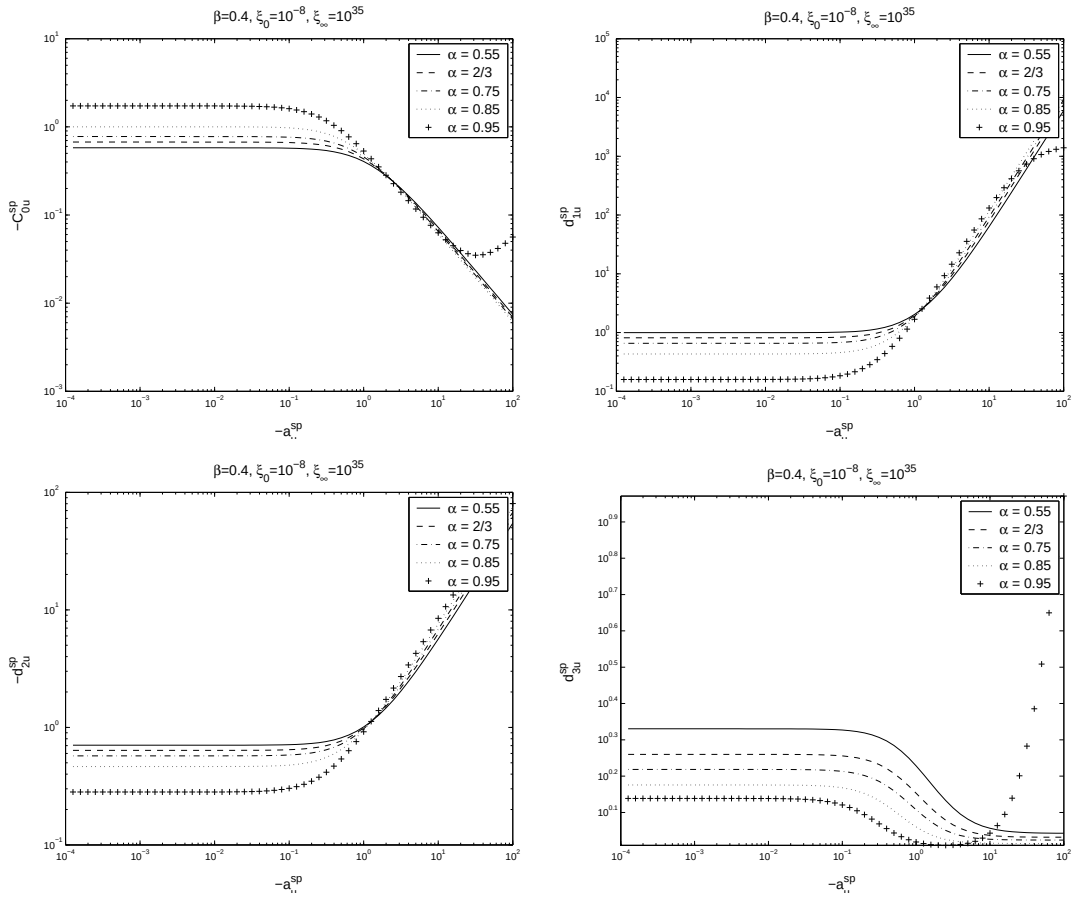

Figure 3-10: Solution profiles for $\beta = 0.4$. Estimates of the upstream far-field similarity parameters, varying the wall similarity parameter a_u^{sp} for selected corner angle values α. The IVP was solved with $\xi_0 = 10^{-8}$, $\xi_\infty = 10^{35}$. Numerical instability is seen for when $-a_u^{sp}$ is $O(10^2)$ for large values of α, especially for d_{3u}^{sp}.

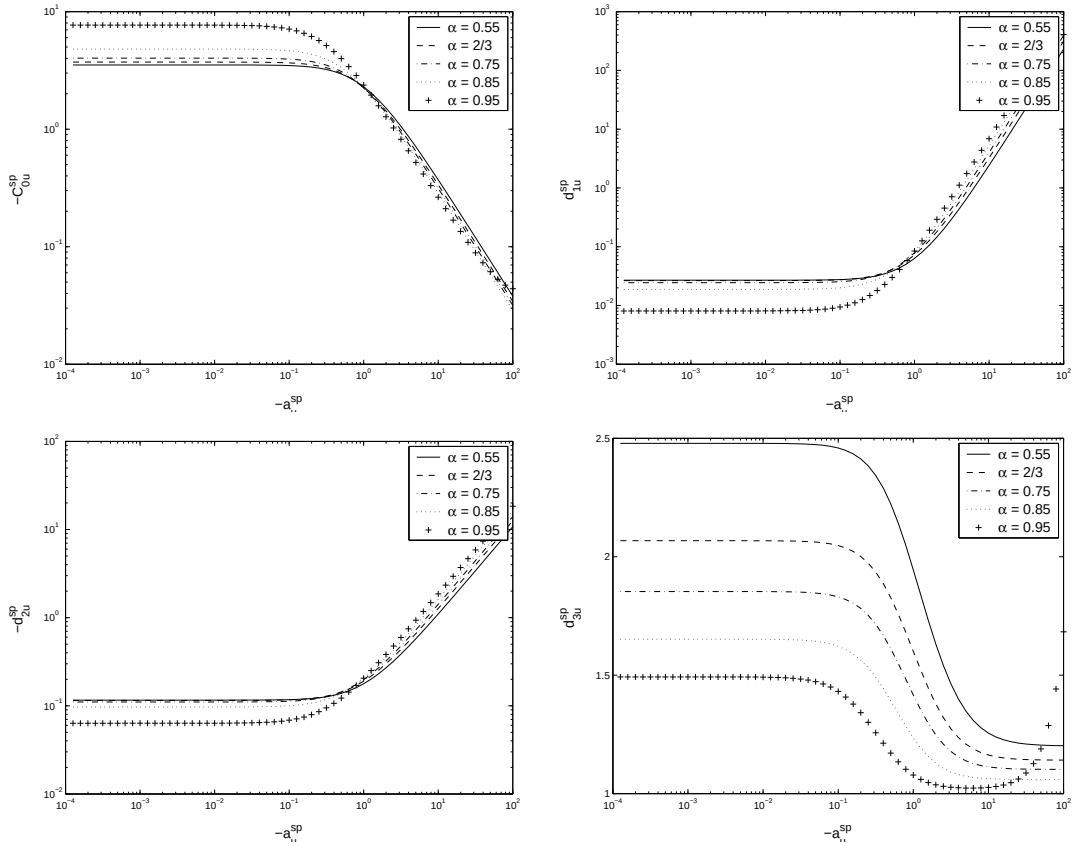

Figure 3-11: Solution profiles for $\beta = 0.8$. Estimates of the upstream far-field similarity parameters, varying the wall similarity parameter a_u^{sp} for selected corner angle values α. The IVP was solved with $\xi_0 = 10^{-9}$, $\xi_\infty = 10^{40}$. Numerical instability is seen for when $-a_u^{sp}$ is $O(10^2)$ for large values of α, especially for d_{3u}^{sp}.

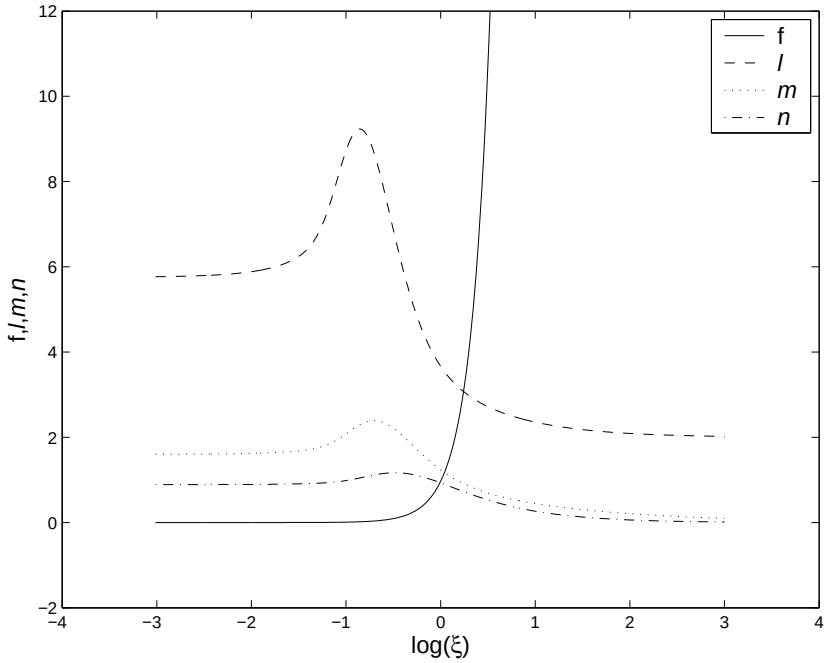

(a) $a_u^{sp} = -1$, $\alpha = 2/3$, $\beta = 1/9$

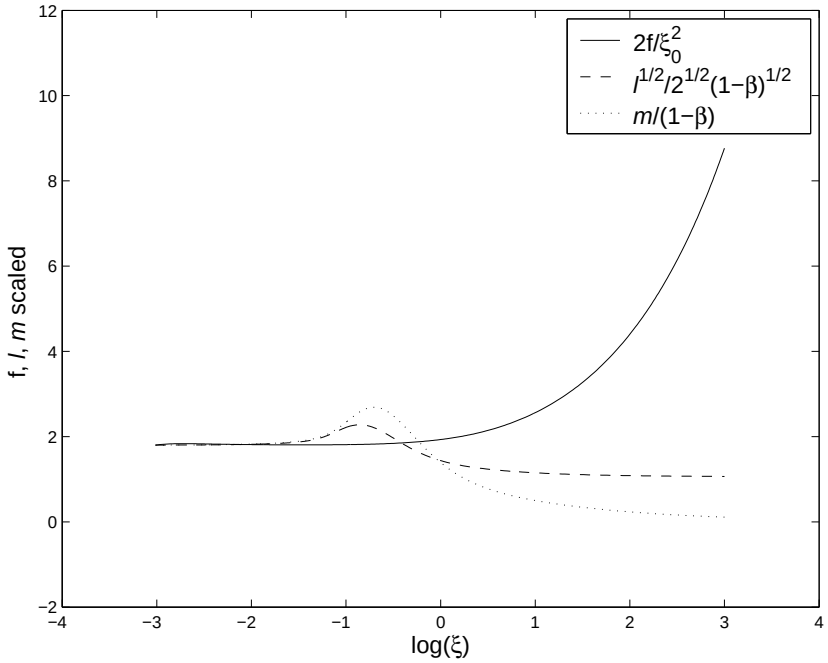

(b) $a_u^{sp} = -1$, $\alpha = 2/3$, $\beta = 1/9$

Figure 3-12: Downstream solutions on a restricted domain with $a_u^{sp} = -1$, $\alpha = 2/3$, $\beta = 1/9$. Residual errors were 9.956×10^{-4} for the BVP with $\xi_0 = 1.65 \times 10^{-4}$, $\xi_\infty = 10^3$. Figure 3-12(a) shows solution profiles, 3-12(b) the behaviour scaled with ξ_0. All three approximations give estimates for $a_d^{sp} \sim 1.803130515942835$ that agree to 15 d.p.

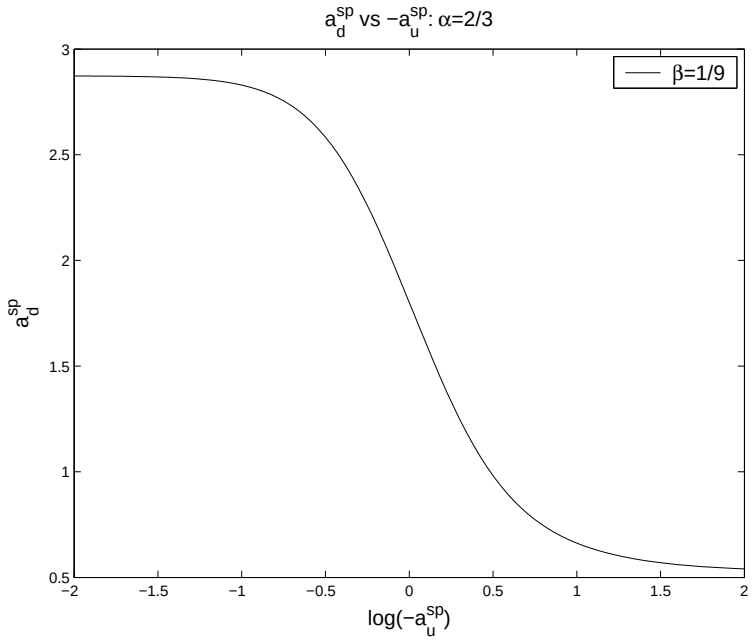

Figure 3-13: Plot showing a_d verses a_u for $\beta = 1/9$.

Chapter 4

Re-entrant corner flow: parameter regimes

The previous chapter has described a similarity solution for the Oldroyd-B fluid at a re-entrant corner where the Weissenberg number has been $O(1)$. Here we investigate the flow in the limits of low and high Weissenberg number limits, where the scalings (3.3) break down. The re-entrant corner UCM flow has been considered in the high and low Weissenberg limiting cases by Evans [19]. The work here is based on that analysis, and is extended here to the Oldroyd-B model (the natural stress formulation is also provided). We also consider the Newtonian limit $\beta \to 1$ (with We=O(1)) which is singular. At the end of chapter we briefly remark as well on the UCM limit $\beta \to 0$.

4.1 The low Weissenberg limit: $We \ll 1, \beta \in [0, 1)$

4.1.1 Introduction to the problem

We are interested in the asymptotic structure of the equations

$$\begin{aligned} &\nabla.\mathbf{v} = 0, \quad \text{Re } (\mathbf{v}.\nabla)\mathbf{v} = -\nabla p + \nabla.\mathbf{T}, \\ &\mathbf{T}^p + \text{We } \overset{\triangledown}{\mathbf{T}^p} = 2(1-\beta)\mathbf{D}, \quad \mathbf{T}^s = 2\beta\mathbf{D}, \quad \mathbf{T} = \mathbf{T}^p + \mathbf{T}^s, \end{aligned} \tag{4.1}$$

where we have written the stress tensor $\mathbf{T}$ to be a combination of the polymer stress $\mathbf{T}^p$ and solvent stress $\mathbf{T}^s$. This is useful for when considering the limiting case $\beta \to 1$, so this formulation is retained for the Weissenberg limiting cases as well. The inertial terms in the momentum equation are found to be subdominant for all asymptotic regions close to the corner, so are omitted. The x, y axes are aligned along the walls with usual no-slip and no normal velocity boundary conditions at the walls prescribed.

The problem setup is similar to the previous chapter, which is referred back to when appropriate. To begin the analysis, we consider the set of equations (4.1) and can naively set We = 0 to see what kind of flow we expect. Our stress equations become

$$\mathbf{T}^p = 2(1-\beta)\mathbf{D}, \quad \mathbf{T}^s = 2\beta\mathbf{D}, \quad \mathbf{T} = \mathbf{T}^p + \mathbf{T}^s = 2\mathbf{D}. \tag{4.2}$$

At distances away from the corner, it is noted in [55] that the velocity gradient and viscous stresses are zero, corresponding to the zero Weissenberg limit, the dominant behaviour therefore being described by the Stokes equation. The results of 2.4 will be of use here. This Newtonian solution behaviour is expected to hold until the point at which the Weissenberg number interacts with the length scale away from the corner where a fuller balance in the governing equations will result. We expect the interaction to give three sets of core and boundary regions represented in figure 4-1. The exterior region gives Newtonian flow, close to the corner we expect Oldroyd-B flow We = $O(1)$ of chapter 3 to dominate, with an intermediate region occuring where a fuller balance of terms is needed due to the upper convected derivative becoming important. This intermediate region is found to be just a matching region between the outer and inner regions, with any subsequent intermediate boundary layer arbitrary due to all terms found to have been retained.

4.1.2 The exterior regions: $We^{\frac{1}{1-\lambda_0}} \ll r \ll 1$

Discussed in the introduction of the problem, the exterior regions at leading order recover Newtonian flow behaviour for the radial distance $r = O(1)$. The Newtonian solution given in chapter (2) will apply here when $r \ll 1$ (but obviously still big enough to be in the exterior region) with important results

$$\text{as } r \to 0, \quad \psi = c_0 r^{1+\lambda_0} f_0(\theta), \quad \mathbf{T} = 2\mathbf{D}, \tag{4.3}$$

where the exponent λ_0 satisfies equation (2.78) (a numerical plot is in figure (2-3)) and the function $f_0(\theta)$ is found in (2.81). The pressure is given in equation (2.86). Critically, for re-entrant corner flow $\lambda_0 < 1$, and from these solutions we may obtain the order of magnitude estimates for the exterior core region as

$$\begin{aligned} \text{for } r = O(1): &\quad \psi = O(1), && \mathbf{T} = O(1), \\ \text{as } r \to 0: &\quad \psi = O(r^{1+\lambda_0}), && \mathbf{T} = O(r^{-1+\lambda_0}). \end{aligned} \tag{4.4}$$

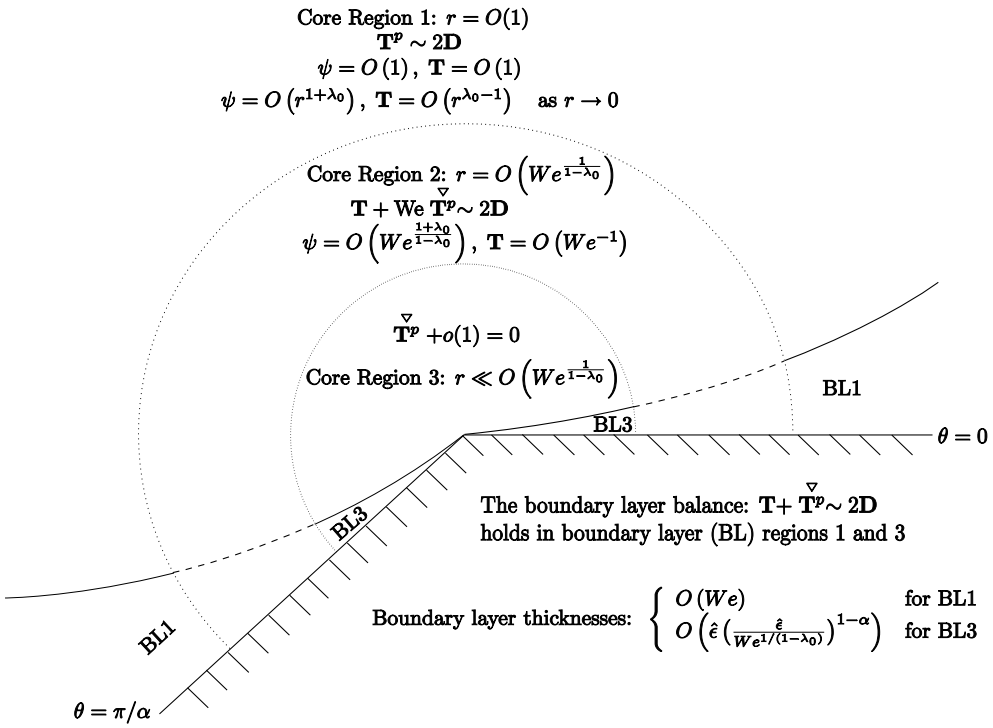

Figure 4-1: Illustration of the main asymptotic regions near to the re-entrant corner in the limit We $\to 0$. Shown are the dominant balances in the constitutive equations for the three core regions. Boundary region 3 is needed due to core region 3 not giving viscometric behaviour at the wall, similarly with the core and boundary layer regions 1. The intermediate region holds up to the walls, hence any boundary layer region in between the two mentioned above would be arbitrary. The exterior regions occur for $\mathrm{We}^{\frac{1}{1-\lambda_0}} \ll r \ll 1$ where Newtonian flow is found. The intermediate region occur on the length scale $r = \mathrm{We}^{\frac{1}{1-\lambda_0}}$ where the upper convected derivative is retrieved. For the inner regions we have $r \ll \mathrm{We}^{\frac{1}{1-\lambda_0}}$, in which we expect Oldroyd-B, We $= O(1)$ behaviour to hold (the linear stress terms and deformation tensor components become subdominant).

Scaling into the core region with the parameter $\hat{\epsilon}$, $\mathrm{We}^a \ll \hat{\epsilon} \ll 1$ with a to be determined, the distance r scales like $r = \hat{\epsilon}\hat{R}^*$ with the remaining scalings being

$$\psi = \hat{\epsilon}^{1+\lambda_0}\hat{\psi}^*, \quad \mathbf{T}^p = \hat{\epsilon}^{-1+\lambda_0}\hat{\mathbf{T}}^{p*}, \quad \mathbf{T}^s = \hat{\epsilon}^{-1+\lambda_0}\hat{\mathbf{T}}^{s*}, \quad p = \hat{\epsilon}^{-1+\lambda_0}\hat{p}^*, \quad \mathbf{v} = \hat{\epsilon}^{\lambda_0}\hat{\mathbf{v}}^*. \tag{4.5}$$

The governing equations are

$$\text{Re}\ \hat{\epsilon}^{2\lambda_0}\hat{\mathbf{v}}^*\cdot\hat{\nabla}^*\hat{\mathbf{v}}^* = -\hat{\epsilon}^{-1+\lambda_0}\hat{\nabla}^* p^* + \hat{\epsilon}^{-1+\lambda_0}\hat{\nabla}^*\cdot\left(\hat{\mathbf{T}}^{p*}+\hat{\mathbf{T}}^{s*}\right), \quad \hat{\nabla}^*\cdot\hat{\mathbf{v}}^* = 0,$$

$$\hat{\psi}^* = c_0\hat{R}^{*(1+\lambda_0)}f_0(\theta), \quad \hat{\mathbf{T}}^{p*} + \text{We}\ \hat{\epsilon}^{-1+\lambda_0}\overset{\triangledown}{\hat{\mathbf{T}}}^{p*} = 2(1-\beta)\hat{\mathbf{D}}^*, \quad \hat{\mathbf{T}}^{s*} = 2\beta\hat{\mathbf{D}}^*. \tag{4.6}$$

As $\theta \to 0$, fixing $f_0(0) = 2$, the behaviours of the stream function and stresses as the wall is approached are

$$\hat{\psi}^* = c_0\hat{X}^{*(\lambda_0-1)}\hat{Y}^{*2}, \quad \hat{p}^* = p_0\hat{X}^{*(\lambda_0-1)}, \tag{4.7}$$

$$\hat{\mathbf{T}}^{s*}_{11} = 4\beta c_0(\lambda_0-1)\hat{X}^{*(\lambda_0-2)}\hat{Y}^*, \quad \hat{\mathbf{T}}^{s*}_{12} = 2\beta c_0\hat{X}^{*(\lambda_0-1)}, \quad \hat{\mathbf{T}}^{s*}_{22} = -\hat{\mathbf{T}}^{s*}_{11}, \tag{4.8}$$

$$\hat{\mathbf{T}}^{p*}_{11} = 4(1-\beta)c_0(\lambda_0-1)\hat{X}^{*(\lambda_0-2)}\hat{Y}^*, \quad \hat{\mathbf{T}}^{p*}_{12} = 2(1-\beta)c_0\hat{X}^{*(\lambda_0-1)}, \quad \hat{\mathbf{T}}^{p*}_{22} = -\hat{\mathbf{T}}^{p*}_{11}. \tag{4.9}$$

Viscometric behaviour isn't recovered in this limit, the boundary layer scalings are

$$\begin{aligned}
&\hat{X}^* = \hat{X}, \quad \hat{Y}^* = \hat{\delta}\hat{Y}, \quad \hat{\psi}^* = \hat{\delta}^2\hat{\Psi}, \quad \hat{p}^* = \hat{p},\\
&\hat{T}^{s*}_{11} = \hat{\delta}\hat{T}^s_{11}, \quad \hat{T}^{s*}_{12} = \hat{T}^s_{12}, \quad \hat{T}^{s*}_{22} = \hat{\delta}\hat{T}^s_{22},\\
&\hat{T}^{p*}_{11} = \hat{\delta}\hat{T}^p_{11}, \quad \hat{T}^{p*}_{12} = \hat{T}^p_{12}, \quad \hat{T}^{p*}_{22} = \hat{\delta}\hat{T}^p_{22}.
\end{aligned} \tag{4.10}$$

With these scalings the governing momentum equations and solvent stresses are

$$\text{Re}\ \hat{\epsilon}^{1-\lambda_0}\delta^2\hat{\mathbf{v}}\cdot\hat{\nabla}\hat{u} = -\frac{\partial\hat{p}}{\partial\hat{X}} + \frac{\partial}{\partial\hat{X}}\left(\delta\hat{T}^p_{11}+\delta\hat{T}^p_{11}\right) + \frac{1}{\delta}\frac{\partial}{\partial\hat{Y}}\left(\hat{T}^p_{12}+\hat{T}^s_{12}\right), \tag{4.11}$$

$$\text{Re}\ \hat{\epsilon}^{1-\lambda_0}\delta^3\hat{\mathbf{v}}\cdot\hat{\nabla}\hat{v} = -\frac{1}{\delta}\frac{\partial\hat{p}}{\partial\hat{Y}} + \frac{\partial}{\partial\hat{X}}\left(\hat{T}^p_{12}+\delta\hat{T}^s_{12}\right) + \frac{\partial}{\partial\hat{Y}}\left(\hat{T}^p_{22}+\hat{T}^s_{22}\right), \tag{4.12}$$

$$\hat{T}^s_{11} = 2\beta\frac{\partial^2\hat{\Psi}}{\partial\hat{X}\partial\hat{Y}}, \quad \hat{T}^s_{12} = \beta\left(\frac{\partial^2\hat{\Psi}}{\partial\hat{Y}^2} - \hat{\delta}^2\frac{\partial^2\hat{\Psi}}{\partial\hat{X}^2}\right), \quad \hat{T}^s_{22} = -2\beta\frac{\partial^2\hat{\Psi}}{\partial\hat{X}\partial\hat{Y}}, \tag{4.13}$$

and constitutive equations

$$\hat{T}^p_{11} + \text{We}\ \hat{\delta}\hat{\epsilon}^{\lambda_0-1}\left(\frac{\partial\hat{\Psi}}{\partial\hat{Y}}\frac{\partial\hat{T}^p_{11}}{\partial\hat{X}} - \frac{\partial\hat{\Psi}}{\partial\hat{X}}\frac{\partial\hat{T}^p_{11}}{\partial\hat{Y}} - \frac{2}{\hat{\delta}^2}\frac{\partial^2\hat{\Psi}}{\partial\hat{Y}^2}\hat{T}^p_{12} - 2\frac{\partial^2\hat{\Psi}}{\partial\hat{X}\partial\hat{Y}}\hat{T}^p_{11}\right) = 2(1-\beta)\frac{\partial^2\hat{\Psi}}{\partial\hat{X}\partial\hat{Y}}, \tag{4.14}$$

$$\hat{T}^p_{22} + \text{We}\ \hat{\delta}\hat{\epsilon}^{\lambda_0-1}\left(\frac{\partial\hat{\Psi}}{\partial\hat{Y}}\frac{\partial\hat{T}^p_{22}}{\partial\hat{X}} - \frac{\partial\hat{\Psi}}{\partial\hat{X}}\frac{\partial\hat{T}^p_{22}}{\partial\hat{Y}} + 2\frac{\partial^2\hat{\Psi}}{\partial\hat{X}^2}\hat{T}^p_{12} + 2\frac{\partial^2\hat{\Psi}}{\partial\hat{X}\partial\hat{Y}}\hat{T}^p_{22}\right) = -2(1-\beta)\frac{\partial^2\hat{\Psi}}{\partial\hat{X}\partial\hat{Y}}, \tag{4.15}$$

$$\hat{T}^p_{12} + \text{We}\ \hat{\delta}\hat{\epsilon}^{\lambda_0-1}\left(\frac{\partial\hat{\Psi}}{\partial\hat{Y}}\frac{\partial\hat{T}^p_{12}}{\partial\hat{X}} - \frac{\partial\hat{\Psi}}{\partial\hat{X}}\frac{\partial\hat{T}^p_{12}}{\partial\hat{Y}} + \hat{\delta}^2\frac{\partial^2\hat{\Psi}}{\partial\hat{X}^2}\hat{T}^p_{11} - \frac{\partial^2\hat{\Psi}}{\partial\hat{Y}^2}\hat{T}^p_{22}\right) = (1-\beta)\left(\frac{\partial^2\hat{\Psi}}{\partial\hat{Y}^2} - \hat{\delta}^2\frac{\partial^2\hat{\Psi}}{\partial\hat{X}^2}\right). \tag{4.16}$$

The only term we may recover from the upper convected derivative whilst still having a thin boundary layer is in the $\hat{T}^p_{11}$ equation, and sets $\hat{\delta} = \text{We}\ \hat{\epsilon}^{\lambda_0-1}$. At leading order then we obtain

$$\hat{T}^s_{11} = 2\beta\frac{\partial^2\hat{\Psi}}{\partial\hat{X}\partial\hat{Y}}, \quad \hat{T}^s_{12} = \beta\left(\frac{\partial^2\hat{\Psi}}{\partial\hat{Y}^2}\right), \quad \hat{T}^s_{22} = -2\beta\frac{\partial^2\hat{\Psi}}{\partial\hat{X}\partial\hat{Y}}, \tag{4.17}$$

$$\hat{T}^p_{11} - 2\frac{\partial^2\hat{\Psi}}{\partial\hat{Y}^2}\hat{T}^p_{12} = 2(1-\beta)\frac{\partial^2\hat{\Psi}}{\partial\hat{X}\partial\hat{Y}}, \quad \hat{T}^p_{22} = -2(1-\beta)\frac{\partial^2\hat{\Psi}}{\partial\hat{X}\partial\hat{Y}}, \quad \hat{T}^p_{12} = (1-\beta)\frac{\partial^2\hat{\Psi}}{\partial\hat{Y}^2}, \tag{4.18}$$

$$0 = \frac{\partial\hat{p}}{\partial\hat{Y}}, \quad \frac{\partial}{\partial\hat{Y}}\left(\hat{T}^p_{12} + \hat{T}^s_{12}\right) = 0. \tag{4.19}$$

Solving the last equation in (4.19) for $\hat{\Psi}$ determines $\hat{\Psi} = \frac{1}{2}a(\hat{X})\hat{Y}^2$ where $a(\hat{X})$ a function arising from the integration (no $O(\hat{Y}^1)$ or $O(\hat{Y}^0)$ terms due to the boundary conditions). Matching with the core solution (4.7)–(4.9) determines $a(\hat{X}) = 2c_0\hat{X}^{\lambda_0-1}$. Hence

$$\hat{\Psi} = c_0\hat{X}^{\lambda_0-1}\hat{Y}^2, \tag{4.20}$$

holds throughout boundary layer one. As a note, for the boundary layer to be small

$$\hat{\delta} = \text{We}\ \hat{\epsilon}^{\lambda_0-1} \ll 1 \implies \hat{\epsilon} \gg \text{We}^{\ \frac{1}{1-\lambda_0}}, \tag{4.21}$$

giving a lower bound on $\hat{\epsilon}$ where core and boundary layer regions one are applicable.

The exterior regions: natural stress basis

We can also formulate the problem in the natural stress variables. From (2.44)–(2.46), we have

$$\lambda = (1-\beta)\frac{1}{\mathrm{We}\,(u^2+v^2)} + \frac{u^2}{(u^2+v^2)^2}T^p_{11} + \frac{2uv}{(u^2+v^2)^2}T^p_{12} + \frac{v^2}{(u^2+v^2)^2}T^p_{22}, \quad (4.22)$$

$$\mu = -\frac{uv}{(u^2+v^2)}T^p_{11} + \frac{uv}{(u^2+v^2)}T^p_{22} + \frac{(u^2-v^2)}{(u^2+v^2)}T^p_{12}, \quad (4.23)$$

$$\nu = \frac{(1-\beta)}{\mathrm{We}}(u^2+v^2) + u^2T^p_{22} + v^2T^p_{11} - 2uvT^p_{12}. \quad (4.24)$$

For small Weissenberg, the first terms of λ and ν dominate where μ retains all the terms. In (2.49)-(2.51), in the second constitutive equation for μ we therefore pull back the term involving $\mathbf{w}$. The balance $\mathbf{T}^p = 2(1-\beta)\mathbf{D}$ holds in the core region in Cartesian variables, substitution of this into (4.22)-(4.24) will give us the core equations in natural stress. To this end we find

$$\lambda = (1-\beta)\frac{1}{\mathrm{We}\,(u^2+v^2)} + \frac{(1-\beta)}{(u^2+v^2)^4}\mathbf{v}\cdot\nabla(u^2+v^2), \quad (4.25)$$

$$\mu = -(1-\beta)(u^2+v^2)\nabla\cdot\mathbf{w}, \quad (4.26)$$

$$\nu = \frac{(1-\beta)}{\mathrm{We}}(u^2+v^2) - (1-\beta)\mathbf{v}\cdot\nabla(u^2+v^2). \quad (4.27)$$

Since We is small, at leading order in We,

$$\lambda \sim (1-\beta)\frac{1}{\mathrm{We}\,(u^2+v^2)}, \quad \mu \sim -(1-\beta)(u^2+v^2)\nabla\cdot\mathbf{w}, \quad \nu \sim \frac{(1-\beta)}{\mathrm{We}}(u^2+v^2). \quad (4.28)$$

We may also obtain (4.25)–(4.27) by substituting the behvaiours (4.28) into the governing equations (2.49)-(2.51).

Scaling into the boundary layer with

$$x = \hat{X}, \quad y = \hat{\delta}\hat{Y}, \quad \psi = \hat{\delta}^2\hat{\Psi}, \quad u = \hat{\delta}\hat{u}, \quad v = \hat{\delta}^2\hat{v},$$
$$\lambda = \hat{\delta}^{-2}\hat{\lambda}, \quad \mu = \hat{\mu}, \quad \nu = \hat{\delta}^2\hat{\nu}, \quad (4.29)$$

the governing equations become

$$\hat{\lambda} + \mathrm{We}\hat{\delta}\left(\hat{\mathbf{v}}\cdot\hat{\nabla}\hat{\lambda} + 2\hat{\delta}^{-1}\hat{\mu}\nabla\cdot\hat{\mathbf{w}}\right) = \frac{(1-\beta)}{\mathrm{We}\left(\hat{\delta}^2\hat{u}^2 + \hat{\delta}^4\hat{v}^2\right)}, \tag{4.30}$$

$$\hat{\mu} + \mathrm{We}\hat{\delta}\left(\hat{\mathbf{v}}\cdot\hat{\nabla}\hat{\mu} + \hat{\nu}\hat{\nabla}\cdot\hat{\mathbf{w}}\right) = 0, \tag{4.31}$$

$$\hat{\nu} + \mathrm{We}\left(\hat{\mathbf{v}}\cdot\hat{\nabla}\hat{\nu}\right) = \frac{(1-\beta)}{\mathrm{We}}(\hat{\delta}^2\hat{u}^2 + \hat{\delta}^4\hat{v}^2). \tag{4.32}$$

From this, we can rearrange the boundary layer equation (4.32) for $\hat{\nu}$, then substitute into (4.31) for $\hat{\mu}$, giving us an expansion again in terms of We. At leading order,

$$\hat{\mu} = -(1-\beta)\frac{\partial}{\partial\hat{Y}}\left(\frac{1}{\hat{u}}\right)\hat{u}^2 = (1-\beta)\hat{u}_{\hat{Y}} + O(\mathrm{We}^2). \tag{4.33}$$

Similarly for $\hat{\lambda}$, the two term boundary layer expansion is

$$\hat{\lambda} = \frac{(1-\beta)}{\mathrm{We}\hat{u}^2} - \hat{\delta}(1-\beta)\hat{\mathbf{v}}\cdot\nabla\left(\frac{1}{\hat{u}^2}\right) - 2\mathrm{We}\hat{\mu}\nabla\cdot\hat{\mathbf{w}} + O(\mathrm{We}^3), \tag{4.34}$$

and finally for $\hat{\nu}$,

$$\hat{\nu} = (1-\beta)\frac{1}{\mathrm{We}}\hat{u}^2 - (1-\beta)\hat{\mathbf{v}}\cdot\nabla\left(\hat{u}^2\right) + O(\mathrm{We}). \tag{4.35}$$

The boundary layer expansions are after substituting in for $\hat{\delta}$,

$$\hat{\mu} = (1-\beta)\hat{u}_{\hat{Y}} + O(\mathrm{We}^2), \tag{4.36}$$

$$\hat{\lambda} = (1-\beta)\frac{1}{\mathrm{We}\,(\hat{u}^2)} + 2\mathrm{We}(1-\beta)\left(\frac{\hat{u}_{\hat{X}}}{\hat{u}^2} + \frac{\hat{v}\hat{u}_{\hat{Y}}}{\hat{u}^3}\right) - 2\mathrm{We}(1-\beta)\frac{\hat{u}_{\hat{Y}}^2}{\hat{u}^2} + O(\mathrm{We}^3), \tag{4.37}$$

$$\hat{\nu} = (1-\beta)\frac{1}{\mathrm{We}}\hat{u}^2 - 2(1-\beta)\hat{u}\left(\hat{u}\hat{u}_{\hat{X}} + \hat{v}\hat{v}_{\hat{Y}}\right) + O(\mathrm{We}) \tag{4.38}$$

and at leading order,

$$\hat{\lambda} \sim (1-\beta)\frac{1}{\mathrm{We}\ \hat{u}^2}, \quad \hat{\mu} \sim (1-\beta)\hat{u}_{\hat{Y}}, \quad \hat{\nu} \sim \frac{(1-\beta)}{\mathrm{We}}\hat{u}^2. \tag{4.39}$$

We can verify this, by writing (2.44)-(2.46) in terms of boundary layer variables. Then

we have

$$\hat{\lambda} = \frac{(1-\beta)}{\mathrm{We}\left(\hat{u}^2+\hat{\delta}^2\hat{v}^2\right)} + \hat{\delta}\frac{\hat{u}^2}{\left(\hat{u}^2+\hat{\delta}^2\hat{v}^2\right)^2}\hat{T}^p_{11} + \frac{2\hat{\delta}\hat{u}\hat{v}}{\left(\hat{u}^2+\hat{\delta}^2\hat{v}^2\right)^2}\hat{T}^p_{12} + \frac{\hat{v}^2\hat{\delta}^3}{\left(\hat{u}^2+\hat{\delta}^2\hat{v}^2\right)^2}\hat{T}^p_{22}, \tag{4.40}$$

$$\hat{\mu} = -\frac{\hat{\delta}^2\hat{u}\hat{v}}{\left(\hat{u}^2+\hat{\delta}^2\hat{v}^2\right)}\hat{T}^p_{11} + \frac{\hat{\delta}^2\hat{u}\hat{v}}{\left(\hat{u}^2+\hat{\delta}^2\hat{v}^2\right)}\hat{T}^p_{22} + \frac{(\hat{u}^2-\hat{\delta}^2\hat{v}^2)}{\left(\hat{u}^2+\hat{\delta}^2\hat{v}^2\right)}\hat{T}^p_{12}, \tag{4.41}$$

$$\hat{\nu} = \frac{(1-\beta)}{\mathrm{We}}(\hat{u}^2+\hat{\delta}^2\hat{v}^2) + \hat{\delta}\hat{u}^2\hat{T}^p_{22} + \hat{\delta}^3\hat{v}^2\hat{T}^p_{11} - 2\hat{\delta}\hat{u}\hat{v}\hat{T}^p_{12}. \tag{4.42}$$

Reordering these equations in terms of a expansion in $\hat{\delta}$,

$$\hat{\lambda} = (1-\beta)\frac{1}{\mathrm{We}\,(\hat{u}^2)} + \hat{\delta}\left(\frac{1}{\hat{u}^2}\hat{T}^p_{11} + \frac{2\hat{v}}{\hat{u}}\hat{T}^p_{12}\right) + O(\hat{\delta}^3), \tag{4.43}$$

$$\hat{\mu} = \frac{(\hat{u}^2-\hat{\delta}^2\hat{v}^2)}{\left(\hat{u}^2+\hat{\delta}^2\hat{v}^2\right)}\hat{T}^p_{12} + O(\hat{\delta}^2), \tag{4.44}$$

$$\hat{\nu} = \frac{(1-\beta)}{\mathrm{We}}\hat{u}^2 + \hat{\delta}\left(\hat{u}^2\hat{T}^p_{22} - 2\hat{u}\hat{v}\hat{T}^p_{12}\right) + O(\hat{\delta}^3), \tag{4.45}$$

and substituting in the boundary layer equations from the Cartesian variables which are

$$\hat{T}^p_{11} - 2\frac{\partial^2\hat{\Psi}}{\partial\hat{Y}^2}\hat{T}^p_{12} = 2(1-\beta)\frac{\partial^2\hat{\Psi}}{\partial\hat{X}\partial\hat{Y}}, \quad \hat{T}^p_{22} = -2(1-\beta)\frac{\partial^2\hat{\Psi}}{\partial\hat{X}\partial\hat{Y}}, \quad \hat{T}^p_{12} = (1-\beta)\frac{\partial^2\hat{\Psi}}{\partial\hat{Y}^2}, \tag{4.46}$$

into (4.40)–(4.42) agrees with (4.36)–(4.36).

We can see that $\hat{\lambda}$ goes very large as We $\to$ 0 , $\hat{\mu}$ is a constant in this limit throughout the core region and $\hat{\nu}$ goes to zero. This is viscometric behaviour in natural stress variables hence the exterior region analysis is complete. We know from the Newtonian Cartesian analysis that the solvent stress dominates the polymer stress for the exterior region. The natural stress basis describes the polymer stress and so it is more instructive to consider this basis for the intermediate and interior regions where the polymer stress components are important.

4.1.3 The main length scale: $r = O\left(We^{\frac{1}{1-\lambda_0}}\right)$

We now determine the length scale at which the Newtonian solution no longer persists, and the fullest balance in the constitutive equations is obtained. Considering distances from the corner of $O(\epsilon)$, with the gauge $\epsilon = \epsilon(We)$ being a small parameter whose

dependency on We is to be found. Initially, we consider an outer region away from the walls via the scalings

$$r = \epsilon R^*, \quad \psi = \gamma \Psi^*, \quad \mathbf{T}^s = \frac{\gamma}{\epsilon^2}\mathbf{T}^*, \quad \mathbf{T}^p = \frac{\gamma}{\epsilon^2}\mathbf{T}^{p*}, \quad p = \frac{\gamma}{\epsilon^2}p^*, \tag{4.47}$$

this intermediate core region holding for $R^* = O(1)$ and γ another gauge. The pressure scaling is determined to be equal to the total stress tensor scaling to achieve balance in the momentum equations. The governing equations in this region are

$$\text{Re}\ \gamma \mathbf{v}^* \cdot \nabla^* \mathbf{v}^* = -\nabla^* p^* + \nabla^* \cdot (\mathbf{T}^{p*} + \mathbf{T}^{s*}) \tag{4.48}$$

$$\mathbf{T}^{p*} + \frac{\text{We}\ \gamma}{\epsilon^2}\ \overset{\triangledown}{\mathbf{T}}{}^{p*} = 2(1-\beta)\mathbf{D}^*, \quad \mathbf{T}^{s*} = 2\beta \mathbf{D}^*. \tag{4.49}$$

Matching with core region one determines $\gamma = \epsilon^{1+\lambda_0}$. Retaining all terms in the constitutive equations implies We $\gamma = \epsilon^2$ and hence $\epsilon = \text{We}^{\,1/(1-\lambda_0)}$: the key length scale is determined. Three critical length scales are now apparent resulting from the interaction between ϵ and Wes:

- $r = O\left(We^{1/(1-\lambda_0)}\right)$: The fullest balance is able to retain all terms in (4.48) - (4.49).
- $r \gg O\left(We^{1/(1-\lambda_0)}\right)$: The linear stress terms dominate over the upper convected derivative leaving the Newtonian balance. This is the exterior region already considered.
- $r \ll O\left(We^{1/(1-\lambda_0)}\right)$: The upper convected stress derivative now dominates over the linear stress terms, and the Oldroyd-B We $= O(1)$ problem is expected to be recovered.

For the boundary layer in this region, the scalings are

$$\begin{aligned} &X^* = X, \quad Y^* = \delta Y, \quad \psi^* = \delta^2 \Psi, \quad p^* = p, \\ &T_{11}^{s*} = \delta T_{11}^s, \quad T_{12}^{s*} = T_{12}^s, \quad T_{22}^{s*} = \delta T_{22}^s, \\ &T_{11}^{p*} = \delta T_{11}^p, \quad T_{12}^{p*} = T_{12}^p, \quad T_{22}^{p*} = \delta T_{22}^p. \end{aligned} \tag{4.50}$$

However since full balance is retained in (4.48) - (4.49), δ would not be determined in the resulting equations. This gives an artificial region and so any boundary layer would be passive. Local wall asymptotic behaviour in (4.20) holds, matching with the leading order boundary layer equations in region 1 (4.17)-(4.19). For natural stress variables, the scalings (4.47) are used, along with the natural stress variable scalings of (found

from balancing terms in (2.41)–(2.43) with each other)

$$\lambda = \epsilon^{-1-\lambda_0}\lambda^*, \quad \mu = \epsilon^{\lambda_0-1}\mu^*, \quad \nu = \epsilon^{3\lambda_0-1}\nu^*. \tag{4.51}$$

Substituting this into the governing equations using $\mathrm{We} = \epsilon^{1-\lambda_0}$ yields

$$\lambda^* + \mathbf{v}^* \cdot \nabla\lambda^* + 2\mu^*\nabla \cdot \mathbf{w}^* = (1-\beta)\frac{1}{(u^{*2}+v^{*2})}, \tag{4.52}$$

$$\mu^* + \mathbf{v}^* \cdot \nabla\mu^* + \nu^*\nabla \cdot \mathbf{w}^* = 0, \tag{4.53}$$

$$\nu^* + \mathbf{v}^* \cdot \nabla\nu^* = (1-\beta)(u^{*2}+v^{*2}), \tag{4.54}$$

and so fullest balance is attained on the same length scale as found with the Cartesian basis. Again there is no need for a boundary layer for the natural stress since all terms that may contribute to viscometric behaviour are automatically included.

4.1.4 The interior regions: $r \ll We^{\frac{1}{1-\lambda_0}}$

The final regions to consider are the interior regions closest to the corner, where we expect to recover the Oldroyd-B $\mathrm{We} = O(1)$ problem due to the upper convected derivative dominating in the core. We introduce the rescaled variables

$$r = \tilde{\epsilon}\tilde{R}^*, \quad x = \tilde{\epsilon}\tilde{X}^*, \quad y = \tilde{\epsilon}\tilde{Y}^*.$$

Assuming Oldroyd-B behaviour, the stream function has the form $\psi \sim \tilde{r}^{n\alpha}$. Care is needed when scaling into the inner region since we need to consider what happens in the intermediate region also (i.e. we scale through the intermediate into the interior region). We have in the intermediate region

$$r = \epsilon R^*, \quad \psi = \epsilon^{1+\lambda_0}\psi^*, \tag{4.55}$$

In the interior region, scaling with $\tilde{\epsilon}$ we have

$$r = \tilde{\epsilon}\tilde{R}^*, \tag{4.56}$$

Hence our scalings for the stream function and velocity vector (where we have essentially scaled through through the intermediate and interior regions in one go) are

$$\psi = \epsilon^{1+\lambda_0-n\alpha}\tilde{\epsilon}^{n\alpha}\tilde{\psi}^*, \quad \mathbf{v} = \epsilon^{1+\lambda_0-n\alpha}\tilde{\epsilon}^{n\alpha-1}\tilde{\mathbf{v}}^*. \tag{4.57}$$

With the upper convected derivative dominating in this region, we can take the self similar solution found in chapter 3,

$$\psi = \tilde{C}_0 r^{n\alpha} \sin^n(\alpha\theta), \quad \mathbf{T}^p = \lambda(\psi)\mathbf{v}\mathbf{v}^T, \quad \lambda(\psi) = \tilde{C}_1 \left(\frac{\psi}{\tilde{C}_0}\right)^{\frac{2}{n}(1-n)}, \tag{4.58}$$

with $n = 3-\alpha$, which allows us to get the scalings for the pressure, stresses and natural stress variables as

$$\begin{aligned}
\mathbf{T}^p &= \epsilon^{(1+\lambda_0-2\alpha)}\tilde{\epsilon}^{2\alpha-2}\tilde{\mathbf{T}}^{*p}, \quad \mathbf{T} = \epsilon^{(1+\lambda_0-2\alpha)}\tilde{\epsilon}^{2\alpha-2}\tilde{\mathbf{T}}^{*}, \\
\mathbf{T}^s &= \epsilon^{(1+\lambda_0-n\alpha)}\tilde{\epsilon}^{n\alpha-2}\tilde{\mathbf{T}}^{*s}, \quad p = \epsilon^{(1+\lambda_0-2\alpha)}\tilde{\epsilon}^{2\alpha-2}\tilde{p}^{*}, \\
\lambda &= \epsilon^{-1-\lambda_0+2\alpha(n-1)}\tilde{\epsilon}^{-2\alpha(n-1)}\tilde{\lambda}^{*}, \quad \mu = \epsilon^{\lambda_0-1+\alpha(1\alpha)}\tilde{\epsilon}^{-\alpha(1-\alpha)}\tilde{\mu}^{*}, \\
\nu &= \epsilon^{3\lambda_0-1-2\alpha}\tilde{\epsilon}^{2\alpha}\tilde{\nu}^{*}, \quad \mathbf{w} = \epsilon^{-\lambda_0-1+n\alpha}\tilde{\epsilon}^{-n\alpha}\tilde{\mathbf{w}}^{*},
\end{aligned}$$

where $\epsilon = \mathrm{We}^{\frac{1}{1-\lambda_0}}$. Our inner core region equations using the above substitutions are

$$\tilde{\mathbf{T}}^{*} = \tilde{\mathbf{T}}^{*p} + \left(\frac{\tilde{\epsilon}}{\epsilon}\right)^{\alpha(n-2)}\tilde{\mathbf{T}}^{*s}, \quad \tilde{\mathbf{T}}^{*s} = 2\beta\tilde{\mathbf{D}}^{*}, \tag{4.59}$$

$$0 = -\tilde{\nabla}\tilde{p}^{*} + \tilde{\nabla}\cdot\tilde{\mathbf{T}}^{*p} + \left(\frac{\tilde{\epsilon}}{\epsilon}\right)^{\alpha(n-2)}\beta\tilde{\nabla}^2\cdot\tilde{\mathbf{v}}^{*}, \tag{4.60}$$

$$\left(\frac{\tilde{\epsilon}}{\epsilon}\right)^{2-n\alpha}\tilde{\mathbf{T}}^{*p} + \overset{\triangledown}{\tilde{\mathbf{T}}}^{*p} = 2(1-\beta)\left(\frac{\tilde{\epsilon}}{\epsilon}\right)^{2-2\alpha}\tilde{\mathbf{D}}^{*}, \tag{4.61}$$

and in natural stress.

$$\left(\frac{\tilde{\epsilon}}{\epsilon}\right)^{(2-n\alpha)}\tilde{\lambda}^{*} + \tilde{\mathbf{v}}^{*}\cdot\tilde{\nabla}\tilde{\lambda}^{*} + 2\left(\frac{\tilde{\epsilon}}{\epsilon}\right)^{(2-\alpha)(1-\alpha)}\tilde{\mu}^{*}\nabla\cdot\tilde{\mathbf{w}}^{*} = (1-\beta)\left(\frac{\tilde{\epsilon}}{\epsilon}\right)^{4-n\alpha-2\alpha}\frac{1}{(\tilde{u}^{*2}+\tilde{v}^{*2})}, \tag{4.62}$$

$$\left(\frac{\tilde{\epsilon}}{\epsilon}\right)^{(2-n\alpha)}\tilde{\mu}^{*} + \tilde{\mathbf{v}}^{*}\cdot\tilde{\nabla}\tilde{\mu}^{*} + \left(\frac{\tilde{\epsilon}}{\epsilon}\right)^{(2-\alpha)(1-\alpha)}\tilde{\nu}^{*}\nabla\cdot\tilde{\mathbf{w}}^{*} = 0, \tag{4.63}$$

$$\left(\frac{\tilde{\epsilon}}{\epsilon}\right)^{(2-n\alpha)}\tilde{\nu}^{*} + \tilde{\mathbf{v}}^{*}\cdot\tilde{\nabla}\tilde{\nu}^{*} = (1-\beta)\left(\frac{\tilde{\epsilon}}{\epsilon}\right)^{\alpha(n-2)}(\tilde{u}^{*2}+\tilde{v}^{*2}). \tag{4.64}$$

neglecting the inertia terms (always subdominant throughout region 3). Using (4.58) to determine the matching behaviour as we approach the wall, i.e. in the limit as $\tilde{Y}^{*} \to 0$,

$(\theta \to 0)$

$$\tilde{\psi}^* \sim \tilde{C}_0 \tilde{X}^{*n(\alpha-1)} \tilde{Y}^{*n}, \quad \tilde{p}^* \sim \frac{1}{2} \tilde{C}_1 \tilde{X}^{*2(\alpha-1)}, \quad \tilde{T}_{11}^{*p} \sim \tilde{C}_1 \tilde{X}^{*2(\alpha-1)} \tag{4.65}$$

$$\tilde{T}_{12}^{*p} \sim \tilde{C}_1 (1-\alpha) \tilde{X}^{*(2\alpha-3)} \tilde{Y}^*, \quad \tilde{T}_{22}^{*p} \sim \tilde{C}_1 (1-\alpha)^2 \tilde{X}^{*(2\alpha-4)} \tilde{Y}^{*2}, \tag{4.66}$$

$$\tilde{\lambda}^* \sim d_1 X^{*2(n-1)(1-\alpha)} \tilde{Y}^{*2(1-n)}, \quad \tilde{\mu}^* \sim d_2 \tilde{X}^{*n(\alpha-1)n_2} \tilde{Y}^{*nn_2}, \tag{4.67}$$

$$\tilde{\nu}^* \sim d_3 \tilde{X}^{*n(\alpha-1)n_3} \tilde{Y}^{*nn_3}, \tag{4.68}$$

where

$$\tilde{C}_0 = \tilde{c}_0 \alpha^n, \quad \tilde{C}_1 = \tilde{c}_0^{\frac{2}{n}} \alpha^2 n^2, \quad nn_2 = \alpha - 1, \quad nn_3 = 2, \tag{4.69}$$

hold. The pressure is retained at leading order in the momentum equation. The boundary layer scalings are

$$\begin{aligned}
&\tilde{X}^* = \tilde{X}, \quad \tilde{Y}^* = \tilde{\delta} \tilde{Y}, \quad \tilde{\psi}^* = \tilde{\delta}^n \tilde{\psi}, \quad \tilde{p}^* = \tilde{p}, \\
&\tilde{T}_{11}^{*p} = \tilde{T}_{11}^p, \quad \tilde{T}_{12}^{*p} = \tilde{\delta} \tilde{T}_{12}^p, \quad \tilde{T}_{22}^{*p} = \tilde{\delta}^2 \tilde{T}_{22}^p, \\
&\tilde{T}_{11}^{*s} = \tilde{\delta}^{n-1} \tilde{T}_{11}^s, \quad \tilde{T}_{12}^{*s} = \tilde{\delta}^{n-2} \tilde{T}_{12}^s, \quad \tilde{T}_{22}^{*s} = \tilde{\delta}^{n-1} \tilde{T}_{22}^s, \\
&\tilde{\lambda}^* = \tilde{\delta}^{2(1-n)} \tilde{\lambda}, \quad \tilde{\mu}^* = \tilde{\delta}^{nn_2} \tilde{\mu}, \quad \tilde{\nu}^* = \tilde{\delta}^{nn_3} \tilde{\nu}, \quad \nabla \cdot \tilde{\mathbf{w}}^* = \tilde{\delta}^{-n} \tilde{\mathbf{w}},
\end{aligned} \tag{4.70}$$

and allow us to retain the fullest balance in the constitutive equations. The gauge $\tilde{\delta}$ is found by considering fullest balance. Substituting into the full equations gives us the constitutive equations

$$\begin{aligned}
&\left(\frac{\tilde{\epsilon}}{\epsilon}\right)^{2-n\alpha} \tilde{T}_{11}^p + \tilde{\delta}^{n-1} \left(\frac{\partial \tilde{\Psi}}{\partial \tilde{Y}} \frac{\partial \tilde{T}_{11}^p}{\partial \tilde{X}} - \frac{\partial \tilde{\Psi}}{\partial \tilde{X}} \frac{\partial \tilde{T}_{11}^p}{\partial \tilde{Y}} - 2 \frac{\partial^2 \tilde{\Psi}}{\partial \tilde{X} \partial \tilde{Y}} \tilde{T}_{11}^p - 2 \frac{\partial^2 \tilde{\Psi}}{\partial \tilde{Y}^2} \tilde{T}_{12}^p \right) \\
&\qquad = 2(1-\beta) \left(\frac{\tilde{\epsilon}}{\epsilon}\right)^{2-2\alpha} \tilde{\delta}^{n-1} \frac{\partial^2 \tilde{\Psi}}{\partial \tilde{X} \partial \tilde{Y}},
\end{aligned} \tag{4.71}$$

$$\begin{aligned}
&\left(\frac{\tilde{\epsilon}}{\epsilon}\right)^{2-n\alpha} \tilde{\delta}^2 \tilde{T}_{22}^p + \tilde{\delta}^{n+1} \left(\frac{\partial \tilde{\Psi}}{\partial \tilde{Y}} \frac{\partial \tilde{T}_{22}^p}{\partial \tilde{X}} - \frac{\partial \tilde{\Psi}}{\partial \tilde{X}} \frac{\partial \tilde{T}_{22}^p}{\partial \tilde{Y}} + 2 \frac{\partial^2 \tilde{\Psi}}{\partial \tilde{X}^2} \tilde{T}_{12}^p + 2 \frac{\partial^2 \tilde{\Psi}}{\partial \tilde{X} \partial \tilde{Y}} \tilde{T}_{22}^p \right) \\
&\qquad = -2(1-\beta) \left(\frac{\tilde{\epsilon}}{\epsilon}\right)^{2-2\alpha} \tilde{\delta}^{n-1} \frac{\partial^2 \tilde{\Psi}}{\partial \tilde{X} \partial \tilde{Y}},
\end{aligned} \tag{4.72}$$

$$\begin{aligned}
&\left(\frac{\tilde{\epsilon}}{\epsilon}\right)^{2-n\alpha} \tilde{\delta} \tilde{T}_{12}^p + \tilde{\delta}^n \left(\frac{\partial \tilde{\Psi}}{\partial \tilde{Y}} \frac{\partial \tilde{T}_{12}^p}{\partial \tilde{X}} - \frac{\partial \tilde{\Psi}}{\partial \tilde{X}} \frac{\partial \tilde{T}_{12}^p}{\partial \tilde{Y}} - \frac{\partial^2 \tilde{\Psi}}{\partial \tilde{Y}^2} \tilde{T}_{22}^p + \frac{\partial^2 \tilde{\Psi}}{\partial \tilde{X}^2} \tilde{T}_{11}^p \right) \\
&\qquad = (1-\beta) \left(\frac{\tilde{\epsilon}}{\epsilon}\right)^{2-2\alpha} \tilde{\delta}^{n-2} \left(\frac{\partial^2 \tilde{\Psi}}{\partial \tilde{Y}^2} - \delta^2 \frac{\partial^2 \tilde{\Psi}}{\partial \tilde{X}^2} \right),
\end{aligned} \tag{4.73}$$

and the momentum equations

$$0 = -\frac{\partial \tilde{p}}{\partial \tilde{X}} + \frac{\partial \tilde{T}^p_{11}}{\partial \tilde{X}} + \frac{\partial \tilde{T}^p_{12}}{\partial \tilde{Y}} + \left(\frac{\tilde{\epsilon}}{\epsilon}\right)^{\alpha(n-2)} \tilde{\delta}^{n-3}\beta\left(\tilde{\delta}^2\frac{\partial^3\tilde{\Psi}}{\partial\tilde{X}^2\partial\tilde{Y}} + \frac{\partial^3\tilde{\Psi}}{\partial\tilde{Y}^3}\right), \tag{4.74}$$

$$0 = -\frac{\partial \tilde{p}}{\partial \tilde{Y}} + \tilde{\delta}^2\left(\frac{\partial \tilde{T}^p_{12}}{\partial \tilde{X}} + \frac{\partial \tilde{T}^p_{22}}{\partial \tilde{Y}}\right) + \left(\frac{\tilde{\epsilon}}{\epsilon}\right)^{\alpha(n-2)} \tilde{\delta}^{n-1}\beta\left(\tilde{\delta}^2\frac{\partial^3\tilde{\Psi}}{\partial\tilde{X}^3} + \frac{\partial^3\tilde{\Psi}}{\partial\tilde{X}\partial\tilde{Y}^2}\right). \tag{4.75}$$

The corresponding natural stress constitutive equations are

$$\left(\frac{\tilde{\epsilon}}{\epsilon}\right)^{(2-n\alpha)} \tilde{\delta}^{1-n}\tilde{\lambda} + \tilde{\mathbf{v}}\cdot\tilde{\nabla}\tilde{\lambda} + 2\left(\frac{\tilde{\epsilon}}{\epsilon}\right)^{(2-\alpha)(1-\alpha)} \tilde{\delta}^{nn_2-1-4n}\tilde{\mu}\tilde{\nabla}\cdot\tilde{\mathbf{w}}$$
$$= (1-\beta)\left(\frac{\tilde{\epsilon}}{\epsilon}\right)^{4-n\alpha-2\alpha} \tilde{\delta}^{1-n}\frac{1}{(\tilde{u}^2)}, \tag{4.76}$$

$$\left(\frac{\tilde{\epsilon}}{\epsilon}\right)^{(2-n\alpha)} \tilde{\delta}^{1-n}\tilde{\mu} + \tilde{\mathbf{v}}\cdot\tilde{\nabla}\tilde{\mu} + \left(\frac{\tilde{\epsilon}}{\epsilon}\right)^{(2-\alpha)(1-\alpha)} \tilde{\delta}^{nn_3-nn_2+1-2n}\tilde{\nu}\tilde{\nabla}\cdot\tilde{\mathbf{w}} = 0, \tag{4.77}$$

$$\left(\frac{\tilde{\epsilon}}{\epsilon}\right)^{(2-n\alpha)} \tilde{\delta}^{1-n}\tilde{\nu} + \tilde{\mathbf{v}}\cdot\tilde{\nabla}\tilde{\nu} = (1-\beta)\left(\frac{\tilde{\epsilon}}{\epsilon}\right)^{\alpha(n-2)} \tilde{\delta}^{n-1-nn_3}(\tilde{u}^2). \tag{4.78}$$

We can determine from this

$$\tilde{\delta} = \left(\frac{\tilde{\epsilon}}{\epsilon}\right)^{1-\alpha}, \quad n = 3-\alpha, \tag{4.79}$$

which is consistent with both formulations. Necessarily $\tilde{\epsilon} \ll \epsilon$, and so $\tilde{\delta}$ is small as required. Thus the boundary layer thickness is determined to be for the inner region

$$\tilde{\epsilon}\left(\frac{\tilde{\epsilon}}{\mathrm{We}^{1/(1-\lambda_0)}}\right)^{1-\alpha}. \tag{4.80}$$

The boundary layer equations can now be given and agree with the Oldroyd-B $\mathrm{We} = O(1)$ case

$$0 = -\frac{\partial \tilde{p}}{\partial \tilde{X}} + \frac{\partial \tilde{T}^p_{11}}{\partial \tilde{X}} + \frac{\partial \tilde{T}^p_{12}}{\partial \tilde{Y}} + \beta\frac{\partial^3\tilde{\Psi}}{\partial\tilde{Y}^3}, \tag{4.81}$$

$$\tilde{T}^p_{11} + \left(\frac{\partial\tilde{\Psi}}{\partial\tilde{Y}}\frac{\partial\tilde{T}^p_{11}}{\partial\tilde{X}} - \frac{\partial\tilde{\Psi}}{\partial\tilde{X}}\frac{\partial\tilde{T}^p_{11}}{\partial\tilde{Y}} - 2\frac{\partial^2\tilde{\Psi}}{\partial\tilde{X}\partial\tilde{Y}}\tilde{T}^p_{11} - 2\frac{\partial^2\tilde{\Psi}}{\partial\tilde{Y}^2}\tilde{T}^p_{12}\right) = 0, \tag{4.82}$$

$$\tilde{T}^p_{22} + \left(\frac{\partial\tilde{\Psi}}{\partial\tilde{Y}}\frac{\partial\tilde{T}^p_{22}}{\partial\tilde{X}} - \frac{\partial\tilde{\Psi}}{\partial\tilde{X}}\frac{\partial\tilde{T}^p_{22}}{\partial\tilde{Y}} + 2\frac{\partial^2\tilde{\Psi}}{\partial\tilde{X}^2}\tilde{T}^p_{12} + 2\frac{\partial^2\tilde{\Psi}}{\partial\tilde{X}\partial\tilde{Y}}\tilde{T}^p_{22}\right) = -2(1-\beta)\frac{\partial^2\tilde{\Psi}}{\partial\tilde{X}\partial\tilde{Y}}, \tag{4.83}$$

$$\tilde{T}^p_{12} + \left(\frac{\partial\tilde{\Psi}}{\partial\tilde{Y}}\frac{\partial\tilde{T}^p_{12}}{\partial\tilde{X}} - \frac{\partial\tilde{\Psi}}{\partial\tilde{X}}\frac{\partial\tilde{T}^p_{12}}{\partial\tilde{Y}} - \frac{\partial^2\tilde{\Psi}}{\partial\tilde{Y}^2}\tilde{T}^p_{22} + \frac{\partial^2\tilde{\Psi}}{\partial\tilde{X}^2}\tilde{T}^p_{11}\right) = (1-\beta)\frac{\partial^2\tilde{\Psi}}{\partial\tilde{Y}^2}. \tag{4.84}$$

The leading order equations in natural stress are found to be

$$\tilde{\lambda} + \tilde{\mathbf{v}} \cdot \tilde{\nabla}\tilde{\lambda} + 2\tilde{\mu}\tilde{\nabla} \cdot \tilde{\mathbf{w}} = 0, \tag{4.85}$$

$$\tilde{\mu} + \tilde{\mathbf{v}} \cdot \tilde{\nabla}\tilde{\mu} + \tilde{\nu}\tilde{\nabla} \cdot \tilde{\mathbf{w}} = 0, \tag{4.86}$$

$$\tilde{\nu} + \tilde{\mathbf{v}} \cdot \tilde{\nabla}\tilde{\nu} = (1-\beta)\tilde{u}^2, \tag{4.87}$$

$$0 = -\tilde{p}_{\tilde{X}} + \tilde{\mathbf{v}} \cdot \nabla(\tilde{\lambda}\tilde{\mu}) + \tilde{\mu}_{\tilde{Y}}. \tag{4.88}$$

Core and boundary layer region three are artificial regions, holding where $\frac{\tilde{\epsilon}}{\epsilon} \ll 1$. They occur for $r \ll \text{We}^{\frac{1}{1-\lambda_0}}$ but as $R^* \to 0$ there isn't a We length scale to determine $\tilde{\epsilon}$ explicitly. The structure for low We re-entrant corner flow has found three asymptotic regions, an exterior region where Newtonian flow is found and an interior region where Oldroyd-B We $= O(1)$ flow holds. An intermediate region is found to transition between these different flow states. The critical length scale We $^{\frac{1}{1-\lambda_0}}$ was found that determines where these flow structures occur, along with core and boundary layer regions for each determined. The results obtained here are similar to those obtained for the low-Weissenberg UCM behaviour obtained by Evans in [19], recovering UCM behaviour in the outer and inner asymptotic regions when setting $\beta = 0$.

4.2 The large Weissenberg limit: $We \gg 1, (1-\beta) \in [0,1)$

4.2.1 Introduction to the problem

We now consider the limit We $\to \infty$ for high Weissenberg number flows. A similar analysis is used to the low limiting case, the main difference requiring an intermediate boundary layer (which was arbitrary in the low We case). To restate, we are interested in the asymptotic structure of the system of governing equations

$$\begin{aligned} &\nabla.\mathbf{v} = 0, \quad 0 = -\nabla p + \nabla.\mathbf{T}, \\ &\mathbf{T}^p + \text{We}\ \overset{\triangledown}{\mathbf{T}}^p = 2(1-\beta)\mathbf{D}, \quad \mathbf{T}^s = 2\beta\mathbf{D}, \quad \mathbf{T} = \mathbf{T}^p + \mathbf{T}^s. \end{aligned} \tag{4.89}$$

As for low Weissenberg flow, the inertia terms in the momentum equation are found to be subdominant for all asymptotic regions close to the corner and thus neglected from the start. To begin the analysis, we consider the set of equations (4.89) setting We $= \infty$ means the upper convected polymer stress derivative dominates in the constitutive equations. Following the analysis in [19] for the UCM fluid, for the interior region close to the corner it is assumed Weissenberg $O(1)$ flow is found. (verified when matching to the exterior regions), motivating consideration initially of a 4 region structure. The

analysis for the high We limit differs from UCM since it is possible to decompose the eventual exterior solution into intermediate and exterior regions if a 'stretching' similarity solution is picked up as the corner is approached. The analysis will proceed as follows for this limit

- The interior regions close to the corner will be picked up first along with the boundary layer thickness. These results are presented separately for Cartesian and natural stress bases.
- The boundary layer thickness is found to be arbitrary to within a constant, fixing this constant to match with the high We boundary layer. A stretching similarity solution is found for $n = 3$ which may or may not be picked up.

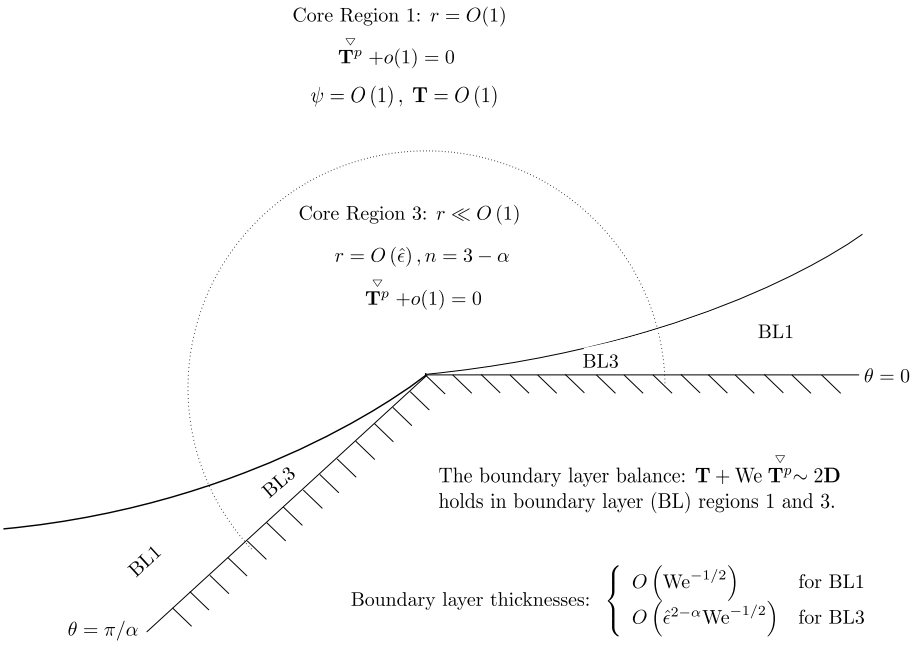

Figure 4-2: Illustration of the main asymptotic regions near to the re-entrant corner in the limit We $\to \infty$. We have the interior regions $r = O(\hat{\epsilon}) \ll 1$ and the exterior regions for $r = O(1)$. The interior regions are artificial and are those of the Oldroyd-B model We $= 1$ in chapter 3. They have a core flow region 3 with boundary layers 3 at the upstream and downstream walls. The exterior regions again have a core region 1 with boundary layers 1 at the walls.

4.2.2 The interior regions

We scale close into the corner with a small parameter $\tilde{\epsilon}$ as

$$r = \tilde{\epsilon}\tilde{R}^*, \quad \psi = \delta_0\tilde{\epsilon}^{n_1\alpha}\tilde{\Psi}^*, \quad \mathbf{T}^p = a\tilde{\epsilon}^{2(\alpha-1)}\tilde{\mathbf{T}}^{p*}, \quad \mathbf{T}^s = \delta_0\tilde{\epsilon}^{n_1\alpha-2)}\tilde{\mathbf{T}}^{s*}, \quad \mathbf{v} = \delta_0\tilde{\epsilon}^{n_1\alpha-1}\tilde{\mathbf{v}}^*,$$
$$\lambda = \hat{a}\tilde{\epsilon}^{2\alpha(1-n_1)}\tilde{\lambda}^*, \quad \mu = \hat{b}\tilde{\epsilon}^{n_2\alpha}\tilde{\mu}^*, \quad \nu = \hat{c}\tilde{\epsilon}^{n_3\alpha}\tilde{\nu}^*, \quad \mathbf{w} = \frac{1}{\delta_0}\tilde{\epsilon}^{1-n_1\alpha}\tilde{\mathbf{w}}^*, \tag{4.90}$$

where $\delta_0 = \delta_0(\mathrm{We})$, $a = a(\mathrm{We})$ are needed for balancing terms later on in the boundary layer. The natural stress variables are scaled with unknown gauges $\hat{a}$, $\hat{b}$, $\hat{c}$. We may use the outer core solution of chapter 3,

$$\psi = \tilde{C}_0 r^{n_1\alpha}\sin^{n_1}(\alpha\theta), \quad \mathbf{T}^p = \lambda(\psi)\mathbf{v}\mathbf{v}^T, \quad \lambda(\psi) = \tilde{C}_1\left(\frac{\psi}{\tilde{C}_0}\right)^{\frac{2}{n_1}(1-n_1)}. \tag{4.91}$$

The gauge $\hat{a}$ can be determined by writing the second expression in (4.91) in core variables

$$a\tilde{\epsilon}^{2(\alpha-1)}\tilde{\mathbf{T}}^{*p} = \hat{a}\delta_0^2\tilde{\epsilon}^{2\alpha(1-n_1)}\tilde{\lambda}^*\tilde{\epsilon}^{2n_1\alpha-2}\tilde{\mathbf{v}}^*\tilde{\mathbf{v}}^{*T}, \quad \Longrightarrow \hat{a} = \frac{a}{\delta_0^2}. \tag{4.92}$$

In the governing equations,

$$0 = -\tilde{\epsilon}^{2(\alpha-1)}a\tilde{\nabla}^*\tilde{p}^* + \tilde{\nabla}^*\cdot\left(a\tilde{\epsilon}^{2(\alpha-1)}\tilde{\mathbf{T}}^{p*} + \delta_0\tilde{\epsilon}^{n_1\alpha-2)}\tilde{\mathbf{T}}^{s*}\right), \tag{4.93}$$

$$0 = -a\tilde{\nabla}^*\tilde{p}^* + \tilde{\nabla}^*\cdot\left(a\tilde{\mathbf{T}}^{p*} + \delta_0\tilde{\epsilon}^{\alpha(n_1-2)}\tilde{\mathbf{T}}^{s*}\right), \tag{4.94}$$

$$\frac{\tilde{\epsilon}^{2-n_1\alpha}}{\delta_0\mathrm{We}}\tilde{\mathbf{T}}^{p*} + \overset{\triangledown}{\tilde{\mathbf{T}}}^{p*} = 2(1-\beta)\frac{\tilde{\epsilon}^{2(1-\alpha)}}{a\mathrm{We}}\tilde{\mathbf{D}}^*, \quad \tilde{\mathbf{T}}^{s*} = 2\beta\tilde{\mathbf{D}}^*, \tag{4.95}$$

and in the natural stress formulation

$$0 = -\tilde{\nabla}^* \tilde{p}^* + \frac{\hat{a}\delta_0^2}{a} \tilde{\mathbf{v}}^* \cdot \tilde{\nabla}^* \left(\tilde{\lambda}^* \tilde{u}^* \right) + O\left(\frac{\hat{b}}{a} \tilde{\epsilon}^{n_2\alpha+2-2\alpha} \right) + O\left(\frac{\hat{c}}{a\delta_0^2} \tilde{\epsilon}^{4-2\alpha-2n_1\alpha+n_3\alpha} \right), \tag{4.96}$$

$$0 = -\tilde{\nabla}^* \tilde{p}^* + \frac{\hat{a}\delta_0^2}{a} \tilde{\mathbf{v}}^* \cdot \tilde{\nabla}^* \left(\tilde{\lambda}^* \tilde{v}^* \right) + O\left(\frac{\hat{b}}{a} \tilde{\epsilon}^{n_2\alpha+2-2\alpha} \right) + O\left(\frac{\hat{c}}{a\delta_0^2} \tilde{\epsilon}^{4-2\alpha-2n_1\alpha+n_3\alpha} \right), \tag{4.97}$$

$$\left(\frac{\tilde{\epsilon}^{2-n_1\alpha}}{\delta_0 \mathrm{We}} \right) \tilde{\lambda}^* + \tilde{\mathbf{v}}^* \cdot \tilde{\nabla}^* \tilde{\lambda}^* + 2 \left(\frac{\hat{b}\tilde{\epsilon}^{n_2\alpha+2-2\alpha}}{\delta_0^2 \hat{a}} \right) \tilde{\mu}^* \tilde{\nabla}^* \cdot \tilde{\mathbf{w}}^* = (1-\beta) \left(\frac{\tilde{\epsilon}^{4-2\alpha-n_1\alpha}}{\delta_0^3 \hat{a} \mathrm{We}^2} \right) \frac{1}{|\mathbf{v}^*|^2}, \tag{4.98}$$

$$\left(\frac{\tilde{\epsilon}^{2-n_1\alpha}}{\delta_0 \mathrm{We}} \right) \tilde{\mu}^* + \tilde{\mathbf{v}}^* \cdot \tilde{\nabla}^* \tilde{\mu}^* + \left(\frac{\hat{c}\tilde{\epsilon}^{n_3\alpha-n_2\alpha+2-2n_1\alpha}}{\delta_0^2 \hat{b}} \right) \tilde{\nu}^* \tilde{\nabla}^* \cdot \tilde{\mathbf{w}}^* = 0, \tag{4.99}$$

$$\left(\frac{\tilde{\epsilon}^{2-n_1\alpha}}{\delta_0 \mathrm{We}} \right) \tilde{\nu}^* + \tilde{\mathbf{v}}^* \cdot \tilde{\nabla}^* \tilde{\nu}^* = (1-\beta) \left(\frac{\delta_0 \tilde{\epsilon}^{n_1\alpha-n_3\alpha}}{\hat{c} \mathrm{We}^2} \right) |\mathbf{v}^*|^2. \tag{4.100}$$

In the natural stress momentum equations, the first two terms are of equal order, the remaining expressions are of the two orders indicated and are eventually found to be subdominant. Under the assumptions

$$\frac{\tilde{\epsilon}^{2-n_1\alpha}}{\delta_0 \mathrm{We}} \ll 1, \quad \frac{\tilde{\epsilon}^{2(1-\alpha)}}{a \mathrm{We}} \ll 1, \tag{4.101}$$

the upper convected derivative will dominate at leading order. The particular solution form will then be as in (4.91),

$$\tilde{\Psi}^* = \tilde{C}_0 \tilde{R}^{*n_1\alpha} \sin^{n_1}(\alpha\theta), \quad \tilde{\mathbf{T}}^{p*} = \tilde{\lambda}^*(\tilde{\Psi}^*) \tilde{\mathbf{v}}^* \tilde{\mathbf{v}}^{*T}, \quad \tilde{\lambda}^* = \tilde{C}_1 \left(\frac{\tilde{\Psi}^*}{\tilde{C}_0} \right)^{\frac{2(1-n_1)}{n_1}}. \tag{4.102}$$

In component form, the extra stress tensor will be

$$\tilde{T}_{11}^{p*} = \tilde{\lambda}^* \left(\frac{\partial \tilde{\Psi}^*}{\partial \tilde{Y}^*} \right)^2, \quad \tilde{T}_{12}^{p*} = -\tilde{\lambda}^* \frac{\partial \tilde{\Psi}^*}{\partial \tilde{Y}^*} \frac{\partial \tilde{\Psi}^*}{\partial \tilde{X}^*}, \quad \tilde{T}_{22}^{p*} = \tilde{\lambda}^* \left(\frac{\partial \tilde{\Psi}^*}{\partial \tilde{X}^*} \right)^2. \tag{4.103}$$

As the upstream wall is approached, $\tilde{Y}^* \to 0$, the core matching conditions are therefore

$$\tilde{\Psi}^* = \tilde{C}_0 \tilde{X}^{*n_1(\alpha-1)} \tilde{Y}^{*n_1}, \tag{4.104}$$

$$\tilde{T}_{11}^{p*} = \tilde{C}_0^2 \tilde{C}_1 n_1^2 \tilde{X}^{*2(\alpha-1)}, \tag{4.105}$$

$$\tilde{T}_{12}^{p*} = -\tilde{C}_0^2 \tilde{C}_1 n_1^2 (\alpha-1) \tilde{X}^{*2(\alpha-1)-1} \tilde{Y}, \tag{4.106}$$

$$\tilde{T}_{22}^{p*} = \tilde{C}_0^2 \tilde{C}_1 n_1^2 (\alpha-1)^2 \tilde{X}^{*2(\alpha-1)-2} \tilde{Y}^2. \tag{4.107}$$

The boundary layer scalings are

$$\tilde{X}^* = \tilde{X}, \quad \tilde{Y}^* = \delta \tilde{Y}, \quad \tilde{\psi}^* = \tilde{\delta}^{n_1} \tilde{\Psi}, \quad \tilde{p}^* = \tilde{p}, \tag{4.108}$$

$$\tilde{T}_{11}^{s*} = \tilde{\delta}^{n_1-1} \tilde{T}_{11}^s, \quad \tilde{T}_{12}^{s*} = \tilde{\delta}^{n_1-2} \tilde{T}_{12}^s, \quad \tilde{T}_{22}^{s*} = \tilde{\delta}^{n_1-1} \tilde{T}_{22}^s, \tag{4.109}$$

$$\tilde{T}_{11}^{p*} = \tilde{T}_{11}^p, \quad \tilde{T}_{12}^{p*} = \tilde{\delta} \tilde{T}_{12}^p, \quad \tilde{T}_{22}^{p*} = \tilde{\delta}^2 \tilde{T}_{22}^p, \tag{4.110}$$

$$\tilde{\lambda}^* = \tilde{\delta}^{2(1-n_1)} \tilde{\lambda}, \quad \tilde{\mu}^* = \tilde{\delta}^{n_2} \tilde{\mu}, \quad \tilde{\nu}^* = \tilde{\delta}^{n_3} \tilde{\nu}, \tag{4.111}$$

$$\tilde{\mathbf{v}}^* \cdot \nabla = \tilde{\delta}^{n_1-1} \tilde{\mathbf{v}} \cdot \nabla, \quad \nabla \cdot \tilde{\mathbf{w}}^* = \tilde{\delta}^{-n_1} \frac{\partial}{\partial \tilde{Y}} \left(\frac{1}{\tilde{u}} \right). \tag{4.112}$$

Substitution into the momentum and constitutive equations then leaves

$$0 = -\frac{\partial \tilde{p}}{\partial \tilde{X}} + \frac{\partial \tilde{T}_{11}^p}{\partial \tilde{X}} + \frac{\partial \tilde{T}_{12}^p}{\partial \tilde{Y}} + \frac{\delta_0 \tilde{\epsilon}^{(n_1-2)\alpha}}{a} \left(\tilde{\delta}^{n_1-1} \frac{\partial \tilde{T}_{11}^s}{\partial \tilde{X}} + \tilde{\delta}^{n_1-3} \frac{\partial \tilde{T}_{12}^s}{\partial \tilde{Y}} \right), \tag{4.113}$$

$$0 = -\frac{\partial \tilde{p}}{\partial \tilde{Y}} + \tilde{\delta} \left(\tilde{\delta} \frac{\partial \tilde{T}_{12}^p}{\partial \tilde{X}} + \tilde{\delta} \frac{\partial \tilde{T}_{22}^p}{\partial \tilde{Y}} + \frac{\delta_0 \tilde{\epsilon}^{(n_1-2)\alpha}}{a} \left(\tilde{\delta}^{n_1-2} \frac{\partial \tilde{T}_{12}^s}{\partial \tilde{X}} + \tilde{\delta}^{n_1-2} \frac{\partial \tilde{T}_{22}^s}{\partial \tilde{Y}} \right) \right), \tag{4.114}$$

$$\frac{\tilde{\epsilon}^{2-n_1\alpha}}{\delta_0 \mathrm{We}} \tilde{T}_{11}^p + \tilde{\delta}^{n_1-1} \left(\frac{\partial \tilde{\Psi}}{\partial \tilde{Y}} \frac{\partial \tilde{T}_{11}^p}{\partial \tilde{X}} - \frac{\partial \tilde{\Psi}}{\partial \tilde{X}} \frac{\partial \tilde{T}_{11}^p}{\partial \tilde{Y}} - 2 \frac{\partial^2 \tilde{\Psi}}{\partial \tilde{Y}^2} \tilde{T}_{12}^p - 2 \frac{\partial^2 \tilde{\Psi}}{\partial \tilde{X} \partial \tilde{Y}} \tilde{T}_{11}^p \right) =$$

$$2(1-\beta) \frac{\tilde{\epsilon}^{2(1-\alpha)} \tilde{\delta}^{n_1-1}}{a\mathrm{We}} \frac{\partial^2 \tilde{\Psi}}{\partial \tilde{X} \partial \tilde{Y}}, \tag{4.115}$$

$$\frac{\tilde{\epsilon}^{2-n_1\alpha} \tilde{\delta}^2}{\delta_0 \mathrm{We}} \tilde{T}_{22}^p + \tilde{\delta}^{n_1+1} \left(\frac{\partial \tilde{\Psi}}{\partial \tilde{Y}} \frac{\partial \tilde{T}_{22}^p}{\partial \tilde{X}} - \frac{\partial \tilde{\Psi}}{\partial \tilde{X}} \frac{\partial \tilde{T}_{22}^p}{\partial \tilde{Y}} + 2 \frac{\partial^2 \tilde{\Psi}}{\partial \tilde{X}^2} \tilde{T}_{12}^p + 2 \frac{\partial^2 \tilde{\Psi}}{\partial \tilde{X} \partial \tilde{Y}} \tilde{T}_{22}^p \right) =$$

$$-2(1-\beta) \frac{\tilde{\epsilon}^{2(1-\alpha)} \tilde{\delta}^{n_1-1}}{a\mathrm{We}} \frac{\partial^2 \tilde{\Psi}}{\partial \tilde{X} \partial \tilde{Y}}, \tag{4.116}$$

$$\frac{\tilde{\epsilon}^{2-n_1\alpha} \tilde{\delta}}{\delta_0 \mathrm{We}} \tilde{T}_{12}^p + \tilde{\delta}^{n_1} \left(\frac{\partial \tilde{\Psi}}{\partial \tilde{Y}} \frac{\partial \tilde{T}_{12}^p}{\partial \tilde{X}} - \frac{\partial \tilde{\Psi}}{\partial \tilde{X}} \frac{\partial \tilde{T}_{12}^p}{\partial \tilde{Y}} + \frac{\partial^2 \tilde{\Psi}}{\partial \tilde{X}^2} \tilde{T}_{11}^p - \frac{\partial^2 \tilde{\Psi}}{\partial \tilde{Y}^2} \tilde{T}_{22}^p \right) =$$

$$(1-\beta) \frac{\tilde{\epsilon}^{2(1-\alpha)} \tilde{\delta}^{n_1-2}}{a\mathrm{We}} \left(\frac{\partial^2 \tilde{\Psi}}{\partial \tilde{Y}^2} - \tilde{\delta}^2 \frac{\partial^2 \tilde{\Psi}}{\partial \tilde{X}^2} \right), \tag{4.117}$$

with the corresponding natural stress formulation being

$$0 = -\tilde{\nabla}p + \frac{\hat{a}\delta_0^2}{a}\tilde{\mathbf{v}}\cdot\tilde{\nabla}\left(\tilde{\lambda}\tilde{u}\right) + O\left(\frac{\hat{b}}{a}\tilde{\epsilon}^{n_2\alpha+2-2\alpha}\right) + O\left(\frac{\hat{c}}{a\delta_0^2}\tilde{\epsilon}^{4-2\alpha-2n_1\alpha+n_3\alpha}\right), \tag{4.118}$$

$$0 = -\tilde{\nabla}p + \frac{\hat{a}\delta_0^2}{a}\tilde{\mathbf{v}}\cdot\tilde{\nabla}\left(\tilde{\lambda}\tilde{v}\right) + O\left(\frac{\hat{b}}{a}\tilde{\epsilon}^{n_2\alpha+2-2\alpha}\right) + O\left(\frac{\hat{c}}{a\delta_0^2}\tilde{\epsilon}^{4-2\alpha-2n_1\alpha+n_3\alpha}\right), \tag{4.119}$$

$$\left(\frac{\tilde{\epsilon}^{2-n_1\alpha}}{\delta_0\mathrm{We}}\right)\tilde{\lambda} + \tilde{\delta}^{n_1-1}\tilde{\mathbf{v}}\cdot\tilde{\nabla}\tilde{\lambda} + 2\left(\frac{\hat{b}\tilde{\epsilon}^{n_2\alpha+2-2\alpha}\tilde{\delta}^{n_2-n_1}}{\delta_0^2\hat{a}\tilde{\delta}^{2-2n_1}}\right)\tilde{\mu}\tilde{\nabla}\cdot\tilde{\mathbf{w}} = (1-\beta)\left(\frac{\tilde{\epsilon}^{4-2\alpha-n_1\alpha}}{\delta_0^3\hat{a}\mathrm{We}^2}\right)\frac{1}{\tilde{u}^2}, \tag{4.120}$$

$$\left(\frac{\tilde{\epsilon}^{2-n_1\alpha}}{\delta_0\mathrm{We}}\right)\tilde{\mu} + \tilde{\delta}^{n_1-1}\tilde{\mathbf{v}}\cdot\tilde{\nabla}\tilde{\mu} + \left(\frac{\hat{c}\tilde{\epsilon}^{n_3\alpha-n_2\alpha+2-2n_1\alpha}\tilde{\delta}^{n_3-n_1}}{\delta_0^2\hat{b}\tilde{\delta}^{n_2}}\right)\tilde{\nu}\tilde{\nabla}\cdot\tilde{\mathbf{w}} = 0, \tag{4.121}$$

$$\left(\frac{\tilde{\epsilon}^{2-n_1\alpha}}{\delta_0\mathrm{We}}\right)\tilde{\nu} + \tilde{\delta}^{n_1-1}\tilde{\mathbf{v}}\cdot\tilde{\nabla}\tilde{\nu} = (1-\beta)\left(\frac{\delta_0\tilde{\delta}^{2(n_1-1)}\tilde{\epsilon}^{n_1\alpha-n_3\alpha}}{\hat{c}\mathrm{We}^2\tilde{\delta}^{n_3}}\right)\tilde{u}^2. \tag{4.122}$$

Balancing the linear with the upper convected stress terms and the leading order term on the right hand side of (4.117) gives

$$\frac{\tilde{\epsilon}^{2-n_1\alpha}}{\delta_0\mathrm{We}} = \tilde{\delta}^{n_1-1}, \quad \tilde{\delta}^2 = \frac{\tilde{\epsilon}^{2(1-\alpha)}}{a\mathrm{We}} \tag{4.123}$$

$$\implies \tilde{\delta} = \frac{\tilde{\epsilon}^{1-\alpha}}{(a\mathrm{We})^{1/2}}, \quad n_1 = 3-\alpha. \tag{4.124}$$

Furthermore, the dominant balances in the natural stress constitutive equations are

$$\left(\frac{\tilde{\epsilon}^{2-n_1\alpha}}{\delta_0\mathrm{We}}\right) = \tilde{\delta}^{n_1-1}, \quad \frac{\hat{b}\tilde{\epsilon}^{n_2\alpha+2-2\alpha}\tilde{\delta}^{n_2-n_1}}{\delta_0^2\hat{a}\tilde{\delta}^{2-2n_1}} = \tilde{\delta}^{n_1-1},$$
$$\frac{\hat{c}\tilde{\epsilon}^{n_3\alpha-n_2\alpha+2-2n_1\alpha}\tilde{\delta}^{n_3-n_1}}{\delta_0^2\hat{b}\tilde{\delta}^{n_2}} = \tilde{\delta}^{n_1-1}, \quad \frac{\delta_0\tilde{\delta}^{2(n_1-1)}\tilde{\epsilon}^{n_1\alpha-n_3\alpha}}{\hat{c}\mathrm{We}^2\tilde{\delta}^{n_3}} = \tilde{\delta}^{n_1-1}. \tag{4.125}$$

Equating the terms on the left hand side in (4.120) gives the same results as in (4.124). Working systematically through the expressions in (4.125): equating the powers of $\tilde{\epsilon}$ gives

$$\hat{a} = \delta_0^{\frac{2}{2-\alpha}}\mathrm{We}^{\frac{\alpha}{2-\alpha}}, \quad n_1 = 3-\alpha, \tag{4.126}$$

$$\hat{b} = \delta_0^{\frac{\alpha}{2-\alpha}}\mathrm{We}^{\frac{2\alpha-2}{2-\alpha}}, \quad n_2 = \alpha-1, \tag{4.127}$$

$$\hat{c} = \delta_0^{\frac{2}{2-\alpha}}\mathrm{We}^{\frac{3\alpha-4}{2-\alpha}}, \quad n_3 = 2, \tag{4.128}$$

thus determining the natural stress core and boundary layer region scalings. These values for n_1, n_2 and n_3 are those found for Weissenberg $O(1)$ flow for the natural stress variables in (3.73) and (3.74), verifying the assumption at the start of this section that $We = O(1)$ flow holds in region 3 close to the corner. With these scalings in mind, at leading order the boundary layer equations are

$$0 = -\frac{\partial \tilde{p}}{\partial \tilde{X}} + \frac{\partial \tilde{T}^p_{11}}{\partial \tilde{X}} + \frac{\partial \tilde{T}^p_{12}}{\partial \tilde{Y}} + \frac{\partial \tilde{T}^s_{12}}{\partial \tilde{Y}}, \quad 0 = -\frac{\partial \tilde{p}}{\partial \tilde{Y}}, \tag{4.129}$$

$$\tilde{T}^p_{11} + \left(\frac{\partial \tilde{\Psi}}{\partial \tilde{Y}} \frac{\partial \tilde{T}^p_{11}}{\partial \tilde{X}} - \frac{\partial \tilde{\Psi}}{\partial \tilde{X}} \frac{\partial \tilde{T}^p_{11}}{\partial \tilde{Y}} - 2\frac{\partial^2 \tilde{\Psi}}{\partial \tilde{Y}^2} \tilde{T}^p_{12} - 2\frac{\partial^2 \tilde{\Psi}}{\partial \tilde{X} \partial \tilde{Y}} \tilde{T}^p_{11} \right) = 0, \tag{4.130}$$

$$\tilde{T}^p_{22} + \left(\frac{\partial \tilde{\Psi}}{\partial \tilde{Y}} \frac{\partial \tilde{T}^p_{22}}{\partial \tilde{X}} - \frac{\partial \tilde{\Psi}}{\partial \tilde{X}} \frac{\partial \tilde{T}^p_{22}}{\partial \tilde{Y}} + 2\frac{\partial^2 \tilde{\Psi}}{\partial \tilde{X}^2} \tilde{T}^p_{12} + 2\frac{\partial^2 \tilde{\Psi}}{\partial \tilde{X} \partial \tilde{Y}} \tilde{T}^p_{22} \right) = -2(1-\beta)\frac{\partial^2 \tilde{\Psi}}{\partial \tilde{X} \partial \tilde{Y}}, \tag{4.131}$$

$$\tilde{T}^p_{12} + \left(\frac{\partial \tilde{\Psi}}{\partial \tilde{Y}} \frac{\partial \tilde{T}^p_{12}}{\partial \tilde{X}} - \frac{\partial \tilde{\Psi}}{\partial \tilde{X}} \frac{\partial \tilde{T}^p_{12}}{\partial \tilde{Y}} + \frac{\partial^2 \tilde{\Psi}}{\partial \tilde{X}^2} \tilde{T}^p_{11} - \frac{\partial^2 \tilde{\Psi}}{\partial \tilde{Y}^2} \tilde{T}^p_{22} \right) = (1-\beta)\frac{\partial^2 \tilde{\Psi}}{\partial \tilde{Y}^2}. \tag{4.132}$$

The natural stress counterpart also determines the pressure to be a function of $\tilde{X}$ only as expected, the pressure related to the velocity via

$$0 = -\frac{\partial \tilde{p}}{\partial \tilde{X}} + \tilde{\mathbf{v}} \cdot \tilde{\nabla} \left(\tilde{\lambda} \tilde{u} \right) + \frac{\partial \tilde{u}}{\partial \tilde{Y}}, \tag{4.133}$$

retaining $\tilde{\mathbf{v}} \cdot \tilde{\nabla} \left(\tilde{\lambda} \tilde{u} \right)$ with the $\tilde{Y}$ pressure derivative and also pulling back an additional velocity derivative term. The leading order constitutive equations are

$$\tilde{\lambda} + \tilde{\mathbf{v}} \cdot \tilde{\nabla} \tilde{\lambda} + 2\tilde{\mu} \frac{\partial}{\partial \tilde{Y}} \left(\frac{1}{\tilde{u}} \right) = 0, \tag{4.134}$$

$$\tilde{\mu} + \tilde{\mathbf{v}} \cdot \tilde{\nabla} \tilde{\mu} + \tilde{\nu} \frac{\partial}{\partial \tilde{Y}} \left(\frac{1}{\tilde{u}} \right) = 0, \tag{4.135}$$

$$\tilde{\nu} + \tilde{\mathbf{v}} \cdot \tilde{\nabla} \tilde{\nu} = (1-\beta)\tilde{u}^2. \tag{4.136}$$

For reference, the relations linking the two different formulations in the boundary layer variables at leading order are given by

$$\tilde{T}_{11} = \tilde{\lambda} \tilde{u}^2, \quad \tilde{T}_{12} = \tilde{\lambda} \tilde{u} \tilde{v} + \tilde{\mu}, \quad \tilde{T}_{22} = -(1-\beta) + \tilde{\lambda} \tilde{v}^2 + \left(\frac{2\tilde{\mu}\tilde{v}}{\tilde{u}} \right) + \left(\frac{\tilde{\nu}}{\tilde{u}^2} \right), \tag{4.137}$$

which are the same as found in (3.85). To recap, in the interior core region, the scalings for the stream function and polymer stress were found to be

$$\psi = \delta_0 \tilde{\epsilon}^{n_1 \alpha} \tilde{\Psi}^*, \quad \mathbf{T}^p = a \tilde{\epsilon}^{2(\alpha-1)} \tilde{\mathbf{T}}^{p*}, \tag{4.138}$$

with the parameter $\tilde{\delta}$ in the boundary layer

$$\tilde{\delta} = \frac{\tilde{\epsilon}^{1-\alpha}}{(a\mathrm{We})^{1/2}}, \tag{4.139}$$

where the value of a is undetermined currently, needing to be matched to the exterior region boundary layer. This region is considered next.

4.2.3 The exterior regions: $r = O(1)$

For this region, $r = O(1)$ so no scaling with ϵ is required for the core region. Following on from the interior region, it is unclear whether the stream function and polymer stresses are scaled with We in the form

$$\psi = A(\mathrm{We})\Psi^*, \quad \mathbf{T}^p = B(\mathrm{We})\mathbf{T}^{p*}. \tag{4.140}$$

For high We flow, the upper convected derivative is expected to dominate in the core region, implying that $\mathrm{We}.A.B \gg B$ and $\mathrm{We}.A.B \gg A$ holds, or alternatively $\mathrm{We}.A, \mathrm{We}.B \gg 1$. For the natural stress basis, the leading order core equations will be

$$\hat{\mathbf{v}}^* \cdot \nabla^* \hat{\lambda}^* + 2\hat{\mu}^* \nabla^* \cdot \hat{\mathbf{w}}^* = 0, \tag{4.141}$$

$$\hat{\mathbf{v}}^* \cdot \nabla^* \hat{\mu}^* + \hat{\nu}^* \nabla^* \cdot \hat{\mathbf{w}}^* = 0, \tag{4.142}$$

$$\hat{\mathbf{v}}^* \cdot \nabla^* \hat{\nu}^* = 0. \tag{4.143}$$

The extra retention of terms in the constitutive equations means that the natural stress variables are unlikely to be of power law form, hence scaling into the boundary layer with δ as

$$\begin{aligned} x = \hat{X}, \quad y = \delta \hat{Y}, \quad \psi = A\delta^n \hat{\Psi}, \quad p = B\hat{p}, \\ T^p_{11} = B\hat{T}^p_{11}, \quad T_{12} = B\delta \hat{T}^p_{12}, \quad T^p_{22} = B\delta^2 \hat{T}^p_{22}, \\ \lambda = \theta_1 \hat{\lambda}, \quad \mu = \theta_2 \hat{\mu}, \quad \nu = \theta_3 \hat{\nu}, \end{aligned} \tag{4.144}$$

for gauges θ_1, θ_2, θ_3, the constitutive equations in Cartesian become

$$\frac{1}{A\delta^{n-1}\mathrm{We}}\hat{T}^p_{11} + \left(\frac{\partial\hat{\Psi}}{\partial\hat{Y}}\frac{\partial\hat{T}^p_{11}}{\partial\hat{X}} - \frac{\partial\hat{\Psi}}{\partial\hat{X}}\frac{\partial\hat{T}^p_{11}}{\partial\hat{Y}} - 2\frac{\partial^2\hat{\Psi}}{\partial\hat{Y}^2}\hat{T}^p_{12} - 2\frac{\partial^2\hat{\Psi}}{\partial\hat{X}\partial\hat{Y}}\hat{T}^p_{11}\right) = 2(1-\beta)\frac{\delta}{B\mathrm{We}}\frac{\partial^2\hat{\Psi}}{\partial\hat{X}\partial\hat{Y}}, \tag{4.145}$$

$$\frac{1}{A\delta^{n-1}\mathrm{We}}\hat{T}^p_{22} + \left(\frac{\partial\hat{\Psi}}{\partial\hat{Y}}\frac{\partial\hat{T}^p_{22}}{\partial\hat{X}} - \frac{\partial\hat{\Psi}}{\partial\hat{X}}\frac{\partial\hat{T}^p_{22}}{\partial\hat{Y}} + 2\frac{\partial^2\hat{\Psi}}{\partial\hat{X}^2}\hat{T}^p_{12} + 2\frac{\partial^2\hat{\Psi}}{\partial\hat{X}\partial\hat{Y}}\hat{T}^p_{22}\right) = -2(1-\beta)\frac{1}{B\delta^2\mathrm{We}}\frac{\partial^2\hat{\Psi}}{\partial\hat{X}\partial\hat{Y}}, \tag{4.146}$$

$$\frac{1}{A\delta^{n-1}\mathrm{We}}\hat{T}^p_{12} + \left(\frac{\partial\hat{\Psi}}{\partial\hat{Y}}\frac{\partial\hat{T}^p_{12}}{\partial\hat{X}} - \frac{\partial\hat{\Psi}}{\partial\hat{X}}\frac{\partial\hat{T}^p_{12}}{\partial\hat{Y}} + \frac{\partial^2\hat{\Psi}}{\partial\hat{X}^2}\hat{T}^p_{11} - \frac{\partial^2\hat{\Psi}}{\partial\hat{Y}^2}\hat{T}^p_{22}\right) = (1-\beta)\frac{1}{B\delta^2\mathrm{We}}\left(\frac{\partial^2\hat{\Psi}}{\partial\hat{Y}^2} - \delta^2\frac{\partial^2\hat{\Psi}}{\partial\hat{X}^2}\right). \tag{4.147}$$

Trying to retain as many terms as possible in the above equations gives the following three relations between A, B, δ and n

$$1 = \mathrm{We}\delta^{n-1}A, \quad B = A\delta^{n-3}, \quad \mathrm{We}\delta^2 B = 1. \tag{4.148}$$

The natural choice is to fix $A = 1$ and $B = 1$, since the interior region is anticipated to be artificial (i.e. the gauge $\tilde{\epsilon}$ is artificial and not dependent on We) and variables should be $O(1)$. Thus,

$$n = 3, \quad \delta = \mathrm{We}^{-1/2} \tag{4.149}$$

which satisfies the inequalities required at the start of this section. For the natural stress formulation, the leading order relations between the two formulations are given in (3.85) (with bars changed to hats). The first relation $\hat{T}^p_{11} = \hat{\lambda}\hat{u}^2$ fixes $\theta_1 = \delta^{-4}$. Similarly the relation for $\hat{T}^p_{12}$ fixes $\theta_2 = \delta$. Having found the scaling for μ the final scaling θ_3 is determined to be $\theta_3 = \delta^6$. The equivalent constitutive equations for natural stress with δ given in (4.149) are

$$\hat{\lambda} + \hat{\mathbf{v}}\cdot\hat{\nabla}\hat{\lambda} + 2\hat{\mu}\frac{\partial}{\partial\hat{Y}}\left(\frac{1}{\hat{u}}\right) = 0, \tag{4.150}$$

$$\hat{\mu} + \hat{\mathbf{v}}\cdot\hat{\nabla}\hat{\mu} + \hat{\nu}\frac{\partial}{\partial\hat{Y}}\left(\frac{1}{\hat{u}}\right) = 0, \tag{4.151}$$

$$\hat{\nu} + \hat{\mathbf{v}}\cdot\hat{\nabla}\hat{\nu} = (1-\beta)\hat{u}^2, \tag{4.152}$$

and the momentum equations

$$0 = -\frac{\partial \hat{p}}{\partial \hat{X}} + \hat{\mathbf{v}} \cdot \hat{\nabla} \left(\hat{\lambda} \hat{u} \right) + \frac{\partial \hat{u}}{\partial \hat{Y}}, \quad 0 = -\frac{\partial \hat{p}}{\partial \hat{Y}}, \tag{4.153}$$

where the terms missing in the core natural stress constitutive equations have been recovered. We are now in a position to determine a. The high We boundary layer thickness in region one was found to be $\delta = \mathrm{We}^{-1/2}$. Recall the interior boundary layer thickness was

$$\tilde{\delta} = \frac{\tilde{\epsilon}^{1-\alpha}}{(a\mathrm{We})^{1/2}}, \tag{4.154}$$

where $\tilde{\epsilon}$ is an artificially small parameter. This suggests taking $a = 1$ so as to retain the artificial nature and also match with the high We boundary layer. If we take a to be this value, then

$$\delta_0 = \mathrm{We}^{-\frac{\alpha}{2}}, \hat{a} = \mathrm{We}, \quad \hat{b} = \mathrm{We}^{\frac{\alpha}{2}-1}, \quad \hat{c} = \mathrm{We}^{-2}, \tag{4.155}$$

are fixed. The high Weissenberg number limit comprises the six-region structure summarised in figure 4-2. In the core regions, the stress singularity is $O(r^{-2(1-\alpha)})$ as for the UCM case. The conclusion for UCM that for re-entrant corners the effect of the singularity will be felt at $O(1)$ distances away from the corner will hold for Oldroyd-B as well, thus posing potential difficulties to any numerical simulation of high Weissenberg flow. In core region 1 a stretching similarity solution may exist for when the stream function $\psi = O(r^{3\alpha})$ differing from the $We = 1$ case where $\psi = O(r^{\alpha(3-\alpha)})$. Also similar to the UCM case is that the $We = 1$ problem is present in the interior regions located at distances less that $O(We^{-1/2})$ away from the corner. Further, the same core balances and boundary layer thickness of $O(\tilde{\epsilon}^{2-\alpha} We^{-1/2})$ are found. The only significant difference between Oldroyd-B and UCM is the difficulty in picking up a solution in the exterior region and thus whether a intermediate region will exist if a similarity solution will exist as the corner is approached. The question of whether such a stretching solution exists away from the corner is left as an open problem.

4.3 The Newtonian limit $\beta \to 1, We = O(1)$

In the Newtonian limit $\beta \to 1$ we would expect to pick up the Newtonian solution in a core region away from the walls. As this is a very different solution from the potential flow solution in the core given in chapter 3, we would expect a transition structure between the two behaviours in this limit. We keep the Weissenberg number

$O(1)$ throughout this section and thus set it to unity.

4.3.1 Introduction to the problem

As usual we consider the asymptotic structure of the governing equations

$$\nabla.\mathbf{v} = 0, \quad 0 = -\nabla p + \nabla.\mathbf{T}^p + \nabla.\mathbf{T}^s,$$
$$\mathbf{T}^s = 2\beta\mathbf{D}, \quad \mathbf{T}^p + \overset{\triangledown}{\mathbf{T}}^p = 2(1-\beta)\mathbf{D}, \tag{4.156}$$

where the inertia terms are anticipated to be negligible as usual and set to zero. To begin the analysis, we consider the set of equations (4.156) with $\beta = 1$. Then $\mathbf{T}^p = 0$ and we have the Newtonian similarity solution of chapter 2.4 holding on small length scales. For β close to 1, we would expect this Newtonian solution to hold in a core region away from the corner and walls, with the solvent stresses $\mathbf{T}^s$ dominating the polymer stresses $\mathbf{T}^p$, i.e. $\mathbf{T}^p \ll \mathbf{T}^s$. Boundary layers will turn out to be needed to recover viscometric behaviour for the polymer stresses. These core and boundary layer regions give the exterior regions.

4.3.2 The exterior regions: $(1-\beta)^{(3-\lambda_0)/(1-\lambda_0^2)} \ll r \ll 1$

Core region 1 is where we get Newtonian dominated flow. We anticipate the balances

$$0 = -\nabla p + \nabla.\mathbf{T}^s, \quad \mathbf{T}^s = 2\mathbf{D}, \quad \overset{\triangledown}{\mathbf{T}}^p = 0, \tag{4.157}$$

for $r \ll 1$ in the governing equations. We then have a separable Newtonian stream function solution of the form,

$$\psi \sim \hat{C}_0 r^{1+\lambda_0} f_0(\theta) \quad \text{for } r \ll 1\ , \tag{4.158}$$

with constant $\hat{C}_0$, eigenvalue λ_0 and eigenfunction $f_0(\theta)$ as defined in section 5.1. For the polymer extra stress we take the stretching solution

$$\mathbf{T}^p \sim \lambda(\psi)\mathbf{v}\mathbf{v}^T, \quad \lambda(\psi) = (1-\beta)\hat{C}_1\left(\frac{\psi}{\hat{C}_0}\right)^{n_1}, \tag{4.159}$$

with constant $\hat{C}_1$ and exponent n_1 to be found. The factor $(1-\beta)$ has been introduced for convenience and is suggested by the constitutive equation. We thus scale in core 1

with

$$r = \hat{\epsilon}\hat{R}^*, \quad x = \hat{\epsilon}\hat{X}^*, \quad y = \hat{\epsilon}\hat{Y}^*, \quad \psi = \hat{\epsilon}^{1+\lambda_0}\hat{\Psi}^*, \quad \mathbf{v} = \hat{\epsilon}^{\lambda_0}\hat{\mathbf{v}}^*,$$
$$\mathbf{T}^s = \hat{\epsilon}^{\lambda_0-1}\hat{\mathbf{T}}^{s*}, \quad \mathbf{T}^p = (1-\beta)\hat{\epsilon}^{n_1(1+\lambda_0)+2\lambda_0}\hat{\mathbf{T}}^{p*}, \quad p = \hat{\epsilon}^{\lambda_0-1}\hat{p}^*, \tag{4.160}$$

with $\hat{\epsilon} \ll 1$ artificial. The governing equations become

$$0 = -\hat{\nabla}\hat{p}^* + \hat{\nabla}\cdot\hat{\mathbf{T}}^{s*} + (1-\beta)\hat{\epsilon}^{(1+n_1)(1+\lambda_0)}\hat{\nabla}\cdot\hat{\mathbf{T}}^{p*}, \tag{4.161}$$

$$\mathbf{T}^{s*} = 2(1-(1-\beta))\hat{\mathbf{D}}^*, \quad \hat{\epsilon}^{1-\lambda_0}\hat{\mathbf{T}}^{p*} + \overset{\triangledown}{\hat{\mathbf{T}}}^{p*} = 2\hat{\epsilon}^{-2\lambda_0-n_1(1+\lambda_0)}\hat{\mathbf{D}}^*. \tag{4.162}$$

Thus we obtain

$$0 = -\hat{\nabla}\hat{p}^* + \beta\hat{\nabla}^{*2}\hat{\mathbf{v}}^*, \quad \hat{\mathbf{T}}^{s*} = 2\hat{\mathbf{D}}^*, \quad \overset{\triangledown}{\hat{\mathbf{T}}}^{p*} = 0, \tag{4.163}$$

at leading order since $1/2 \leq \lambda_0 < 1$ and provided

$$(1-\beta)\hat{\epsilon}^{(1+n_1)(1+\lambda_0)} \ll 1, \quad \hat{\epsilon}^{-2\lambda_0-n_1(1+\lambda_0)} \ll 1. \tag{4.164}$$

Using (4.158)–(4.159) we thus have the core 1 solution

$$\hat{\psi}^* \sim \hat{C}_0 R^{*1+\lambda_0} f_0(\theta), \quad \hat{\mathbf{T}}^{s*} = 2\hat{\mathbf{D}}^*, \tag{4.165}$$

$$\hat{\mathbf{T}}^{p*} \sim \hat{\lambda}^*(\hat{\Psi}^*)\hat{\mathbf{v}}^*\hat{\mathbf{v}}^{*T}, \quad \hat{\lambda}^*(\hat{\Psi}^*) = (1-\beta)\hat{C}_1\left(\frac{\hat{\Psi}^*}{\hat{C}_0}\right)^{n_1}. \tag{4.166}$$

The behaviour as the upstream wall is approached as $\hat{Y} \to 0$ is

$$\hat{\Psi}^* \sim \hat{C}_0\hat{X}^{*\lambda_0-1}\hat{Y}^{*2}, \quad \hat{p}^* \sim p_0\hat{X}^{*\lambda_0-1} \tag{4.167}$$

$$\hat{T}_{11}^{p*} \sim 4\hat{C}_0^2\hat{C}_1\hat{X}^{*n_1(\lambda_0-1)+2(\lambda_0-1)}\hat{Y}^{*2(1+n_1)}, \tag{4.168}$$

$$\hat{T}_{12}^{p*} \sim 2\hat{C}_0^2\hat{C}_1(\lambda_0-1)\hat{X}^{*n_1(\lambda_0-1)+2(\lambda_0-1)-1}\hat{Y}^{*2(1+n_1)+1}, \tag{4.169}$$

$$\hat{T}_{22}^{p*} \sim \hat{C}_0^2\hat{C}_1(\lambda_0-1)^2\hat{X}^{*n_1(\lambda_0-1)+2(\lambda_0-1)2}\hat{Y}^{*2(1+n_1)+2}, \tag{4.170}$$

$$\hat{T}_{11}^{s*} \sim 4\beta\hat{C}_0(\lambda_0-1)\hat{X}^{*\lambda_0-2}\hat{Y}^*, \quad \hat{T}_{12}^{s*} \sim 2\beta\hat{C}_0\hat{X}^{*\lambda_0-1}, \quad \hat{T}_{22}^{s*} \sim 4\beta\hat{C}_0(1-\lambda_0)\hat{X}^{*\lambda_0-2}\hat{Y}^*. \tag{4.171}$$

Scaling into the wall with a small parameter $\hat{\delta}$, the wall behaviour (4.167)–(4.171) suggest the boundary layer scalings

$$\begin{aligned}
&\hat{X}^* = \hat{X}, \quad \hat{Y}^* = \hat{\delta}\hat{Y}, \quad \hat{\Psi}^* = \hat{\delta}^2\hat{\Psi}, \quad \hat{p}^* = \hat{p},\\
&\hat{T}^{*s}_{11} = \hat{\delta}\hat{T}^s_{11}, \quad \hat{T}^s_{12} = \hat{T}^s_{12}, \quad \hat{T}^{*s}_{22} = \hat{\delta}\hat{T}^s_{22},\\
&\hat{T}^{*p}_{11} = \hat{\delta}^{2(1+n_1)}\hat{T}^p_{11}, \quad \hat{T}^p_{12} = \hat{\delta}^{2(1+n_1)+1}\hat{T}^p_{12}, \quad \hat{T}^{*p}_{22} = \hat{\delta}^{2(1+n_1)+2}\hat{T}^p_{22}.
\end{aligned} \tag{4.172}$$

The governing equations become

$$0 = -\frac{\partial\hat{p}}{\partial\hat{X}} + \frac{\partial\hat{T}^s_{11}}{\partial\hat{X}} + \frac{1}{\hat{\delta}}\frac{\partial\hat{T}^s_{12}}{\partial\hat{Y}} + (1-\beta)\hat{\epsilon}^{(1+n_1)(1+\lambda_0)}\hat{\delta}^{2(1+n_1)}\left(\frac{\partial\hat{T}^p_{11}}{\partial\hat{X}} + \frac{\partial\hat{T}^p_{12}}{\partial\hat{Y}}\right), \tag{4.173}$$

$$0 = -\frac{1}{\hat{\delta}}\frac{\partial\hat{p}}{\partial\hat{Y}} + \frac{\partial\hat{T}^p_{12}}{\partial\hat{X}} + \frac{\partial\hat{T}^p_{22}}{\partial\hat{Y}} + (1-\beta)\hat{\epsilon}^{(1+n_1)(1+\lambda_0)}\hat{\delta}^{2(1+n_1)+1}\left(\frac{\partial\hat{T}^p_{12}}{\partial\hat{X}} + \frac{\partial\hat{T}^p_{22}}{\partial\hat{Y}}\right), \tag{4.174}$$

$$\frac{\hat{\epsilon}^{1-\lambda_0}}{\hat{\delta}}\hat{T}^p_{11} + \left(\frac{\partial\hat{\Psi}}{\partial\hat{Y}}\frac{\partial\hat{T}^p_{11}}{\partial\hat{X}} - \frac{\partial\hat{\Psi}}{\partial\hat{X}}\frac{\partial\hat{T}^p_{11}}{\partial\hat{Y}} - 2\frac{\partial^2\hat{\Psi}}{\partial\hat{Y}^2}\hat{T}^p_{12} - 2\frac{\partial^2\hat{\Psi}}{\partial\hat{X}\partial\hat{Y}}\hat{T}^p_{11}\right) = 2\hat{\delta}^2\hat{\theta}\frac{\partial^2\hat{\Psi}}{\partial\hat{X}\partial\hat{Y}}, \tag{4.175}$$

$$\frac{\hat{\epsilon}^{1-\lambda_0}}{\hat{\delta}}\hat{T}^p_{22} + \left(\frac{\partial\hat{\Psi}}{\partial\hat{Y}}\frac{\partial\hat{T}^p_{22}}{\partial\hat{X}} - \frac{\partial\hat{\Psi}}{\partial\hat{X}}\frac{\partial\hat{T}^p_{22}}{\partial\hat{Y}} + 2\frac{\partial^2\hat{\Psi}}{\partial\hat{X}^2}\hat{T}^p_{12} + 2\frac{\partial^2\hat{\Psi}}{\partial\hat{X}\partial\hat{Y}}\hat{T}^p_{22}\right) = -2\hat{\theta}\frac{\partial^2\hat{\Psi}}{\partial\hat{X}\partial\hat{Y}}, \tag{4.176}$$

$$\frac{\hat{\epsilon}^{1-\lambda_0}}{\hat{\delta}}\hat{T}^p_{12} + \left(\frac{\partial\hat{\Psi}}{\partial\hat{Y}}\frac{\partial\hat{T}^p_{12}}{\partial\hat{X}} - \frac{\partial\hat{\Psi}}{\partial\hat{X}}\frac{\partial\hat{T}^p_{12}}{\partial\hat{Y}} + \frac{\partial^2\hat{\Psi}}{\partial\hat{X}^2}\hat{T}^p_{11} - \frac{\partial^2\hat{\Psi}}{\partial\hat{Y}^2}\hat{T}^p_{22}\right) = \hat{\theta}\left(\frac{\partial^2\hat{\Psi}}{\partial\hat{Y}^2} - \hat{\delta}^2\frac{\partial^2\hat{\Psi}}{\partial\hat{X}^2}\right), \tag{4.177}$$

where

$$\hat{\theta} = \frac{\hat{\epsilon}^{-2\lambda_0 - n_1(1+\lambda_0)}}{\hat{\delta}^{2(1+n_1)+2}}. \tag{4.178}$$

Balancing in the constitutive equations (4.175)–(4.177) determines $\hat{\delta}$ and $\hat{\theta}$ to be

$$\hat{\delta} = \hat{\epsilon}^{1-\lambda_0}, \quad \hat{\theta} = 1, \tag{4.179}$$

and hence

$$n_1 = \frac{2(\lambda_0 - 2)}{3 - \lambda_0}. \tag{4.180}$$

This gives the leading order momentum equations to be

$$\frac{\partial\hat{T}^s_{12}}{\partial\hat{Y}} = 0, \quad \frac{\partial\hat{p}}{\partial\hat{Y}} = 0, \tag{4.181}$$

hence

$$\hat{T}^s_{12} = 2\beta\hat{C}_0\hat{X}^{\lambda_0-1}, \quad \hat{p} = p_0\hat{X}^{\lambda_0-1}, \tag{4.182}$$

holds throughout boundary layer 1, after matching with $\hat{T}^s_{12}$ and $\hat{p}$ in (4.167) and (4.171). Since

$$\hat{T}^s_{12} = \beta\frac{\partial^2\hat{\Psi}}{\partial\hat{Y}^2} \tag{4.183}$$

in the boundary layer, we may integrate twice and using no slip and normal velocity at the walls determines $\hat{\Psi}$ as

$$\hat{\Psi} = \hat{C}_0\hat{X}^{\lambda_0-1}\hat{Y}^2. \tag{4.184}$$

This matches with the stream function behaviour in (4.167) from core 1. Hence the solvent stresses, pressure and stream function are unchanged at leading order through the boundary layer with explicit solutions

$$\begin{gathered}\hat{\Psi} = \hat{C}_0\hat{X}^{\lambda_0-1}\hat{Y}^2, \quad \hat{p} = \hat{p}_0\hat{X}^{\lambda_0-1}, \\ \hat{T}^s_{11} \sim 4\beta\hat{C}_0(\lambda_0-1)\hat{X}^{\lambda_0-2}\hat{Y}, \quad \hat{T}^s_{12} \sim 2\beta\hat{C}_0\hat{X}^{\lambda_0-2}, \quad \hat{T}^s_{22} \sim 4\beta\hat{C}_0(\lambda_0-1)\hat{X}^{\lambda_0-2}\hat{Y}.\end{gathered} \tag{4.185}$$

The polymer stresses do change throughout the boundary layer which we will describe next. The leading order constitutive equations are

$$\begin{aligned}&\hat{T}^p_{11} + \left(\frac{\partial\hat{\Psi}}{\partial\hat{Y}}\frac{\partial\hat{T}^p_{11}}{\partial\hat{X}} - \frac{\partial\hat{\Psi}}{\partial\hat{X}}\frac{\partial\hat{T}^p_{11}}{\partial\hat{Y}} - 2\frac{\partial^2\hat{\Psi}}{\partial\hat{Y}^2}\hat{T}^p_{12} - 2\frac{\partial^2\hat{\Psi}}{\partial\hat{X}\partial\hat{Y}}\hat{T}^p_{11}\right) = 0, \\ &\hat{T}^p_{22} + \left(\frac{\partial\hat{\Psi}}{\partial\hat{Y}}\frac{\partial\hat{T}^p_{22}}{\partial\hat{X}} - \frac{\partial\hat{\Psi}}{\partial\hat{X}}\frac{\partial\hat{T}^p_{22}}{\partial\hat{Y}} + 2\frac{\partial^2\hat{\Psi}}{\partial\hat{X}^2}\hat{T}^p_{12} + 2\frac{\partial^2\hat{\Psi}}{\partial\hat{X}\partial\hat{Y}}\hat{T}^p_{22}\right) = -2(1-\beta)\frac{\partial^2\hat{\Psi}}{\partial\hat{X}\partial\hat{Y}}, \\ &\hat{T}^p_{12} + \left(\frac{\partial\hat{\Psi}}{\partial\hat{Y}}\frac{\partial\hat{T}^p_{12}}{\partial\hat{X}} - \frac{\partial\hat{\Psi}}{\partial\hat{X}}\frac{\partial\hat{T}^p_{12}}{\partial\hat{Y}} + \frac{\partial^2\hat{\Psi}}{\partial\hat{X}^2}\hat{T}^p_{11} - \frac{\partial^2\hat{\Psi}}{\partial\hat{Y}^2}\hat{T}^p_{22}\right) = (1-\beta)\frac{\partial^2\hat{\Psi}}{\partial\hat{Y}^2}.\end{aligned} \tag{4.186}$$

This is invariant under the one parameter scaling group

$$\begin{gathered}\hat{X} = \gamma X, \quad \hat{Y} = \gamma^{2-\lambda_0}Y, \quad \hat{\Psi} = \gamma^{3-\lambda_0}\Psi, \\ \hat{T}^p_{11} = \gamma^{2(\lambda_0-1)}T^p_{11} \quad \hat{T}^p_{12} = \gamma^{\lambda_0-1}T^p_{12} \quad \hat{T}^p_{22} = \gamma T^p_{22},\end{gathered} \tag{4.187}$$

which suggests the similarity solution

$$\xi = \frac{\hat{Y}}{\hat{X}^{2-\lambda_0}}, \quad \hat{\Psi} = \hat{X}^{3-\lambda_0}\xi^2, \quad \hat{T}^p_{11} = \hat{X}^{2(\lambda_0-1)}t^p_{11}, \quad \hat{T}^p_{12} = \hat{X}^{\lambda_0-1}t^p_{12} \quad \hat{T}^p_{22} = t^p_{22}. \tag{4.188}$$

Putting these scalings into the constitutive equations gives

$$-\hat{C}_0\xi^2(-3+\lambda_0)t^{p'}_{11} + 4\hat{C}_0 t^p_{12} - t^p_{11} = 0, \tag{4.189}$$

$$\xi^2\hat{C}_0(-3+\lambda_0)t^{p'}_{22} + \left(1+\left(-4+4\lambda_0\xi\hat{C}_0\right)\right)t^p_{22} + 2\left(2+\xi\left(-2+\lambda_0\right)t^p_{12}\right)\xi\hat{C}_0(\lambda_0-1) = 0, \tag{4.190}$$

$$\xi^2\hat{C}_0(-3+\lambda_0)t^{p'}_{12} + \left(1+\left(2\lambda_0-2\right)\xi\hat{C}_0\right)t^p_{12} + \xi^2\hat{C}_0(\lambda_0-1)(-2+\lambda_0)t^p_{11} - 2\hat{C}_0(t^p_{22}+1) = 0, \tag{4.191}$$

where $'$ denotes derivatives with respect to ξ. At the wall we have the leading order behaviour as $\xi \to 0$

$$t^p_{11} \sim 8\hat{C}_0^2, \tag{4.192}$$

$$t^p_{12} \sim 2\hat{C}_0, \tag{4.193}$$

$$t^p_{22} \sim 4(1-\lambda_0)\hat{C}_0\xi. \tag{4.194}$$

In the far field we have the matching conditions as $\xi \to \infty$

$$t^p_{11} \sim 4C_1^{sp}\xi^{2(\lambda_0-1)/(3-\lambda_0)}, \tag{4.195}$$

$$t^p_{12} \sim 2(1-\lambda_0)C_1^{sp}\xi^{(\lambda_0+1)/(3-\lambda_0)}, \tag{4.196}$$

$$t^p_{22} \sim (1-\lambda_0)^2C_1^{sp}\xi^{4/(3-\lambda_0)}, \tag{4.197}$$

where we introduce the similarity parameter $C_1^{sp} = \hat{C}_1\hat{C}_0^2$. We record here illustrative numerical solutions using Cartesian variables. The numerical domain we take here for ξ is $[\xi_0, \xi_\infty]$, with the wall behaviour (4.192) imposed at ξ_0 and far field behaviour (4.195) at ξ_∞. To implement we use MATLAB's solver ode15s with absolute and relative tolerances set at 10^{-11}. The two figures in (4.3.2) show the solutions for a re-entrant corner with parameter values $\lambda_0 = 0.56, \xi_0 = 10^{-6}, \xi_\infty = 10^{10}$ and $\lambda_0 = 0.9, \xi_0 = 10^{-6}, \xi_\infty = 10^{10}$ respectively. Convergence to far-field behaviour is demonstrated to ten significant figures.

The asymptotic behaviours in (4.192), (4.195) determines how many conditions are imposed on this third order system. The wall behaviour (4.192) imposes three

conditions on (4.189) thus leaving no degrees of freedom as $\xi \to 0$. In the far field, the parameter $\hat{C}_1^{sp}$ is free with two further free parameters present but existing as higher order expansion terms. The problem can thus be posed as an initial value problem. The downstream boundary layer requires the natural stress formulation for its solution, which is left as further work.

For reference, we note that scaling directly into the boundary layer from the outer region we use the scalings

$$\begin{aligned} x = \hat{\epsilon}\hat{X}, \quad y = \hat{\epsilon}^{2-\lambda_0}\hat{Y}, \quad \psi = \hat{\epsilon}^{3-\lambda_0}\hat{\Psi}, \quad p = \hat{\epsilon}^{4(\lambda_0-1)/(3-\lambda_0)}\hat{p} \\ T_{11}^s = \hat{T}_{11}^s, \quad T_{12}^s = \hat{\epsilon}^{\lambda_0-1}\hat{T}_{12}^s, \quad T_{22}^s = \hat{T}_{22}^s, \\ T_{11}^p = \hat{\epsilon}^{2(\lambda_0-1)}\hat{T}_{11}^p, \quad T_{12}^p = \hat{\epsilon}^{\lambda_0-1}\hat{T}_{12}^p, \quad T_{22}^p = \hat{T}_{22}^p. \end{aligned} \tag{4.198}$$

We can now determine the main length scale that will motivate consideration of an intermediate region closer to the corner. Since $(1-\beta)$ is a small quantity, in the core region, we know the scalings of $\mathbf{T}^p$ and $\mathbf{T}^s$ to be

$$\mathbf{T}^p = O\left((1-\beta)r^{(1+\lambda_0)n_1+2\lambda_0}\right) = O\left((1-\beta)r^{4(\lambda_0-1)/(3-\lambda_0)}\right), \quad \mathbf{T}^s = O\left(r^{\lambda_0-1}\right). \tag{4.199}$$

The balance of core region 1 holds until the polymer and solvent extra stress become the same size i.e. $\mathbf{T}^p = O(\mathbf{T}^s)$. This occurs when the sizes in (4.199) are of similar order and determines the main length scale to be

$$r = O\left((1-\beta)^{(3-\lambda_0)/(1-\lambda_0^2)}\right). \tag{4.200}$$

We note that the conditions (4.164) can be verified with the first condition being

$$(1-\beta)^{(3-\lambda_0)/(1-\lambda_0^2)} \ll \hat{\epsilon}, \tag{4.201}$$

this being the lower limit on the length scale for core region 1. The core and boundary layer equations have been found for the exterior region, now we look at an intermediate region.

4.3.3 The main length scale: $r \leq (1-\beta)^{(3-\lambda_0)/(1-\lambda_0^2)}$

In this region we have $\mathbf{T}^p = O(\mathbf{T}^s)$ and introduce the small parameter ϵ to represent the length (4.200). We scale with

$$\begin{aligned} r = \epsilon R^*, \quad x = \epsilon X^*, \quad y = \epsilon Y^*, \quad \psi = \epsilon^q \Psi^*, \quad \mathbf{v} = \epsilon^{q-1}\mathbf{v}^*, \\ \mathbf{T}^s = \epsilon^{q-2}\mathbf{T}^{s*}, \quad \mathbf{T}^p = \epsilon^{q-2}\mathbf{T}^{p*}, \quad p = \epsilon^{q-2}p^*, \end{aligned} \tag{4.202}$$

where q is an as yet undetermined arbitrary scaling for the stream function. Into the governing equations we get

$$0 = -\nabla^* p^* + \nabla^* \cdot \mathbf{T}^{p*} + \nabla^* \cdot \mathbf{T}^{s*} \tag{4.203}$$

$$\mathbf{T}^{p*} + \epsilon^{q-2} \overset{\triangledown}{\mathbf{T}}^{p*} = 2(1-\beta)\mathbf{D}^*. \tag{4.204}$$

We would expect $q < 2$, for example to match with core region 1 we require $q = 1 + \lambda_0$ as $R^* \to \infty$, hence the leading order core equations are

$$0 = -\nabla^* p^* + \nabla^* \cdot \mathbf{T}^{p*} + \nabla^* \cdot \mathbf{T}^{s*}, \quad \mathbf{T}^{s*} = 2\beta\mathbf{D}^*, \quad \overset{\triangledown}{\mathbf{T}}^{p*} = 0. \tag{4.205}$$

Seeking viscometric behaviour at the walls, we scale into the wall boundary layers using a small parameter δ with the scalings

$$\begin{aligned} &X^* = X, \quad Y^* = \delta Y, \quad \Psi^* = \gamma\Psi, \quad p^* = \theta p \\ &T_{11}^* = \theta T_{11}, \quad T_{12}^* = \theta\delta T_{12}, \quad T_{22}^* = \theta\delta^2 T_{22}, \\ &T_{11}^{s*} = \frac{\gamma}{\delta} T_{11}^s, \quad T_{12}^{s*} = \frac{\gamma}{\delta^2} T_{12}^s, \quad T_{22}^{s*} = \frac{\gamma}{\delta} T_{22}^s, \\ &T_{11}^{p*} = \theta T_{11}^p, \quad T_{12}^{p*} = \theta\delta T_{12}^p, \quad T_{22}^{p*} = \theta\delta^2 T_{22}^p, \end{aligned} \tag{4.206}$$

for gauges γ and θ to be determined and where we have chosen to balance the pressure with the polymer stress component T^p_{11}. Into the constitutive equations we get

$$\theta T^p_{11} + \frac{\theta\gamma\epsilon^{q-2}}{\delta}\left(\frac{\partial\Psi}{\partial Y}\frac{\partial T^p_{11}}{\partial X} - \frac{\partial\Psi}{\partial X}\frac{\partial T^p_{11}}{\partial Y} - 2\frac{\partial^2\Psi}{\partial Y^2}T^p_{12} - 2\frac{\partial^2\Psi}{\partial X\partial Y}T^p_{11}\right) = 2(1-\beta)\frac{\gamma}{\delta}\frac{\partial^2\Psi}{\partial X\partial Y}, \tag{4.207}$$

$$\theta T^p_{22} + \frac{\theta\gamma\epsilon^{q-2}}{\delta}\left(\frac{\partial\Psi}{\partial Y}\frac{\partial T^p_{22}}{\partial X} - \frac{\partial\Psi}{\partial X}\frac{\partial T^p_{22}}{\partial Y} + 2\frac{\partial^2\Psi}{\partial X^2}T^p_{12} + 2\frac{\partial^2\Psi}{\partial X\partial Y}T^p_{22}\right) = -2(1-\beta)\frac{\gamma}{\delta^3}\frac{\partial^2\Psi}{\partial X\partial Y}, \tag{4.208}$$

$$\theta T^p_{12} + \frac{\theta\gamma\epsilon^{q-2}}{\delta}\left(\frac{\partial\Psi}{\partial Y}\frac{\partial T^p_{12}}{\partial X} - \frac{\partial\Psi}{\partial X}\frac{\partial T^p_{12}}{\partial Y} + \frac{\partial^2\Psi}{\partial X^2}T^p_{11} - \frac{\partial^2\Psi}{\partial Y^2}T^p_{22}\right) = (1-\beta)\frac{\gamma}{\delta^3}\left(\frac{\partial^2\Psi}{\partial Y^2} - \delta^2\frac{\partial^2\Psi}{\partial X^2}\right). \tag{4.209}$$

Balancing the linear stress terms with the upper convected stress derivative terms, along with the r.h.s. terms in T^p_{12} and T^p_{22} determines γ and δ to be

$$\delta = \frac{(1-\beta)^{1/2}}{\theta^{1/2}}\epsilon^{1-q/2}, \quad \gamma = \frac{(1-\beta)^{1/2}}{\theta^{1/2}}\epsilon^{3(1-q/2)}. \tag{4.210}$$

Considering the momentum equations, we have

$$0 = -\frac{\partial p}{\partial X} + \frac{\partial T^p_{11}}{\partial X} + \frac{\partial T^p_{12}}{\partial Y} + \frac{\epsilon^{2(1-q/2)}}{\theta}\frac{\partial T^s_{11}}{\partial X} + \frac{\theta}{(1-\beta)}\frac{\partial T^s_{12}}{\partial Y}, \tag{4.211}$$

$$0 = -\frac{\partial p}{\partial Y} + \delta^2\left(\frac{\partial T^p_{12}}{\partial X} + \frac{\partial T^p_{22}}{\partial Y}\right) + \frac{\gamma}{\delta\theta}\left(\frac{\partial T^s_{11}}{\partial X} + \frac{\partial T^s_{12}}{\partial Y}\right). \tag{4.212}$$

To retain the solvent shear stress we require $\theta = (1-\beta)$ and thus $\delta = \epsilon^{1-q/2}, \gamma = \epsilon^{3(1-q/2)}$. The leading order boundary layer equations for the momentum equations are thus

$$0 = -\frac{\partial p}{\partial X} + \frac{\partial T^p_{11}}{\partial X} + \frac{\partial T^p_{12}}{\partial Y} + \frac{\partial T^s_{12}}{\partial Y}, \quad 0 = -\frac{\partial p}{\partial Y}, \tag{4.213}$$

provided

$$\frac{\gamma}{\delta\theta} = \frac{\epsilon^{2-q}}{(1-\beta)} \ll 1, \tag{4.214}$$

which at least holds for $q = 1 + \lambda_0$. The polymer extra stresses satisfy

$$T_{11}^p + \left(\frac{\partial \Psi}{\partial Y} \frac{\partial T_{11}^p}{\partial X} - \frac{\partial \Psi}{\partial X} \frac{\partial T_{11}^p}{\partial Y} - 2 \frac{\partial^2 \Psi}{\partial Y^2} T_{12}^p - 2 \frac{\partial^2 \Psi}{\partial X \partial Y} T_{11}^p \right) = 0, \tag{4.215}$$

$$T_{22}^p + \left(\frac{\partial \Psi}{\partial Y} \frac{\partial T_{22}^p}{\partial X} - \frac{\partial \Psi}{\partial X} \frac{\partial T_{22}^p}{\partial Y} + 2 \frac{\partial^2 \Psi}{\partial X^2} T_{12}^p + 2 \frac{\partial^2 \Psi}{\partial X \partial Y} T_{22}^p \right) = -2 \frac{\partial^2 \Psi}{\partial X \partial Y}, \tag{4.216}$$

$$T_{12}^p + \left(\frac{\partial \Psi}{\partial Y} \frac{\partial T_{12}^p}{\partial X} - \frac{\partial \Psi}{\partial X} \frac{\partial T_{12}^p}{\partial Y} + \frac{\partial^2 \Psi}{\partial X^2} T_{11}^p - \frac{\partial^2 \Psi}{\partial Y^2} T_{22}^p \right) = \frac{\partial^2 \Psi}{\partial Y^2}. \tag{4.217}$$

A simple similarity solution to these boundary layer equations and the core is not anticipated for the whole of this intermediate region. On smaller length scales in this intermediate region we would expect to obtain the similarity solution detailed in chapter 3.

4.4 Discussion

For the re-entrant corner geometry, we have considered three parameter limits of the Oldroyd-B equations. Those were low and high We with $\beta < 1$ and the Newtonian limit $\beta \to 1$ with We $= O(1)$. The majority of the analysis has been done using the Cartesian formulation with the natural stress formulations not providing any further information.

For the low Weissenberg limit we found three asymptotic regions, an exterior region where Newtonian flow is found and an interior region where Oldroyd-B We $= O(1)$ flow holds. An intermediate or matching region was found to transition between these different flow states. The critical length scale We $^{\frac{1}{1-\lambda_0}}$ was found that determines where these flow structures occur, along with core and boundary layer regions for each determined. The results obtained here are very similar to those obtained for the low-Weissenberg UCM behaviour obtained by Evans in [19], recovering UCM behaviour in the asymptotic regions when setting $\beta = 0$.

As discussed previously, the high Weissenberg number limit comprises a six-region structure. In the core regions, the stress singularity is $O(r^{-2(1-\alpha)})$ as for the UCM case. In the outer core region a stretching similarity solution may exist for when the stream function $\psi = O(r^{3\alpha})$ is different from the $We = 1$ case where $\psi = O(r^{\alpha(3-\alpha)})$. Also similar to the UCM case is that the $We = 1$ problem is present in the interior regions located at distances less that $O(We^{-1/2})$ away from the corner. Where the analysis differs from UCM is the difficulty in picking up a solution in the exterior region and thus whether a intermediate matching region can be found as the corner is approached.

The Newtonian limit $\beta \to 1$ has identified the main regions in which Newtonian

flow is obtained and the length scale on which it breaks down closer to the corner. This region we termed the intermediate region, the finer details of which is left as unfinished work.

It would be of interest to see if the structures presented here can be validated through full numerical simulation of the equations. The low Weissenberg number limit and the Newtonian limit should cause numerical schemes no difficulties, although the high Weissenberg limit is still likely to prove notoriously difficult. The double limits involving both $\beta \to 1$ and We are likely to form even more complicated asymptotic structures with additional regions needing to be included.

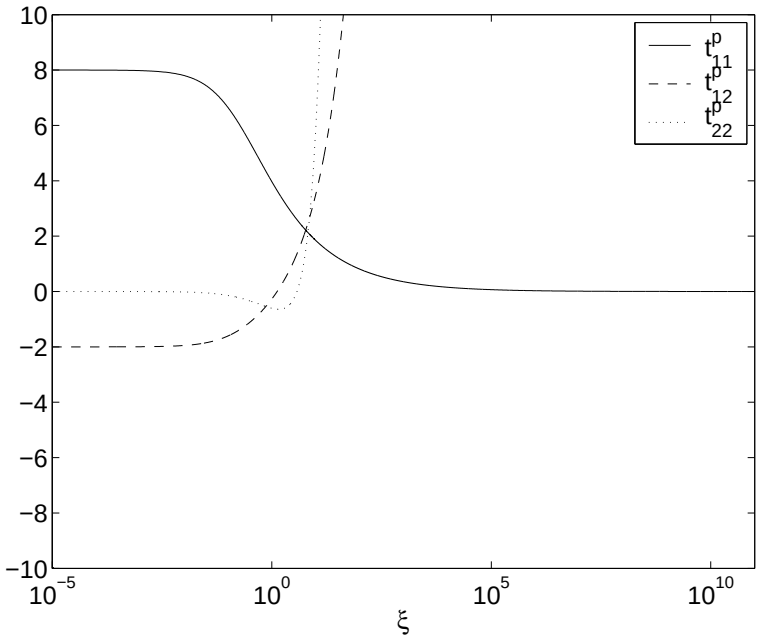

(a) Solution profiles for t^p_{11}, t^p_{12}, t^p_{22},

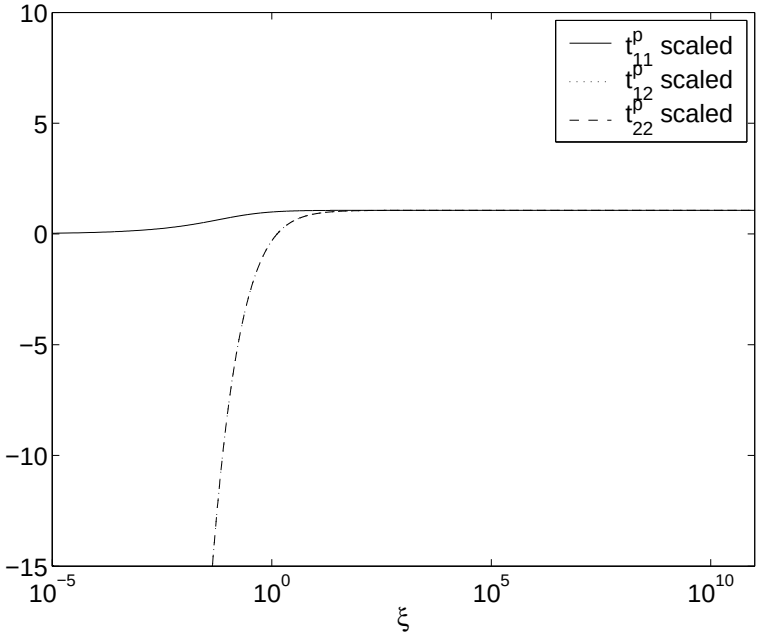

(b) Solution profiles for t^p_{11}, t^p_{12}, t^p_{22} scaled with ξ. All should (and do) tend to $C_1^{sp} = 1.0678176398$ to 10 decimal places which is sufficient convergence.

Figure 4-3: To implement we use MATLAB's solver ode15s with absolute and relative tolerances set at 10^{-11}. We have the solution for an upstream re-entrant corner with parameter values $\lambda_0 = 0.56, \xi_0 = 10^{-6}, \xi_\infty = 10^{10}$. In the second picture, we scale with the far-field behaviour aiming to pick up an estimate for C_1^{sp}. Convergence is found with $C_1^{sp} = 1.0678176398$ to 10 decimal places.

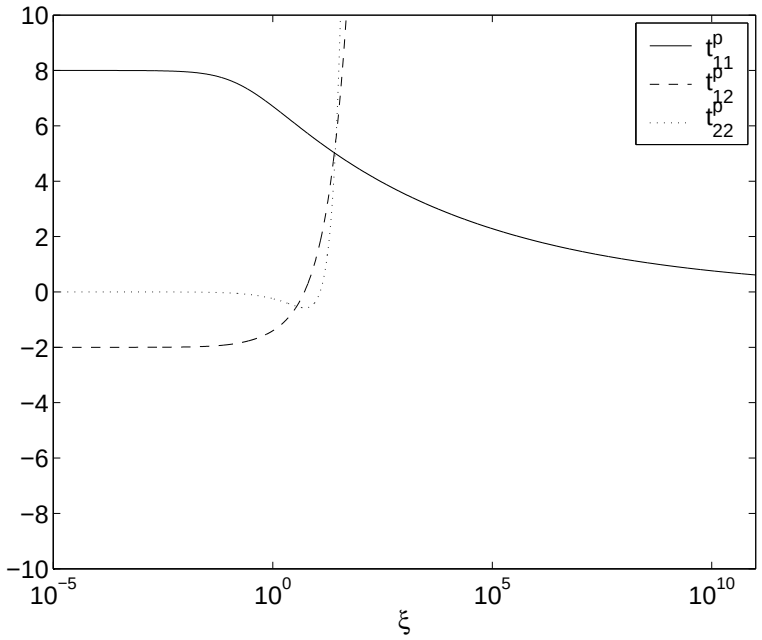

(a) Solution profiles for t^p_{11}, t^p_{12}, t^p_{22} with $\lambda = 0.9$. t^p_{11} slopes off much slower as λ increases, decreasing the rate of convergence.

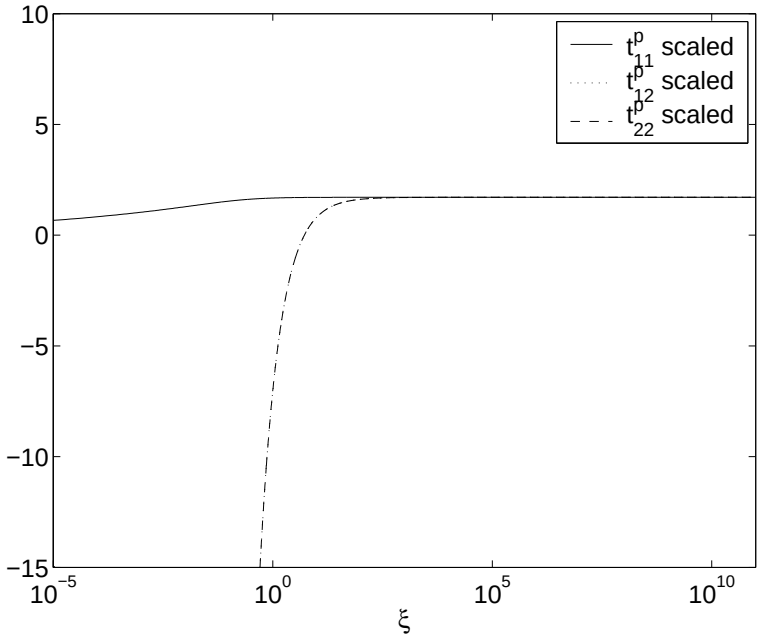

(b) Solution profiles for t^p_{11}, t^p_{12}, t^p_{22} scaled with ξ. All should (and do) tend to $C_1^{sp} = 1.70986761423$ to 10 decimal places which is sufficient convergence.

Figure 4-4: Implementation of the similarity problem with parameter values $\lambda_0 = 0.90, \xi_0 = 10^{-6}, \xi_\infty = 10^{10}$ with the same tolerances as in 4.3.2. Convergence to C_1 is found with $C_1^{sp} = 1.70986761423$ to 10 decimal places.

Chapter 5

Salient Corner Flow

In this chapter we will consider Salient corner flow for the Oldroyd-B fluid. Preliminary results on Newtonian flow first discussed in section 2.4 will be used for Oldroyd-B flow in section 5.1, where we shall show that the Newtonian solution dominates in a core outer region away from the walls.

5.1 Salient corner flow of the Oldroyd-B fluid

We consider now the salient corner flow of the Oldroyd-B fluid with the usual governing equations

$$\begin{aligned} &\nabla.\mathbf{v} = 0, \quad \text{Re } (\mathbf{v}.\nabla)\mathbf{v} = -\nabla p + \nabla.\mathbf{T}^p + \beta\nabla^2\mathbf{v}, \\ &\mathbf{T}^p + \text{We } \overset{\triangledown}{\mathbf{T}}{}^p = 2(1-\beta)\mathbf{D}. \end{aligned} \tag{5.1}$$

As for the re-entrant corner there is no natural length scale, so the Weissenberg number can be scaled out of the problem and set to unity. The geometry to consider is shown in figure (5-1). In this geometry, as opposed to the re-entrant corner, we are about to show that the velocity gradient and upper convected polymer stress are small (for example see [55]) in the core region, with the dominant behaviour being described by the Stokes equation. So we assume the flow in the core region away from the walls satisfies

$$\mathbf{T}^p \sim 2(1-\beta)\mathbf{D}. \tag{5.2}$$

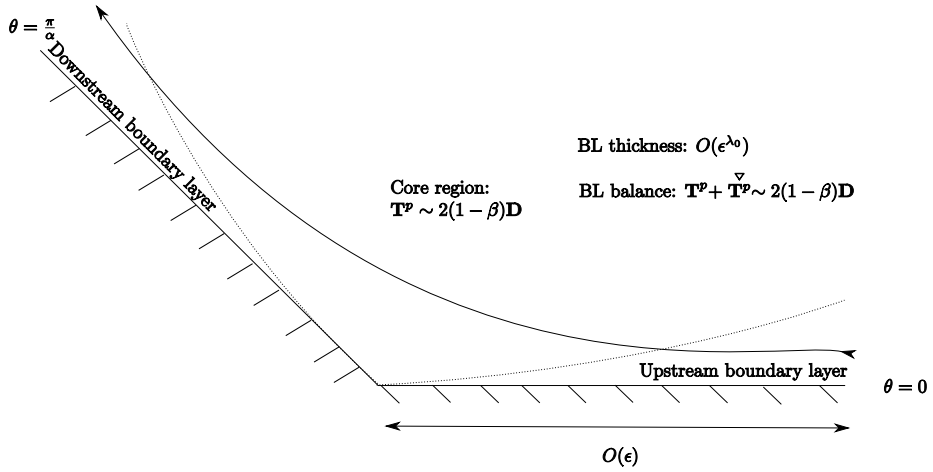

Figure 5-1: Salient corner geometry, with the main asymptotic regions shown and dominant balances given. Distances to the corner are of $O(\epsilon)$, and are assumed to be small. This geometry differs from the re-entrant corner as here the corner angle depends upon α in the range $\alpha \in (1, \infty)$. Viscometric behaviour is not recovered in the core region so a boundary layer is present. For corner angles less than 146.3°, eddies will be present as discussed in section 2.4. This figure then illustrates the flow pattern for corner angles between 180° and 146.3°.

Using the small parameter ϵ, the core scalings will be

$$\begin{aligned} &r = \epsilon R^*, \quad x = \epsilon X^*, \quad y = \epsilon Y^*, \quad \psi = \epsilon^q \Psi^* \\ &\mathbf{v} = \epsilon^{q-1}\mathbf{v}^*, \quad \mathbf{T}^p = \epsilon^{q-2}\mathbf{T}^{p*}, \quad p = \epsilon^{q-2}p^*, \end{aligned} \tag{5.3}$$

with unknown parameter q, where the exponent for p is chosen the same as for $\mathbf{T}^p$ due to the momentum equation. In the governing equations we have

$$\begin{aligned} &\text{Re } \epsilon^q(\mathbf{v}^* \cdot \nabla^*)\mathbf{v}^* = -\nabla^* p^* + \nabla^*.\mathbf{T}^{p*} + \beta\nabla^{*2}\mathbf{v}^*, \\ &\mathbf{T}^{p*} + \epsilon^{q-2}\,\overset{\triangledown}{\mathbf{T}}{}^{p*} = 2(1-\beta)\mathbf{D}^*, \end{aligned} \tag{5.4}$$

so for the balance (5.2) in the constitutive equations we require $q > 2$. At leading order in the core region we have

$$\nabla^* p^* = \nabla^* . \mathbf{T}^{p*} + \beta \nabla^{*2} \mathbf{v}^*, \quad \mathbf{T}^{p*} = 2(1-\beta)\mathbf{D}^*, \tag{5.5}$$

or combining the equations

$$\nabla^* p^* = \nabla^2 \mathbf{v}^*. \tag{5.6}$$

This may then be solved as for the Newtonian case since the same balance occurs. Hence, we determine $q = \lambda_0 + 1$, found from the Newtonian stream function behaviour. The analysis of section 2.4 is then relevant here, noting that for salient corners we have α in the range $\alpha \in (1, \infty)$. Thus the stream function exponent λ_0 satisfies $\mathrm{Re}(\lambda_0) > 1$. This is crucial as now $q = \mathrm{Re}(\lambda_0) + 1 > 2$ does hold.

Using the wall behaviour as $y \to 0$ from (2.99) in current variables, we have

$$\begin{aligned}
&\Psi^* \sim c_0 X^{*\lambda_0 - 1} Y^{*2}, \quad p^* \sim p_0 X^{*\lambda_0 - 1} + 2(1-\lambda_0) c_0 X^{*\lambda_0 - 2} Y^*, \\
&T_{11}^{s*} \sim 4(\lambda_0 - 1)\beta c_0 X^{*\lambda_0 - 2} Y^*, \quad T_{12}^{s*} \sim 2\beta c_0 X^{*\lambda_0 - 1}, \\
&T_{22}^{s*} \sim -4(\lambda_0 - 1)\beta c_0 X^{*\lambda_0 - 2} Y^*, \\
&T_{11}^{p*} \sim 4(\lambda_0 - 1)(1-\beta) c_0 X^{*\lambda_0 - 2} Y^*, \quad T_{12}^{p*} \sim 2c_0(1-\beta) X^{*\lambda_0 - 1}, \\
&T_{22}^{p*} \sim -4(\lambda_0 - 1)(1-\beta) c_0 X^{*\lambda_0 - 2} Y^*.
\end{aligned} \tag{5.7}$$

We may see that although it is a Newtonian shearing flow, it does not give Oldroyd-B viscometric behaviour for the polymer extra stresses. Needing to find wall boundary layers, we can use the behaviours (5.7) to suggest the scalings

$$\begin{aligned}
&X^* = \bar{X}, \quad Y^* = \delta \bar{Y}, \quad \Psi^* = \delta^2 \bar{\Psi}, \quad p^* = \bar{p}_0(\bar{X}) + \delta \bar{p}, \\
&T_{11}^{p*} = \delta \bar{T}_{11}^p, \quad T_{12}^{p*} = \bar{T}_{12}^p, \quad T_{22}^{p*} = \delta \bar{T}_{22}^p.
\end{aligned} \tag{5.8}$$

The momentum equations become

$$\begin{aligned}
\mathrm{Re}\ \epsilon^{\lambda_0 - 1}\delta^3 \left(\frac{\partial \bar{\Psi}}{\partial \bar{Y}} \frac{\partial^2 \bar{\Psi}}{\partial \bar{X} \partial \bar{Y}} - \frac{\partial \bar{\Psi}}{\partial \bar{X}} \frac{\partial^2 \bar{\Psi}}{\partial \bar{Y}^2} \right) &= -\left(\delta \frac{\partial \bar{p}_0}{\partial \bar{X}} + \delta^2 \frac{\partial \bar{p}}{\partial \bar{X}} \right) \\
&\quad + \delta^2 \frac{\partial \bar{T}_{11}^p}{\partial \bar{X}} + \frac{\partial \bar{T}_{12}^p}{\partial \bar{Y}} + \delta^2 \beta \frac{\partial^3 \bar{\Psi}}{\partial \bar{X}^2 \partial \bar{Y}} + \beta \frac{\partial^3 \bar{\Psi}}{\partial \bar{Y}^3},
\end{aligned} \tag{5.9}$$

$$\begin{aligned}
\mathrm{Re}\ \epsilon^{\lambda_0 - 1}\delta^3 \left(-\frac{\partial \bar{\Psi}}{\partial \bar{Y}} \frac{\partial^2 \bar{\Psi}}{\partial \bar{X}^2} + \frac{\partial \bar{\Psi}}{\partial \bar{X}} \frac{\partial^2 \bar{\Psi}}{\partial \bar{X} \partial \bar{Y}} \right) &= \\
&\quad - \frac{\partial \bar{p}}{\partial \bar{Y}} + \frac{\partial \bar{T}_{12}^p}{\partial \bar{X}} + \frac{\partial \bar{T}_{22}^p}{\partial \bar{Y}} - \delta^2 \beta \frac{\partial^3 \bar{\Psi}}{\partial \bar{X}^3} - \beta \frac{\partial^3 \bar{\Psi}}{\partial \bar{X} \partial \bar{Y}^2},
\end{aligned} \tag{5.10}$$

and the constitutive equations

$$\bar{T}^p_{11} + \frac{\epsilon^{\lambda_0-1}}{\delta}\left(\delta^2\left(\frac{\partial\bar{\Psi}}{\partial\bar{Y}}\frac{\partial\bar{T}^p_{11}}{\partial\bar{X}} - \frac{\partial\bar{\Psi}}{\partial\bar{X}}\frac{\partial\bar{T}^p_{11}}{\partial\bar{Y}} - 2\frac{\partial^2\bar{\Psi}}{\partial\bar{X}\partial\bar{Y}}\bar{T}^p_{11}\right) - 2\frac{\partial^2\bar{\Psi}}{\partial\bar{Y}^2}\bar{T}^p_{12}\right)$$
$$= 2(1-\beta)\frac{\partial^2\bar{\Psi}}{\partial\bar{X}\partial\bar{Y}}, \tag{5.11}$$

$$\bar{T}^p_{22} + \epsilon^{\lambda_0-1}\delta\left(\frac{\partial\bar{\Psi}}{\partial\bar{Y}}\frac{\partial\bar{T}^p_{22}}{\partial\bar{X}} - \frac{\partial\bar{\Psi}}{\partial\bar{X}}\frac{\partial\bar{T}^p_{22}}{\partial\bar{Y}} + 2\frac{\partial^2\bar{\Psi}}{\partial\bar{X}^2}\bar{T}^p_{12} + 2\frac{\partial^2\bar{\Psi}}{\partial\bar{X}\partial\bar{Y}}\bar{T}^p_{22}\right)$$
$$= -2(1-\beta)\frac{\partial^2\bar{\Psi}}{\partial\bar{X}\partial\bar{Y}}, \tag{5.12}$$

$$\bar{T}^p_{12} + \epsilon^{\lambda_0-1}\left(\delta\left(\frac{\partial\bar{\Psi}}{\partial\bar{Y}}\frac{\partial\bar{T}^p_{12}}{\partial\bar{X}} - \frac{\partial\bar{\Psi}}{\partial\bar{X}}\frac{\partial\bar{T}^p_{12}}{\partial\bar{Y}} - \frac{\partial^2\bar{\Psi}}{\partial\bar{Y}^2}\bar{T}^p_{22}\right) + \delta^3\frac{\partial^2\bar{\Psi}}{\partial\bar{X}^2}\bar{T}^p_{11}\right)$$
$$= (1-\beta)\frac{\partial^2\bar{\Psi}}{\partial\bar{Y}^2} - \delta^2\frac{\partial^2\bar{\Psi}}{\partial\bar{X}^2}. \tag{5.13}$$

The only possible balance which allows a thin boundary layer, is that of $\delta = \epsilon^{\lambda_0-1}$ from (5.11) (giving a boundary layer thickness of ϵ^{λ_0}). Hence we have

$$\text{Re }\epsilon^{4(\lambda_0-1)}\left(\frac{\partial\bar{\Psi}}{\partial\bar{Y}}\frac{\partial^2\bar{\Psi}}{\partial\bar{X}\partial\bar{Y}} - \frac{\partial\bar{\Psi}}{\partial\bar{X}}\frac{\partial^2\bar{\Psi}}{\partial\bar{Y}^2}\right) = -\left(\epsilon^{(\lambda_0-1)}\frac{\partial\bar{p}_0}{\partial\bar{X}} + \epsilon^{2(\lambda_0-1)}\frac{\partial\bar{p}}{\partial\bar{X}}\right)$$
$$+ \epsilon^{2(\lambda_0-1)}\frac{\partial\bar{T}^p_{11}}{\partial\bar{X}} + \frac{\partial\bar{T}^p_{12}}{\partial\bar{Y}} + \epsilon^{2(\lambda_0-1)}\beta\frac{\partial^3\bar{\Psi}}{\partial\bar{X}^2\partial\bar{Y}} + \beta\frac{\partial^3\bar{\Psi}}{\partial\bar{Y}^3}, \tag{5.14}$$

$$\text{Re }\epsilon^{4(\lambda_0-1)}\left(-\frac{\partial\bar{\Psi}}{\partial\bar{Y}}\frac{\partial^2\bar{\Psi}}{\partial\bar{X}^2} + \frac{\partial\bar{\Psi}}{\partial\bar{X}}\frac{\partial^2\bar{\Psi}}{\partial\bar{X}\partial\bar{Y}}\right) =$$
$$- \frac{\partial\bar{p}}{\partial\bar{Y}} + \frac{\partial\bar{T}^p_{12}}{\partial\bar{X}} + \frac{\partial\bar{T}^p_{22}}{\partial\bar{Y}} - \epsilon^{2(\lambda_0-1)}\beta\frac{\partial^3\bar{\Psi}}{\partial\bar{X}^3} - \beta\frac{\partial^3\bar{\Psi}}{\partial\bar{X}\partial\bar{Y}^2}, \tag{5.15}$$

and

$$\bar{T}^p_{11} + \epsilon^{2(\lambda_0-1)}\left(\frac{\partial\bar{\Psi}}{\partial\bar{Y}}\frac{\partial\bar{T}^p_{11}}{\partial\bar{X}} - \frac{\partial\bar{\Psi}}{\partial\bar{X}}\frac{\partial\bar{T}^p_{11}}{\partial\bar{Y}} - 2\frac{\partial^2\bar{\Psi}}{\partial\bar{X}\partial\bar{Y}}\bar{T}^p_{11}\right) - 2\frac{\partial^2\bar{\Psi}}{\partial\bar{Y}^2}\bar{T}^p_{12}$$
$$= 2(1-\beta)\frac{\partial^2\bar{\Psi}}{\partial\bar{X}\partial\bar{Y}}, \tag{5.16}$$

$$\bar{T}^p_{22} + \epsilon^{2(\lambda_0-1)}\left(\frac{\partial\bar{\Psi}}{\partial\bar{Y}}\frac{\partial\bar{T}^p_{22}}{\partial\bar{X}} - \frac{\partial\bar{\Psi}}{\partial\bar{X}}\frac{\partial\bar{T}^p_{22}}{\partial\bar{Y}} + 2\frac{\partial^2\bar{\Psi}}{\partial\bar{X}^2}\bar{T}^p_{12} + 2\frac{\partial^2\bar{\Psi}}{\partial\bar{X}\partial\bar{Y}}\bar{T}^p_{22}\right)$$
$$= -2(1-\beta)\frac{\partial^2\bar{\Psi}}{\partial\bar{X}\partial\bar{Y}}, \tag{5.17}$$

$$\bar{T}^p_{12} + \epsilon^{2(\lambda_0-1)}\left(\frac{\partial\bar{\Psi}}{\partial\bar{Y}}\frac{\partial\bar{T}^p_{12}}{\partial\bar{X}} - \frac{\partial\bar{\Psi}}{\partial\bar{X}}\frac{\partial\bar{T}^p_{12}}{\partial\bar{Y}} - \frac{\partial^2\bar{\Psi}}{\partial\bar{Y}^2}\bar{T}^p_{22}\right) + \epsilon^{4(\lambda_0-1)}\frac{\partial^2\bar{\Psi}}{\partial\bar{X}^2}\bar{T}^p_{11}$$
$$= (1-\beta)\frac{\partial^2\bar{\Psi}}{\partial\bar{Y}^2} - \epsilon^{2(\lambda_0-1)}\frac{\partial^2\bar{\Psi}}{\partial\bar{X}^2}. \tag{5.18}$$

At leading order in ϵ we thus obtain

$$0 = \frac{\partial \bar{T}^p_{12}}{\partial \bar{Y}} + \beta \frac{\partial^3 \bar{\Psi}}{\partial \bar{Y}^3}, \quad 0 = -\frac{\partial \bar{p}}{\partial \bar{Y}} + \frac{\partial \bar{T}^p_{12}}{\partial \bar{X}} + \frac{\partial \bar{T}^p_{22}}{\partial \bar{Y}} - \beta \frac{\partial^3 \bar{\Psi}}{\partial \bar{X} \partial \bar{Y}^2}. \tag{5.19}$$

$$\bar{T}^p_{11} - 2\frac{\partial^2 \bar{\Psi}}{\partial \bar{Y}^2} \bar{T}^p_{12} = 2(1-\beta)\frac{\partial^2 \bar{\Psi}}{\partial \bar{X} \partial \bar{Y}}, \bar{T}^p_{22} = -2(1-\beta)\frac{\partial^2 \bar{\Psi}}{\partial \bar{X} \partial \bar{Y}}, \bar{T}^p_{12} = (1-\beta)\frac{\partial^2 \bar{\Psi}}{\partial \bar{Y}^2}, \tag{5.20}$$

Eliminating $\bar{T}^p_{12}$ from the first equation in (5.19) using the third in (5.20) and then integrating with respect to $\bar{Y}$ gives

$$\bar{\Psi} = \frac{1}{2}\bar{a}(\bar{X})\bar{Y}^2 + \bar{b}(\bar{X})\bar{Y} + \bar{c}(\bar{X}), \tag{5.21}$$

for some functions $\bar{a}(\bar{X})$, $\bar{b}(\bar{X})$ and $\bar{c}(\bar{X})$. The no-slip and no normal velocity conditions imposed on the wall imply that $\bar{\Psi} = \frac{\partial \bar{\Psi}}{\partial \bar{Y}} = 0$ on $\bar{Y} = 0$, and thus $\bar{b}(\bar{X}) = \bar{c}(\bar{X}) = 0$, leaving

$$\bar{\Psi} = \frac{1}{2}\bar{a}(\bar{X})\bar{Y}^2. \tag{5.22}$$

We can solve now for the polymer stress components in (5.20) and integrate the pressure equation in (5.19) to obtain

$$\bar{T}^p_{11} = 2(1-\beta)\left(\bar{a}'(\bar{X})\bar{Y} + \bar{a}(\bar{X})^2\right), \quad \bar{T}_{12} = (1-\beta)\bar{a}(\bar{X}), \quad \bar{T}^p_{22} = -2(1-\beta)\bar{a}'(\bar{X})\bar{Y},$$
$$\bar{p} = -\bar{a}'(\bar{X})\bar{Y} + \bar{p}_0(\bar{X}), \tag{5.23}$$

which is an explicit solution to the boundary layer equations in terms of the unknown functions $\bar{a}(\bar{X})$ and $\bar{p}_0(\bar{X})$. Recalling the far-field behaviour as $\theta \to 0$ from (5.7), writing these in terms of inner barred variables (equivalent to the limit as $\bar{Y} \to \infty$) gives

$$\begin{aligned}
&\bar{\Psi} \sim c_0 \bar{X}^{\lambda_0 - 1}\bar{Y}^2, \quad \bar{p} \sim p_0 \bar{X}^{\lambda_0 - 1} + 2(1-\lambda_0)c_0 \bar{X}^{\lambda_0 - 2}\bar{Y}, \\
&\bar{T}^p_{11} \sim 4(\lambda_0 - 1)(1-\beta)c_0 \bar{X}^{\lambda_0 - 2}\bar{Y}, \quad \bar{T}^p_{12} \sim 2(1-\beta)c_0 \bar{X}^{\lambda_0 - 1}, \\
&\bar{T}^p_{22} \sim -4(\lambda_0 - 1)(1-\beta)c_0 \bar{X}^{\lambda_0 - 2}\bar{Y}, \qquad \text{as } \bar{Y} \to \infty.
\end{aligned} \tag{5.24}$$

By comparing with (5.23) and the expression for the pressure in (5.8) we may determine the functions $\bar{a}(\bar{X})$ and $p_0(\bar{X})$ to be

$$\bar{a} = 2c_0 \bar{X}^{\lambda_0 - 1}, \quad \bar{p}_0 = p_0 \bar{X}^{\lambda_0 - 1}. \tag{5.25}$$

Thus we can write the solution of the leading order boundary layer equations as

$$\bar{\Psi} = c_0 \bar{X}^{\lambda_0 - 1} \bar{Y}^2, \quad \bar{T}^p_{11} = 2(1-\beta)\left(2(\lambda_0 - 1)c_0 \bar{X}^{\lambda_0 - 2}\bar{Y} + 4c_0^2 \bar{X}^{2(\lambda_0 - 1)}\right),$$
$$\bar{T}^p_{12} = 2(1-\beta)c_0 \bar{X}^{\lambda_0 - 1}, \quad \bar{T}^p_{22} = -4(1-\beta)(\lambda_0 - 1)c_0 \bar{X}^{\lambda_0 - 2}\bar{Y},$$
$$\bar{p} = p_0 \bar{X}^{\lambda_0 - 1}, \tag{5.26}$$

satisfying Oldroyd-B viscometric behaviour as $\bar{Y} \to 0$. In the boundary layer the solvent extra stresses are their Newtonian like behaviour

$$T^s_{11} = \epsilon^{2(\lambda_0 - 1)}\bar{T}^s_{11}, \quad T^s_{12} = \epsilon^{(\lambda_0 - 1)}\bar{T}^s_{11}, \quad T^s_{22} = \epsilon^{2(\lambda_0 - 1)}\bar{T}^s_{22}, \tag{5.27}$$

where

$$\bar{T}^s_{11} = -\bar{T}^s_{22} = 2\beta \frac{\partial^2 \bar{\Psi}}{\partial \bar{X} \partial \bar{Y}} \sim 4\beta(\lambda_0 - 1)c_0 \bar{X}^{\lambda_0 - 2}\bar{Y},$$
$$\bar{T}^s_{12} = \beta\left(\frac{\partial^2 \bar{\Psi}}{\partial \bar{Y}^2} - \frac{\partial^2 \bar{\Psi}}{\partial \bar{X}^2}\right) \sim 2\beta c_0 \bar{X}^{\lambda_0 - 1}, \tag{5.28}$$

at leading order in ϵ.

The above boundary layer analysis has focused on the ('upstream') wall $\theta = 0$ and is expected to apply to the ('downstream') wall $\theta = \pi/\alpha$. For the 'downstream' layer, Cartesian axes are taken with the x axis along the 'downstream' wall $\theta = \pi/\alpha$ and y orthogonal to the wall along $\theta = \pi/\alpha + \pi/2$, preserving the orientation relative to the 'upstream' axes. In terms of polar co-ordinates we have $x = r\cos(\pi/\alpha - \theta)$, $y = -r\sin(\pi/\alpha - \theta)$. In outer variables, $R^* \sim X^*$ as normal, but $(\pi/\alpha - \theta) \sim -Y^*/X^*$ as the downstream wall is approached. From the separable solution form of ψ (2.69), as the downstream wall $\theta = \pi/\alpha$ is approached

$$\psi \sim r^{1+\lambda_0} c_0 (\pi/\alpha - \theta)^2, \quad \text{since } f_0 \sim (\pi/\alpha - \theta)^2 \tag{5.29}$$
$$= x^{1+\lambda_0} c_0 \frac{y^2}{x^2} = c_0 x^{\lambda_0 - 1} y^2. \tag{5.30}$$

In terms of boundary layer variables, the equivalent expression for ψ in (5.24) is

$$\frac{1}{2} c_0 \bar{X}^{\lambda_0 - 1} \bar{Y}^2. \tag{5.31}$$

From (2.79), or using the fact that f_0 is symmetric around $\theta - \pi/2$, $f_0''(\pi/\alpha) = f_0''(0)$. The governing equations are therefore unchanged from the upstream case, so the above analysis applies still. Consequently, (5.26) gives the solution for the stream function, solvent stresses and pressure in the downstream region, with the difference being the

domain is now

$$\bar{X} \geq 0, \quad \bar{Y} \leq 0. \tag{5.32}$$

Figure 5-2 shows the downstream axes alignment.

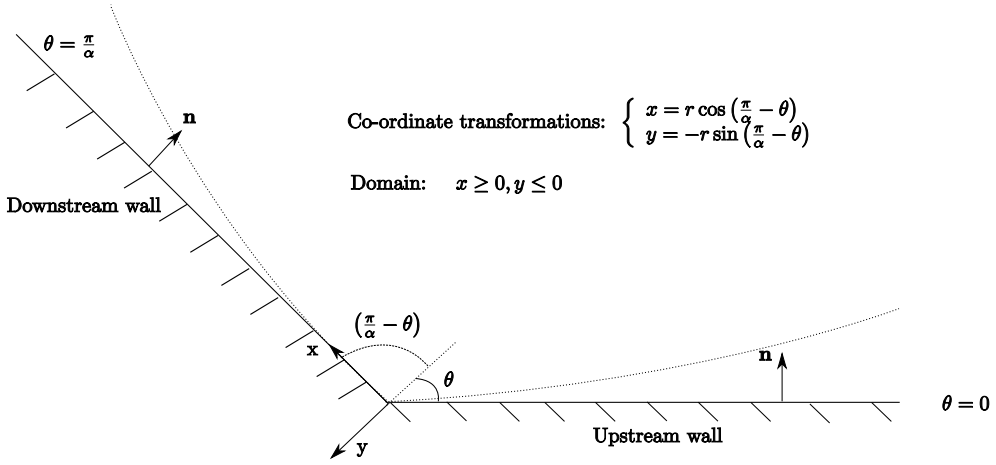

Figure 5-2: Salient corner geometry, with the downstream axes alignment shown. The normals n are given on both 'upstream' and 'downstream' walls, along with the (x, y) alignment shown for the 'downstream' wall. The domain (5.32) is given, where y is now aligned into the wall now rather than out from it as in the 'upstream' case. The co-ordinate transformations from Cartesian to polars are given, with the relevant angles indicated on the corner.

5.2 Discussion

The salient corner flow of the Oldroyd-B fluid has been determined as a one parameter family of solutions with respect to the stream function multiplicative constant c_0. The flow, dominated by Newtonian behaviour, has zero velocity gradient and polymer stresses at the corner in comparison to the singular behaviour of these in re-entrant corner flow. These features allow the analysis to be far more straightforward, indeed as far as to have an analytical solution in the core and boundary layer regions. It is notable how significantly different the boundary layer equations (5.20) are in the salient case compared to those of the re-entrant corner in chapter 3. Only one component term in the upper convected stress derivative is present, whilst in comparison all the component terms are retained in the boundary layer equations at the re-entrant corner.

The solution derived is valid for $\beta \in [0,1]$. The UCM results can be deduced by simply setting $\beta = 0$. In the Newtonian limit $\beta \to 1^-$, we obtain zero polymer extra stresses in both the outer region (5.2) and in the boundary layer (5.26). As such nothing special happens in these two limits.

Another limit of interest is the flat wall case $\alpha \to 1^+$. In this limit, the plot in figure 2-3 shows that $\lambda_0 \to 1^+$, or indeed directly from equation (2.78) it can be calculated that $\lambda_0 = 1$ when $\alpha = 1$. Thus the asymptotic structure breaks down as the boundary layer thickness becomes order one and is no longer thin. The boundary layer solution (5.26) gives the simple shear solution

$$\bar{\Psi} = c_0 \bar{Y}^2, \quad \bar{T}^p_{11} = 8(1-\beta)c_0^2, \quad \bar{T}^p_{12} = 2(1-\beta)c_0, \quad \bar{T}^p_{22} = 0, \tag{5.33}$$

with analogous expressions for the solvent stresses. We note that the outer core stream function does give simple shear, since setting $\alpha = \lambda_0 = 1$ in (2.81) gives

$$f_0 = \frac{1}{2}\left(1 + \cos(2\theta - \pi)\right) = \sin^2\theta,$$

and thus

$$\psi \to c_0 r^2 \sin^2\theta \quad \text{as} \quad \alpha \to 1^+. \tag{5.34}$$

The solution of section 5.1 is only guaranteed to hold for corner angles $\theta \in (146.3^o, 180^o)$ due to the complex nature of the Newtonian eigenvalue λ_0 for smaller corner angles. Further work to understand eddy formation for Oldroyd-B (as in [39] for Newtonian flow) is required. Also the analysis has been done for We = 1 and the limits of low and high Weissenberg number are also of interest.

Chapter 6

Discussion

The asymptotic structure local to both the re-entrant and salient corners has been described for classes of self-similar solutions of the Oldroyd-B equations in relevant parameter regimes. Discussion of the results in each chapter has been previously presented. Here we discuss the results and limitations of the work presented, along with possible future lines of enquiry to be pursued.

Prior to this thesis, the re-entrant corner problem was well understood for UCM fluids, but arguably less so for the more complicated Oldroyd-B fluids. The work of Rallison and Hinch [47], Hinch [30] provided the basic solution approach. Here we have extended this work, primarily investigating in more detail:
(i) the relationship between the Cartesian and natural stress variables,
(ii) the parameter dependence of the solution on both the retardation parameter and Weissenberg number, and
(iii) providing an alternative numerical scheme to solve the downstream boundary layer equations.
The other regime of a salient corner problem has also been discussed. This has been assumed to be straightforward due to the anticipation of a Newtonian flow field dominating, for example see Renardy [54], although no details have previously been presented.

The model equations have been presented here in terms of two dimensionless parameters, the Weissenberg number We and the retardation parameter (or dimensionless solvent viscosity) β. The base parameter regime is that of $\mathrm{We} = O(1)$ with $\beta \in (0, 1)$, the singular behaviour of the Oldroyd-B equations near a sharp corner being described in chapters 3 and 5. In both the re-entrant and salient corner regimes, boundary layers are present, although their equations are markedly different.

For the re-entrant corner case, the main single parameter limits of (i) high and low

Weissenberg with $\beta \in (0,1)$ fixed, and then (ii) $\beta \to 1^-$ with Weissenberg kept fixed and order one, have been described in chapter 4. The three region asymptotic structure of chapter 3 occurs at the heart of the high and low Weissenberg structures, which is expected since the Weissenberg number can be scaled out of the problem. The combined double parameter limits involving both We and β have been left as open problems and are likely to have even more complicated structures. Understanding the asymptotics in these parameter limits is particularly useful as it aids numerical schemes which can encounter significant difficulties. This aid to the numerics may be by incorporating the analytical behaviour of the corner stress singularity into a numerical scheme, or simply by identifying narrow regions where large changes in stress or velocity gradients can occur and which need appropriate resolution, for example, the cusp like elastic boundary layers at the walls. As a case in point, numerical schemes tend to have trouble converging with increasing Weissenberg number (although cope more easily with low Weissenberg number due to the Newtonian flow behaviour which dominates). As such the asymptotics of this limit is of use in the understanding of the high Weissenberg number problem (an overview discussion of which is given in Owens and Philips [43]). The analytical results of chapter 3 give the following asymptotic stress and velocity field behaviours near to the corner of

$$\mathbf{T}^p = O(r^{-2(1-\alpha)}), \quad \mathbf{T}^s = O(r^{-(1-\alpha)(2-\alpha)}), \quad \mathbf{v} = O(r^{(3-\alpha)\alpha-1}) \ \text{ as } r \to 0, \tag{6.1}$$

with corresponding elastic wall boundary layers of thickness $O(r^{2-\alpha})$. These behaviours are known from the earlier work of Hinch [30], Rallison and Hinch [47] and Evans [18]. However, numerical results in Alves et al. [5] (as well as Singh and Leal [56], Baaijens [8], Xue et al. [60], Phillips and Williams [46], Alves et al. [4], Aboubacar and Webster [2], Aboubacar et al. [1] amongst others) have only confirmed these behaviours in the benchmark case of a 270^o corner angle i.e. for $\alpha = 2/3$. It would be of interest to validate the behaviours (6.1) for other corner angles and moreover to see if numerics can support the asymptotic structures of chapters 3 and 4 (by simply comparing numerical sizes of terms in different regions).

For the salient corner case, the Newtonian core similarity solution has been successfuly matched to wall boundary layers in chapter 5 for corner angles greater than 146.3^o i.e. $\alpha < 1.23$. The boundary layers are of thickness r^{λ_0} and retrieve viscometric behaviour for the polymer stresses. Since only one term of the upper convected stress derivative is recovered at leading order these boundary layer equations are very different to those of the re-entrant corner case where all terms in the upper convected stress derivative are present. The complex mathematical machinery of the natural

stress formulation is unnecessary in this case to analyse the boundary layer equations and an explicit solution is available. The retardation parameter β plays less of role for this solution with the polymer stresses vanishing in the Newtonian limit $\beta \to 1^-$. The analysis has been performed for the main case of We $= 1$, with the limits of low and high Weissenberg numeber being left for future work. For smaller corner angles, the eigenvalue is complex and the real part of the stream function is taken. Complex eigenvalues correspond to a sequence of recirculating regions or eddies, the size and intensity of which are described in Moffatt [39]. The details of the boundary layer equations accommodating such circulating core flows for this corner range have not yet been been done.

The main extensions to this work can be categorised (not mutually exclusive) in regard to

- model generalisation ;
- geometry ; and
- other flow types and problems.

Common generalisations of the Oldroyd-B model are the Phan-Thien–Tanner ([45]) and Giesekus ([27]) models. These add quadratic stress terms to the polymer constitutive equation which allows these models to capture shear-thinning effects commonly associated with polymeric fluids. Also these correct the deficiency of Oldroyd-B noted in chapter 2 in regard to the unrestrictedly growing extensional viscosity at finite extension rates in uni- and bi-axial extensional flows. Analogous results to (6.1) for the re-entrant corner exist for these models (see Renardy [53] and Evans [22, 23]), namely

$$\mathbf{T}^p = \begin{cases} O(r^{-\frac{4(1-\lambda_0)}{(5+\lambda_0)}}), & \text{PTT}, \\ O(r^{-\frac{(1-\lambda_0)(3-\lambda_0)}{4}}), & \text{Giesekus}, \end{cases} \qquad \mathbf{T}^s = O(r^{-(1-\lambda_0)}), \mathbf{v} = O(r^{\lambda_0}), \quad \begin{cases} \text{PTT}, \\ \text{Giesekus}. \end{cases} \tag{6.2}$$

Here $\lambda_0 \in [1/2, 1)$ is the Newtonian flow eigenvalue (as defined in chapter 5, but now applied for the range $\alpha < 1$). The behaviours are thus very different:

- For Oldroyd-B, the polymer stress dominates the solvent stress. These stress behaviours hold for the UCM model obtained in the limit $\beta \to 0^+$. However, they breakdown in the Newtonian limit $\beta \to 1^-$ as remarked upon in chapter 4.
- For PTT and Giesekus, the solvent stress dominates the polymer stress. These stress behaviours hold for the Newtonian limit $\beta \to 1^-$, but breakdown in the limit $\beta \to 0^+$.

- For $\beta = 0$, the PTT model shares the same stress singularity as UCM (but different velocity behaviours) as described in Evans and Sibley [24, 25]. However, this solution for the PTT model only holds for angles between 180^o and 270^o. Results for larger angles are outstanding as are those entirely for Giesekus in this limit.

- The boundary layer thickneses for $\beta \in (0, 1)$ are very different, with Oldroyd-B the thinnest at $O(r^{2-\alpha})$, then $O(r^{\frac{(3-\lambda_0)}{2}})$ for Giesekus and the thickest being $O(r^{\frac{(4-\lambda_0)}{3}})$ for PTT.

More complex models, include those such as FENE-P and Rollie-Poly [35]. As these become more widely used in numerical simulations, the need to understand the asymptotic behaviours near singularities (to benchmark the numerical algorithms) also increases. Understanding the "simpler" models first though is beneficial since they are usually more tractable analytically and tend to be contained within (i.e. are valid limits of) the more involved constitutive laws.

Attention has focused entirely on the two-dimensional planar geometry. Equally important are the circular contraction geometries, so that the axis-symmetric case is important to study. Much experimental and numerical simulation in the axisymmetic case has been done (and surveyed in Philips and Owen [46]), whilst no analytical results are available. This is also the case for the fully 3-D contraction flows.

Another restriction of the flow considered here is that it is assumed to be complete around the re-entrant corner. The presence of a separating streamline at the upstream wall may be of relevance to the situation of a lip vortex, which is often seen in experimental and numerical simulation of viscoelastic fluids (and not for Newtonian fluids). This situation has not been discussed. However, if the separating streamline attached to the corner makes an acute angle $\pi/\alpha' < \pi/2$ with the upstream wall then there may be an effective re-entrant corner between the separating streamline and the downstream wall. Care needs to be taken since the boundary conditions along the seperation streamline are quite different from those at the solid wall; and the dividing streamline may not be a straight line (though it will be at a close enough distance to the corner). The core and downstream boundary layer analysis may still be relevant in this situation, although more general core flows would be anticipated since fluid is now not originating from the upstream boundary layer. If $\pi/\alpha' = \pi/2$, then the results here are unlikely to be applicable.

It is worth mentioning that for the salient corner, antisymmetric flows were only considered. Following Moffat [39], it is possible to consider symmetric flows, where the symmetry line is a free surface. The flow structure is very similar to the antisymmetric

case with a Newtonian similarity solution dominating between the free surface and the wall at which a boundary layer of the type obtained in chapter 5 occurs. The main difference is that the eigenvalues now satisfy a slightly different transcendental equation and the behaviour near the free surface needs investigation. Unlike for Newtonian fluids, general salient corner flows for Oldroyd-B are not simply linear combinations of the symmetric and antisymmetric flows due to the nonlinearity of the constitutive equations.

Further situations possessing both geometric and stress singularities are those associated with source/sink flows in wedges/cones, stick-slip or slip-stick as well as flows with general separation points. Very little analytically is available, other than the recent sink flow in a wedge by Evans and Hagan [26].

Appendix A

Full far field coefficients

Here we record the coefficients in the far-field expansion of the Cartesian variables (3.141)–(3.144) in chapter 3. The superscript *sp* denoting similarity parameters have been dropped in the below expressions for C_0 and C_1.

$$F_1 = \frac{\beta C_0(\alpha-2)(\alpha-3)^2}{C_1(3\alpha-2)} \tag{A.1}$$

$$F_2 = \frac{\beta^2 C_0^2(\alpha-2)(27\alpha^4-102\alpha^3+135\alpha^2-73\alpha+14)(\alpha-3)^3}{2C_1^2(3\alpha-2)^2(2\alpha-1)^2} \tag{A.2}$$

$$\begin{aligned} F_3 = \frac{(\alpha-3)}{4C_1\alpha^2(3\alpha-2)\xi^2}\Big(&\alpha^5(4\beta C_0C_4+6)+\alpha^4(14\beta C_0C_4+40+\beta) \\ &+\alpha^3(10\beta C_0C_4+84+3\beta)+\alpha^2(4\beta C_0C_4-46)-32\alpha+24\Big) \end{aligned} \tag{A.3}$$

$$\begin{aligned} F_4 = \frac{\beta^3 C_0^3(\alpha-1)(\alpha-2)(\alpha-3)^4}{3C_1^3(3\alpha-1)(5\alpha-2)(2\alpha-1)^2(3\alpha-2)^3}\Big(&3690\alpha^7-20722\alpha^6+47879\alpha^5 \\ &-58763\alpha^4+41304\alpha^3-16672\alpha^2+3592\alpha-320\Big) \end{aligned} \tag{A.4}$$

$$\begin{aligned} F_5 = \frac{\beta^4 C_0^4(\alpha-1)(\alpha-2)(\alpha-3)^5}{24C_1^4(4\alpha-1)(3\alpha-1)(5\alpha-2)(2\alpha-1)^4(3\alpha-2)^4}\Big(&4177800\alpha^{12} \\ &-36056365\alpha^{11}+139910175\alpha^{10}-322540510\alpha^9+491709868\alpha^8 \\ &-521994001\alpha^7+395586577\alpha^6-215620945\alpha^5+83898211\alpha^4 \\ &-22728136\alpha^3+4069032\alpha^2-432208\alpha+20592\Big) \end{aligned} \tag{A.5}$$

$$F_6 = \frac{\beta C_0(\alpha-3)^2}{6C_1^2\alpha^2(\alpha+2)(\alpha+1)(2\alpha-1)^2(3\alpha-2)^2}\Big(\alpha^{10}(48C_0C_4\beta+72)$$
$$+\alpha^9(-12\beta-38C_0C_4\beta-408)+\alpha^8(-518\beta C_0C_4+394-17\beta)$$
$$+\alpha^7(740\beta C_0C_4+1204+260\beta)+\alpha^6(1028\beta C_0C_4-1526-270\beta)$$
$$+\alpha^5(-3100-182\beta-2356\beta C_0C_4)+\alpha^4(275\beta+6484+1124\beta C_0C_4)$$
$$+\alpha^3(-78\beta-3326+16\beta C_0C_4)+\alpha^2(-80\beta C_0C_4-332)+696\alpha-144\Big) \quad \text{(A.6)}$$

$$A_1 = \frac{2\beta C_0(\alpha-1)(\alpha-2)(\alpha-3)}{C_1(3\alpha-2)} \quad \text{(A.7)}$$

$$A_2 = \frac{(\alpha-1)(\alpha-2)(25\alpha^3-66\alpha^2+50\alpha-12)\beta^2C_0^2}{C_1^2(3\alpha-2)^2(2\alpha-1)} \quad \text{(A.8)}$$

$$A_3 = \frac{(\alpha-1)(\alpha-2)(3\alpha^3+(\alpha^3-\alpha^2)\beta C_0C_4-8\alpha^2-5\alpha+6)}{C_1\alpha^2(3\alpha-2)(\alpha+1)} \quad \text{(A.9)}$$

$$A_4 = \frac{(\alpha-1)(\alpha-2)(\alpha-3)^3\beta^3C_0^3}{C_1^3(3\alpha-2)^2(2\alpha-1)^2(5\alpha-2)}\Big(775\alpha^6-3693\alpha^5$$
$$+6883\alpha^4-6420\alpha^3+3199\alpha^2-816\alpha+84\Big) \quad \text{(A.10)}$$

$$A_5 = \frac{(\alpha-1)(\alpha-2)(\alpha-3)^4\beta^4C_0^4}{3C_1^4(3\alpha-2)^4(2\alpha-1)^3(5\alpha-2)(3\alpha-1)}\Big(505395\alpha^{11}-4022929\alpha^{10}$$
$$+14185420\alpha^9-29241956\alpha^8+39170793\alpha^7$$
$$-35834263\alpha^6+22872182\alpha^5-10198476\alpha^4$$
$$+3116896\alpha^3-622496\alpha^2+73184\alpha-3840\Big) \quad \text{(A.11)}$$

$$A_6 = \frac{(\alpha-3)\beta C_0}{6\alpha C_1^2(3\alpha-2)^2(2\alpha-1)^2}\Big(\alpha^9(+48\alpha^9C_0C_4\beta+72\alpha^9)$$
$$+\alpha^8(-232\beta C_0C_4-552-12\alpha^8\beta)+\alpha^7(+338\beta C_0C_4+1514+56\beta)$$
$$+\alpha^6(-32\beta C_0C_4-1864-59\beta)+\alpha^5(-332\beta C_0C_4+1670-21\beta)$$
$$+\alpha^4(+346\beta C_0C_4+65\beta-3182)+\alpha^3(-200\beta C_0C_4-35\beta+5108)$$
$$+\alpha^2(+80\beta C_0C_4-4066+6\beta)+\alpha(-16\beta C_0C_4+1520)-216\Big) \quad \text{(A.12)}$$

$$A_7 = \frac{(\alpha-1)(-3+2\alpha)}{2\alpha C_0(\alpha+1)(\alpha-2)(\alpha-3)^2}\Big(4\alpha^3C_0C_5-\alpha^2(16C_0C_5-2C_0C_4^2)$$
$$+\alpha(C_4+6C_0C_4^2+4C_0C_5)+24C_0C_5-4C_0C_4^2-3C_4\Big) \quad \text{(A.13)}$$

$$B_1 = \frac{\beta C_0(2\alpha-1)(\alpha-3)(\alpha-2)^2}{C_1(3\alpha-2)(\alpha-1)} \tag{A.14}$$

$$B_2 = \frac{2(\alpha-2)(\alpha-3)^2(25\alpha^5-117\alpha^4+197\alpha^3-146\alpha^2+49\alpha-6)\beta^2C_0^2}{C_1^2(3\alpha-2)^2(2\alpha-1)^2} \tag{A.15}$$

$$B_3 = \frac{2(\alpha-2)(3\alpha^3+(\alpha^3-\alpha^2)\beta C_0C_4-8\alpha^2-5\alpha+6)}{C_1\alpha^2(3\alpha-2)(\alpha+1)} \tag{A.16}$$

$$\begin{aligned} B_4 = \frac{(\alpha-2)(\alpha-3)^3\beta^3C_0^3}{2C_1^3(3\alpha-2)^2(2\alpha-1)^2(5\alpha-2)(3\alpha-1)}\Big(&4650\alpha^8-30913\alpha^7 \\ &+84613\alpha^6-123649\alpha^5+105184\alpha^4-53509\alpha^3+15958\alpha^2-2556\alpha+168\Big) \end{aligned} \tag{A.17}$$

$$\begin{aligned} B_5 = \frac{2(\alpha-2)(\alpha-3)^4\beta^4C_0^4}{3C_1^4(3\alpha-2)^4(2\alpha-1)^3(5\alpha-2)(3\alpha-1)}\Big(&1010790\alpha^{13}-9864353\alpha^{12} \\ &+43122976\alpha^{11}-111668429\alpha^{10}+190927218\alpha^9 \\ &-227482449\alpha^8+194275242\alpha^7-120407718\alpha^6 \\ &+54151965\alpha^5-17447730\alpha^4+3911344\alpha^3-576824\alpha^2+50032\alpha-1920\Big) \end{aligned} \tag{A.18}$$

$$\begin{aligned} B_6 = \frac{(\alpha-3)\beta C_0}{12\alpha C_1^2(3\alpha-2)^2(2\alpha-1)^2(\alpha-1)(\alpha+1)}\Big(&\alpha^{11}(144+96C_0C_4\beta) \\ &+\alpha^{10}(-512C_0C_4\beta-24\beta-1176)+\alpha^9(124\beta+668C_0C_4\beta+3148) \\ &+\alpha^8(-2170-126\beta+700\beta C_0C_4)+\alpha^7(-2086\beta C_0C_4-1512-207\beta) \\ &+\alpha^6(990\beta C_0C_4-6590+387\beta)+\alpha^5(558\beta C_0C_4+25078-51\beta) \\ &+\alpha^4(-622\beta C_0C_4-213\beta-22676)+\alpha^3(376\beta C_0C_4+134\beta-906) \\ &+\alpha^2(-232\beta C_0C_4+11828-24\beta)+\alpha(64\beta C_0C_4-6200)+1008\Big) \end{aligned} \tag{A.19}$$

$$\begin{aligned} B_7 = \frac{(\alpha^2-3\alpha+3)}{\alpha C_0(\alpha+1)(\alpha-2)(\alpha-3)^2}\Big(&4\alpha^3C_0C_5+\alpha^2(-16C_0C_5-2C_0C_4^2) \\ &+\alpha(C_4+6C_0C_4^2+4C_0C_5)+24C_0C_5-4C_0C_4^2-3C_4\Big) \end{aligned} \tag{A.20}$$

$$D_1 = \frac{2\beta C_0(\alpha-2)(\alpha-3)(\alpha^2-3\alpha+1)}{C_1(3\alpha-2)(\alpha-1)} \tag{A.21}$$

$$D_2 = \frac{(\alpha-2)(\alpha-3)^2\beta^2 C_0^2}{C_1^2(3\alpha-2)^2(2\alpha-1)^2(\alpha-1)^2}\Big(50\alpha^7 - 36\alpha^6 + 1041\alpha^5 - 1547\alpha^4 + 1272\alpha^3 - 578\alpha^2 + 134\alpha - 12\Big) \tag{A.22}$$

$$D_3 = \frac{1}{(\alpha+1)(3\alpha-2)(\alpha-1)^2 C_1\alpha^2}\Big(\alpha^7(\beta C_0C_4+3) + \alpha^6(-11-2\beta C_0C_4) + \alpha^5(-6\beta C_0C_4-15) + \alpha^4(16\beta C_0C_4+104-3\beta) + \alpha^3(-96-11\beta C_0C_4-\beta) + \alpha^2(6\beta C_0C_4+2\beta-57) + 108\alpha - 36\Big) \tag{A.23}$$

$$D_4 = \frac{(\alpha-2)(\alpha-3)^3\beta^3 C_0^3}{C_1^3(3\alpha-2)^3(2\alpha-1)^2(5\alpha-2)(3\alpha-1)(\alpha-1)}\Big(6975\alpha^{10} - 61827\alpha^9 + 234261\alpha^8 - 498701\alpha^7 + 658958\alpha^6 - 563825\alpha^5 + 316358\alpha^4 - 114941\alpha^3 + 25838\alpha^2 - 3228\alpha + 168\Big) \tag{A.24}$$

$$D_5 = \frac{(\alpha-2)(\alpha-3)^4\beta^4 C_0^4}{3C_1^4(3\alpha-2)^4(2\alpha-1)^3(5\alpha-2)(3\alpha-1)(\alpha-1)(4\alpha-1)}\Big(4043160\alpha^{15} - 47742182\alpha^{14} + 255195011\alpha^{13} - 819193720\alpha^{12} + 1765689807\alpha^{11} - 2705857782\alpha^{10} + 3044714741\alpha^9 - 2560985636\alpha^8 + 1623126047\alpha^7 - 774886220\alpha^6 + 276205926\alpha^5 - 72105876\alpha^4 + 13318912\alpha^3 - 1637936\alpha^2 + 119264\alpha - 3840\Big) \tag{A.25}$$

$$D_6 = \frac{(\alpha-3)\beta C_0}{6\alpha C_1^2(3\alpha-2)^2(2\alpha-1)^2(\alpha-1)^2(\alpha+1)}\Big(\alpha^{12}(72+48C_0C_4\beta) + \alpha^{11}(-696-12\beta-328C_0C_4\beta) + \alpha^{10}(80\beta+2330+658C_0C_4\beta) + \alpha^9(-2420+170C_0C_4\beta-147\beta) + \alpha^8(-1962-51\beta-2156\beta C_0C_4) + \alpha^7(-640+393\beta+2784\beta C_0C_4) + \alpha^6(25220-300\beta-2394\beta C_0C_4) + \alpha^5(-47560-117\beta+3346\beta C_0C_4) + \alpha^4(253\beta+30450-3472\beta C_0C_4) + \alpha^3(-117\beta+4648+1528\beta C_0C_4) + \alpha^2(-15490+18\beta-136\beta C_0C_4) + \alpha(7152-48\beta C_0C_4) - 1080\Big) \tag{A.26}$$

$$D_7 = \frac{1}{2\alpha C_0(\alpha+1)(\alpha-2)(\alpha-1)^2(\alpha-3)^2}\Big(\alpha^7(8C_0C_5) + \alpha^6(-76C_0C_5 - 4C_0C_4^2)$$
$$+ \alpha^5(284C_0C_5 + 34C_0C_4^2 + 2C_4) + \alpha^4(-504C_0C_5 - 126C_0C_4^2 - 17C_4)$$
$$+ \alpha^3(254C_0C_4^2 + 316C_0C_5 + 59C_4) + \alpha^2(-290C_0C_4^2 + 300C_0C_5 - 105C_4)$$
$$+ \alpha(+180C_0C_4^2 - 600C_0C_5 + 93C_4) - 48C_0C_4^2 + 288C_0C_5 - 36C_4\Big) \qquad \text{(A.27)}$$

Appendix B

$\alpha = 2/3$ Full-far field case

Here are presented the modified expansions analogous to (3.141)–(3.144) in the case $\alpha = 2/3$. These terms are fully determined down to $\xi^{-8/3}$ where the eigenmodes associated with C_0, C_2, C_3, C_4 and C_5 are retained. The structure of the expansion is similar to that found by Sibley [57] for the PTT model involving algebraic powers of $\ln(\xi)$. This expansion below completes the far-field analysis for the Cartesian stress basis. The supercript *sp* has again been dropped from C_0 and C_1 for convenience.

$$
\begin{aligned}
f(\xi) \sim \xi^{7/3} \Bigg(& 1 + (F_1 \ln(\xi) + C_2) \frac{1}{\xi^{2/3}} + C_3 \frac{1}{\xi^1} \\
& + \left(F_2 \ln^2(\xi) + F_3 \ln(\xi) + C_4\right) \frac{1}{\xi^{4/3}} \\
& + \left(F_4 \ln^3(\xi) + F_5 \ln(\xi)^2 + F_6 \ln(\xi) + F_7\right) \frac{1}{\xi^2} \\
& + \left(F_8 \ln^4(\xi) + F_9 \ln(\xi)^3 F_{10} \ln^2(\xi) + F_{11} \ln(\xi) + C_5\right) \frac{1}{\xi^{8/3}} \Bigg), \qquad \text{(B.1)} \\
t^p_{11}(\xi) \sim C_1 \Bigg(& 1 + (A_1 \ln(\xi) + A_2) \frac{1}{\xi^{2/3}} \\
& + \left(A_3 \ln^2(\xi) + A_4 \ln(\xi) + A_5\right) \frac{1}{\xi^{4/3}} \\
& + \left(A_6 \ln(\xi)^2 + A_7 \ln(\xi) + A_8\right) \frac{1}{\xi^2} \\
& + \left(A_9 \ln^4(\xi) + A_{10} \ln(\xi)^3 A_{11} \ln^2(\xi) + A_{12} \ln(\xi) + A_{13}\right) \frac{1}{\xi^{8/3}} \Bigg), \qquad \text{(B.2)}
\end{aligned}
$$

$$t_{12}^{p}(\xi)\frac{1}{3} \sim C_1\xi\Bigg(1 + (B_1\ln(\xi) + B_2)\,\frac{1}{\xi^{2/3}} + B_3\frac{1}{\xi} + \left(B_4\ln^2(\xi) + B_5\ln(\xi) + B_6\right)\frac{1}{\xi^{4/3}} + \left(B_7\ln(\xi)^2 + B_8\ln(\xi) + B_9\right)\frac{1}{\xi^2} + \left(B_{10}\ln^4(\xi) + B_{11}\ln(\xi)^3 B_{12}\ln^2(\xi) + B_{13}\ln(\xi) + B_{14}\right)\frac{1}{\xi^{8/3}}\Bigg), \tag{B.3}$$

$$t_{22}^{p}(\xi) \sim \frac{1}{9} \sim C_1\xi^2\Bigg(1 + (D_1\ln(\xi) + D_2)\,\frac{1}{\xi^{2/3}} + D_3\frac{1}{\xi} + \left(D_4\ln^2(\xi) + D_5\ln(\xi) + D_6\right)\frac{1}{\xi^{4/3}} + \left(D_7\ln(\xi)^3 D_8\ln(\xi)^2 + D_9\ln(\xi) + D_{10}\right)\frac{1}{\xi^2} + \left(D_{11}\ln^4(\xi) + D_{12}\ln(\xi)^3 D_{13}\ln^2(\xi) + D_{14}\ln(\xi) + D_{15}\right)\frac{1}{\xi^{8/3}}\Bigg). \tag{B.4}$$

The constants F_i, A_i, B_i, D_i are presented separately

$$F_1 = \frac{196}{27}\frac{\beta C_0}{C_1}, \quad F_2 = \frac{2744}{81}\frac{\beta^2 C_0^2}{C_1^2}, \quad F_3 = \frac{28}{9}\frac{\beta C_0(3C_1C_2 + 49\beta C_0)}{C_1^2},$$
$$F_4 = \frac{4533088}{59049}\frac{\beta^3 C_0^3}{C_1^3}, \quad F_5 = \frac{4571504}{6561}\frac{\beta^3 C_0^3}{C_1^3},$$
$$F_6 = \frac{7}{26244}\frac{\beta(3616592\beta^2 C_0^3 + 12312C_1^2C_0^2C_4 - 1215C_1^2)}{C_1^3}$$
$$F_7 = \frac{1}{104976}\frac{(31752C_1^2(C_0\beta C_4 + 33)^2 - 107163C_1^2\beta + 86512832\beta^3 C_0^3)}{C_1^3},$$
$$F_8 = \frac{158658080}{1594323}\frac{\beta^4 C_0^4}{C_1^4}, \quad F_9 = \frac{991747456}{531441}\frac{\beta^4 C_0^4}{C_1^4},$$
$$F_{10} = \frac{49}{196830}\frac{\beta C_0(37510480\beta^3 C_0^3 + 32400C_0\beta C_1^2C_4 + 135C_1^2\beta - 5616C_1^2)}{C_1^4},$$
$$F_{11} = \frac{1}{104976}\frac{1}{C_1^4}\Bigg(781734240C_0\beta C_1^2(C_0\beta C_4 + 1021/24620) + 654885C_1^2\beta^2 C_0 + 131597465440\beta^4 C_0^4\Bigg) \tag{B.5}$$

$$A_1 = \frac{56}{271}\frac{\beta C_0}{C_1}, \quad A_2 = \frac{2}{63}\frac{196\beta C_0 + 9C_1C_2}{C_1}, \quad A_3 = \frac{-3136}{729}\frac{\beta^2 C_0^2}{C_1^2},$$

$$A_4 = \frac{2}{2835}\frac{30184\beta^2 C_0^2 - 756\beta C_0(49\beta C_0 + 3C_1C_2) + 588\beta C_0 C_2 C_1}{C_1^2}$$

$$A_5 = \frac{1}{11340}\frac{-1944C_0(-1/6C_2^2 + C_4)C_1^2 + (33264C_0^2\beta C_2 C_1 + 729C_1^2) + 932960\beta^2 C_0^3}{C_1^3 C_0}$$

$$A_6 = \frac{-219520}{2187}\frac{\beta^3 C_0^3}{C_1^3}, \quad A_7 = \frac{1}{21870}\frac{1944C_0\beta C_1^2 C_4 - 729C_1^2\beta - 9521680\beta^3 C_0^3}{C_1^3},$$

$$A_8 = \frac{1}{29160}\frac{(-44712C_0\beta C_4 - 68040)C_1^2 + 16767C_1^2\beta + 10097920\beta^3 C_0^3}{C_1^3}$$

$$A_9 = \frac{49172480}{1594323}\frac{\beta^4 C_0^4}{C_1^4}, \quad A_{10} = \frac{242635456}{531441}\frac{\beta^4 C_0^4}{C_1^4}$$

$$\begin{aligned} A_{11} = \frac{1}{3582306}\frac{1}{C_1^4}\Big(& -221997343568/9\beta^4 C_0^4 - 9814896C_1^2\beta^2 C_0^2 C_4 - 4144959C_1^2\beta^2 C_0 \\ & + 637\beta C_0(37510480\beta^3 C_0^3 + 32400C_0\beta C_1^2 C_4 + 135C_1^2\beta - 5616C_1^2)\Big) \end{aligned}$$

$$\begin{aligned} A_{12} = \frac{1}{3980340}\frac{1}{C_1^4}\Big(& 17912552022820/81\beta^4 C_0^4 + 118025908C_1^2\beta^2 C_0^2 C_4 \\ & - 122967117/4C_1^2\beta^2 C_0 + 26754000C_1^2\beta C_0 - 83447/12\beta C_0(37510480\beta^3 C_0^3 \\ & + 32400C_0\beta C_1^2 C_4 + 135C_1^2\beta - 5616C_1^2) \\ & + 188195280C_0\beta C_1^2(C_0\beta C_4 + 1021/24620)\Big) \end{aligned}$$

$$\begin{aligned} A_{13} = \frac{1}{57153600}\frac{1}{C_0^2 C_1^4}\Big(& -1749600(C_4^2 - 70/3C_5)C_0^2 C_1^4 - 3280500C_4 C_1^4 C_0 \\ & + (1476225C_1^4 + (-4280804640C_0^4\beta^2 C_4 - 635658576C_0^3\beta)C_1^2) \\ & + 429231915C_1^2\beta^2 C_0^3 - 191400805120C_0^6\beta^4\Big) \end{aligned} \tag{B.6}$$

$$B_1 = \frac{-112}{27}\frac{\beta C_0}{C_1}, \quad B_2 = \frac{4}{63}\frac{-9C_1C_2 + 245\beta C_0}{C_1}, \quad B_3 = \frac{-9}{7}C_3, \quad B_4 = \frac{-31360}{729}\frac{\beta^2 C_0^2}{C_1^2},$$

$$B_5 = \frac{4}{567}\frac{-756\beta C_0(49\beta C_0 + 3C_1C_2) + 4802\beta^2 C_0^2 + 588\beta C_0 C_2 C_1}{C_1^2},$$

$$B_6 = \frac{1}{1134}\frac{1}{C_1^2 C_0}\Big(3024C_0^2\beta(49\beta C_0 + 3C_1C_2) + 324C_1^2C_0C_2^2 - 1944C_1^2C_0C_4$$
$$+ 729C_1^2 - 3780C_1\beta C_2 C_0^2 + 101528\beta^2 C_0^3\Big)$$

$$B_7 = \frac{-439040}{729}\frac{\beta^3 C_0^3}{C_1^3}, \quad B_8 = \frac{1}{10935}\frac{5832C_0\beta C_1^2C_4 - 2187C_1^2\beta - 35178080\beta^3C_0^3}{C_1^3},$$

$$B_9 = \frac{1}{14580}\frac{(-131544C_0\beta C_4 - 204120)C_1^2 + 49329C_1^2\beta + 2112880\beta^3C_0^3}{C_1^3}$$

$$B_{10} = \frac{255696896}{1594323}\frac{\beta^4 C_0^4}{C_1^4}, \quad B_{11} = \frac{1336108480}{531441}\frac{\beta^4 C_0^4}{C_1^4}$$

$$B_{12} = \frac{1}{49601160}\frac{1}{C_1^4}\Big(-1684669141120\beta^4C_0^4 - 706672512C_1^2\beta^2C_0^2C_4 - 298437048C_1^2\beta^2C_0$$
$$+ 45864\beta C_0(37510480\beta^3C_0^3 + 32400C_0\beta C_1^2C_4 + 135C_1^2\beta - 5616C_1^2)\Big)$$

$$B_{13} = \frac{1}{49601160}\frac{1}{C_1^4}\Big(13938926324624\beta^4C_0^4 + 7560976752C_1^2\beta^2C_0^2C_4 - 2085427701C_1^2\beta^2C_0$$
$$+ 1733659200C_1^2\beta C_0 - 437913\beta C_0(37510480\beta^3C_0^3 + 32400C_0\beta C_1^2C_4$$
$$+ 135C_1^2\beta - 5616C_1^2) + 12195054144C_0\beta C_1^2(C_0\beta C_4 + 1021/24620)\Big)$$

$$B_{14} = \frac{1}{771573600}\frac{1}{C_0^2C_1^4}\Big(-122821920(C_4^2 - 70/3C_5)C_0^2C_1^4 - 230291100C_4C_1^4C_0$$
$$(103630995C_1^4 + (-284515701120C_0^4\beta^2C_4 - 29880727632C_0^3\beta)C_1^2)$$
$$+ 24179961645C_1^2\beta^2C_0^3 - 20542004819840C_0^6\beta^4\Big) \tag{B.7}$$

$$D_1 = \frac{-280}{27}\frac{\beta C_0}{C_1}, \quad D_2 = \frac{2}{63}\frac{784\beta C_0 - 45C_1C_2}{C_1}, \quad D_3 = \frac{-18}{7}C_3, \quad D_4 = \frac{-31360}{729}\frac{\beta^2 C_0^2}{C_1^2},$$

$$D_5 = \frac{-2}{945}\frac{32928\beta^2 C_0^2 + 4788\beta C_0(49\beta C_0 + 3C_1C_2) - 8764\beta C_0 C_2 C_1}{C_1^2}$$

$$D_6 = \frac{1}{79380}\frac{1}{C_1^2 C_0}\Big(- 258552C_0(C_4 - 313/798C_2^2)C_1^2 + (96957C_1^2 - 762048C_0^2\beta C_2 C_1)$$
$$+ 35342720\beta^2 C_0^3\Big)$$

$$D_7 = \frac{878080}{2187}\frac{\beta^3 C_0^3}{C_1^3}, \quad D_8 = \frac{2063488}{2187}\frac{\beta^3 C_0^3}{C_1^3},$$

$$D_9 = \frac{1}{21870}\frac{441288C_0\beta C_1^2 C_4 - 165483C_1^2\beta - 247755760\beta^3 C_0^3}{C_1^3}$$

$$D_{10} = \frac{1}{9720}\frac{(-440424C_0\beta C_4 - 220320)C_1^2 + 252639C_1^2\beta + 19208000\beta^3 C_0^3}{C_1^4}$$

$$D_{11} = \frac{1789878272}{1594323}\frac{\beta^4 C_0^4}{C_1^4}, \quad D_{12} = \frac{11158926016}{531441}\frac{\beta^4 C_0^4}{C_1^4},$$

$$D_{13} = \frac{1}{12400290}\frac{1}{C_1^4}\Big(- 2257685654560\beta^4 C_0^4 - 1246964544C_1^2\beta^2 C_0^2 C_4 - 518406966C_1^2\beta^2 C_0$$
$$+ 80262\beta C_0(37510480\beta^3 C_0^3 + 32400C_0\beta C_1^2 C_4 + 135C_1^2\beta - 5616C_1^2)\Big)$$

$$D_{14} = \frac{1}{24800580}\frac{1}{C_1^4}\Big(49076975672704\beta^4 C_0^4 + 25824727152C_1^2\beta^2 C_0^2 C_4 + 1052578800C_1^2\beta C_0$$
$$- 8347854816C_1^2\beta^2 C_0 - 1415610\beta C_0(37510480\beta^3 C_0^3 + 32400C_0\beta C_1^2 C_4 + 135C_1^2\beta$$
$$- 5616C_1^2) + 42682689504C_0\beta C_1^2(C_0\beta C_4 + 1021/24620)\Big)$$

$$D_{15} = \frac{1}{154314720}\frac{1}{C_0^2 C_1^4}\Big(- 205962912C_0^2 C_1^4(-6370/327C_5 + C_4^2) - 386180460C_4 C_1^4 C_0$$
$$+ (173781207C_1^4 + (-270294361344C_0^4\beta^2 C_4 - 22869187488C_0^3\beta)C_1^2)$$
$$+ 31723546239C_1^2\beta^2 C_0^3 - 24598692930560C_0^6\beta^4\Big) \qquad \text{(B.8)}$$

Bibliography

[1] M. Aboubacar, H. Matallah and M.F. Webster, Highly elastic solutions for Oldroyd-B and Phan-Thien/Tanner fluids with a finite volume/element method: planar contraction flows, *J. Non-Newtonian Fluid Mech.* **103** (2002), 65–103.

[2] M. Aboubacar and M.F. Webster, A cell-vertex finite volume/element method on triangles for abrupt contraction viscoelastic flows, *J. Non-Newtonian Fluid Mech.* **98** (2001), 83–106.

[3] D.J. Acheson, *Elementary Fluid Dynamics*, OUP, (1990).

[4] M.A. Alves, F.T. Pinho and P.J. Oliveira, Effect of a high-resolution differencing scheme on finite-volume predictions of viscoelastic flows, *J. Non-Newtonian Fluid Mech.* **93** (2000), 287–314.

[5] M.A. Alves, P.J. Oliveira and F.T. Pinho, Benchmark solutions for the flow of Oldroyd-B and PTT fluids in planar contractions, *J. Non-Newtonian Fluid Mech.* **110** (2003), 45–75.

[6] M.A. Alves, F.T. Pinho and P.J. Oliveira, Viscoelastic flow of Boger Fluids in a 4:1 Square/Square contraction, *J. Braz. Soc. Mechanical Sciences and Engineering* Paper: CIT04-0217 (2004), 287–314.

[7] J. Azaiez, R. Guenette and A. Ait-Kadi, Numerical simulation of viscoelastic flows through a planar contraction, *J. Non-Newtonian Fluid Mech.* **62** (1996), 253–277.

[8] F.P.T. Baaijens, An iterative solver for the DEVSS/DG method with application to smooth and non-smooth flows of the upper convected Maxwell fluid, *J. Non-Newtonian Fluid Mech.* **75** (1998), 119–138.

[9] F.P.T. Baaijens, Mixed finite element methods for viscoelastic flow analysis: a review, *J. Non-Newtonian Fluid Mech.* **79** (1998), 361–385.

[10] D.V. Boger, Viscoelastic flows through contractions, *Annual Review of Fluid Mech.* **19** (2000), 157–182.

[11] D.V. Boger, Model polymer fluid systems, *Pure and App. Chem.* **57** (1985), 921–930.

[12] P.J. Coates, R.C. Armstrong and R.A. Brown, Calculation of steady-state viscoelastic flow through axisymmetric contractions with the EEME formulation, *J. Non-Newtonian Fluid Mech.* **42** (1992), 141–188.

[13] L. Davidson, *Fundamentals of Shock Wave Propagation in Solids*, Springer (2008).

[14] A.R. Davies and J. Devlin, On corner flows of Oldroyd-B fluids, *J. Non-Newtonian Fluid Mech.* **50** (1993), 173–191.

[15] W.R. Dean and P.E. Montagnon, On the steady motion of viscous liquid in a corner, *Proc. Cambridge. Phil. Soc.* **45** (1949), 389–394.

[16] S. Dupont, J.M. Marchal and M.J. Crochet, Finite element simulation of viscoelastic fluids of the integral type, *J. Non-Newtonian Fluid Mech.* **17** (1985), 157–183.

[17] J.D. Evans, Re-entrant corner flows of the upper convected Maxwell fluid, *Proc. Roy. Soc. A.* **461** (2005), 117–142.

[18] J. D. Evans, Re-entrant corner flows of Oldroyd-B fluids, *Proc. Roy. Soc. A.* **461** (2005), 2573–2603.

[19] J.D. Evans, Re-entrant corner flows of upper convected Maxwell fluids: the small and high Weissenberg number limits, *Proc. Roy. Soc. A.* **462** (2006), 3749–3774.

[20] J.D. Evans, Re-entrant corner flows of UCM fluids: The Cartesian stress basis, *J. Non-Newtonian Fluid Mech.* **150** (2008), 116–138.

[21] J.D. Evans, Re-entrant corner flows of UCM fluids: The natural stress basis, *J. Non-Newtonian Fluid Mech.* **150** (2008), 139–153.

[22] J.D. Evans, Re-entrant corner behaviour of the PTT fluid with a solvent viscosity, *J. Non-Newtonian Fluid Mech.* **165** (2010), 527–537.

[23] J.D. Evans, Re-entrant corner behaviour of the Giesekus fluid with a solvent viscosity, *J. Non-Newtonian Fluid Mech.* **165** (2010), 538–543.

[24] J.D. Evans and D.N. Sibley, Re-entrant corner flows of PTT fluids in the Cartesian stress basis, *J. Non-Newtonian Fluid Mech.* **153** (2008), 12–24.

[25] J.D. Evans and D.N. Sibley, Re-entrant corner flows of PTT fluids in the natural stress basis, *J. Non-Newtonian Fluid Mech.* **157** (2009), 79–91.

[26] J.D. Evans and T. Hagen, Viscoelastic sink flow in a wedge for the UCM and Oldroyd-B models, *J. Non-Newtonian Fluid Mech.* **154** (2008), 39–46.

[27] H. Giesekus, A unified approach to a variety of constitutive models for polymer fluids based on the concept of configuration dependent molecular mobility, *Rheol. Acta.* **21** (1982), 366–375.

[28] M.I. Gerritsma and T.N. Philips, On the characteristics and compatibility equations for the UCM model fluid, *ZAAM.Z.Angew. Math. Mech.* **88** (2008), 529–539.

[29] M.I. Gerritsma and T.N. Philips, On the use of characteristic variables in viscoelastic flow problems, *IMA Jour. Appl. Math.* **66** (2001), 127–147.

[30] E.J. Hinch, The flow of an Oldroyd Fluid around a sharp corner, *J. Non-Newtonian Fluid Mech.* **50** (1993), 161–171.

[31] D.D. Joseph, *Fluid Dynamics of Viscoelastic Liquids*, Applied Mathematical Sciences **84**, Springer-Verlag, (1990).

[32] D.D. Joseph, M. Renardy and J.C. Saut, Hyperbolicity and change of type in the flow of viscoelastic fluids, *Arch. Rat. Mech. Anal.* **87** (1985), 213–251.

[33] R.A. Keiller, Entry-flow caluclations for the Oldroyd-B and FENE equations, *J. Non-Newtonian Fluid Mech.* **46** (1992), 143–178.

[34] R. Keunings, On the high Weissenberg number problem, *J. Non-Newtonian Fluid Mech.* **20** (1986), 209–226.

[35] A.E. Likhtman and R.S. Graham, Simple constitutive equation for linear polymer melts derived from molecular theory: RoliePoly equation, *J. Non-Newtonian Fluid Mech.* **114** (2003), 1–12.

[36] G.G. Lipscomb, R. Keunings and M.M. Denn, Implications of boundary singularities in complex geometries, *J. Non-Newtonian Fluid Mech.* **24** (1987), 85–96.

[37] J. Lubliner, *Plasticity Theory*, Macmillan Publishing Company, (1990).

[38] H. Matallah, K.S. Sujatha, M.J. Banaai and M.F. Webster Multi-mode simulation of filament stretching flows, *Swansea CSR Report 11* **10** (2006), [Online] Available at http://www.cs.swan.ac.uk/reports/yr2006/

[39] H.K. Moffatt, Viscous and resistive eddies near a sharp corner, *J. Fluid Mech.* **18** (1964), 1–18.

[40] J.G. Oldroyd, Non-Newtonian effects in steady motion of some idealized elastico-viscous liquids, *Proc. R. Soc. A.* **245** (1958), 278–297.

[41] J.G. Oldroyd, On the Formulation of Rheological Equations of State, *Proc. Roy. Soc. A.* **200** (1950), 523–541.

[42] P.J. Oliveira, Alternative derivation of differential constitutive equations of the Oldroyd-B type, *J. Non-Newtonian Fluid Mech.* **160** (2009), 40–46.

[43] R.G. Owens and T.N. Phillips, *Computational Rheology*, Imperial College Press (2002).

[44] N. Phan-Thien, *Understanding Viscoelasticity*, Springer, (2002).

[45] N. Phan-Thien and R. I. Tanner, A new constitutive equation derived from network theory, *J. Non-Newtonian Fluid Mech.* **2** (1977), 353–365.

[46] T.N. Philips and A.J. Williams, Viscoelastic flow through a planar contraction using a semi-Lagrangian finite volume method, *J.Non-Newtonian Fluid Mech.* **87** (1999), 215–246.

[47] J.M. Rallison and E.J. Hinch, The flow of an Oldroyd fluid past a reentrant corner: the downstream boundary layer, *J. Non-Newtonian Fluid Mech.* **116** (2004), 141–162.

[48] M. Renardy, The stresses of an upper convected Maxwell fluid in a Newtonian velocity field near a re-entrant corner, *J. Non-Newtonian Fluid Mech.* **50** (1993), 127–134.

[49] M. Renardy, How to integrate the upper convected Maxwell (UCM) stresses near a singularity (and maybe elsewhere, too), *J. Non-Newtonian Fluid Mech.* **52** (1994), 91–95.

[50] M. Renardy, The high Weissenberg number limit of the UCM model and the Euler equations, *J. Non-Newtonian Fluid Mech.* **69** (1997), 293–301.

[51] M. Renardy, A matched solution for corner flow of the upper convected Maxwell fluid, *J.Non-Newtonian Fluid Mech.* **58** (1995), 83–89.

[52] M Renardy, High Weissenberg number boundary layers for the upper convected Maxwell fluid, *J. Non-Newtonian Fluid Mech.* **68** (1997), 125–132.

[53] M. Renardy, Re-entrant corner behaviour of the PTT fluid, *J. Non-Newtonian Fluid Mech.* **69** (1997), 99–104.

[54] M. Renardy, *Mathematical Analysis of Viscoelastic Flows*, SIAM, (2000).

[55] M. Renardy, Current issues in non-Newtonian flows: a mathematical perspective, *J. Non-Newtonian Fluid Mech.* **90** (2000), 293–301.

[56] P. Singh and L.G. Leal, Finite element simulation of flow around a $3\pi/2$ corner using the FENE dumbell model, *J. Non-Newtonian Fluid Mech.* **58** (1995), 279–313.

[57] D.N.Sibley *Viscoelastic flows of PTT fluids*, PHD thesis, Bath University (2010).

[58] R.I. Tanner, *Engineering Rheology*, OUP, (1985).

[59] R.I. Tanner, The stability of some numerical schemes for model viscoelastic fluids, *J. Non-Newtonian Fluid Mech.* **10** (1982), 169–174.

[60] S.-C. Xue, N. Phan-Thien and R.I. Tanner, Three dimensional numerical simulations of viscoelastic flows through planar contractions, *J. Non-Newtonian Fluid Mech.* **74** (1998), 195–245.

[61] S. Zahorski *Mechanics of viscoelastic fluids*, M.N. Publishers, (1978).